



# Imperial College London

STRUCTURAL AND AEROELASTIC VIBRATION ANALYSIS  
OF BLADED SYSTEMS

BY

M IMREGUN

Dynamics Group

Mechanics I Engineering

THESIS SUBMITTED TO THE UNIVERSITY OF LONDON  
FOR THE DEGREE OF DOCTOR OF PHILOSOPHY

**STRUCTURAL AND AEROELASTIC  
VIBRATION ANALYSIS OF BLADED SYSTEMS**

*by*

**M. Imregun**

*A thesis submitted to the University of London  
for the degree of Doctor of Philosophy*

**Department of Mechanical Engineering  
Imperial College of Science and Technology  
London SW7**

**December 1983**

*Les souvenirs sont cors de chasse  
Dont meurt Le brutt dans le vent.*

*Guillaume Apollinaire*

### ABSTRACT

*This study deals with the vibration analysis of bladed systems and can be divided into two parts (i) Structural analysis of packed bladed discs and (ii) Aeroelastic characteristics of bladed systems. Both parts share the feature that vibration properties are complicated by a lack of symmetry.*

*The aim of the first part is to seek effective and efficient ways of predicting the vibrational behaviour of turbine blades when grouped into packets on a disc. Several theoretical models based on various techniques were developed to investigate different aspects of the problem. Finite element modelling was used to analyse isolated blade packets while substructuring via receptance coupling was needed to investigate the complete bladed system. The latter model led to the formulation of two new methods of analysis, results from which were checked by a series of experiments and good agreement was obtained in all cases. A lumped parameter technique was used for qualitative studies and it was found that this particular model was adequately representative of packed bladed disc behaviour provided quantitative predictions were not required.*

*The second part deals with the aerodynamic analysis and flutter stability of bladed discs, with particular interest in mistuned systems. A simple structural model based on the lumped parameter configuration used in (i) was combined with existing unsteady aerodynamic theories for two-dimensional unstalled cascades of flat plates. The effects of mistuning and the levels of forced response were investigated for a number of bladed systems in order to find and to categorize patterns of qualitative behaviour. Finally, a finite element model of a cantilevered flat plate subject to axial aerodynamic loading was developed to analyse the flutter stability of an isolated blade. A numerical study was conducted to predict the natural frequencies and the mode shapes for both in vacuum and under aerodynamic loading and also the amount of aerodynamic damping was determined in the latter case.*

CONTENTS

<b>ABSTRACT</b>	iii
<b>PREFACE</b>	vii
<b>LIST OF FIGURES</b>	viii
<b>LIST OF TABLES</b>	x
<b>NOMENCLATURE</b>	xi

*Part I*

STRUCTURAL ANALYSIS

<b>1 INTRODUCTION</b>	<b>2</b>
1.1 The Nature of the Problem	2
1.2 Literature Survey	3
1.3 Objectives and Scopes of the Present <b>Analysis</b>	6
<b>2 FINITE ELEMENT ANALYSIS OF CANTILEVERED BLADE PACKETS</b>	<b>8</b>
2.1 Finite Element Model	8
2.2 Numerical Study	10
2.3 Concluding <b>Remarks</b>	13
<b>3 RECEPTANCE COUPLING ANALYSIS OF PACKETED BLADED DISCS</b>	<b>15</b>
3.1 Theoretical Analyses	15
3.1.1 Direct Method	16
3.1.2 Cyclic Symmetry Method	19
3.2 Derivation of Disc Receptances	20
3.3 Derivation of Packet Receptances	23
3.3.1 Finite Element Method	23
3.3.2 Receptance Coupling	25
<b>4 NUMERICAL STUDY</b>	<b>28</b>
4.1 General	28
4.2 Continuously-Shrouded Disc	29
4.3 Ten Packets with Three Blades Each	30
4.3.1 Analysis via Direct Method	32
4.3.2 Analysis via Cyclic <b>Symmetry</b> Method	33
4.3.3 Further Considerations	34
4.4 Additional Calculations	38
4.5 A Rationale for <b>Packeted</b> Bladed Disc Analysis	40
<b>5 EXPERIMENTAL PROGRAMME, PROCEDURE AND RESULTS</b>	<b>50</b>
5.1 Objective	50
5.2 General Procedure	50
5.2.1 Testpiece	50

5.2.2	Description of the Apparatus and Experimental Procedure	51
5.3	Results	52
5.4	Discussion of Results	52
5.5	Concluding Remarks	54
6	<b>LUMPED PARAMETER ANALYSIS OF PACKETED BLADED DISCS</b>	62
6.1	Lumped <b>Parameter Model</b>	62
6.2	<b>Numerical Study</b>	63
6.2.1	Derivation of the Model <b>Parameters</b>	63
6.2.2	Case Studies	65
6.3	Forced <b>Response</b> Calculations	66
6.3.1	Basic Theory	66
6.3.2	Case Study	67
6.4	Concluding Remarks	68
7	<b>CONCLUSIONS</b>	73
7.1	<b>Summary</b> of Conclusions of Preceding Chapters	73
7.2	Limitations and Extension of the Present Work	77

## Part II

### AEROELASTIC ANALYSIS

8	<b>INTRODUCTION</b>	79
8.1	The Nature of the Problem	79
8.1.1	Aeroelastic Phenomena	79
8.1.2	Types of Flutter	80
8.2	Survey of Previous Work	82
8.2.1	Aeroelastic Studies	82
8.2.2	Aerodynamic Studies	85
8.3	Objectives and <b>Scopes of the Present Analysis</b>	87
9	<b>DERIVATION OF THE AEROELASTIC MODEL</b>	90
9.1	<b>Structural Model</b>	90
9.2	<b>Aerodynamic Model</b>	92
9.2.1	Fundamentals of the Two-Dimensional Cascade <b>Theory</b>	93
9.2.2	Force and Moment Coefficients	96
9.3	Aeroelastic <b>Model</b>	98
9.3.1	Derivation of the Overall Equations of Motion	98
9.3.2	Forced Aeroelastic Response	101
10	<b>NUMERICAL STUDY</b>	106
10.1	Details of the Computer Program	106
10.2	<b>Force and Moment</b> Coefficients	109
10.2.1	Direct Use of the Coefficients for Flutter Predictions	109
10.2.2	Further Considerations	110

10.3	Case Study: Twelve-Bladed <b>Disc</b>	113
10.3.1	Tuned System	115
10.3.2	Effects of Mistuning	119
10.3.3	The Special Case of Alternate Mistuning	124
10.4	Aeroelastic <b>Response</b> to <b>Forced</b> Vibration	126
10.5	Concluding Remarks	130
11	<b>FLUTTER ANALYSIS OF A CANTILEVERED PLATE</b>	146
11.1	Introduction	1 %
11.2	Structural <b>Model</b>	146
11.3	<b>Aerodynamic Model</b>	147
11.3.1	Pressure Distribution	147
11.3.2	Pinite <b>Element</b> Discretization	148
11.4	Aeroelastic <b>Model</b>	150
11.5	Numerical Study	151
11.5.1	Preliminary Calculations	151
11.5.2	Case Study	<b>155</b>
11.6	Concluding <b>Remarks</b>	157
12	<b>CONCLUSIONS</b>	165
12.1	<b>Summary</b> of Conclusions of Preceding Pour Chapters	165
12.2	Limitations and Extension of the Present Work	167
	<b>APPENDICES</b>	169
I	<i>List of Computer Programs Developed in this Study</i>	170
II	<i>Tabulated Results from Chapters 4, 5 and 6</i>	171
III	<i>Aeroetasttc Equations of Motion for the Lumped Parameter Model</i>	182
IV	<i>Derivation of the Mass, Sttffness and Aeroetasttc Matrices</i>	184
	<b>REFERENCES</b>	194

PREFACE

This thesis is the final report of the work carried out by the author at Imperial College between October 1980 and September 1983. and acknowledgement is made to Professor D. J. Ewins. the project supervisor. for his continual encouragement and guidance throughout this period.

The author is indebted to present and past members of the Imperial College Dynamics Group for many useful discussions and exchange of ideas. Special thanks are due to Dr. B. Hillary, Mr. J. Griffin, Mr. J. Sidhu, Mr. J. Antonio, Dr. D. Afolabi, Dr. J. Kirshenboim and Mr. R. Gunn. the laboratory technician, without whose help the experimental programme could be in jeopardy. The author also wishes to thank Miss Ft. Moore for her careful and persevering typing of a difficult manuscript.

It is the author's strong belief that the main purpose of undertaking a doctoral study lies in assimilating the method of attack to a general problem rather than presenting a series of results and conclusions on a specific topic. This philosophy, wherever possible, has been incorporated into the preparation of the thesis: instead of concentrating on results from one single model, emphasis has been given to illustrate several possible approaches to analyse the behaviour of a same system. the results in' themselves being of secondary importance.



LIST OF FIGURES

Figure	Title	Page
2. 1	12 DOP beam element	14
2. 2	Three-bladed packet	14
3. 1	Typical blade packet	26
3. 2	Loads and responses at disc rim and $j^{\text{th}}$ blade root	26
3. 3	Disc sector - Blade packet coupling	27
3. 4	Coupling sequence for packet receptance matrix computation	27
4. 1	Three-bladed packet	42
4. 2	Natural frequencies of the continuously-shrouded disc	42
4. 3	Schematic representation of the shrouding arrangement	42
4. 4	Variation of the characteristic determinant with frequency	44
4. 5	Natural frequencies of the 30-bladed disc via direct method	43
4. 6	Natural frequencies of the 30-bladed disc via cyclic symmetry method	43
4. 7	Receptance curves of the blade packet	44
4. 8	Natural frequencies of the 30-bladed disc	45
4. 9	Packeted bladed disc mode shapes	45
4.10	Various packeting arrangements together with their Fourier series representation	46
4.11	Natural frequencies of the 30-bladed disc for further packeting arrangements	48
4.12	Modal interference diagrams	49
5. 1	Test structure	56
5. 2	Experimental apparatus	57
5. 3	Comparison of theoretical and experimental results	58
5. 4	Predicted and measured mode shapes together with their DPT	59
5. 5	Correlation between predicted and measured natural frequencies	60
5. 6	Radial stresses in the blade packet	59
5. 7	Measured response curves in the neighbourhood of single packet cantilever frequencies	60
6. 1	Lumped parameter model of a three-bladed packet	70
6. 2	2 DOP cantilevered blade model	72
6. 3	Natural frequencies of the 30-bladed disc	71
6. 4	Response of the continuously-shrouded and packeted assemblies to 5EO excitation	72

8. 1	Variation of system's stability in time	89
8. 2	Types of fan/compressor flutter	89
9. 1	Lumped parameter model	104
9. 2	Aerofoil details	105
9. 3	<b>Geometry of tuned cascade</b>	105
10. 1	<b>Test case: 25-bladed cascade</b>	131
10. 2	Stability plots for various flow regimes	132
10. 3	Variation of the Fourier components with g/c	131
10. 4	Variation of the $C_{M\alpha}$ coefficient for small changes in $\lambda$ and $M$	134
10. 5	Pressure distribution due to torsional motion	135
10. 6	Natural frequencies of the unloaded system	134
10. 7	Modal properties of the 12-bladed system under aerodynamic load	136
10. 8	Convergence of the damped natural frequency	137
10. 9	Effect of structural damping	137
10.10	Correlation between the computed eigenvalue and the $C_{M\alpha}$ coefficient	138
10.11	Stability diagrams for various types of mistuning	139
10.12	DFT components of the eigenvectors associated with modes 0, and 2	142
10.13	Variation of modal damping with increasing mistuning (Disc A)	143
10.14	Variation of global damping with increasing mistuning	144
10.15	Variation of modal damping with increasing mistuning (Disc B)	144
10.16	Effect of modal damping on forced response levels	144
10.17	<b>Forced response of the tuned and mistuned systems</b>	145
11. 1	Finite element model of a cantilevered plate	158
11. 2	Pressure distribution along the chord	158
11. 3	The first 10 modes of the cantilevered plate for vacuum conditions	159
11. 4	Pressure distribution functions $P_h$ and $P_\alpha$	160
11. 5	Aeroelastic coefficients resulting from the pressure distribution given in Fig. 11. 4	161
11. 6	The first 10 modes of the cantilevered plate under aerodynamic load	162
11. 7	Amplitudes resulting from the difference of the loaded and unloaded modes shapes	163
11. 8	Mode shapes of the cantilevered plate with and without aerodynamic loading	164
<b>IV-1</b>	<b>Rectangular plate element of uniform thickness</b>	<b>184</b>
<b>IV-2a</b>	<b>Element stiffness matrix</b>	<b>191</b>
<b>IV-2b</b>	<b>Element mass matrix</b>	<b>191</b>

**LIST OF TABLES**

Table	Title	Page
2. 1	Packet data	11
2. 2	Variation of cantilevered packet natural frequencies with number of blades in the packet	12
4. 1	Disc details	28
6. 1	Model parameters for the 30-bladed disc	65
10. 1	Variation of $C_{M\alpha}$ for small changes in $\lambda$ and $M$	112
10. 2	Aeroelastic system data	114
10. 3	Convergence of the damped natural frequency	116
10. 4	Mistuning data	122
10. 5	Variation of $C_{M\alpha}$ with frequency	125
11. 1	Plate data	152
11. 2	Convergence of the non-dimensional frequency with mesh size	153
11. 3	Convergence of $\omega = \Omega + i\eta$ with mesh size	154
11. 4	Natural frequency and aerodynamic damping values for the first 10 modes	155
II- 1	Continuous uniform shroud (BLISC)	171
II- 2	Non-interlocking shroud (BLISC)	172
II- 3	10 packets of 3 blades (Direct method)	172
II- 4	10 packets of 3 blades (Direct method)	173
II- 5	10 packets of 3 blades (Cyclic symmetry method)	173
II- 6	15 packets of 2 blades (Direct method)	174
II- 7	6 packets of 5 blades (Direct method)	174
II- 8	6 packets of 5 blades (Cyclic symmetry method)	175
II- 9	5 packets of 6 blades (Direct method)	175
II-10	3 packets of 10 blades (Direct method)	176
II-11	Continuous uniform shroud (Lumped parameter model)	176
II-12	Non-interlocking shroud (Lumped parameter model)	177
II-13	10 packets of 3 blades (Lumped parameter model)	177
II-14	10 packets of 3 blades (Experimental results)	178
II-15	Comparison of predicted and measured mode shapes	181

NOMENCLATURE

*Part I*

$a_1$ to $a_{12}$	Constants in the beam shape functions
A	Cross-sectional area
D	<b>Flexural</b> rigidity
E	Young's modulus
f	Force at blade root
F	Force at disc rim
{F}	<b>External</b> force vector
g	Grounding stiffness
G	Torsional rigidity
h	<b>Sectorial</b> disc stiffness Disc thickness
$I_y, I_z$	Area moments of inertia
J	Polar moment
k	Stiffness between tip mass and clapper mass
K	Stiffness between clapper mass and disc sector
[K]	Stiffness matrix
l	Beam length
m	Blade mass between tip and clapper point Moment at blade root
M	Maximum possible number of nodal diameters Moment on disc rim Blade mass between root and clapper point
[M]	Massmatrix
n	Nodal diameter number Rotational speed
$n_b$	Number of elements along the blade
$n_s$	Number of elements along the shroud segment
N	Total number of blades
p	<b>Number</b> of blades in the packet
P	Total number of packets
{Q}	Load vector
{q}	Response <i>or</i> deflection vector

<b>r</b>	Engine order of excitation
<b>R</b>	Number of modes in the <b>modal summation</b>
<b>s</b>	<b>Upper</b> shroud stiffness
<b>S</b>	Lower shroud stiffness
<b>t</b>	Time
<b>T</b>	Kinetic energy
<b>U</b>	Deflection in the X direction
<b>U</b>	Potential energy
<b>V</b>	Deflection in the Y direction
<b>W</b>	Deflection in the Z direction
<b>W</b>	Mass of disc sector
<b>z</b>	Axial co-ordinate for blade
<b>Z</b>	Axial co-ordinate for disc
<b>[α]</b>	Disc receptance matrix (full)
<b>[β]</b>	Blade receptance matrix
<b>[γ<sub>n</sub>]</b>	Disc receptance matrix (reduced)
<b>[δ]</b>	Packet receptance matrix
<b>2ε</b>	Angle subtended at disc centre by blade <b>root</b>
<b>θ</b>	Rotation about the Z axis
<b>θ<sub>y</sub></b>	Rotational co-ordinate for blade
<b>θ<sub>z</sub></b>	Rotational co-ordinate for disc
<b>λ</b>	Eigenvalue
<b>[Δ]</b>	Defined in equation (6-11)
<b>ν</b>	Poisson's ratio
<b>ρ</b>	Material density
<b>φ</b>	Rotation about the X axis
<b>[Φ]</b>	Eigenvector matrix
<b>ψ</b>	Rotation about the Y axis
<b>ω</b>	Frequency

Superscripts

<b>G</b>	Global
<b>R</b>	Reduced
<b>S</b>	<b>Shroud</b>
<b>T</b>	Transpose

' Slope-force or Displacement-moment  
" ~~Slope-moment~~

Subscripts

**B** Blade  
**D** Disc  
**e** Element  
**i** Position index  
**j** Position index  
**n** Nodal diameter  
**r** Mode counter  
**R** Root

*Part II*

**a** Element length  
**[a<sub>r</sub>]** Aerodynamic matrix due to motion in r<sup>th</sup> mode  
**[A]** Global aerodynamic (or aeroelastic) matrix  
**b** Semi-chord length  
Element width  
**c** Chord length  
Blade torsional stiffness  
**[C]** Defined in equation (9-16)  
**C<sub>Fh</sub>, C<sub>Fα</sub>, C<sub>Fw</sub>** Aerodynamic force coefficients  
**C<sub>Mh</sub>, C<sub>Mα</sub>, C<sub>Mw</sub>** Aerodynamic moment coefficients  
**C<sub>hhr</sub>, C<sub>hαr</sub>** Aeroelastic coefficients for axial force  
**C<sub>αhr</sub>, C<sub>ααr</sub>** Aeroelastic coefficients for radial moment  
**C<sub>θhr</sub>, C<sub>θαr</sub>** Aeroelastic coefficients for tangential moment  
**d** Offset distance  
**D** Plexural rigidity  
**e** Co-ordinate along blade chord  
**CBI** Defined in equation (9-11)  
**f** Pressure distribution function

$F_j$	Aerodynamic force acting on $j^{\text{th}}$ blade
$F_r$	Axial force at node $r$
$\{F_w\}$	Force due to wakes
$g$	Grounding stiffness
$h$	Translational co-ordinate
$\dot{h}$	Translational velocity
$h_{ar}$	Bending deflection in $r^{\text{th}}$ mode of tuned system
$[H]$	Damping matrix
$i$	Square root of $-1$
$I$	Mass moment of inertia
$[I]$	Unit matrix
$j$	Blade index
$k$	Blade stiffness in translation
$K$	Interdisc stiffness
$[K]$	Stiffness matrix
$K(x)$	Kernel function
$L$	Blade length
$l_{hxr}, l_{h\alpha r}, l_{hw r}$	Non-dimensional aerodynamic force coefficients
$l_{mxr}, l_{m\alpha r}, l_{mw r}$	Non-dimensional aerodynamic moment coefficients
$m$	Blademass
$M$	Disc mass
$[M]$	Massmatrix
$M_{\alpha r}$	Radial moment at node $r$
$M_{\theta r}$	Tangential moment at node $r$
$n$	Rotational speed
$N$	Number of blades
$P$	Non-dimensional forcing frequency parameter
$[P]$	Stability matrix
$P_h, P_\alpha$	Pressure distribution functions
$\{q\}$	Deflection vector
$\{q_{ar}\}$	Deflection vector of tuned cascade in $r^{\text{th}}$ mode
$\{Q\}$	Response or load vector
$r$	Modal index
$r_1, r_2, r_3$	Pressure distribution coefficients for bending
$R$	Order of excitation
$s$	Interblade phase angle index
$s_1, s_2, s_3$	Pressure distribution coefficients for torsion

$S_h$	Shroud stiffness in translation
$S_\alpha$	Shroud stiffness in rotation
$t$	<b>Time</b>
$T_j$	<b>Aerodynamic moment acting on <math>j^{\text{th}}</math> blade</b>
$v_i$	Induced velocity
$v_u$	<b>Upwash velocity</b>
$V$	Relative flow velocity in the chord direction
$w$	Velocity of disturbance due to wakes
$y$	Disc co-ordinate
$Y_{ar}$	Disc deflection in $r^{\text{th}}$ mode of tuned system
$a$	Rotational co-ordinate
$a_{ar}$	Torsional deflection in $r^{\text{th}}$ mode of tuned system
$\beta_r$	Interblade phase angle associated with $r^{\text{th}}$ mode
$\gamma$	Fluid density
$\eta$	Aerodynamic damping
$\eta_h, \eta_\alpha$	Structural damping for bending and torsion
$A$	Reduced frequency
$\mu$	Non-dimensional mass parameter
$\nu$	Poisson's ratio
$\rho$	Material density
$\sigma$	Global amount of aerodynamic damping
$\omega$	Complex frequency
$\omega_0$	Reference frequency

Superscripts

*	<b>Non-dimensionalized</b>
	Complex conjugate
T	Transpose

Subscripts

e	Element
h	Bending
i, j	Position indexes
r	<b>Modal index</b>



	Element node counter
	Iteration index
W	wakes
a	Torsional
o	vacuum

- 1 -

*Part I*

**STRUCTURAL ANALYSIS**

## CHAPTER 1

### INTRODUCTION

#### 1.1 THE NATURE OF THE PROBLEM

Vibration induced fatigue has always been one of the chief hazards to turbomachinery blading and hence the theoretical prediction of natural frequencies, mode shapes and forced response levels is of vital importance for designing away from ranges where the stresses are likely to be high. As suggested by Smith in Ref. SD-I, it is convenient to distinguish between globally- and locally-occurring vibration problems. The first type involves the motion of the whole structure while the second is restricted to a few internal components such as discs, blades and shroud attachments. Failures due to problems of the first kind are usually related to bearings and/or shafts and their study is outside the scope of this work which will focus on bladed disc vibration.

The blades, especially in steam turbines and to a lesser extent in gas turbines, are often grouped together at some point along their span via a metal band or wiring lace referred to as shroud which can be continuous (continuously-shrouded disc) or segmented (packeted bladed disc). Although both structures may appear very similar, the broken cyclic symmetry of the latter gives rise to a much more complex vibration problem than the one presented by the former. Both analyses are

further compounded by the complexity of the blade geometry and thermal and centrifugal effects which customarily are not included in the theoretical model.

## 1.2 LITERATURE SURVEY

Although bladed disc vibration problems have been the subject of numerous investigations, most of the published work deals with the continuously-shrouded or unshrouded assemblies and the case where the blades are grouped into packets is somewhat neglected. Nevertheless, as early as 1927 (even earlier, including publications in German), Stodola [Ref. SD-21] pioneered the theoretical study by estimating the fundamental frequency of a blade packet. His analysis was based on Lagrange's energy equation and on account of the complexity of the calculations, no estimates were given for higher modes. Sezewa [Ref. SD-31] studied the transverse vibrations of an infinite number of beams grouped together and found that the deviation of the packet cantilever frequencies from the single blade frequencies was governed by the ratio of blade to shroud cross-sectional area. Smith [Ref. SD-41] considered the in-plane or tangential vibrations and derived a frequency equation for a general number ( $N$ ) of blades in the form of a determinant of order  $(N + 1)$ . He studied six- and twenty-bladed packets and showed the existence of a qualitative behaviour which could be related to the number of blades in the packet. His work was extended by Prohl [Ref. SD-51] and Weaver and Prohl [Ref. SD-61] to include out-of-plane or axial vibrations. An analytical method of calculation, subject to the usual limitations of elementary beam theory, was presented and used to compute axial, tangential and torsional natural frequencies of various

packets together with the associated mode shapes and stress levels.

Using a finite difference technique, Eliington and McCallion [Ref. SD-71] derived the frequency equations for the symmetric and asymmetric modes of vibration of a packet of laced turbine blades. Their work was based on Ref. SD-4 and made extensive use of the *Vibration Analysis Tables* later published as Ref. SD-8. It was found that the blades could be considered as clamped-clamped or clamped-hinged, depending on the shroud to blade stiffness ratio. Rieger and McCallion [Ref. SD-91] investigated the oscillations of a single-storey, single-bay portal frame comprised of uniform prismatic beams. Although their analysis was not developed specifically with turbine blades in mind, the generality of the model used allows their results and conclusions to be directly applicable into this area. Based on an exact solution of the Bernoulli-Euler differential equation for transverse motion, a series of non-dimensional tables were presented to help the evaluation of in-plane natural frequencies by simple interpolation.

Advances in computational methods led to the formulation of finite element models and such a technique has been used by Thomas and Belek [Ref. FE-11] to investigate the in-plane vibrations of an isolated blade packet, represented once again using uniform beams. The effects of various weight, flexural rigidity and length ratios between blades and shroud segments were systematically studied and it was found that the vibration characteristics of a multibladed packet could be predicted, with reasonable accuracy, from the behaviour of the corresponding two-bladed packet. A similar study was also undertaken by Salama, Petyt and Soares [Ref. FE-21] who incorporated the effects of a rigid disc with finite

radius. Their analysis was restricted to in-plane vibrations but it included the dynamic response to periodic loading which was considered with reference to a six-bladed packet. They also investigated the variation of the packet's natural frequencies with blade number and obtained similar results to the ones reported by Sezewa in Ref. SD-3.

Recent studies, based on substructuring techniques, considered both in-plane and out-of-plane motions of packeted bladed discs. Afolabi [Ref. SD-101] used Timoshenko beam theory to predict the dynamic response of a single packet of cantilevered blades. His work was further developed by Dimitriadis [Ref. SD-111] who modelled the whole bladed assembly by including a disc of finite radius and rigidity. The process in his method involved numerous matrix inversions, thus making it very inefficient in terms of computation time. Stathyanopoulos [Ref. SD-121] used a lumped-parameter model, similar to the one originally proposed by Dye and Henry in Ref. SD-13, to investigate the similarities between the vibrational behaviour of the two types of assembly; the packeted bladed and continuously-shrouded discs. Some of the work described above is summarized in Ref. SD-14 in an attempt to rationalise packeted bladed disc behaviour and to relate it to the one of two much simpler assemblies, namely the continuously-shrouded disc and a single packet of cantilevered blades.

Singh and Schiffer [Ref. SD-151] used a three-dimensional finite element model to predict the natural frequencies and the associated mode shapes of a 90-bladed disc arranged in 15 packets of 6 blades each. Their analysis was complemented by the use of a mass-spring model and it was concluded that this simplified representation was accurately

descriptive of bladed disc assemblies.

### 1.3 OBJECTIVES AND SCOPES OF THE PRESENT ANALYSIS

Although the vibration of blade packets has been studied by several authors, there are still a number of questions which can be raised with respect to packeted bladed assemblies.

- (i) What are the additional effects of packeting on the assembly's natural frequencies and mode shapes over the continuously-shrouded case?
- (ii) In the case of a **symmetrical** packeting arrangement, can these be predicted qualitatively without having to undertake a lengthy and perhaps superfluous analysis ? and/or
- (iii) Can these always be estimated quantitatively from knowledge of the two much simpler assemblies, namely the continuously-shrouded disc and a packet of cantilevered blades?
- (iv) The inherent circular **symmetry** being destroyed, how is the response in any one mode to periodic loading will be affected?

The existing analytical models being either incomplete or too expensive to use, there is an obvious need for the formulation of more advanced ones. In order to address the problems above and the present study aims to undertake a thorough analysis of packeted bladed disc vibration from both theoretical and experimental aspects. As customarily done, the blades and the shroud arcs will be modelled by uniform beams of rectangular cross-section and the disc as a circular plate of constant thickness. A further objective of this study lies in showing that the incorporation of more complex blade geometries into this simplified model is possible and

this feature will be discussed on a case study.

The packeted bladed disc assembly will be considered to be undamped. an assumption which can be justified in view of the light damping present in the system. The reasons for this approach are threefold: Firstly, it is difficult to estimate the damping amount for each mode; secondly, the damped and undamped solutions are known to be very close for lightly damped systems; and thirdly, the inclusion of damping necessitates the use of complex algebra, thus doubling the computational effort.

A number of theoretical models based on

- (i) finite elements,
- (ii) substructuring via receptance coupling and/or finite elements,
- (iii) lumped parameter techniques

will be used to predict the vibration properties of a 30-bladed disc which is considered as the datum case throughout this study. Also, a series of experiments will be carried out to check the validity of the theoretical analyses. Although it is expected that all models above will yield similar qualitative predictions, other important aspects of packeted bladed disc vibration - such as the accuracy of quantitative predictions and the relative computational effort - will be investigated in detail.



## CHAPTER 2

### FINITE ELEMENT ANALYSIS OF CANTILEVERED BLADE PACKETS

Before undertaking a complete packeted bladed disc analysis. It was decided to investigate the behaviour of a single packet of cantilevered blades. The present study is an extension of the work reported in Ref. FE-1 to all six co-ordinate directions with inclusion of finite disc radius and rigidity. The objectives of this Introductory analysis are twofold:

- (i) to establish the vibration properties of blade packets in order to draw parallels with those of the complete assembly;
- (ii) to look for permissible simplifications in order to facilitate the construction of a full bladed disc model.

#### 2.1 FINITE ELEMENT MODEL

The blade packet is idealized using 12 degree-of-freedom uniform one-dimensional beam elements of rectangular cross-section. A typical element, together with the global and local co-ordinate systems used, is shown in Fig. 2. 1. All three translational deflections within the element are approximated to cubic polynomials of the form:

$$\begin{aligned}u(x) &= a_1 + a_2(x/l) + a_3(x/l)^2 + a_4(x/l)^3 \\v(x) &= a_5 + a_6(x/l) + a_7(x/l)^2 + a_8(x/l)^3 \\w(x) &= a_9 + a_{10}(x/l) + a_{11}(x/l)^2 + a_{12}(x/l)^3\end{aligned}\tag{2.1}$$

and the rotational deflections are:

$$\phi = du/dx ; \quad \psi = dv/dx ; \quad \theta = dw/dx \quad (2.2)$$

The element mass and stiffness matrices can be derived by equating different expressions for the kinetic and potential energies stored in a typical element: that is to say:

$$\begin{aligned} T &= 1/2 \rho A \int_0^l [(\partial u/\partial t)^2 + (\partial v/\partial t)^2 + (\partial w/\partial t)^2] dx + 1/2 \rho J \int_0^l (\partial \phi/\partial t)^2 dx \\ &= 1/2 \{q\}_e^T [M]_e \{q\}_e \end{aligned} \quad (2.3)$$

$$\begin{aligned} U &= 1/2 EI_y \int_0^l (\partial^2 w/\partial x^2)^2 dx + 1/2 EI_z \int_0^l (\partial^2 v/\partial x^2)^2 dx \\ &\quad + 1/2 EA \int_0^l (\partial u/\partial x)^2 dx + 1/2 GJ \int_0^l (\partial \phi/\partial x)^2 dx \\ &= 1/2 \{q\}_e^T [K]_e \{q\}_e \end{aligned} \quad (2.4)$$

A list of all symbols used is given in the nomenclature and explicit formulations of the mass and stiffness matrices above can be found in the published literature [See Ref. FE-3]. It should be noted that these were first computed in local coordinates and then expressed in global ones via the appropriate transformation matrix. The overall mass and stiffness matrices, denoted by [M] and [K], were assembled using the

stiffness method described in Ref. FE-4 and they have a banded configuration, the width of which depends on the number of blades per packet. The overall equation of motion is:

$$[K]\{q\} = \omega_r^2 [M]\{q\} \quad (2.5)$$

the solution of which yields the natural frequencies  $\omega_r$  and the associated mode shapes  $\{q\}$  of the blade packet.

Fig. 2.2 shows a typical packet geometry with three blades. In the present formulation, the blade stagger can be accounted for and Bernoulli-Euler or Timoshenko beam theories can be used at will.

## 2.2 NUMERICAL STUDY

A computer program, namely FINPAC, was written to analyse the vibrational behaviour of free-free or cantilevered blade packets. A set of preliminary calculations were made to investigate the convergence of the eigensolution for various mesh sizes. It was found that 3 elements per blade and also per shroud segment were sufficient to compute the first 30 natural frequencies within a relative error bound of 1% and the accuracy obtained was considered to be adequate for the purpose of this study. In any case, the overall equation of motion for a cantilevered packet is of order:

$$6 [p n_b + (p-1)(n_s-1)] \quad (2.6)$$

where  $p$  is the number of blades, and  $n_b$  and  $n_s$  the numbers of finite elements along the blade and shroud segment respectively. This yields a medium size eigenproblem which can be solved using standard routines and subroutine FO2AEF from the Numerical Algorithms Group (NAG) library was used throughout this study. Also, a few test runs were made to check the results against those given in Refs. FE-I, SD-8 and SD-10 and very good agreement was obtained in all cases considered.

The substantial body of numerical work reported in the first part of this thesis will be carried out for the data listed below in Table 2. 1.

No of blades	= 1,2,3,4,5 and 6	Blade length (Rad)	= 200.7 mm
Young's modulus	= 207 GN/m <sup>2</sup>	Blade thickness (Ax)	= 12.7 mm
Density	= 7850 Kg/m <sup>3</sup>	Blade width (Tang)	= 17.3 mm
Blade stagger	= 0°	Shroud thickness (Rad)	= 3.1 mm
Disc radius	= 262.6 mm	Shroud width (Ax)	= 12.7 mm

Table 2.1 Packet data

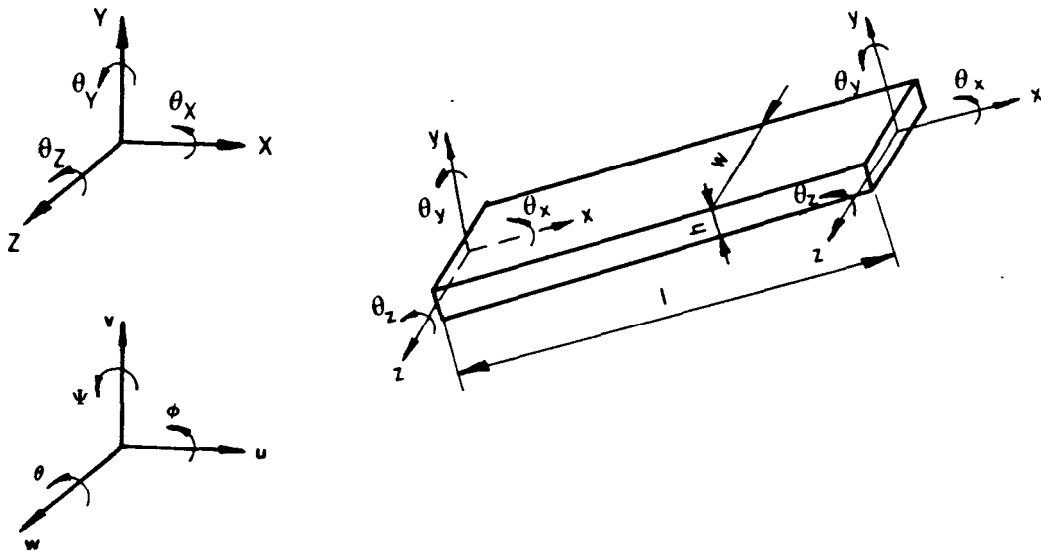
It should be noted that the one-bladed packet is nothing but a single blade cantilevered at its root and that Timoshenko beams were used throughout the analysis. The results obtained are listed in Table 2.2.

Family	p=1	p=2	p=3	p=4	p=5	p=6
<b>1A</b>	261.18	241.19 504.21	235.34 365.44 707.92	232.76 308.95 518.62 808.04	231.21 280.83 417.80 639.04 857.89	230.48 290.58 375.04 526.43 876.32
<b>1T</b>	355.20	331.25 1494.11	324.43 1490.03 1490.70	321.22 1470.67 1487.33 1496.97	319.35 1438.52 1485.34 1493.98 1497.81	325.87 1403.76 1480.34 1482.56 1491.86 1492.52
<b>2A</b>	1618.95	1504.78 1628.08	1468.23 1549.48 1683.70	1454.78 1502.28 1586.36 1728.97	1454.19 1477.43 1534.60 1619.48 1766.04	1451.55 1489.32 1535.88 1571.21 1649.94 1818.31
<b>2T</b>	2181.24	<b>1798.31</b> 2050.23	1758.64 1809.96 2017.31	1780.03 1798.37 1814.51 2002.58	1777.26 1790.66 1805.69 1816.69 1994.26	1761.65 1766.02 1798.30 1808.26 1814.32 2038.49
<b>3A</b>	3506.94	3397.82 4380.69	3335.34 3920.34 4373.06	3305.90 3760.86 4024.97 4363.18	3288.75 3629.16 3953.30 4045.29 4356.75	3287.05 3575.05 3869.36 4008.06 4053.66 4344.77

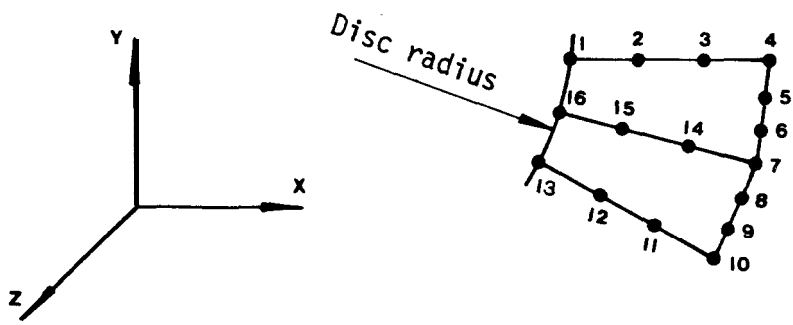
Table 2.2      **Variation of cantilevered packet natural frequencies (Hz) with number of blades in the packet (p)**  
**A: Axial or out-of-plane**  
**T: Tangential or in-plane**

### 2.3 CONCLUDING REMARKS

- (i) The blades being unstaggered, the in-plane (tangential) and out-of-plane (axial) vibrations are uncoupled. This has been done for the sake of clarity and also to provide a datum case for the following chapters.
- (ii) For each single-blade cantilever frequency, the grounded packet exhibits a number of natural frequencies equal to the number of blades in the packet, thus covering all possible mode shapes. As will be shown in Chapter 4, this feature has significant effects on the packeted bladed disc behaviour.
- (iii) As can be seen from Table 2.2, the tangential or in-plane vibration characteristics of a multi-bladed packet follow a certain pattern which can be predicted with reasonable accuracy from the behaviour of the corresponding 2-bladed packet. This matter is discussed in detail in Ref. FE-I.
- (iv) The axial or out-of-plane vibrations however, do not show a similar trend. The natural frequencies being spread over a much wider range, the multi-bladed disc behaviour cannot be predicted by simple interpolation. This can be explained by the fact that the shroud has a much more pronounced effect axially and, also, that bending and torsion are closely coupled in this direction. Unfortunately, most of the published literature is restricted to tangential vibration analysis, axial vibrations being somehow neglected.
- (v) Finally, it should be noted that the axial vibrations are much more likely to be affected by the disc flexibility than are the tangential ones since the disc is relatively stiff in this latter direction. Thus the rigid disc assumption can only be applied to in-plane vibrations and the model used here has to be improved for the out-of-plane analysis. This problem will be addressed in Chapters 3 and 4.



**Fig. 2. 1 12 DOF beam element**



**Fig. 2.2 Three-bladed packet ( 3 elements per blade and also per shroud segment)**

### CHAPTER 3

#### RECEPTANCE COUPLING ANALYSIS OF PACKETED BLADED DISCS

##### 3.1 THEORETICAL ANALYSES

The problem of studying assemblies which have a complex geometry can be greatly simplified by subdividing the structure into components which are directly amenable to mathematical analysis. The characteristics of the initial structure can then be determined by synthesis of these individual components and the process is referred to as substructure analysis.

In the case of a packeted bladed disc, the two main components are the disc and a single packet of blades - sometimes called *superblade* - which, in turn, can be subdivided into individual blades and shroud segments. The coupling process will ultimately take place at specific points on the disc rim where the blades are mounted. The complete analysis of the motion at these points would require the consideration of all possible six co-ordinates, thus limiting the analysis to a small number of blades for obvious reasons of memory storage and computation time. Fortunately, as concluded in Ref. SD-17, not all six co-ordinates are strictly necessary, only axial translation and tangential rotation being of primary importance to bladed disc vibration since the disc is much more flexible in these two degrees of freedom. The remaining four co-ordinates will be considered to be grounded at the blade roots throughout the analysis. Although the effect of the root flexibility can be



modelled by using translational and torsional springs in the appropriate co-ordinate directions. it will be excluded from the present formulation. chiefly because of the computational effort required to conduct a parametric study.

In common with many other studies [Refs. SD-10, SD-11, SD-16, SD-17, SD-18, SD-19, SD-20, SD-21], blades and shroud arcs will be represented as prismatic beams of rectangular cross-section and the disc as a uniform circular plate of constant thickness. Receptance expressions for such idealised components are already available in analytical form and can be found in Refs. SD-8 and SD-21. A typical three-bladed packet together with the co-ordinate system used is shown in Fig. 3. 1.

Two methods of analysis will be presented below. one which considers the assembly as a whole and the other which takes advantage of its cyclic symmetry. Both techniques assume that the receptance matrix  $[\delta]$  of a typical packet has already been computed either by receptance coupling of blades and shroud segments or by modal summation of a finite element eigensolution. In the interests of continuity, the governing equations of motion will be derived first and the explicit formulation of the component receptance matrices will follow later.

### 3. 1. 1 Direct Method

The so-called direct method is a full analysis in the sense that the bladed disc is considered as a whole without depending on or using the cyclic symmetry of the system. It is an extension of Ewins' unshrouded

disc work [Ref. SD-161 to packeted bladed discs. The coupling process takes place at the N points around the disc rim where the blades are mounted and, as two coupling co-ordinates per blade are used. the system is of order 2N.

Fig. 3.2 shows the co-ordinates used together with the forces and moments acting on the blade roots and the disc rim.  $(z_j, \theta_{yj})$  and  $(Z_j, \Theta_{Yj})$  denote the displacement and slope at the root of the  $j^{\text{th}}$  blade and at the corresponding point on the disc rim while  $(f_j, m_j)$  and  $(F_j, M_j)$  are the force and moment acting at these locations in the same order.  $[\alpha]$  and  $[\beta]$  are the disc and packet receptance matrices whose explicit forms will be given later.

The response/load relationship for a disc with N blades is:

$$\{q\}_D = [\alpha] \{Q\}_D \quad (3-1)$$

where  $\{q\}_D$  and  $\{Q\}_D$  are the response and load vectors at the disc rim whose explicit forms are given by:

$$\{q\}_D^T = \{z_1, \dots, z_j, \dots, \theta_{y1}, \dots, \theta_{yj}, \dots\}_{1 \times 2N} \quad (3-2)$$

$$\{Q\}_D^T = \{F_1, \dots, F_j, \dots, M_1, \dots, M_j, \dots\}_{1 \times 2N}$$

Similarly, the response/load relationship for the N blades is:

$$\{q\}_B = [\beta] \{Q\}_B \quad (3-3)$$

where  $\{q\}_B$  and  $\{Q\}_B$  are the response and load vectors at the blade roots whose explicit forms are given by:

$$\{q\}_B^T = \{z_1, \dots, z_j, \dots, \theta_{y1}, \dots, \theta_{yj}, \dots\}_{1 \times 2N} \quad (3-4)$$

$$\{Q\}_B^T = \{f_1, \dots, f_j, \dots, m_1, \dots, m_j, \dots\}_{1 \times 2N}$$

The equations of motion are derived by considering the dynamic equilibrium of all loads applied and the compatibility of responses obtained, that is to say:

$$\text{Equilibrium: } \{Q\}_D + \{Q\}_B = \{0\} \quad (3-5)$$

$$\text{Compatibility: } \{q\}_D = \{q\}_B$$

Combining equations (3-1), (3-3) and (3-5) we obtain:

$$[[\alpha] + [\beta]] \{Q\}_D = - [[\alpha] + [\beta]] \{Q\}_B = \{0\} \quad (3-6)$$

The necessary and sufficient condition for a non-trivial solution of the above system of 2N simultaneous linear equations is:

$$\det |[\alpha] + [\beta]| = 0 \quad (3-7)$$

The roots of equation (3-7) are the natural frequencies of the bladed disc system and several well-established numerical techniques, some of which will be discussed later, are available for the solution of this determinantal equation. Once a natural frequency has been located, the corresponding load vector (i.e. the modal shape by linearity) can be found by setting any one of its elements to unity and solving (2N-1) linear simultaneous equations for the remaining (2N-1) elements. if required, the response vector can be recovered from equations (3-1) or (3-3).

### 3.1.2 Cyclic Symmetry Method

In 1955 Armstrong presented a method of analysis for discs with identical blades [Ref. SD-221 and his technique has now been developed to incorporate symmetrical packeting arrangements. Unlike the continuously-shrouded case, each packeted bladed disc mode is known to contain more than one diametral component and hence Armstrong's method is not directly applicable. Nevertheless, it is assumed that the wheel vibrates with a dominant  $n$  nodal diameter shape, that is to say contributions from other diametral patterns are negligible. (A similar assumption, concerning the interblade phase angle of an aeroelastic system, will be made later in Chapters 9 and 10). Also, it is assumed that the blade displacements follow a cosine fluctuation both in time and angular position around the circumference. Thus, for example, the response of the  $j^{\text{th}}$  blade can be written as:

$$q_j = q_0 \cos 2\pi n j / N \quad (3-8)$$

where  $q_0$  is some arbitrary amplitude and  $n$  and  $N$  are the nodal diameter and total blade numbers respectively.

This time, the packet is considered as a multi-root blade (or superblade) and the coupling, as shown in Fig. 3.3, takes place between these roots and the corresponding points on the disc sector. If  $p$  is the number of blades per packet, the system's matrix will be of order  $2p$  and hence a very substantial saving in the central memory requirement is achieved.

Let  $[\gamma_n]$  be the receptance matrix of the disc sector for the  $n$  nodal diameter mode whose explicit form will be given later and  $[\delta]$  the receptance matrix of a single packet. Proceeding as above for the direct method. it can be shown that the governing equation of motion is:

$$([\gamma_n] + [\delta]) \{Q\}_R = \{0\} \quad (3-9)$$

where

$$\begin{aligned} \{Q\}_R^T &= \{z_1, \theta_{y1}, z_2, \theta_{y2}, \dots, z_p, \theta_{yp}\} \\ &= \{z_1, \theta_{y1}, z_2, \theta_{y2}, \dots, z_p, \theta_{yp}\} \end{aligned} \quad (3.10)$$

The natural frequencies of the packeted bladed disc while vibrating mainly in its  $n$  nodal diameter shape can be found from the determinantal equation :

$$\det |[\gamma_n] + [\delta]| = 0 \quad (3-11)$$

Each of the two analyses described above requires the formulation of a matrix pair,  $([a], [\beta])$  or  $([\gamma_n], [\delta])$ , whose derivation will be discussed below.

### 3.2 DERIVATION OF DISC RECEPTANCES

The equation governing the harmonic motion of a thin, uniform, isotropic, fiat, circular plate, expressed in polar co-ordinates. is:

$$(\nabla^2 + k^2)(\nabla^2 - k^2) w = 0 \quad (3-12)$$

where  $\nabla^2$  is the Laplacian operator.

$w$  the transverse deflection at the plate mid-plane.

$$k^4 = \rho h \omega^2 / D \quad \text{and} \quad D = E h^3 / 12 (1 - \nu^2);$$

with  $\omega$  frequency of vibration,

$h$  plate thickness,

$\rho$  density.

$E$  Elastic modulus,

$\nu$  Poisson's ratio.

and  $D$  is sometimes called as flexural rigidity.

The solution of equation (3-12) can be found in the published literature and will not be reproduced here. As shown in Ref. SD-16, the general expressions for transfer receptances between points  $i$  and  $j$  on the disc rim, where the  $i^{\text{th}}$  and  $j^{\text{th}}$  blades are mounted, can be expressed as an infinite Fourier series of the form:

$$a_{ij} = 1/\pi \{ 1/2 \alpha_0 + \sum_{n=1}^{\infty} \alpha_n \cos [2\pi n(i-j)/N] \} \quad (3-13)$$

where  $\alpha_n$  is a combination of Bessel functions of order  $n$  and also depends on the disc properties and the frequency of vibration. In practice, this series is truncated at integer multiples of the highest possible nodal diameter number. As there are two coupling co-ordinates per blade root, there will be three types of receptances relating (i) displacements to forces, (ii) displacements to moments or slopes to forces and (iii) slopes to moments. Cases (ii) and (iii) will be distinguished by superscripts ' and " respectively. Once these transfer (or point if  $i$  coincides with  $j$ ) receptances are known, the overall disc receptance matrix  $[\alpha]$  can easily be derived using the circular symmetry. Such a formulation yields:

$$\text{Cal} = \begin{matrix} \begin{matrix} \text{(i)} & \text{(ii)} \\ \begin{bmatrix} [\alpha]_s \\ [\alpha']_s \end{bmatrix} & \begin{bmatrix} [\alpha']_s \\ [\alpha'']_s \end{bmatrix} \\ \text{(ii)} & \text{(iii)} \end{matrix} & \left| \begin{matrix} \text{where } [\alpha]_s \\ 2N \times 2N \end{matrix} \right. & = & \begin{bmatrix} \alpha_{11} & \alpha_{12} & \dots & \alpha_{1N} \\ - & - & - & - \\ \alpha_{N1} & \alpha_{N2} & \dots & \alpha_{NN} \end{bmatrix} \end{matrix} \quad (3-14)$$

Because of the inherent symmetry, it may be shown [Ref. SD-161 that:

$$\alpha_{j, j+q} = \alpha_{j, j+N-q} = \alpha_q \quad (3-15)$$

where q is some arbitrary Integer. This feature makes the submatrix  $[\alpha]_s$  a circulant of the Toeplitz type. properties of which can be found in Ref. MA-1.

As explicitly shown by equation (3-13), receptance expressions in the  $[\alpha]$  matrix contain contributions from all possible nodal diameters, a feature which makes the analysis general. The cyclic symmetry approach, which assumes a priori an n nodal diameter pattern, requires only receptances of order n but these must be expressed compatibly with the discontinuous lumped loading of the form imposed by the chosen modal shape. Armstrong, Ref. SD-22, showed that:

$$\alpha_n^G = N/2\pi \{ \sin(n\epsilon) / n\epsilon \cdot \alpha_n + \sin[(N-n)\epsilon] / [(N-n)\epsilon] \cdot \alpha_{N-n} + \dots \} \quad (3-16)$$

where  $\epsilon$  is half the angle subtended at the disc centre by the blade root width and the superscript  $^G$  indicates that receptances are expressed in the global co-ordinate system. The receptance matrix of the disc sector, to which p blades are mounted, can now be written as:

$$[\gamma_n] = \begin{matrix} \text{Blade 1} & \text{Blade p} \\ \left[ \begin{array}{ccc} [\gamma]_s & \dots & [\gamma]_s \end{array} \right]_{2p \times 2p} \end{matrix} \quad \text{where } [\gamma]_s = \begin{bmatrix} \alpha_n^G & \alpha'_{n^G} \\ \alpha'_{n^G} & \alpha''_{n^G} \end{bmatrix}_{2 \times 2} \quad (3-17)$$

where the superscripts ' and '' have their previous meaning.

### 3.3 DERIVATION OF PACKET RECEPTANCES

Two different approaches will be used to derive the packet receptance matrix.

#### 3.3.1 Finite Element Method

The finite element model described in the previous chapter can also be used to obtain the packet receptance matrix at the blade roots. For free harmonic vibrations, the equation of motion is:

$$([\mathbf{K}] - \omega^2 [\mathbf{M}]) \{\mathbf{q}\} = 0 \quad (3-18)$$

where all symbols have their customary meaning. The formal solution of equation (3-18) yields the eigenvalues  $[\omega_r^2]$  and the mass-normalized eigenvectors  $[\Phi]$  from which the complete packet receptance matrix can be obtained as:

$$[\Delta]_{6p \times 6p} = [\Phi]_{6p \times R} [-(\omega_r^2 - \omega^2)^{-1}]_{R \times R} [\Phi]^T_{R \times 6p} \quad (3-19)$$
$$R \geq 6p$$

where  $p$  is the number of blades per packet and  $R$  the number of modes to be included in the modal summation.

As explained in Section 3.1, it was decided to use two coupling co-ordinates only, namely axial translation and tangential rotation, the remaining four being grounded throughout the analysis. The co-ordinate deletion has to be carried out on the packet dynamic stiffness matrix defined as:



$$[D]_{6px6p} = [\Delta]^{-1}_{6px6p} \quad (3-20)$$

which after the grounding process reduces to:

$$[d] = [D]_{2px2p}^R \quad (3-21)$$

and the packet receptance matrix is obtained via re-inversion.

$$[\delta]_{2px2p} = [d]^{-1} \quad (3-22)$$

This latter can then be written explicitly as:

$$[\delta] = \begin{bmatrix} \delta_{z_1z_1} & \delta_{z_1\theta_1} & \dots & \delta_{z_1\theta_p} \\ \delta_{\theta_1z_1} & \delta_{\theta_1\theta_1} & \dots & \delta_{\theta_1\theta_p} \\ \dots & \dots & \dots & \dots \\ \delta_{\theta_pz_1} & \delta_{\theta_p\theta_1} & \dots & \delta_{\theta_p\theta_p} \end{bmatrix}_{2px2p} \quad (3-23)$$

The overall packet receptance matrix  $[\beta]$ , which is required by the direct method, can now be formed from the elements of the individual packet receptance matrix in the following manner:

$$[\beta] = \begin{bmatrix} \text{Packet 1} & \text{Packet } \frac{N}{p} & \text{Packet 1} & \text{Packet } \frac{N}{p} \\ \hline [\beta]_s & \dots & [\beta']_s & \dots & [\beta']_s \\ \hline [\beta']_s & \dots & [\beta'']_s & \dots & [\beta'']_s \\ \hline & & & & [\beta'']_s \end{bmatrix}_{2Nx2N} \quad (3-24)$$

where

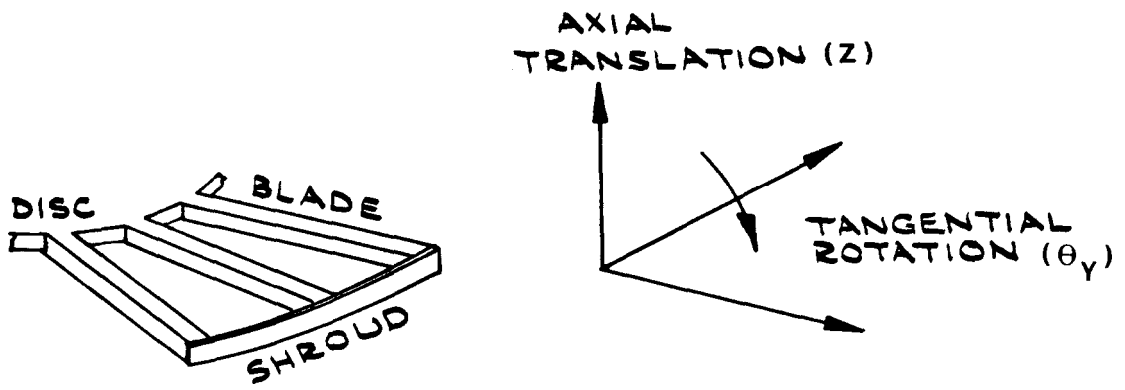
$$\begin{aligned} [\beta]_s &= \begin{bmatrix} \delta_{z_1z_1} & \delta_{z_1z_2} & \dots & \delta_{z_1z_p} \\ \dots & \dots & \dots & \dots \\ \dots & \dots & \dots & \dots \end{bmatrix}_{pxp} \\ [\beta']_s &= \begin{bmatrix} \delta_{z_1\theta_1} & \delta_{z_1\theta_2} & \dots & \delta_{z_1\theta_p} \\ \dots & \dots & \dots & \dots \\ \dots & \dots & \dots & \dots \end{bmatrix}_{pxp} \\ [\beta'']_s &= \begin{bmatrix} \delta_{\theta_1\theta_1} & \delta_{\theta_1\theta_2} & \dots & \delta_{\theta_1\theta_p} \\ \dots & \dots & \dots & \dots \\ \dots & \dots & \dots & \dots \end{bmatrix}_{pxp} \end{aligned} \quad (3-25)$$

### 3.3.2 Receptance Coupling

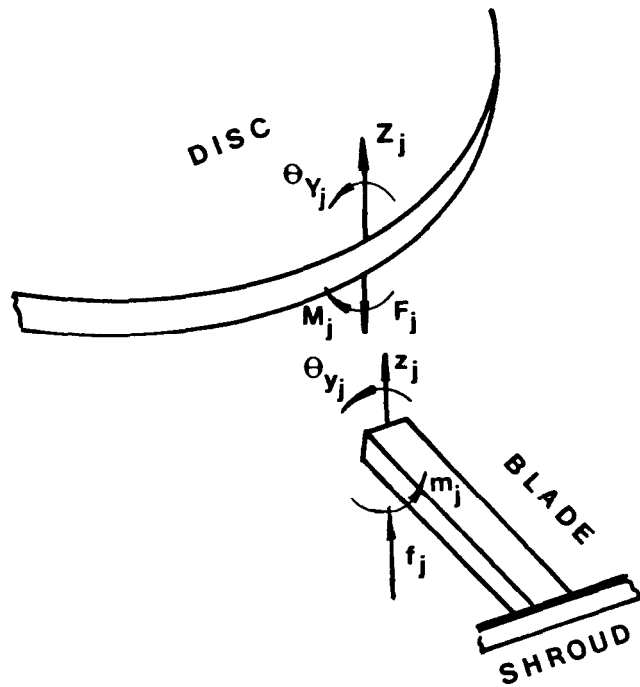
The packet receptance matrix can also be formed by coupling the individual blade and shroud segments which, once again, are considered as prismatic beams of rectangular cross-section. Although this is a straightforward process, it involves numerous matrix inversions and hence optimization of the coupling sequence is necessary. To ensure compatibility between the two approaches, a single global co-ordinate system, shown in Fig. 2. 1. was used for both the finite element and receptance coupling models. The coupling was performed in all six co-ordinates and the following sequence was used.

- 1) The blade and shroud impedance matrices were computed directly from tabulated expressions.
- 2) The first blade, then all shroud segments and finally the last blade were coupled end-to-end to form the external frame of the packet.
- 3) The remaining blades, 2 to p-1, were placed in-between the shroud segments and hence the impedance matrix of the complete packet, as shown in Fig. 3.4. was obtained. To be aligned with the global OXYZ co-ordinate system, all beam elements had to be rotated through an angle  $\phi$ , this being the angle between the global OX and the local Ox axes.
- 4) Only two co-ordinates, namely axial translation and tangential rotation, were retained at the blade roots; the remaining four being deleted from the packet impedance matrix, since they are considered to be effectively grounded.
- 5) Finally, the packet receptance matrix  $[\delta]$  was obtained by inverting the reduced impedance matrix formed above and then deleting all but the blade root-root receptances.

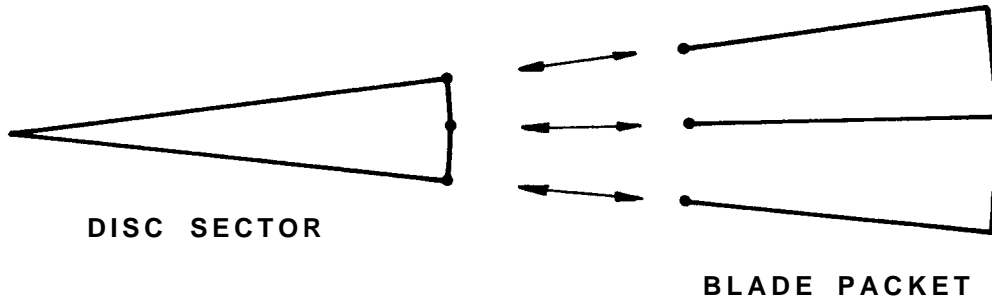
Once the single packet receptances are computed, the overall packet matrix  $[\beta]$  can be assembled as indicated by equations (3-24) and (3-25).



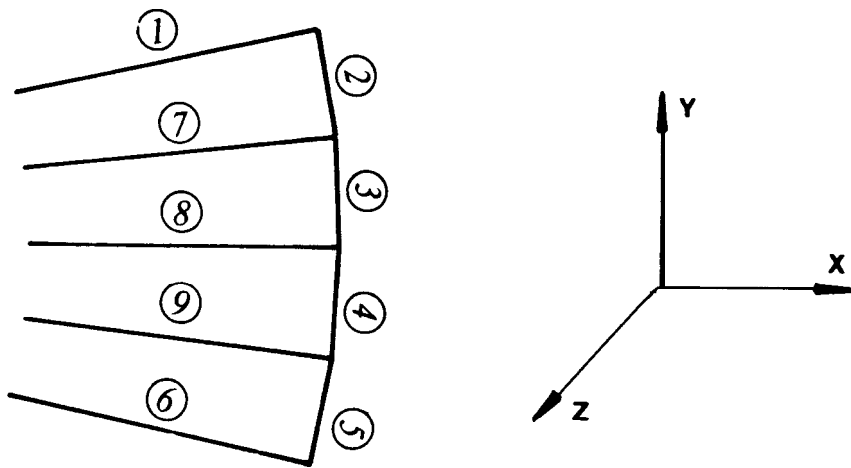
**Fig. 3.1** Typical blade packet



**Fig. 3.2** Loads and responses at disc rim and  $j$ <sup>th</sup> blade root



**Fig. 3.3** Disc sector - Blade packet coupling



**Fig. 3.4** Coupling sequence for packet receptance matrix computation

CHAPTER 4

NUMERICAL STUDY

4.1 GENERAL

Two computer programs based on the methods described in Sections 3.1.1 and 3.1.2, namely **MULPAC** and **SINPAC**, were written for the numerical study. These programs share a common **LIBRARY** containing component receptance routines and other general purpose subroutines such as matrix inversion, determinant evaluation, discrete Fourier transforms, etc.

Although based on receptance coupling models, the analysis which will be presented below is a natural extension of that initiated in Chapter 2 in the sense that the effects of a flexible disc are now being considered. The packet data were given in Table 2.1 and the disc details are listed below in Table 4.1. All cases will be run for  $N=30$ , where  $N$  is the number of blades on the disc, and Timoshenko beam theory will be used throughout the analysis. A typical packet together with the co-ordinates used is shown in Fig. 4.1.

Inner radius = 0 mm	Young's Modulus = 207 GN/m <sup>2</sup>
Outer radius = 262.6 mm	Density = 7850 Kg/m <sup>3</sup>
Thickness = 12.7 mm	Poisson's ratio = .287

Table 4.1 Disc details

Because of the restriction on the number and position of coupling co-ordinates, all graphs - which will be presented in natural frequency vs nodal diameter format - refer to axial vibration. In other more symmetric bladed disc configurations, it is well known that each vibration mode may be characterised by a shape containing  $n$  nodal diameters. This notation will also be used here but it must be observed at the outset that each mode of a packeted assembly is more complex in its shape than is implied by  $n$  nodal diameters and does in fact, contain several diametral components. For convenience, each mode will be labelled by the largest diametral component in its mode shape. In order to minimize the computational effort, the study will further be focussed on the variation of the first three families, sometimes associated with 0, 1 and 2 nodal circle(s).

#### 4.2 CONTINUOUSLY-SHROUDED DISC

Before investigating the effects of packeting, it was decided to study the case of a continuously shrouded disc. An existing Disc-Blade-Shroud receptance coupling program, BLISC [Refs. SD-17 and SD-271], was further developed for this purpose. To ensure compatibility with the present analysis, coupling was performed in all six co-ordinates at the blade tips but only in two at the roots, these being axial translation and tangential rotation. Two particular types of shroud attachment, which were considered to be the two limiting cases of a packeting configuration, were used:

- (i) a uniform continuous shroud which is a circular ring connecting blade tips;

(ii) a non-interlocking shroud which is modelled as a series of rigid blocks possessing mass and inertia and attached at blade tips.

Results are given in Tables II. 1 and II. 2 of Appendix II and plotted below in Fig. 4.2. The natural frequencies in Fig. 4.2 exhibit the well-known tendency of grouping into families, each one being associated with the disc behaviour at low nodal diameter numbers and the blade dominance increasing thereafter. An inspection of the individual blade mode shapes revealed that the first two families were mainly in bending while the third one showed torsional characteristics. These findings are in total agreement with Cottney [Ref. SD-171] who studied both the unshrouded and shrouded versions of the same disc. In the former case, the identification of the families is much easier due to the asymptotic approach towards the single blade cantilever frequencies. The same type of behaviour is also observed with the non-interlocking shroud curves which tend to the cantilever frequencies of an isolated blade at the tip of which the shroud mass and inertia are concentrated. This is due to the stiffening of the disc which behaves almost as a rigid body in high diametral modes. Also, the gap between the two shrouded assembly curves diminishes with increasing frequency and decreasing nodal diameter number. This suggests that the effect of packeting is likely to be more pronounced on the lower families as well as on higher modes in each family.

#### 4.3 TEN PACKETS WITH THREE BLADES EACH

For the 30-bladed disc used in this study, there are six possible regular packeting configurations, each comprising 15, 10, 6, 5, 3 or 2 identical

packets. The three-bladed packeting arrangement will be considered as the reference case and studied in great detail. Also, results for other configurations will be reported.

Fig. 4.3 illustrates the shrouding pattern used together with a schematic representation of its Discrete Fourier Transform (DFT). It is seen that this particular arrangement renders all coefficients zero but the ones of order 0 and 10, suggesting that the cyclic symmetry has been broken at least once, this being in the case of the 10 nodal diameter shape since the term of order 0 corresponds to the continuously-shrouded case. This can be explained by considering the single and double modes in which a bladed disc assembly is known to vibrate [Ref. SD-161. In a tuned system, a single mode possesses only one natural frequency and its associated mode shape is circumferentially symmetrical due to the fact that each blade experiences the same loading. The only possible single modes, for which the circular symmetry cannot be maintained, are those with 0 and  $N/2$  nodal diameters, the latter occurring only in the case of discs with even blade numbers. All the remaining modes are double in the sense that they occur in pairs having identical frequencies and the corresponding mode shapes are also identical except for their circumferential orientation. When the blades are grouped into packets, the cyclic symmetry is broken for some of these double modes which then split into two single ones with distinct frequencies and similar mode shapes. In the case of 10 packets, or superblades, it is obvious that there will be one *preferred orientation* of the 5 nodal diameter pattern due to the matching symmetry between the packeting arrangement and the modal shape. The same argument also applies to 10 nodal diameter modes, simply because 10 is an integer multiple of 5.



#### 4.3.1 Analysis via Direct Method

The first part of the numerical study was conducted using computer program MULPAC which is based on the direct method of Chapter 3. The natural frequencies of the ~~packeted~~ ~~bladed~~ disc were determined by searching for the roots of equation (3-7) within the 100-4000 Hz frequency range. A frequency step of 25 Hz was first used to locate the single and double roots which were then pinpointed using repeated bisections combined with a special root-finding algorithm described in detail in Refs. SD-23 and SD-24. The essence of the method lies in setting up and reducing the system's matrix into upper triangular form at two distinct frequencies. The number of negative elements (or sign count) on the leading diagonal is calculated in both cases, the difference giving the number of sign changes (i.e. number of natural frequencies minus number of poles) within the interval considered. Unfortunately, the process is polluted by the presence of many poles which occur at each subcomponent free-free natural frequency and hinder location of the true natural frequencies. A typical plot of the system's characteristic determinant against frequency showing one single and two double roots is given in Fig. 4.4. As can be seen from the figure, the frequency determinant exhibits very sharp and sudden changes, a characteristic feature of the direct analysis method which makes the finding of certain modes very difficult. Once a natural frequency was located, the associated shape was identified by solving equation (3-6) for the load vector, i.e. the mode shape by linearity. Some difficulties were encountered for closely-situated roots whose modal shapes were distorted due to numerical pollution.

Two sets of results, each corresponding to a different formulation of the packet receptance matrix, will be presented below. In the first set, the blades and shroud segments are coupled end-to-end to yield the packet receptances while these are derived via modal summation in the second. Results are given in Tables II-3 and II-4 of Appendix II and plotted in Fig. 4.5. The natural frequencies are once again grouped into families but this time the frequency versus nodal diameter curves exhibit discontinuities due to the splitting of the 5 and 10 nodal diameter modes which together with those for 0 and 15 diameters constitute the single modes of the system, all others being double modes. This rather singular behaviour is characteristic of packeted bladed disc assemblies and will be discussed further and generalised in the following sections.

#### 4.3.2 Analysis via Cyclic Symmetry Method

The second part of the numerical study was conducted using computer program SINPAC which is based on the cyclic symmetry method of Chapter 3. The natural frequencies of the packeted bladed disc were determined by searching the roots of equation (3-11) within the 100-4000 Hz frequency range. The root-finding algorithm described in the previous section was also used here. It should be noted that the method considering a typical disc sector with only one packet rather than the whole assembly, the solution of equation (3-11) always yields single roots though some of them may well represent double modes. Furthermore, unlike the previous case, there is no need to identify the modal shape since precognition of a dominant  $n$  nodal diameter component was imposed in the first instance.

The natural frequencies of the 10 packeted configuration, as predicted by SINPAC, are listed in Table II-5 and plotted in Fig. 4.6. All results were computed in the case of a packet receptance matrix derived via coupling of individual components. As can be seen from Fig. 4.6, each family is now represented by three curves, each approaching a single packet cantilever frequency at high nodal diameter numbers. In the light of the previous bladed disc studies and also of the results obtained via the direct method, it is immediately seen that the correct vibrational properties can only be represented by the single curve drawn in bold, coinciding in turn with each of the initial three curves and the take-over occurring at 5 and 10 nodal diameters. While there is very good agreement with the results previously obtained via the direct method, the physical significance of these superfluous predicted values, so-called *ghost* modes, is not entirely clear. The answer to this question almost certainly lies in the assumption that each mode has a pure  $n$  nodal diameter shape while in reality each comprises several components. This feature will be discussed in Section 4.5.

#### 4.3.3 Further Considerations

Accuracy of the finite element modelling.

Although the two sets of results shown in Fig. 4.5 are in good agreement, there are a few discrepancies which merit closer inspection. As everything else remained the same throughout both analyses, it was decided to plot the packet receptance curves derived from the two methods, and Figs. 4. 7a and 4. 7b show the variation of the translational

and rotational receptances ( $\beta_{z_1, z_1}$  and  $\beta_{\theta y_1, \theta y_1}$ ) of the three-bladed packet with frequency. Both the receptance coupling and modal summation curves follow each other closely within the 100-4000 Hz frequency range. It should be noted that the locations of the natural frequencies on these figures do not correspond to the free-free conditions since the packet was effectively grounded at the blade roots in four out of the six co-ordinates. The slight deviations in these theoretically-generated curves is partly due to the inevitable inaccuracies involved in the finite element method. In this study both the blade and the shroud segments were modelled using 3 elements and the criterion was the convergence of the first 30 modes ( $f_{30} = 4924.9$  Hz) of the free blade packet. This resulted in a 16 node/96 degree-of-freedom model and consequently in 96 modes, out of which only the first 75 were included in the modal summation ( $f_{75} = 31029.5$  Hz). Thus the finite element method leads to the computation of the packet receptances by truncating an infinite series - and this by definition of finite elements - as opposed to the receptance coupling method which uses the closed form solution and hence effectively incorporates all possible modes. The introduction of a finer mesh would permit the inclusion of more modes and hence improve the accuracy but this could only be done at the expense of increased computing time and memory requirements. Another major difficulty is associated with the rigid body mode shapes which always contain *impurities* or *residuals* due to the fact that these zero modes are numerically unstable and ill-conditioned.

The main purpose of deriving packet receptances via a finite element eigen-solution was to investigate the possibility of incorporating complex blade geometries into the basic model of Chapter 3, and the related set

of results is not of relevance to the general method of analysis and hence will be excluded from further discussion.

Survey of **packeted** bladed disc behaviour.

Fig. 4.8 recapitulates all bladed disc results obtained so far with the exception of those related to finite element modelling. It is observed that:

- (i) As the number of nodal diameters increases, all three families approach a cantilever frequency of the single blade packet. A similar phenomenon, reported in Ref. SD-17, is known to occur in the case of an unshrouded disc whose families become asymptotic to blade cantilever frequencies. This is due to the stiffening of the disc at high nodal diameters.
- (ii) The most striking difference between the continuously-shrouded and **packeted** bladed disc behaviour is the discontinuous pattern exhibited by the latter. As discussed earlier, the broken cyclic symmetry forces some of the double modes to split – in this case 5 and 10 nodal diameters – and this can be predicted by considering the DFT of the complete **packeting** arrangement. It should be noted that the direct method predicts the double and single modes correctly in the sense that the corresponding roots are also single or double. The cyclic symmetry method however, always yields single roots and hence additional information is required. A rationale will be given in Section 4.5.
- (iii) An at least as important, but a much less obvious, difference lies in the modal shapes. The **packeted** bladed disc exhibits complicated modes which contain more than one diametral component as opposed to its continuously shrouded counterpart whose modes are always pure in shape. The direct method being a full analysis, the various diametral components

contained in any one mode can be obtained from the DFT of the corresponding modal shape. Some examples are given in Fig. 4.9 and a systematic study will be presented later.

- (iv) The continuously-shrouded discs (uniform or non-interlocking) can effectively be considered as the two limiting cases of their packeted bladed counterparts. It is clearly seen that packeting has no significant effect at low nodal diameter numbers and also at high frequencies where the continuous and non-interlocking shroud curves stay together and hence the 1F family (first flapwise) is most vulnerable to packeting effects. The amount of splitting in the 5 and 10 nodal diameter modes is proportional to the gap between these two curves which increases with nodal diameter number and decreases with frequency.
- (v) The 1F family presents a somewhat distinct feature vis-à-vis the location of its natural frequencies which can be estimated from knowledge of the properties of two much simpler assemblies, the continuously-shrouded disc and a single packet of cantilevered blades.
- (vi) The packeted bladed disc yields higher natural frequencies for some nodal diameters than its continuously-shrouded counterpart. This should be attributed to the fact that the corresponding set of results presented in Fig. 4.0 was compiled using different computer programs and hence different techniques of analysis. This feature will be discussed further in the next section.

#### Review of the two methods of analysis.

- (i) From a numerical viewpoint, the cyclic symmetry method has some distinct advantages. It requires considerably less computational effort and it is applicable to assemblies with large blade numbers. Furthermore the root-finding process is less tedious and the mode shapes need not be identified.

- (ii) The cyclic symmetry method however, cannot predict the various diametral components which are present in any one mode nor distinguish between the single and double modes of packeted bladed disc vibration and hence additional information must be supplied.
- (iii) Blade-to-blade differences and/or unsymmetrical packeting arrangements can only be considered through the direct method since each blade in the assembly is always modelled individually whether the symmetry exists or not.

#### 4.4 ADDITIONAL CALCULATIONS

To study the effects of packeting further, it was decided to extend the analysis above to other possible packeting configurations of the 30-bladed disc. Fig. 4. 10 illustrates the shrouding arrangements considered together with their DFT. Calculations were performed via MULPAC and complemented in some cases using SINPAC. Results are listed in Tables II. 6 to II. 11 and plotted in Fig. 4. 11 from which it can be seen that all packeting configurations of the 30-bladed disc follow the same qualitative trend which has been established in the previous section.

- (i) Discs with continuous and non-interlocking shrouds can still be considered as the two limiting cases of their packeted counterpart. This is clearly observed for the 2- and 3-bladed packets while the others lead to higher natural frequencies. The discrepancies are believed to be due to the use of two different computer programs, BLISC and MULPAC, which model the shroud as a circular hoop and a polygon of straight beams respectively. As discussed in Ref. SD-17, the hoop curvature is expected to couple in-plane flexure to tangential translation,

and out-of-plane flexure to tangential rotation. Since this coupling effect is of particular importance at the blade Ups, the straight beam approximation is much more acceptable for a 2-bladed packet than for a 10-bladed one. Also, certain modes of the packeted configuration are likely to be more sensitive to stiffness changes due to the gaps in the shroud, a feature which depends on the nodal diameter orientation.

- (ii) The double modes which split can be predicted with the aid of the corresponding Fourier diagrams although there may be more modes which split than given by the Fourier analysis. These are due to the global symmetry inherent in the assembly. in physical terms, a mode will split each time its associated shape is forced to have a preferred orientation. This can be visualized best by checking whether some or all of the nodal diameters could pass through the gaps in the shrouding in a symmetrical manner.
- (iii) Although totally within the general behaviour outlined above, the case of the 2-bladed packet presents a somewhat distinguishing feature. in spite of the absence of a splitting double mode, the characteristic curves still show a discontinuous jump occurring between 7 and 8 nodal diameter modes. in this case there are 15 gaps in the shroud and hence these two modes are the closest ones to have a preferred orientation.
- (iv) As can be seen from Fig. 4. 1 lb. a dominant  $n$  nodal diameter assumption used the cyclic symmetry method yields accurate results even when the number of blades per packet has been increased to 5. in this case the modal shapes, which contain up to 5 nodal diametral components, are considerably more complicated than the ones of the 3-bladed packet with a maximum of three components.



#### 4.5 A RATIONALE FOR PACKETED BLADED DISC ANALYSIS

it has already been established that **packeted** bladed disc vibration is **characterized** by:

- (i) the splitting of certain double modes into single ones;
- (ii) the **complexity** of each mode shape which contains at least two nodal **diametral** components.

From design **considerations**, it is very important to be able to predict these two qualitative properties before undertaking a lengthy and perhaps superfluous analysis involving the numerical solution of a determinantal equation. Furthermore, in order to be used on its own, the cyclic symmetry method requires this extra information. These two essential features of **packeted** bladed **disc** assemblies, (i) and (ii) above, can be anticipated using the modal interference diagrams shown in Fig. 4. 12 which may be drawn using  $M$ , the maximum possible number of nodal **diameters**, and  $P$ , the total number of packets in the assembly. These diagrams are constructed by drawing the two  $45^\circ$  lines emanating from each integer multiple of  $P$  on the nodal diameter axes (e. g. at 5, 10, and 15 In Fig. **4. 12d** or at 3, 6, 9 and 12 In **Fig. 4. 12f**) and including the main diagonal.

- (i) The nodal diameters at which the modes are split into two different frequencies are found from the intersections of the interference lines with the leading diagonal and for a given **packeting** arrangement, they correspond to the preferred locations of the nodal lines.
- (ii) Also, columns or rows of the modal interference diagrams indicate the **combinations** of nodal diameter components which

exist together in the (complicated) mode shapes of the packeted biaded disc. For example, referring again to fig. 4.12d, it is seen that all modes will have shapes whose diametral components are either:

- (a) 0, 5, 10 and 15;
- (b) 1, 4, 6, 9, 11 and 14;
- (c) 2, 3, 7, 8, 12 and 13.

No other combinations are possible. This result has significant implications for prediction methods which can exploit the limited number of diametral components present in any one mode. It also has implications for the susceptibility of each mode to forced excitation, as will be examined in Chapter 6.

Finally, it is stressed that the interference diagrams, introduced in this work, are applicable to any biaded disc assembly provided the packeting arrangement is symmetrical. Numerous cases with different blade and packet numbers have been studied and found to be within the rules above.

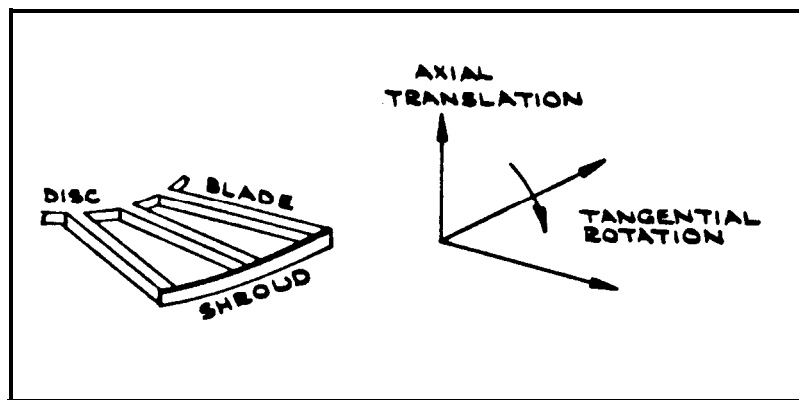


Fig. 4.1 Three-bladed packet

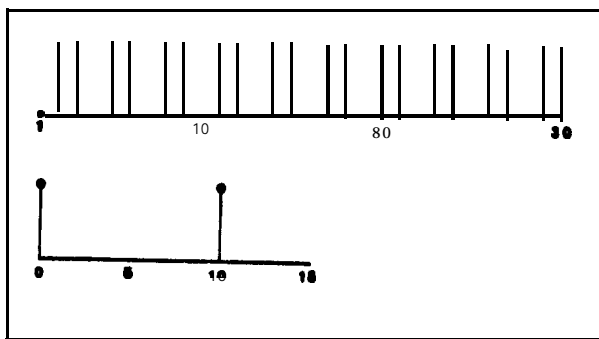


Fig. 4.3 Schematic representation of the shrouding arrangement

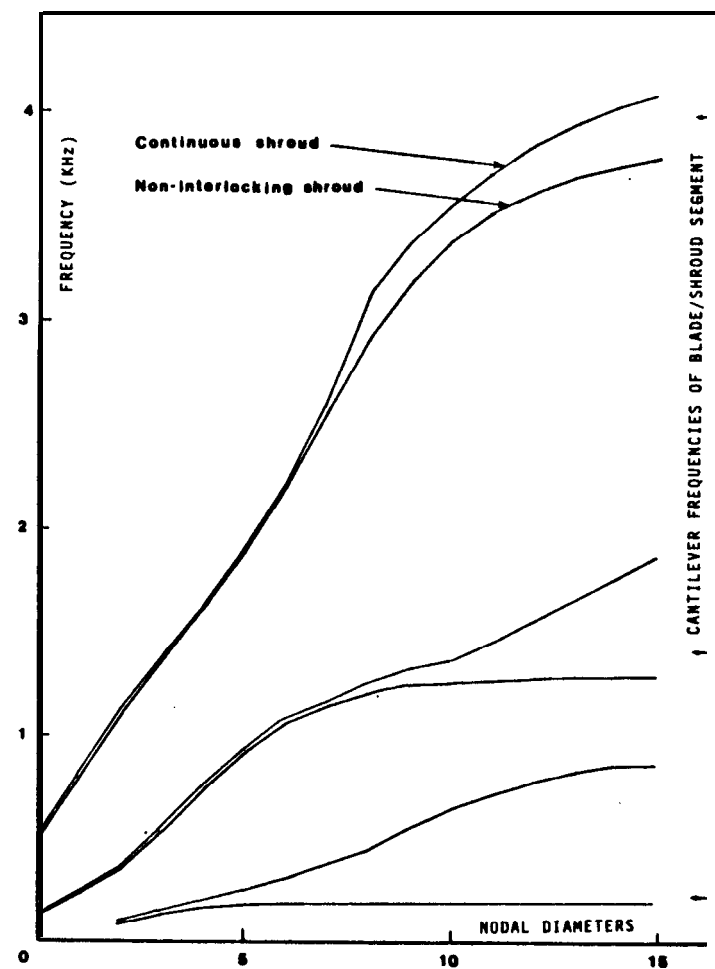


Fig. 4.2 Natural frequencies of the continuously-shrouded disc

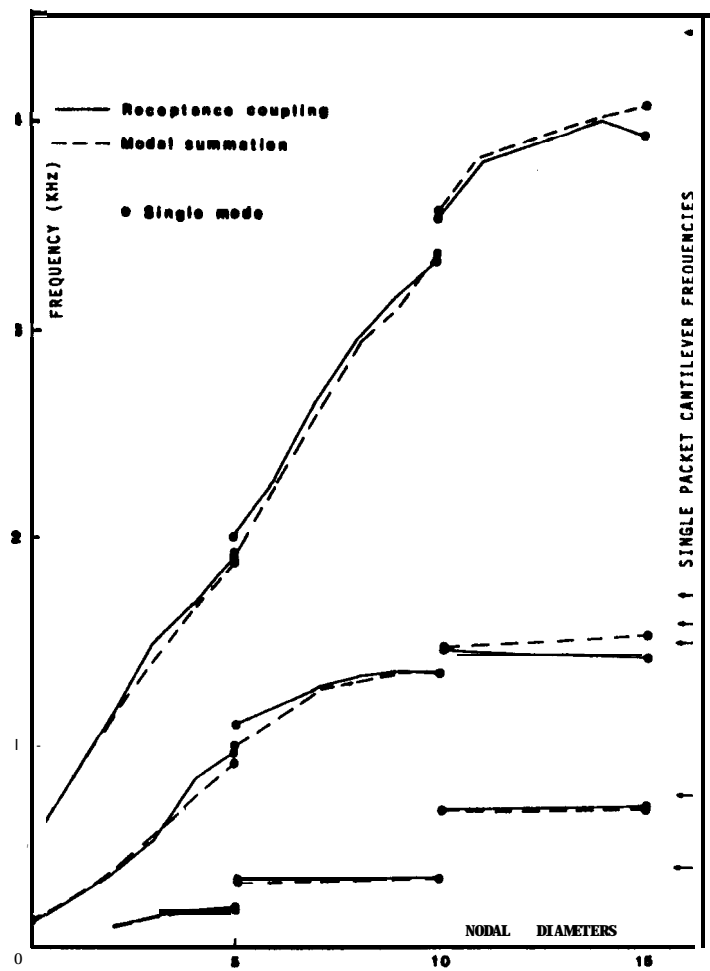


Fig. 4.5 Natural frequencies of the 30-bladed disc via direct method (10 packets)

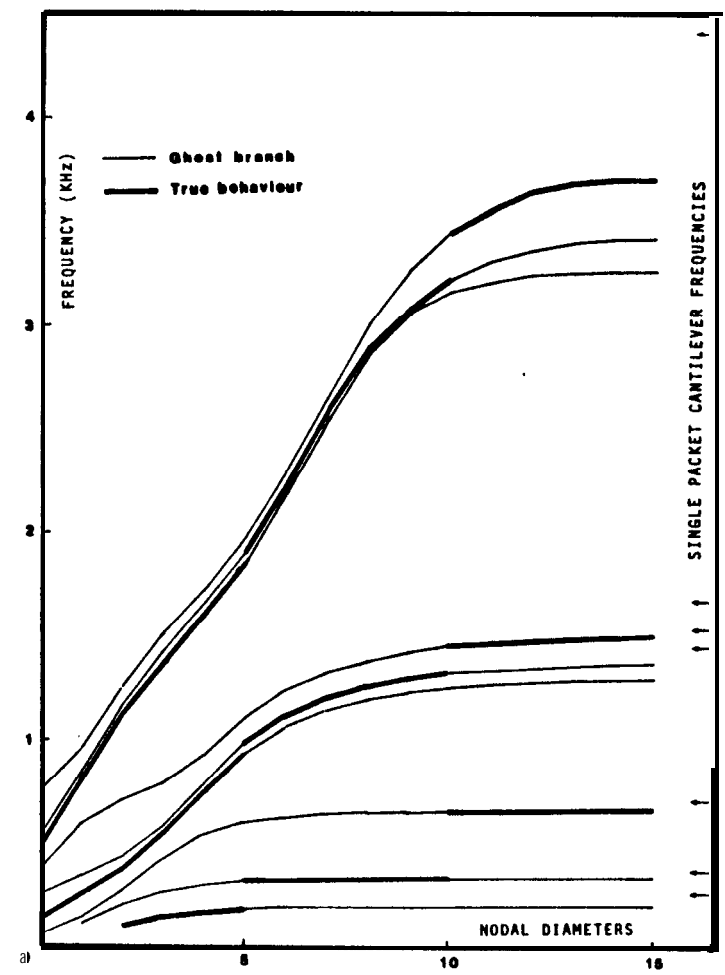


Fig. 4.6 Natural frequencies of the 30-bladed disc via cyclic symmetry method (10 packets)

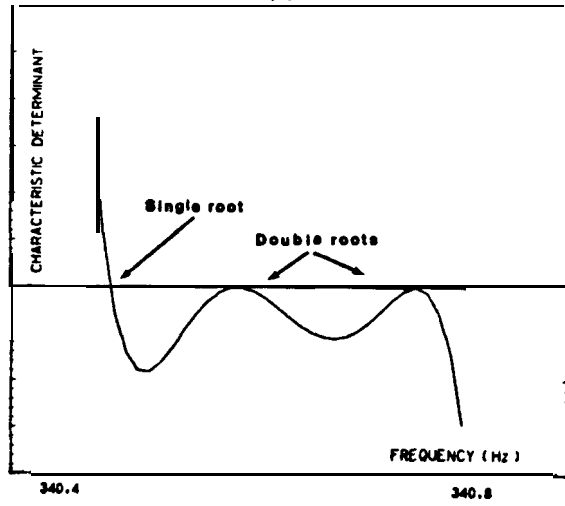


Fig. 4.4 Variation of the characteristic determinant with frequency

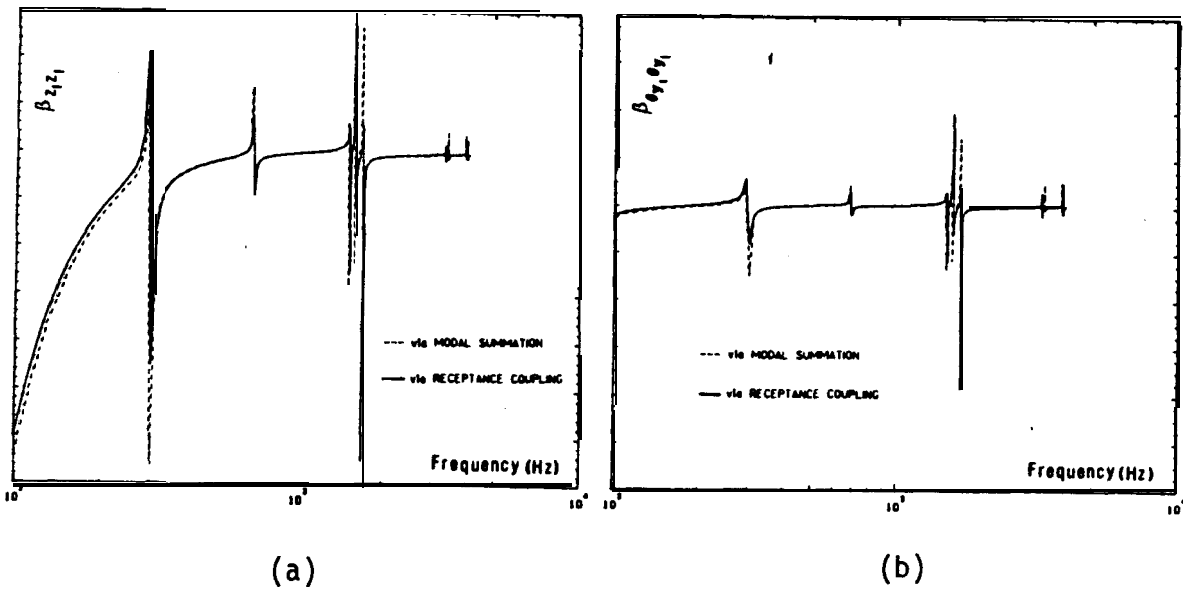


Fig. 4.7 Receptance curves of the blade packet

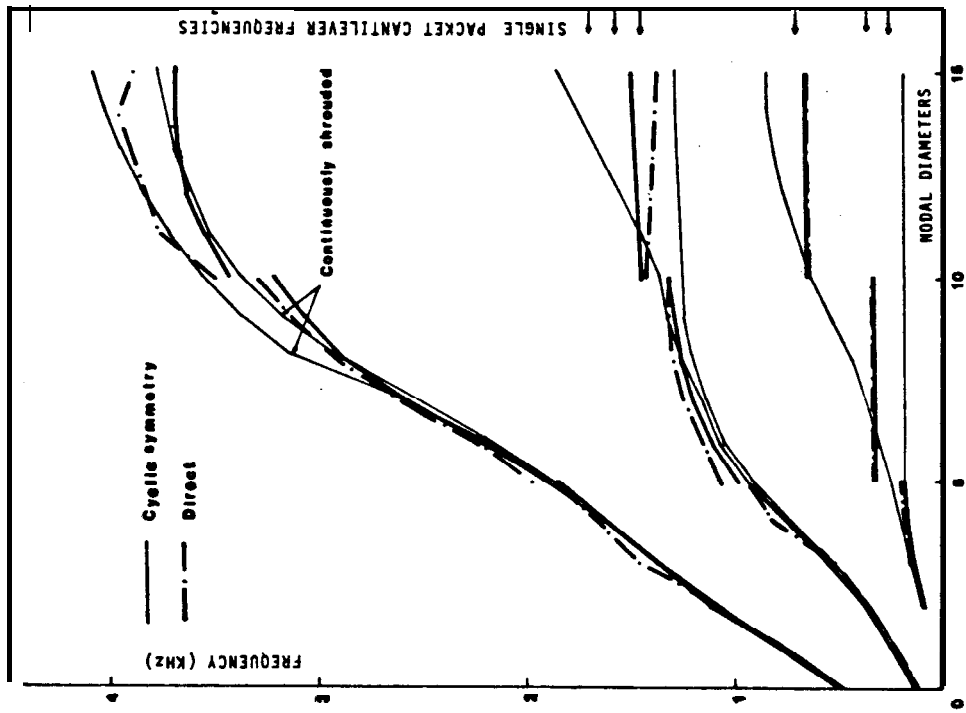


Fig. 4.8 Natural frequencies of the 30-bladed disc  
(10 packets of 3 blades)

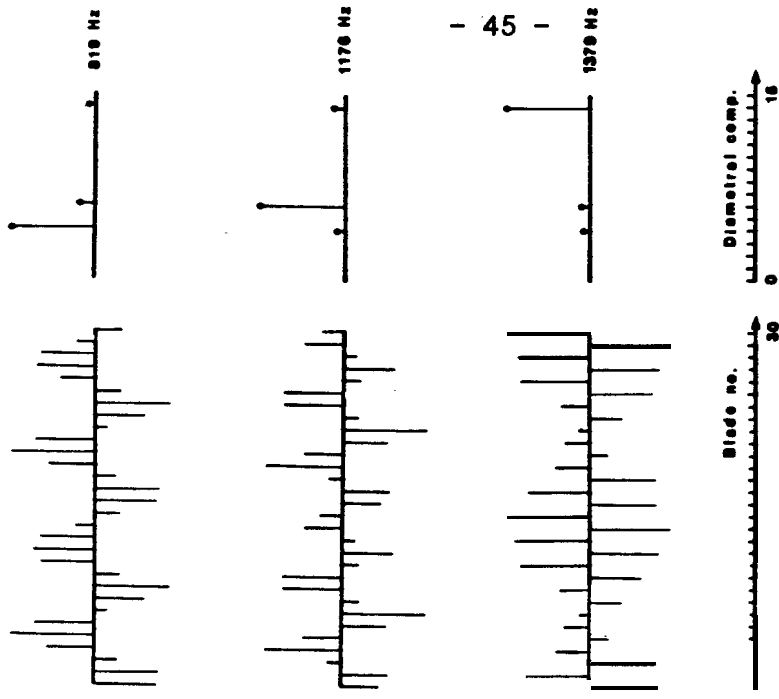
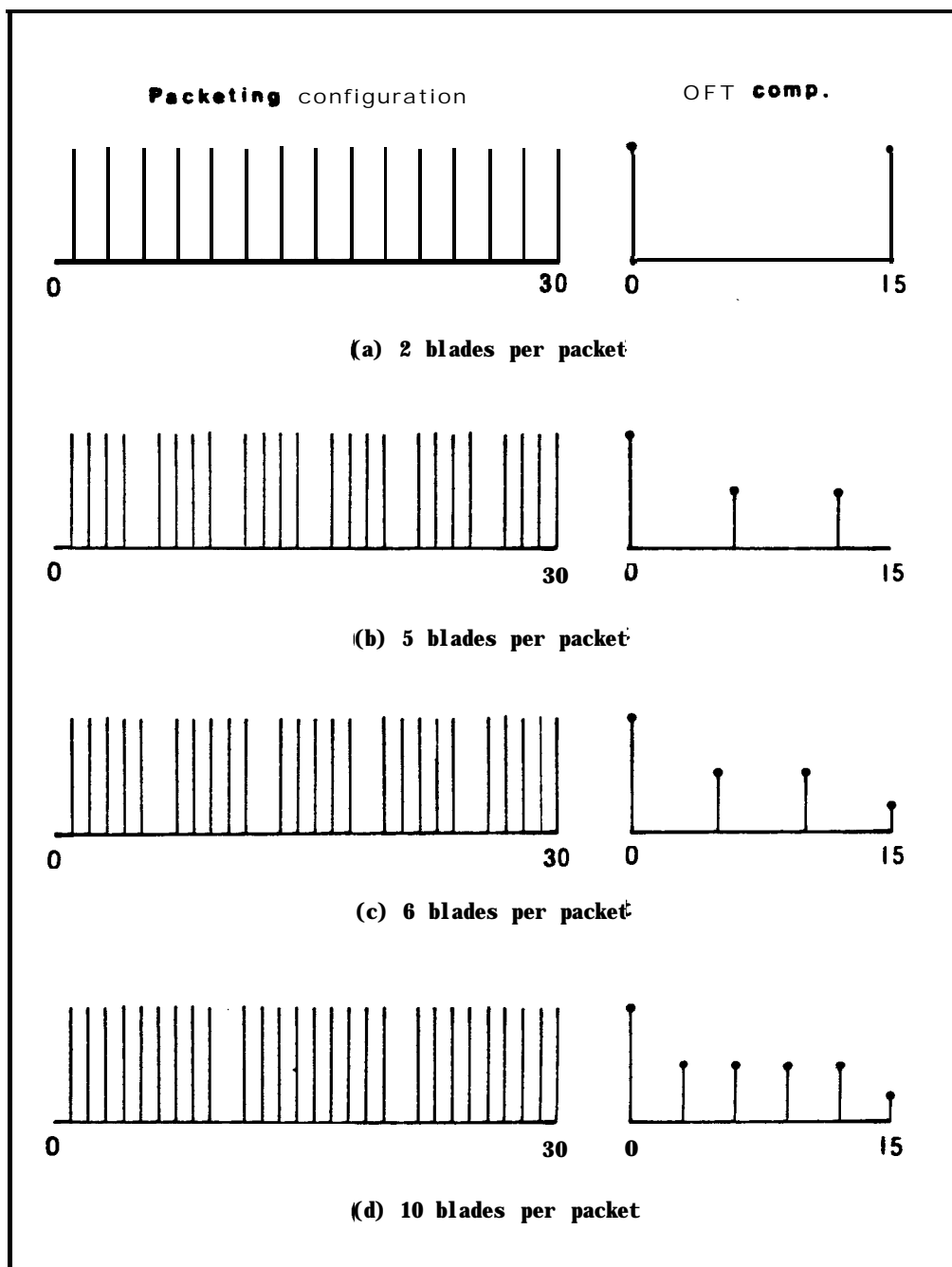
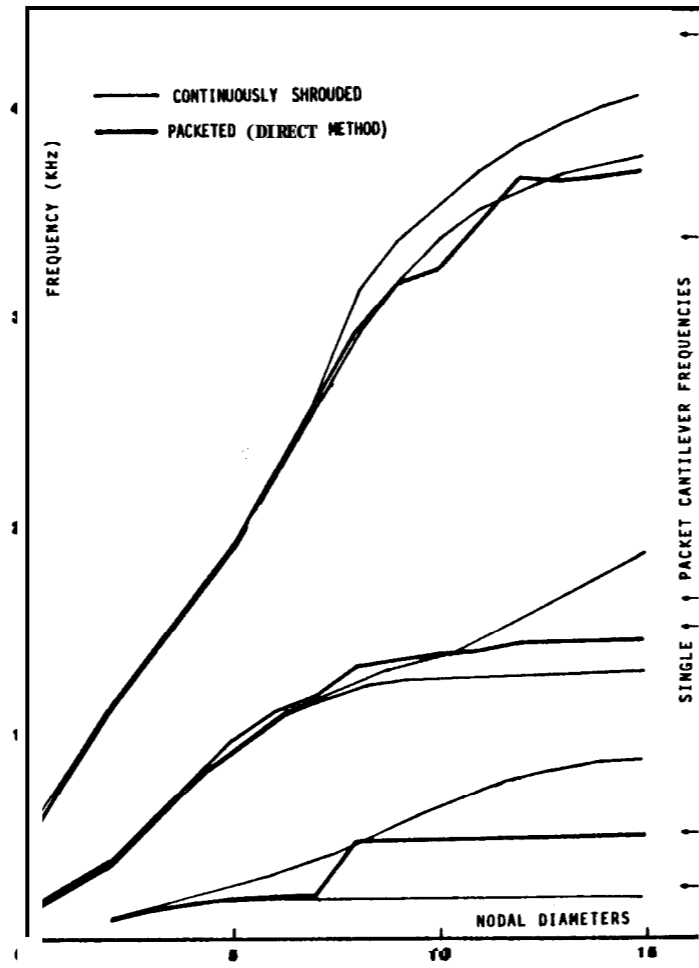


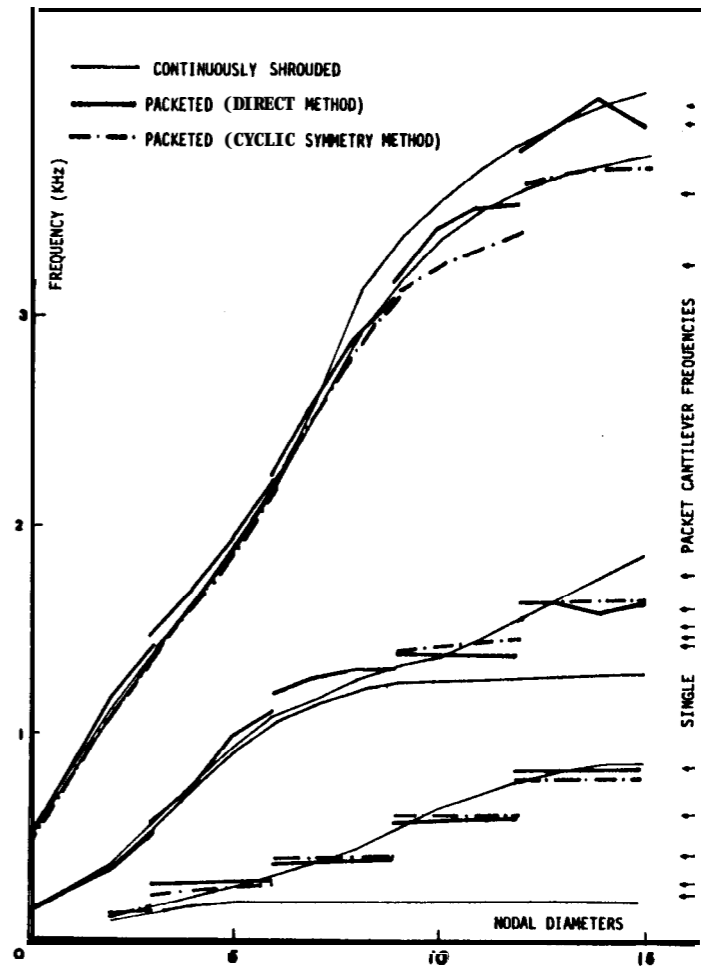
Fig. 4.9 Packeted-bladed disc mode shapes  
(10 packets of 3 blades)



**Fig. 4.10** Various packeting arrangements together with their Fourier series representation



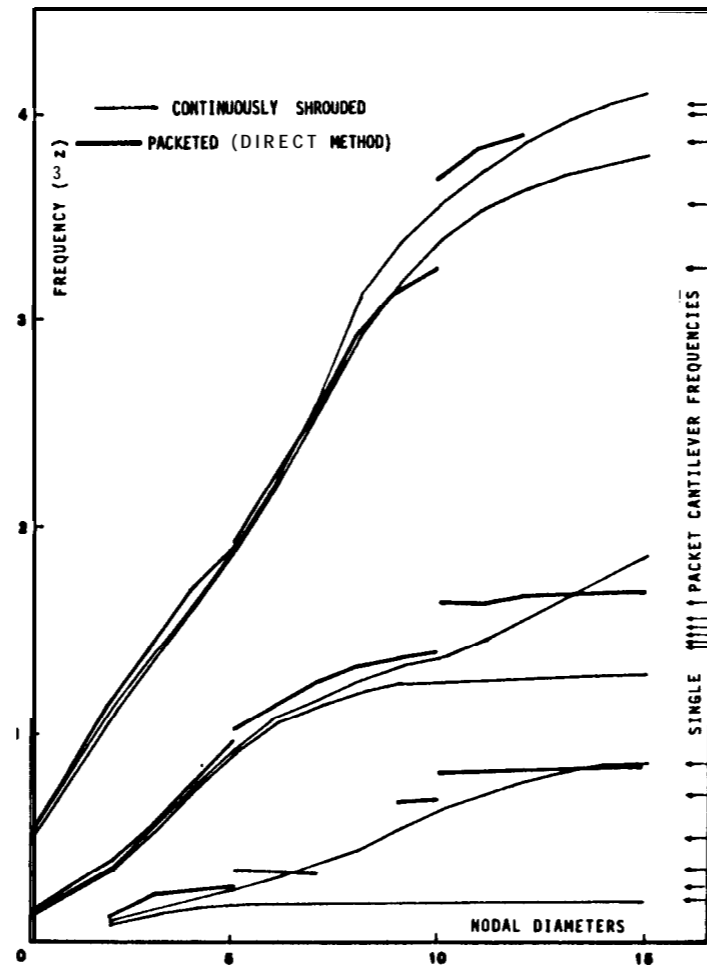
(a) 15 packets of 2 blades.



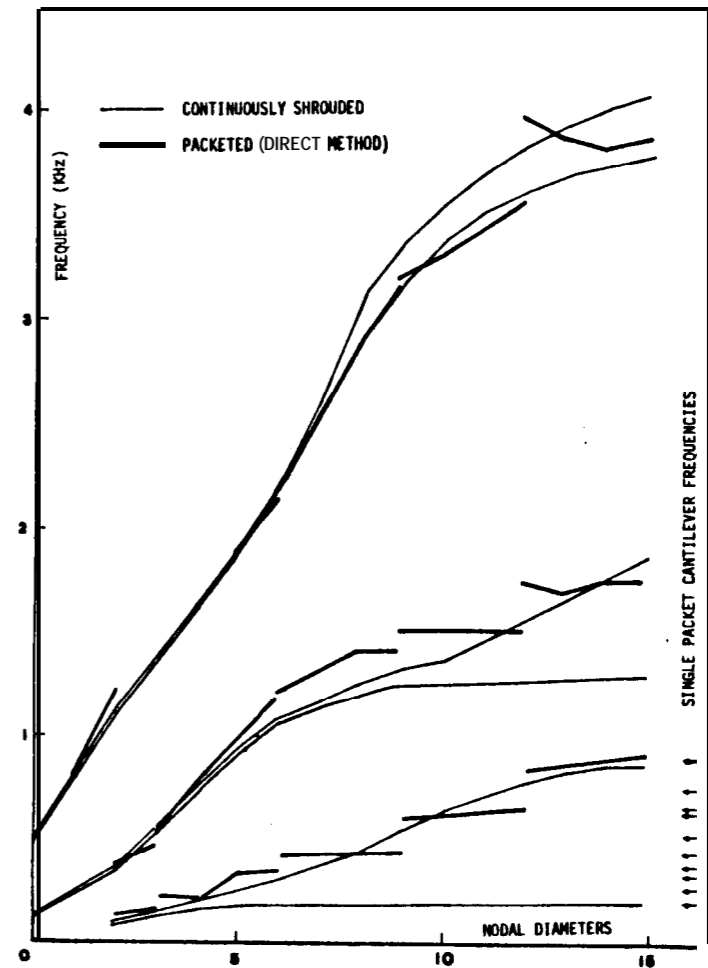
(b) 6 packets of 5 blades

**Fig. 4.11** Natural frequencies of the 30-bladed disc for further packeting arrangements (continued)



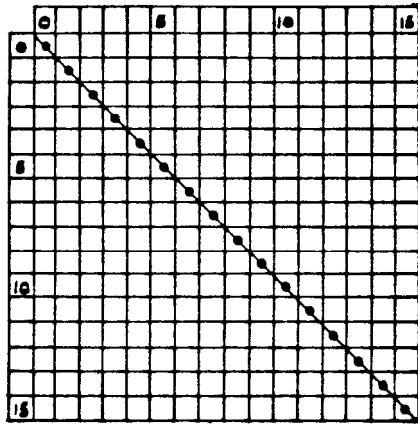


(c) 5 packets of 6 blades

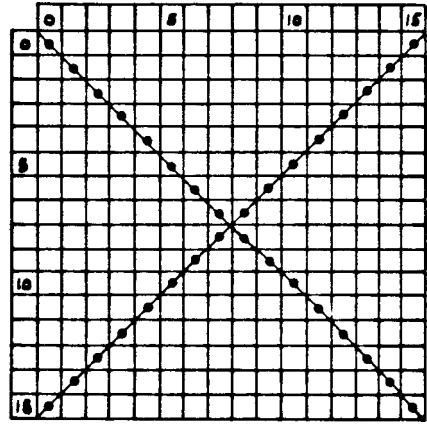


(d) 3 packets of 10 blades

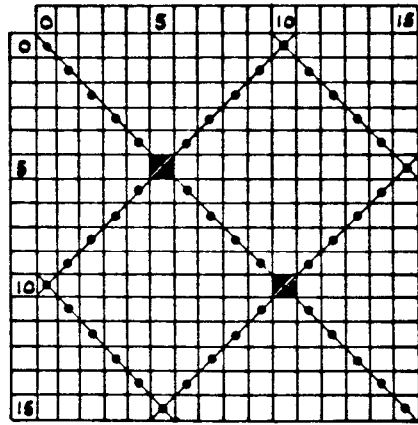
**Fig. 4.11** Natural frequencies of the 30-bladed disc for further packeting arrangements (concluded)



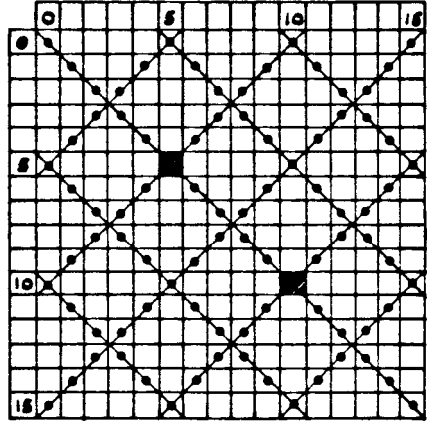
(a) Continuously shrouded



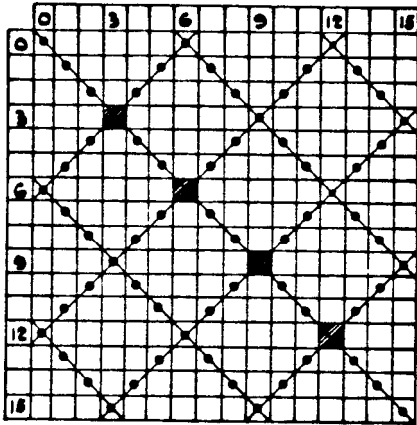
(b) 15 packets of 2 blades



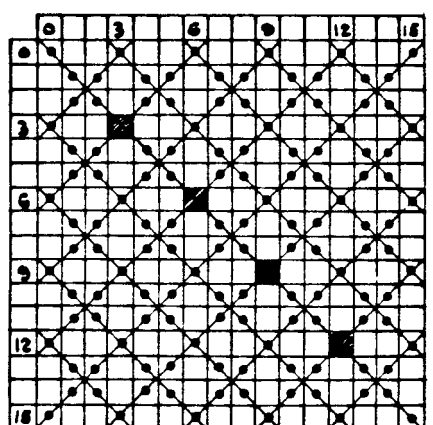
(c) 10 packets of 3 blades



(d) 5 packets of 6 blades



(e) 6 packets of 5 blades



(f) 3 packets of 10 blades

**Fig. 4.12** Modal interference diagrams

## CHAPTER 5

### EXPERIMENTAL PROGRAMME, PROCEDURE AND RESULTS

#### 5.1 OBJECTIVE

Two methods, both based on substructuring, have been proposed for the theoretical analysis of packeted bladed discs and an extensive numerical study of the various packeting arrangements of a 30-bladed disc has been conducted. There is an obvious need to undertake an experimental investigation in order to provide a check on the calculations and observations reported in Chapter 4 and this will be done in the case of the 10-packeted configuration for which computations from both methods can be compared with measurements. The main objective of this exercise is to check whether the two receptance coupling programs, MULPAC and SINPAC, can fulfil their purpose of predicting the assembly's natural frequencies and mode shapes reliably and accurately.

#### 5.1 GENERAL PROCEDURE

##### 5.2.1 Testpiece

As can be seen from Fig. 5. 1, the testpiece used is a plane disc with 30 uniform unstaggered blades grouped into 10 identical packets. The relevant dimensions and material properties are listed in Tables 2. 1 and 4.1. The experimental model was designed so as to match the analytical

model as closely as possible and to this effect it was manufactured as a single integral component from a mild steel plate, except where the shroud arcs were attached to form the blade packets. This practice was thought to be warranted to avoid introducing unknown conditions at the blade roots since the root flexibility is known to have a crucial bearing on bladed disc vibration [Ref. SD-251 and this complication is outside the scope of the present analysis.

### 5.2.2 Description of the Apparatus and Experimental Procedure

The apparatus used in the experimental investigation was arranged as shown in the schematic diagram of Fig. 5.2. During the experiments, the testpiece rested on a partially inflated automobile inner tube and the foundations were isolated from all unwanted noise disturbances. The structure was excited <sup>axially</sup> via an electro-magnetic shaker at a point near the disc rim while the response was measured at the blade tips using an accelerometer. The position of the shaker had to be changed several times because it happened to be on or near a nodal line of particular modes which could then not be properly excited. The experiments were carried out in two phases.

- (1) First, the natural frequencies of the structure were located using white noise excitation and processing the response signal through a digital spectrum analyser. This technique produced with a reasonably accurate description of the natural frequency locations within the 80 - 4000 Hz range,
- (2) Next, a sinusoidal excitation was used throughout the second phase for all frequency response function measurements. A fine resolution about the suspected resonances ensured the accurate determination

of the natural frequencies. The modal shapes were then identified using sand which, as shown in Fig. 5. 1. settled on nodal lines. Also, for checking against theoretical predictions. a few mode shapes were determined accurately by measuring the response at the tip of each blade.

### 5.3 RESULTS

All measured frequencies together with the corresponding theoretical predictions are listed in Table II. 14 of Appendix II and plotted In Fig. 5.3. Also, the tip response of each blade was measured when the disc vibrated in 3 diameters. 0 circles and 10 diameters, 1 circle modes. These measured mode shapes together with their DFTs are compared with the theoretically generated ones in Table II. 15. it should be noted that all mode shapes and their corresponding Fourier transforms are normalized such that the largest element has a value of 100. Table II. 15 Is plotted In Fig. 5.4.

### 5.4 DISCUSSION OF RESULTS

- (i) As can be seen from Fig. 5.3. correlation between theory and experiment is satisfactory with natural frequency errors rarely exceeding 5% and usually being less than 2%. The average error. defined as the absolute arithmetic mean of individual relative errors. is about 3.2% for the direct method and 1. 8% for the cyclic symmetry method. a feature more explicitly shown in Fig. 5.5 where the correlation between predicted and measured values is displayed. The cyclic symmetry method being based on a simplified analysis, this result is somewhat surprising and merits a closer look. As can be seen from Fig. 5.5a. the direct method usually overestimates the natural frequencies. suggesting that the Young's modulus to density

ratio used in the theoretical calculations was too high. These predicted frequencies being on average 3.2% higher than the measured ones, the solid line of Fig. 5.5 was adjusted accordingly. The broken line representing the corrected correlation, it is seen that the direct method yields closer predictions. Further discrepancies between the computed and measured values can be explained as follows:

in the analytical model, the shroud is represented by a series of straight beams joined end-to-end while the testpiece has packets formed by circular arcs attached at the blade tips:

as shown in Fig. 5.6. the shroud attachment causes radial blade stresses, a phenomenon which has not been allowed for in the analytical model;

as the hole in the shroud was considerably larger than the Allen screw diameter. a certain amount of slip between the blade tip and the inner shroud surface was inevitable. This was partly remedied by cementing the tip connection but it was believed that some motion was still possible, especially in radial rotation. It will be recalled from Chapter 3 that blade tips and shroud segments are rigidly connected in the analytical model, this being imposed by compatibility equations.

- (ii) Some modes of vibration are missing from Table II. 14 and Fig. 5.3. These fall into two distinct categories:
  - (a) although the force into the structure was applied at various points to avoid any possible nodes, certain modes of vibration could not be excited at all;
  - (b) some very closely-spaced natural frequencies were located in the frequency sweep but the associated modal shapes could not be identified because of the heavy interferences from the neighbouring modes. This particular problem arose each time the assembly's natural frequencies were expected to approach a cantilever frequency of the single

packet. The frequency response function shown in Fig. 5.7a indicates the presence of 5 modes near the packet cantilever frequency predicted at 707 Hz. Out of these, only 2 modes, namely the 11 and 12 nodal diameter ones, were identified during the second phase using sinusoidal excitation and entered in Table II. 14. A further example, this time for the second family, is given in Fig. 5.7b.

- (III) As can be seen from Fig. 5.4, the correlation between predicted and measured mode shapes is as good as can be expected within experimental accuracy. The 3 diameters, 0 circles mode at 154.8 Hz being very close to the 0 diameter, 0 circle mode at 143.0 Hz, the effect of that latter (umbrella mode) on the measured response is significant and results in a shift which accounts for the constant Fourier term being the largest. Otherwise, it is clearly seen that the 3 nodal diameters mode has also components of order 7 and 13, a feature correctly predicted by the modal interference diagram of Fig. 4. Similarly, the 10 diameters, 1 circle mode includes a term of order 0.

#### 5.5 CONCLUDING REMARKS

Two methods have been developed to compute the natural frequencies of a packeted bladed disc. Both give very similar results and these in turn compare well with the measurements made on a physical testpiece.

Further, it is confirmed experimentally that the packeted bladed disc modes are complex in shape, always having more than one diametral component. However, all modal shapes identified exhibited a dominant nodal diameter number, contributions from the others being negligible.

This suggests that the cyclic symmetry model, together with the modal Interference diagrams, is adequately representative of tuned packeted bladed assemblies.

All results were found to be within the expected experimental accuracy and no contradictory behaviour towards the theory outlined in Chapter 4 was encountered.



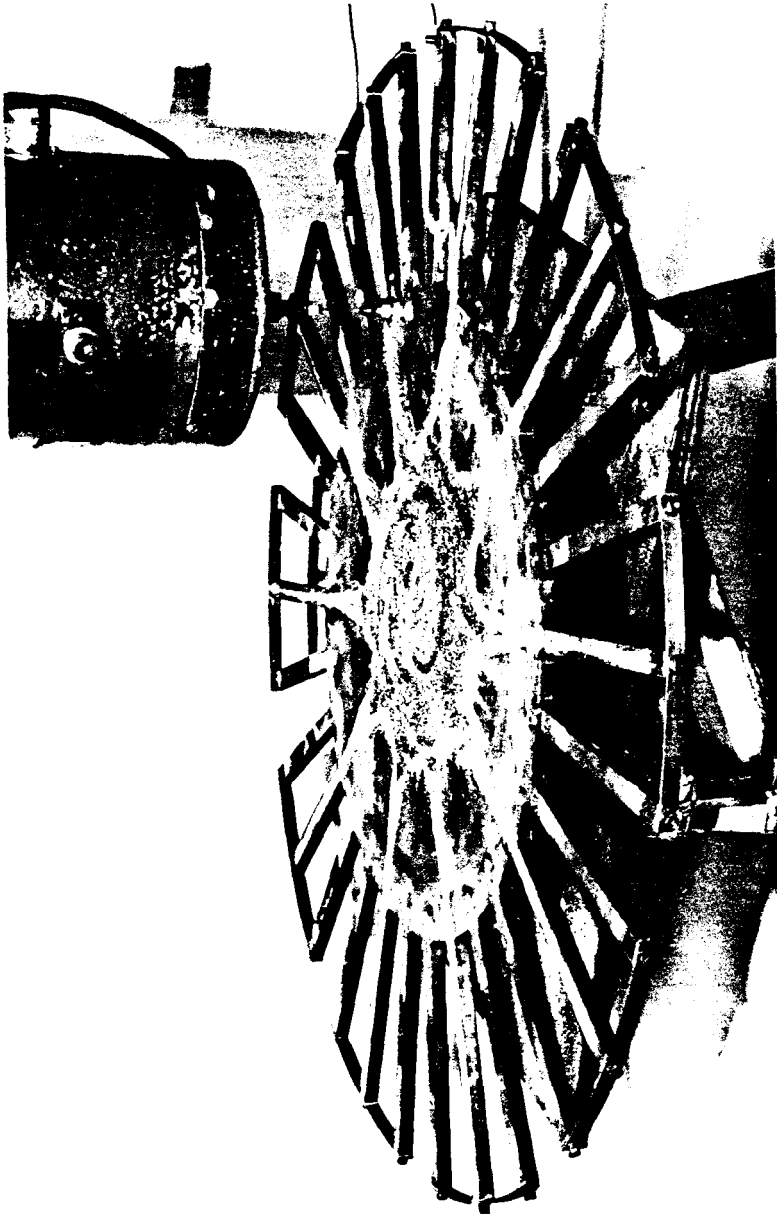


Fig. 5.1 Test structure

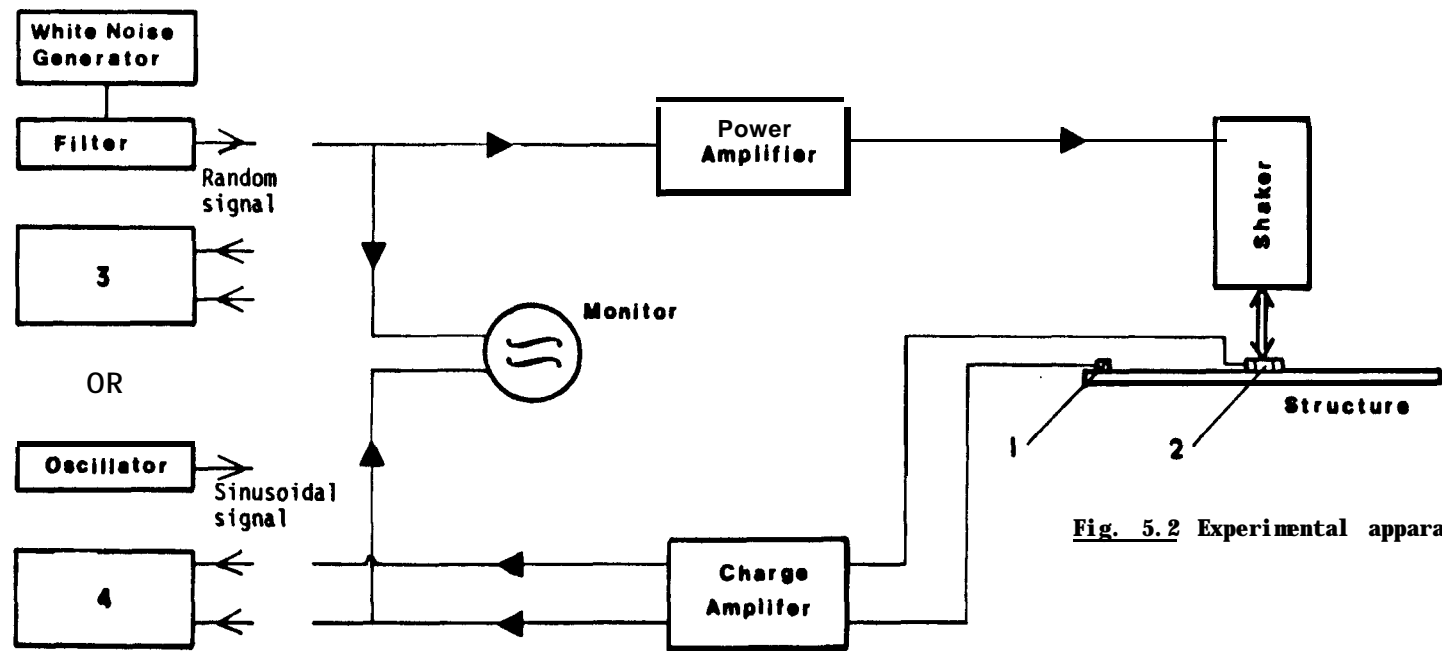


Fig. 5.2 Experimental apparatus

- (1) Bruel & Kjer type 4344 accelerometer
- (2) Bruel & Kjær type 8200 force gauge
- (3) Hewlett-Packard Digital Signal Analyser 5420A
- (4) Solatron 1170 Frequency Response Analyser

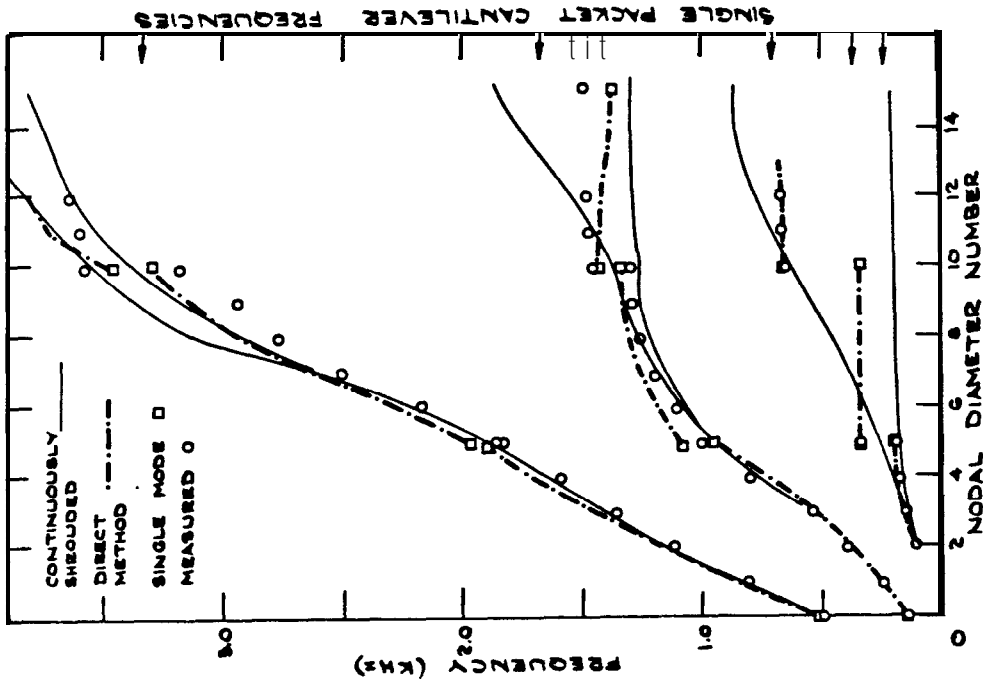
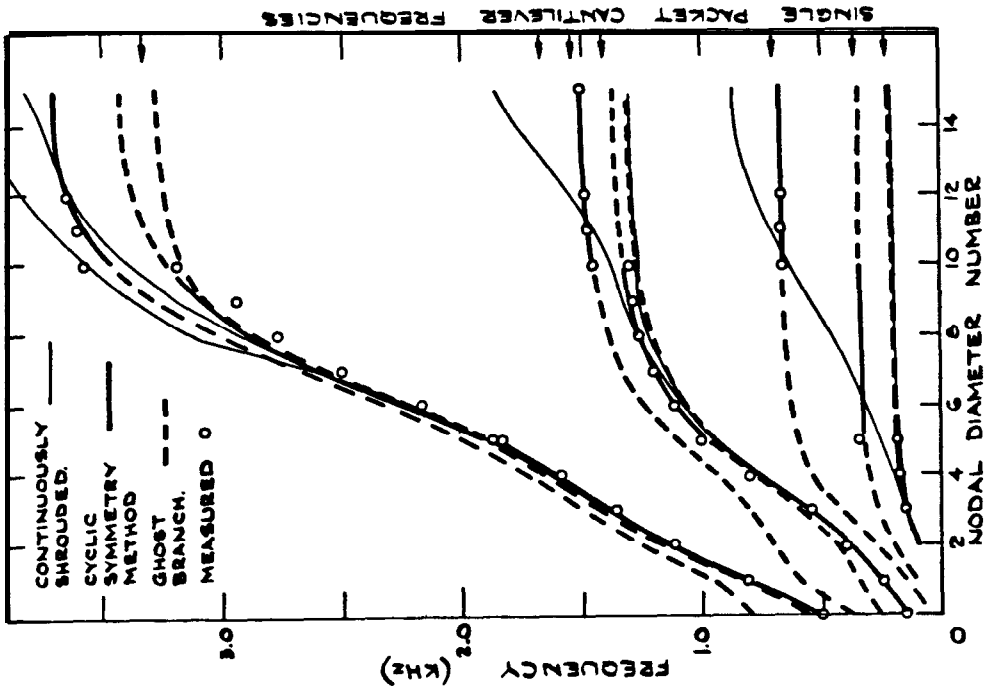
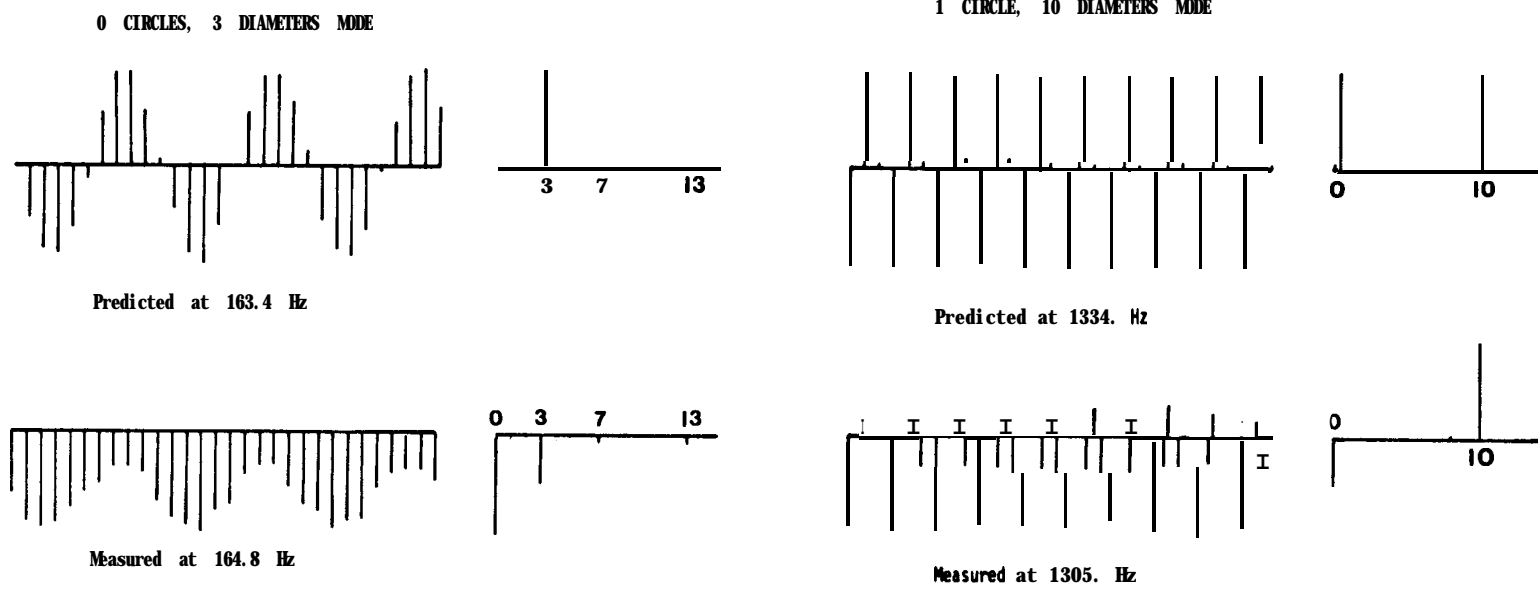
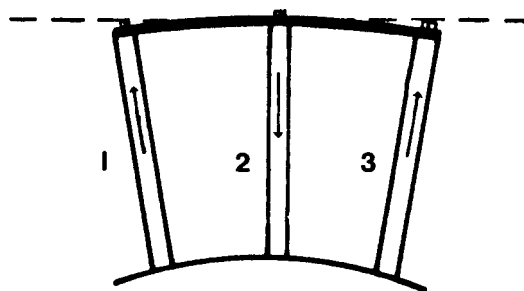


Fig. 5.3 rison of theoretical and experimental results



**Fig. 5.4 Predicted and measured mode shapes together with their DFT**



**Fig. 5.6 Radial stresses in the blade packet**  
 Note that blades 1 and 3 are in tension while blade 2 is in compression.

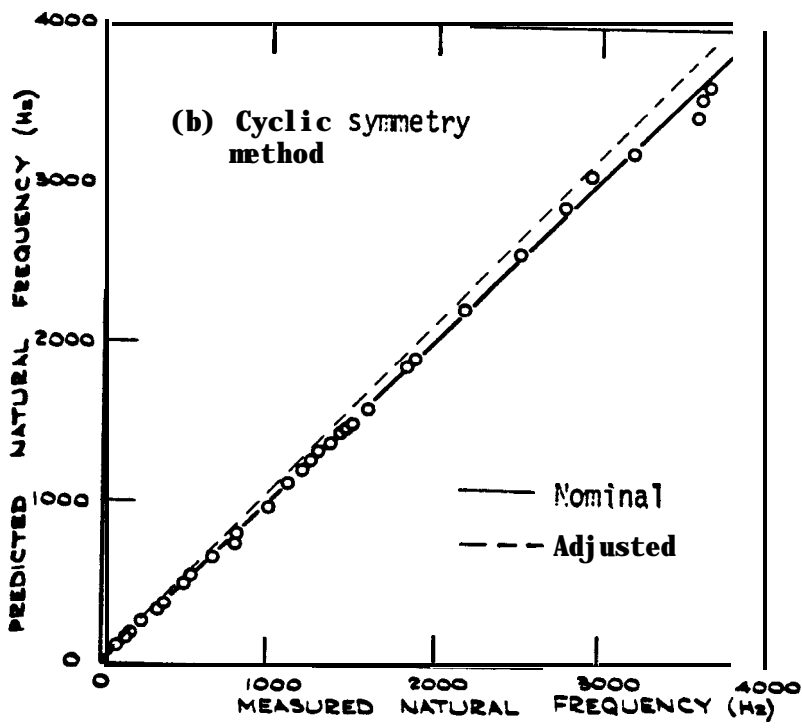
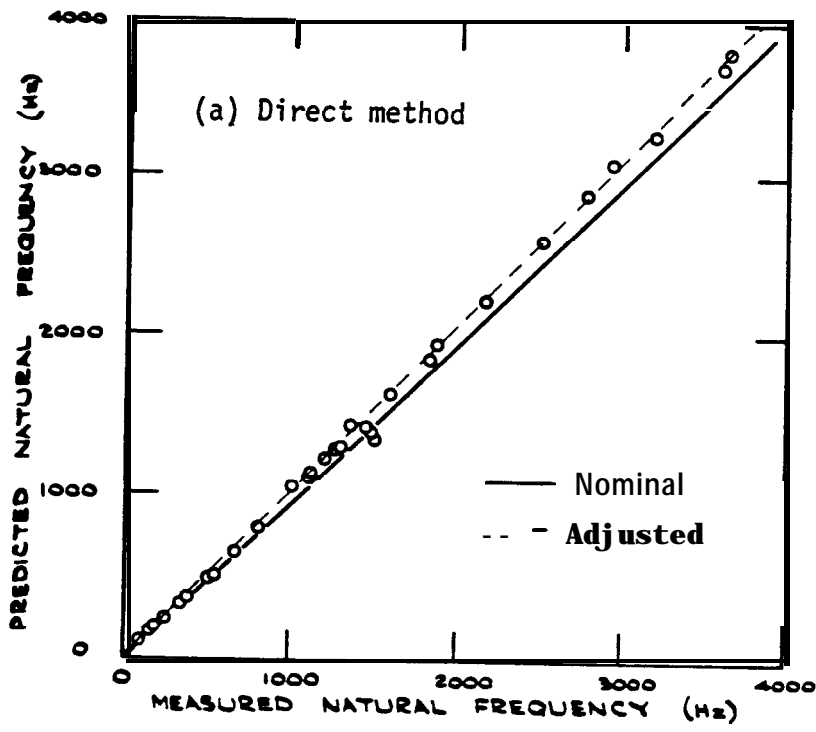
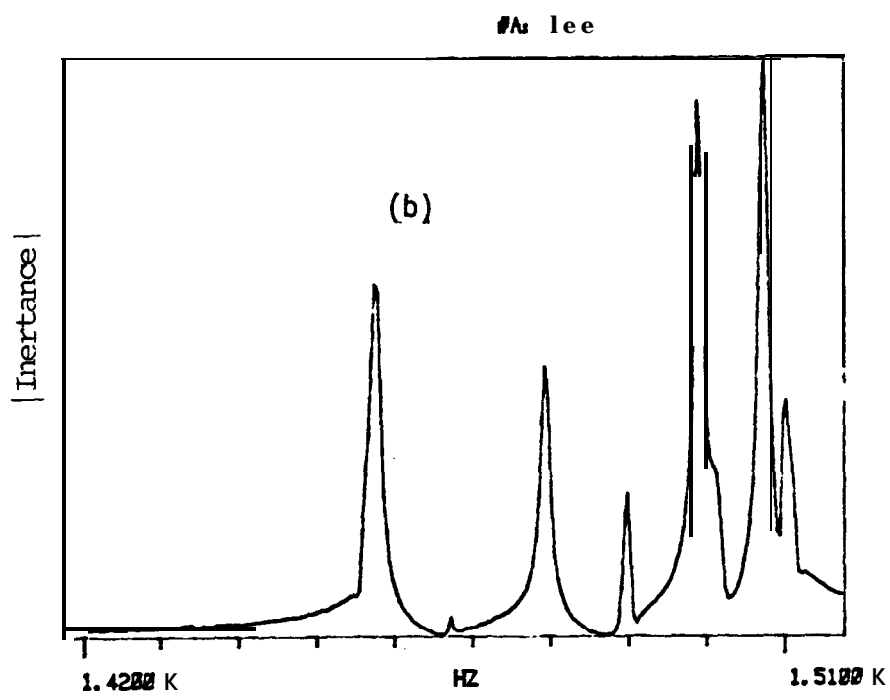
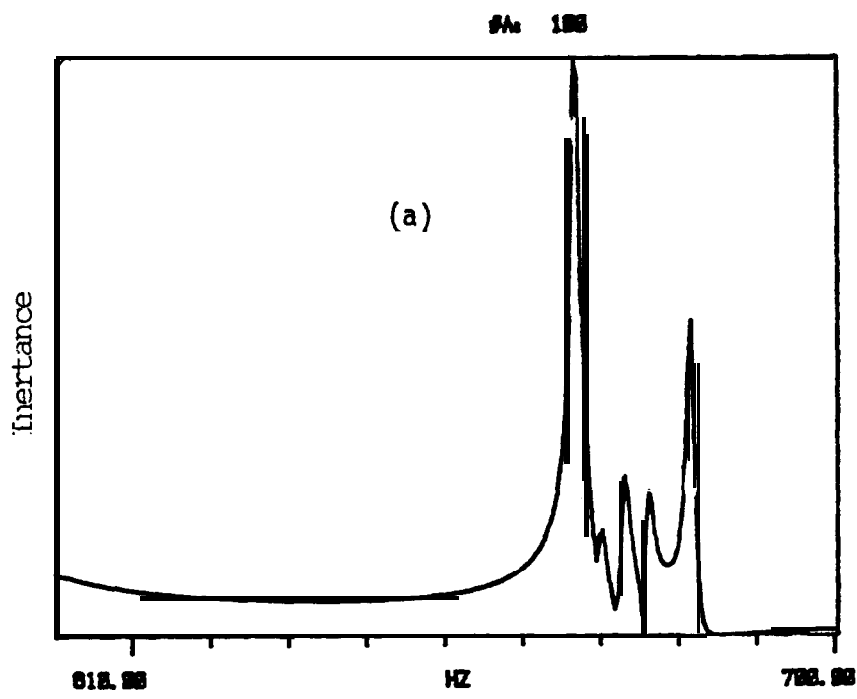


Fig. 5.5 Correlation between predicted and measured natural frequencies



**Fig. 5.7 Measured frequency response curves in the neighbourhood of single packet cantilever frequencies**

## CHAPTER 6

### **LUMPED PARAMETER ANALYSIS OF PACKETED BLADED DISCS**

Although two satisfactory analytical models based on receptance coupling have been developed and used with success to predict the packeted bladed disc behaviour quantitatively, these cannot be put in use to conduct parametric studies in view of the computational effort required. There is an obvious need to devise a simpler and more economical model yielding qualitative results for standard bladed disc analyses such as blade mistuning and forced response levels. The main purpose of this chapter is to demonstrate that the lumped parameter technique, successfully used in the case of continuously-shrouded discs, is also applicable to packeted configurations. Although some numerical examples will be given, this is by no means an attempt to a parametric study.

#### 6.1 LUMPED PARAMETER MODEL

In the original lumped parameter model of a compressor rotor proposed by Dye and Henry [Ref. SD-131], a single mass was used to represent the blade while the sectorial mass of the disc was lumped at the root. An improved version of this model, in which the blade is modelled via two lumped masses, was developed by Afolabi [Ref. SD-261] to investigate the effects of random mistuning on the vibration of coupled turbomachine blades. His work has now been extended to incorporate blade packets

and the model used is shown in Fig. 6. 1.

The equations of motion for the  $j^{\text{th}}$  blade can be written as:

$$\begin{aligned}m\ddot{x}_j - sx_{j-1} + (k+2s)x_j - sx_{j+1} - ky_j &= 0 \\M\ddot{y}_j - Sy_{j-1} + (K+k+2S)y_j - Sy_{j+1} - kx_j - Kz_j &= 0 \\W\ddot{z}_j - hz_{j-1} + (K+g+2h)z_j - hz_{j+1} - Ky_j &= 0\end{aligned}\tag{6-1}$$

where all symbols used are defined in Fig. 6.1. Assuming simple harmonic motion. the analysis is reduced to the following linear eigenvalue problem of order  $3N$ :

$$([\mathbf{K}] - \omega^2[\mathbf{M}]) \{\mathbf{q}\} = 0\tag{6-2}$$

where  $N$  is the number of blades on the disc, and  $E, I, [M], \omega$  and  $\{q\}$  have their customary meaning.

## 6.2 Numerical Study

LUMPAC, a computer program based on Afolabi's original. was written and used for the numerical study.

### 6.2. 1 Derivation of the Model Parameters

The actual values of the lumped mass and stiffness parameters used in the model above can be derived for any given bladed disc by using a semi-empirical method described in Ref. SD-26. for the 30-bladed disc. these values were computed as follows:



- 1) The total mass ( $M_D$ ) of the blade was divided into two masses  $m$  and  $M$  such that:

$$m + M = (M_D) \quad (6-3)$$

$$m = aM$$

- 2) If the first two cantilever frequencies of an Individual blade are 1CF and 2CF, the blade springs  $k$  and  $K$  can be determined from the two-degree-of-freedom cantilever model illustrated in Fig. 6.2. It can be shown that:

$$K = M [G + \sqrt{G^2 - 4H(1 + a)}] / 2 \quad (6-4)$$

$$k = aGM^2/K$$

$$\text{where } G = (1CF)^2 + (2CF)^2 \text{ and } H = (1CF)^2 (2CF)^2$$

- 3) If the total mass of the disc alone is ( $M_D$ ), the sectorial mass  $W$  is given by:

$$W = (M_D)/N \quad (6-5)$$

where  $N$  is the total number of blades.

- 4) The disc model stiffnesses  $h$  and  $g$  are determined using a curve-fitting technique. Let  $\omega_2$  and  $\omega_3$  denote the natural frequencies of the unshrouded disc for the 2 and 3 nodal diameter modes respectively. By setting the shroud stiffnesses  $s$  and  $S$  to zero and assuming values for the disc stiffnesses  $h$  and  $g$ , the natural frequencies of the 2 and 3 diameter modes are forced to converge towards  $\omega_2$  and  $\omega_3$  while the higher modes are expected to approach the first cantilever frequency asymptotically.
- 5) The shroud springs are determined in the same way, using this time the natural frequencies  $\omega^{(s)}$  of the continuously-shrouded disc.

The model parameters of the 30-bladed disc are listed in Table 6.1.

$(M_D)$ = .35 Kg	$m$ = .115 Kg
$a$ = .5	$M$ = .321 Kg
$(M_D)$ = 21.6 Kg	$w$ = .720 Kg
$1CF$ = 262. Hz	$k$ = ,317 x $10^6$ N/m
$2CF$ = 1640. Hz	$K$ = 24.171 x $10^6$ N/m
$\omega_2$ = 102. Hz	$h$ = 2.6 x $10^6$ N/m
$\omega_3$ = 151. Hz	$g$ = 60.0 N/m
$\omega^{(s)}_9$ = 556. Hz	$s$ = 5.000 x $10^5$ N/m
$\omega^{(s)}_{15}$ = 866. Hz	$s$ = 8.000 x $10^5$ N/m

Table 6.1 Model parameters for the 30-bladed disc

### 6.2.2 Case Studies

The following is a list of cases studied using LUMPAC :

- (i) a single packet comprising three cantilevered blades,
- (ii) the disc with a uniform continuous shroud,
- (iii) the disc with a non-interlocking shroud,
- (iv) the disc with 10 packets of 3 blades.

All cases above were run with the parameters given in Table 6.1 except for (i) where  $h$  and  $g$  were set to  $10^{20}$  and for (iii) where  $S=0, s=200$  N/m and  $m=.146$  kg. Results are listed in Tables II. 11. II. 12 and II. 13 and plotted in Fig. 6.3. As can be seen from Figs. 4.8 and 6.3. there is excellent qualitative agreement between the two approaches used and hence It can be stated that the lumped parameter formulation is adequately representative of bladed disc systems if quantitative analysis is of no primary importance. The investigation of the forced response

levels. for which a global picture of a qualitative nature is usually satisfactory. can therefore be carried out on this simplified model to economize on computational effort. This idea will be developed in the next section.

## 6.3 FORCED RESPONSE CALCULATIONS

### 6.3.1 Basic Theory

The equation of motion for forced harmonic vibrations is:

$$[[K] - \omega^2 [M]] \{q\} e^{i\omega t} = \{F\} \quad (6-6)$$

where  $\{q\}^T = \{ \dots, x_j, y_j, z_j, \dots \}$

$$\{F\}^T = \{ \dots, F_{xj}, F_{yj}, F_{zj}, \dots \}$$

and  $x_j, y_j$  and  $z_j$  are the  $j^{\text{th}}$  blade deflections at the tip, the clapper point and the root; and  $F_{xj}, F_{yj}$  and  $F_{zj}$  the forces applied at these locations in the same order. It can be shown that:

$$F_{xj} = F_j = F_0 e^{ir[nt + 2\pi(j-1)/N]} \quad (6-7)$$

where  $r$  is the engine order of the excitation,  
 $N$  the total number of blades,  
 $F_0$  an arbitrary constant,  
 $t$  the time,  
 $n$  the rotational speed.

For the sake of clarity. It has been assumed that the external forces are applied at the blade tips only. Remembering that  $rn = \omega$ , the frequency of vibration, equation (6-7) reduces to:

$$P_j = P_0 e^{2\pi i r(j-1)/N} \cdot e^{i\omega t} \quad (6-8)$$

which combined together with equation (6-6) yields a response vector of the form:

$$\{q\} = [[K] - \omega^2 [M]]^{-1} \{P_0 e^{2\pi i r(j-1)/N}\}_{j=1,N} \quad (6-9)$$

The matrix  $[[K] - \omega^2 [M]]^{-1}$  is simply the receptance matrix of the bladed system which can also be expressed as:

$$[[K] - \omega^2 [M]]^{-1} = [\alpha(\omega)] = [\phi] [\Lambda] [\phi]^T \quad (6-10)$$

where  $[\phi]$  is the eigenvector matrix from the free vibration analysis and  $[\Lambda]$  is a diagonal matrix whose  $(j,j)$  element is of the form  $(\lambda_j - \omega^2)^{-1}$ ,  $\lambda_j$  being the  $j^{\text{th}}$  eigenvalue from the free vibration analysis. Substituting equation (6-10) into equation (6-9) gives the final form for the response vector:

$$\{q\}_{3N \times 1} = [\phi]_{3N \times R} [\Lambda]_{R \times R} [\phi]^T_{R \times 3N} \{P\}_{3N \times 1} \quad (6-11)$$

where  $R$  is the number of modes to be included in the modal summation.

### 6.3.2 Case Study

A 5<sup>th</sup> engine order (5EO) excitation was applied to both continuously-shrouded and packeted assemblies and the response curves, computed at the tip of the middle blade in the packet, are shown in Fig. 6.4. The frequency range for which calculations were made includes up to six nodal diameter modes of the first family of the continuously-shrouded

wheel and it is clearly seen that the 5EO excitation generates a response in the five-diameter mode only. This is a well-known result for tuned systems [Ref. SD-I 81.

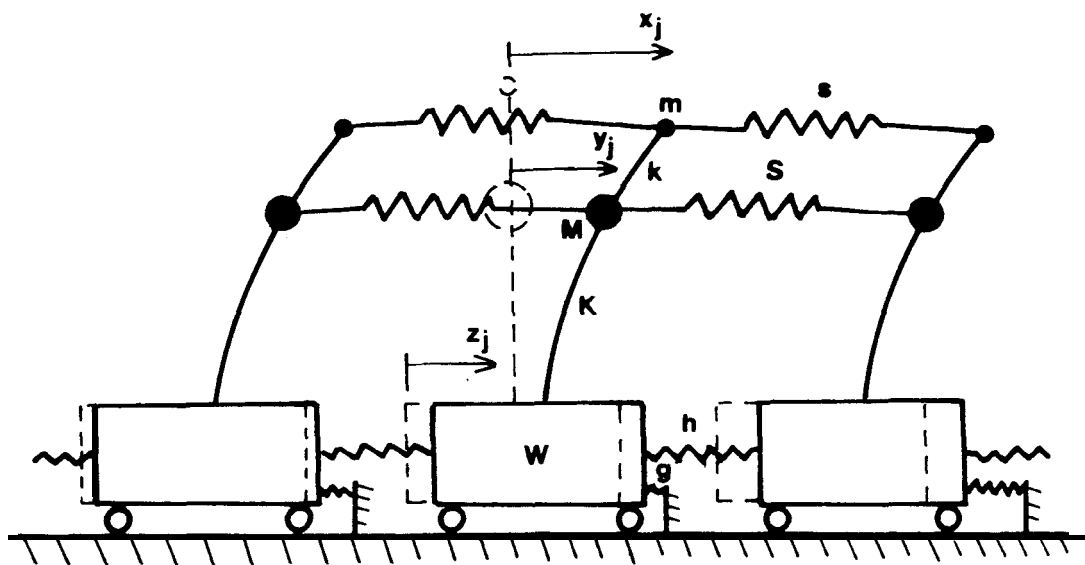
The presence of gaps in the shroud disturbs the cyclic symmetry for the five-diameter mode which splits into two single modes, both of which are susceptible to 5EO excitation. The third resonance at 332 Hz occurs at another single five nodal diameter mode. This time belonging to the second family. Hence the packeting is seen to have the effect of bringing additional modes into excitation and this feature should be duly considered at any design stage.

#### 6.4 CONCLUDING REMARKS

Both the receptance coupling and the lumped parameter methods yield the same qualitative results, showing that the latter can adequately represent bladed disc systems provided no quantitative predictions are required. The implications of this are threefold:

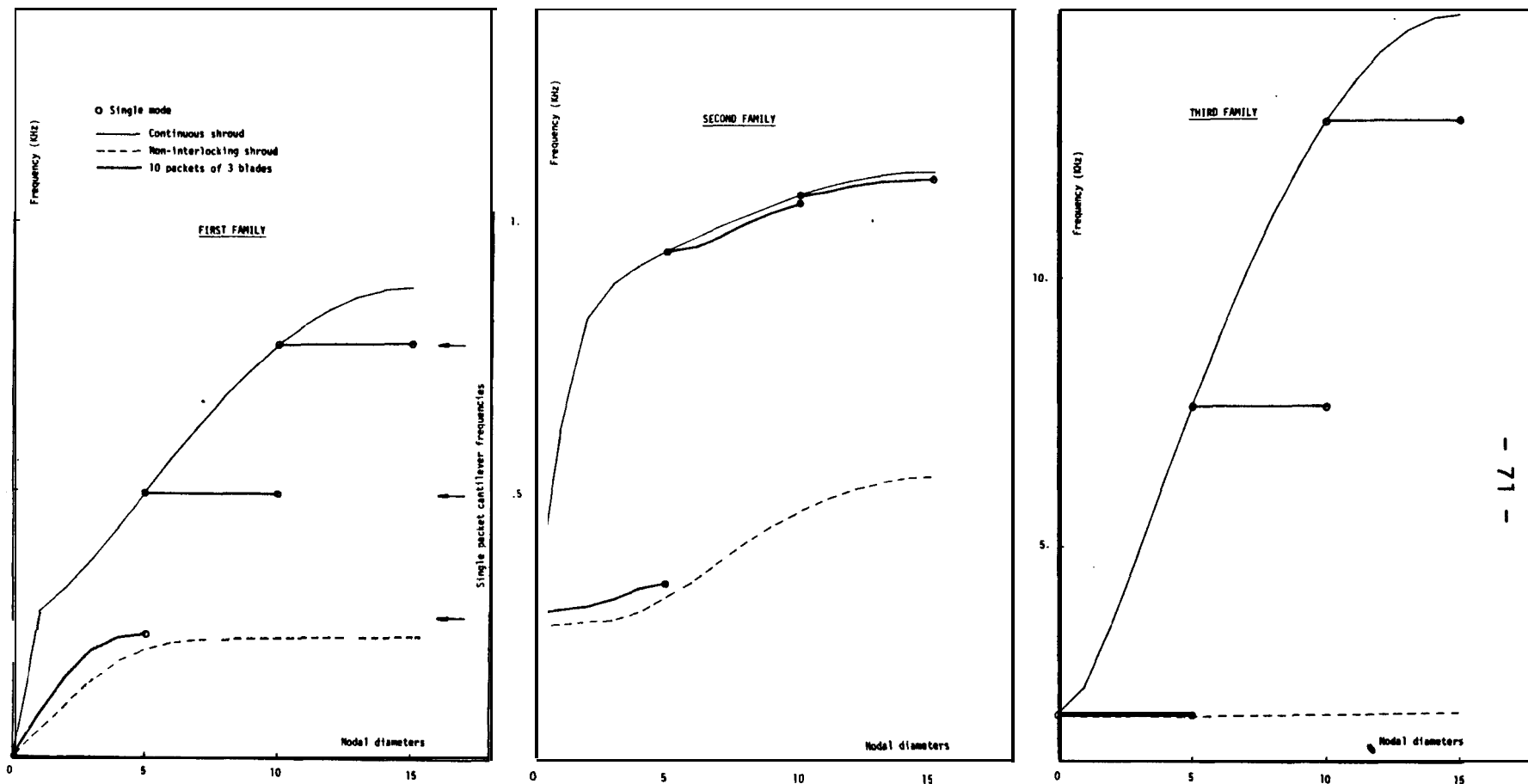
- (i) several important aspects of packeted bladed disc vibration, such as asymmetrical packeting arrangements, importance of individual blade tunes, root-flexibility effects, influence of various parameters on forced response levels etc. , can be investigated without requiring a prohibitive computational effort:
- (ii) other results, experimental or theoretical, can be checked to see whether they are within the bounds of the expected qualitative behaviour:
- (iii) the lumped parameter method can also serve as a reliable structural basis to a first generation of aeroelastic models

yielding qualitative stability predictions. This will be discussed  
In Chapter 8.



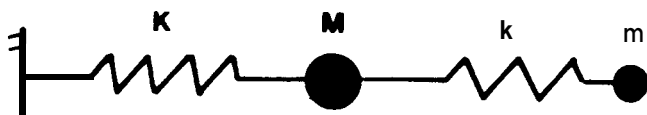
**Fig. 6.1** Lumped parameter model of a three-bladed packet

- $x_j$  Tip deflection of  $j^{\text{th}}$  blade,
- $y_j$  Clapper point deflection of  $j^{\text{th}}$  blade,
- $z_j$  Root deflection of  $j^{\text{th}}$  blade;
  
- $m$  Blade mass between tip and clapper point,
- $M$  Blade mass between root and clapper point,
- $W$  Mass of disc sector,
- $s$  Upper shroud stiffness,
- $S$  Lower shroud stiffness,
- $k$  Stiffness between tip mass and clapper mass,
- $K$  Stiffness between clapper mass and disc sector,
- $h$  Sectorial disc stiffness,
- $g$  Grounding stiffness.

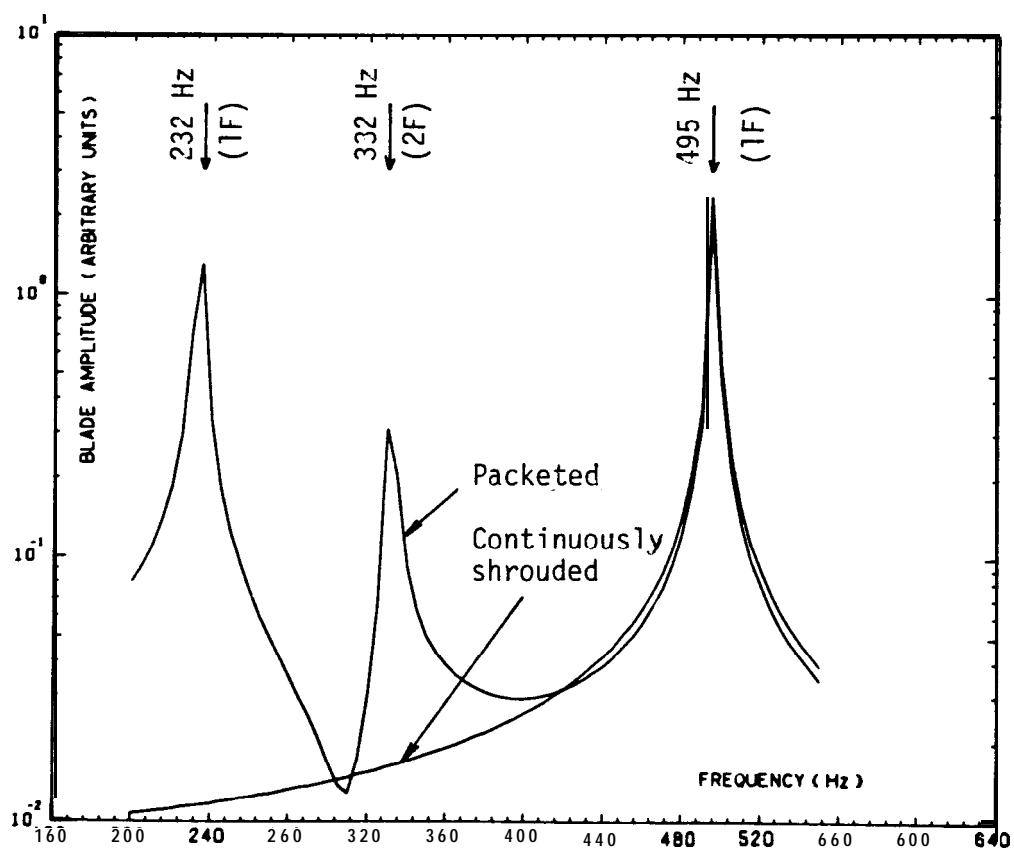


**Fig. 6.3** Natural frequencies of the 30-bladed disc





**Fig. 6.2** 2 DOF cantilevered blade model



**Fig. 6.4** Response of the continuously-shrouded and packeted assemblies to 5E0 excitation

## CHAPTER 7

### CONCLUSIONS

#### 7.1 SUMMARY OF CONCLUSIONS OF PRECEDING CHAPTERS

The work described in the first part of this thesis represents an effort to rationalize the vibrational behaviour of packeted bladed discs. To this end, several independent analytical models have been formulated to study both qualitative and quantitative aspects of the problem and some of the theoretical findings have been checked experimentally. With respect to the models used, it is found that:

- (i) In the case of a stiff disc with relatively flexible blades grouped into identical packets, the cantilevered packet (finite element) model is adequate for determining the natural frequencies and mode shapes of the whole assembly. In any event, this model is particularly useful if only in-plane vibrations are of interest.
- (ii) The direct method (receptance coupling) is a general packeted bladed disc analysis tool, capable of dealing with asymmetric arrangements and/or individual blade mistuning. However, due to restrictions on Central Memory storage, its use is limited to relatively small blade numbers.
- (iii) The cyclic symmetry method (receptance coupling) is ideally suited for studying bladed discs with symmetrical packeting arrangements. It is applicable to any number of blades and requires less computational effort than the direct method.

- (iv) Used in the case of a 30-bladed disc. the models in (ii) and (iii) above gave very similar results which in turn compared well with the experimental measurements on a physical testpiece. The implications of this are twofold: firstly. receptance coupling is fully capable of analysing packeted bladed systems and secondly. correct choice of coupling co-ordinates at the blade root was made.
- (v) A lumped parameter study of the same disc showing very good qualitative agreement with the previously-obtained results. it is concluded that this model is adequately representative of packeted bladed disc assemblies provided quantitative analysis is of secondary importance. An immediate application area is the investigation of the response levels due to forced vibration where only a global picture of a qualitative nature is required.
- (vi) Packet receptances derived from a finite element eigensoiution can be substituted into the basic models (ii) and (iii) to incorporate more complex blade geometries. Although the basic steps of this relatively new technique have been established. some difficulties in both finite element modelling and the truncation of the modal series are anticipated in view of the slightly different results obtained when using simple beams.

Although this particular study was conducted for a 30-bladed disc, it is the author's conclusion that the methods of analysis are general and applicable to any packeted bladed assembly and some of the results obtained are representative of universal bladed disc behaviour. it is found that:

- (i) The natural frequencies of a cantilevered blade packet are grouped into families. each exhibiting a number of modes equal to the number of blades in the packet. The lowest natural frequency in each family corresponds to a blade cantilever

frequency and its limiting value can be estimated by allowing for some concentrated mass and inertia at the blade tip due to the shroud.

The in-plane or tangential vibration characteristics of a multi-bladed unstaggered blade packet follow a certain predictable pattern: in each family with  $N$  modes,  $(N-1)$  natural frequencies are grouped together and the  $N^{\text{th}}$  frequency, which is either the lowest or the highest of that family, is somehow isolated. This finding is in agreement with Smith [Ref. SD-41] who reached a similar conclusion using an approximate method. Also, as discussed in Ref. FE-I, the in-plane behaviour of a multi-bladed packet can be deduced from the one of the corresponding two-bladed packet. The out-of-plane or axial vibrations however, do not show a similar trend. The packet's natural frequencies being randomly dispersed between the first and the last frequency in each family.

- (ii) The packeted bladed disc exhibits:
- double modes (i.e. two modes with identical natural frequencies and almost identical mode shapes) which arise from the circular symmetry or;
  - single modes which occur when the cyclic symmetry is destroyed.

The latter fall into two distinct categories: the first contains modes for which the symmetry cannot be maintained in any case. These are common to both packeted and continuously-shrouded assemblies and occur for 0 and  $N/2$  nodal diameters where  $N$  is the total number of blades and even. The second category consists of split double modes for which the circular symmetry has been broken by the presence of packeting. They have two distinct but close natural frequencies and they are both associated with the same nodal diameter pattern.

- (iii) Unlike its continuously-shrouded counterpart, a packeted bladed disc's modes are complex in shape, containing several nodal diameter components. However, diametral components from single modes are coupled only with components from other single modes and the same is true for double modes.
- (iv) Both the modes which split and the modal composition in terms of nodal diameter components can be predicted from the modal interference diagrams introduced in this work.
- (v) As for the continuously-shrouded case, the natural frequencies of the packeted bladed disc exhibit the well-known tendency to group into families, each becoming asymptotic to a cantilever frequency of the single packet.
- (vi) Discs with continuous and non-interlocking shrouds can effectively be considered as the two limiting cases of their packeted bladed counterparts. The families from both analyses being very close to each other at low nodal diameter numbers, packeting has no significant effect on the corresponding natural frequency locations. Also, the curves depart from each other with increasing frequency and hence the effects of packeting will be more pronounced on families associated with 0 and 1 nodal circle(s). Furthermore, the first family presents a somewhat distinct feature vis-a-vis the single packet cantilever frequencies: the natural frequency locus can be predicted with reasonable accuracy from knowledge of these former together with the two continuously-shrouded cases.
- (vii) The packeted bladed disc response to engine order excitation always occurs in more than one mode, due to the presence of several diametral components. This feature must be duly considered at the design stage.

## 7.2 LIMITATIONS AND EXTENSION OF THE PRESENT WORK

Although the analytical models were formulated for the more general case of coupled axial/tangential vibrations. both numerical and experimental studies focussed on the out-of-plane analysis. chiefly to illustrate patterns of typical behaviour more clearly. It is suggested that the effects of changing the blade stagger angle are investigated and more coupling co-ordinates at the blade root used if necessary. Due to storage considerations, this can only be done in the case of the cyclic symmetry method which can easily be extended to all possible 6 co-ordinate directions.

The effect of blade root flexibility was totally excluded from the present analysis. This feature can be incorporated into the existing models using translational and rotational springs in the appropriate co-ordinate directions but it is anticipated the cost of such an exercise will be high. The cantilevered packet finite element model is suggested as a starting point. Damping was also excluded from the analysis but it is believed that its inclusion would not bring any significant changes to the results obtained.

Finally, there is an obvious need for more accurate modelling of the blade geometry. This can be achieved via a finite element model. the eigensolution from which can be used to evaluate packet receptances. Although the basic steps of this approach have been established in this study. several difficulties are anticipated in the case of more advanced finite elements. namely the size of the eigenproblem. the reduction techniques which must be employed and the compatibility of a particular element with the analytical disc model used.

*Part II*

**AEROELASTIC ANALYSIS**

## CHAPTER 8

### INTRODUCTION

#### 8.1 THE NATURE OF THE PROBLEM

##### 8.1.1 Aeroelastic Phenomena

The term *aeroelasticity* was first used by aeronautical engineers to describe an important class of problems encountered in aircraft design. It is often defined as a science which involves the mutual interaction between the aerodynamic, elastic and inertial forces which act on the structure. Structural flexibility may not be objectionable in itself or even desirable in some cases but aeroelastic phenomena arise when structural deformations induce additional aerodynamic forces. These additional aerodynamic forces may also produce additional structural deformations which then will cause still greater aerodynamic forces. Such interactions may tend to become smaller and smaller until a condition of stable equilibrium is reached, or diverge and destroy the structure. In spite of the presence of external (aerodynamic) forces applied to the structure, this type of vibrational behaviour is fundamentally different from the one frequently encountered in structural dynamic analysis, namely forced vibration. Referring to the former as self-excited vibration, Ref. AE-1 forwards the following distinction.

*In a self-excited vibration the alternating force that sustains the motion is created and/or controlled by the motion itself; when the motion stops the alternating force disappears.*



***In a forced vibration. the sustaining alternating force exists independently of the motion and persists even when the vibratory motion is stopped.***

A self-excited vibration can also be considered as a free vibration with **negative damping**, and this approach will **be** adopted throughout this work. With positive damping. the damping force does negative work since it is always opposed to the motion, and **hence the** energy is **taken** out from the system. in the case of negative damping, **however**, the damping force (which now is a driving force) does positive work and this results in energy **being** fed into the system and then used to **increase** the amplitude of vibration. With a perfectly **linear** self-excited system. this response would become infinitely larger in time **because** Of the **continuous** energy **input to the** System. in most real structures. **however, the** mechanisms of self-excitation and damping exist simultaneously and separately. thus allowing the system to recover and oscillate about a dynamically changing point of **equilibrium**. This phenomenon IS schematically **illustrated** in Fig. 8. I.

#### 8. 1.2 Types of Flutter

Although more than one type of **self-excited** vibration **due** to **aerodynamic** effects is encountered in practice. this work **will** be restricted to the study of a particular kind, namely **the** flutter of axial turbomachinery blades. Flutter can be defined as the dynamic instability of an elastic body in **a** gas flow. it occurs when the unsteady aerodynamic forces and moments **created** by periodic blade vibrations do positive work on the blade during each cycle and **the** mechanical damping is insufficient to dissipate this work input. Flutter is **most** commonly encountered on bodies subjected to large lateral aerodynamic loads of the lift type. such

as aircraft wings, turbomachinery blades and Venetian blinds. although no research is known to have been done in this last case.

At the outset. two different regimes of flutter must be distinguished: (i) stall flutter with large angles of incidence where there is flow separation from the aerofoil surface: and (ii) classical or unstalled flutter with small angles of incidence where the flow remains attached to the aerofoil surface. The former type is mainly encountered on compressor blades operating at near-surge conditions and will be excluded from this study. A comprehensive review of subsonic stall flutter in axial turbomachines is given in Ref. AE-2. Unstalled flutter has always been a major concern for aircraft wings - but a minor one for turbomachinery blades when operating at relatively low speeds. With the introduction of high-speed jet engines however. the supersonic unstalled flutter became one of the most serious technological problems associated with the fan stage of modern compressors. Two more types of flutter - encountered in practice - are reported in Ref. AE-3 and summarized below:

- transonic (ie. mixed subsonic/supersonic) choke flutter which becomes important when the blade is operating at near-choke conditions;
- A-100 type supersonic torsional flutter which occurs above a threshold level pressure ratio.

Typical flutter boundaries that have been observed on modern compressors are shown in Fig. 8.2. However, this study will be centered on classical or unstalled flutter and when flutter is henceforth referred to, this type is implied.

## 8.2 SURVEY OF PREVIOUS WORK

in most cases. aeroelastic equations are derived by equating (the work done by) the aerodynamic forces and moments to (the work done by) the elastic and inertial ones so that the basic model is usually independent of the flow type until numerical values are required. Hence the survey of previous work on flutter will focus firstly on the evolution of aeroelastic models irrespective of the flow type used and a review of the existing unsteady aerodynamic theories will be given later.

### 8.2.1 Aeroelastic Studies

Although most of the early research work on flutter is related to aeroplane-wing stability and not to turbomachinery blades. the models and techniques used are relevant to the present study and a précis will be given here. Theodorsen [Ref. AE-41 and Theodorsen and Garrick [Ref. AE-5] were the first to approach the bending/torsion flutter problem by considering an aerofoil of finite aspect ratio, moving with small oscillatory amplitudes at constant velocity through an incompressible non-viscous fluid. The aerodynamic forces were determined by considering the problem as one of two-dimensional potential flow. Furthermore. it was assumed that the distributed inertial and geometric properties of the aerofoil could be conservatively represented at a typical section - usually at the 3/4 span - using a lumped parameter technique. The problem was further simplified by considering the system's motion as a combination of the fundamental bending, fundamental torsion and the aileron motion about the hinge line. The aerofoil was then represented by an equivalent typical section of unit span length restrained by springs

against translational and rotational motions. This basic model was later to become a standard textbook feature [Refs. AE-1. AE-6 and AE-71 as well as a basis for a number of subsequent studies [Refs. AE-8. AE-9. AE-10. AE-17. AE-12. AE-13. AE-14. AE-15. ~~AE-16~~], including the present one. The first exact treatment of the bending/torsion flutter is due to Goland [Ref. AE-171 who solved the partial differential equations of motion for a uniform cantilevered bar under known aerodynamic load.

The flow through an axial compressor or turbine stage is much more complicated than the flow past a single aerofoll due to the presence of many blades per stage and. in general. of several stages which introduce severe Interference effects. In view of these complicated interactions between rotor and stator blades. most analyses concentrate on a single blade row: unwrapping an annulus of differential radial height from the flow passage of an axial-flow compressor, fan or turbine produces the two-dimensional cascade flow model which is generally used in turbomachinery studies.

Multi-bladed cascade analysis initiated from the study of wind tunnel interference effects for an Isolated aerofoll situated between two solid walls. This is equivalent to an unstaggered cascade In which all blades are vibrating out-of-phase with each other [Refs. AD-1. AD-2. AD-3 and AD-41. The solution for the generalized cascade was obtained by Lane [Ref. AE-181 who showed that a system of *N identical blades* can be reduced, wlt h no loss of generality whatsoever, into a *single equivalent* blade so long as a linear analysis is permissible. His method was based on discretizing the variation of the interblade phase angle to N equally spaced values within the interval  $10. 2\pi$  and this technique is now a

standard feature for most two-dimensional cascade studies including the present one [Refs. AE-8, AE-11, AE-12, AE-13, AE-14, AE-15, AE-16, and AE-201.

Whitehead [Ref. AE-81 investigated the single-degree-of-freedom torsional flutter of unstalled blades at zero deflection. He was the first to study the effects of small differences between the blades and he concluded that mistuning had always a stabilizing outcome. He later extended his work to investigate the effects of mistuning on the forced aeroelastic response of bladed disc assemblies [Refs. AE-21 and AE-221. For a mistuned assembly with N blades, he showed that although the amplitude of any one blade could theoretically increase by a factor of  $[1 + \sqrt{(N/2)}]/2$  or  $(1 + \sqrt{N})/2$ , this upper limit would not be reached under normal circumstances. Hanamura and Tanaka [Ref. AE-131 investigated the special case of alternate mistuning on torsional flutter and concluded that this particular mistuning had greatly increased flutter velocity. Srinivasan [Ref. AE-121 developed Whitehead's basic model to incorporate mechanical coupling among the blades via a shroud attachment. He conducted a series of parametric studies for a particular bladed disc assembly with emphasis on mistuning.

Carta [Ref. AE-9] applied an energy method to predict the flutter boundaries of a bladed shrouded disc. His technique was based on evaluating the logarithmic decrement of the system as the ratio of the work done by aerodynamic forces and moments to the average kinetic energy of the system. This approach was later generalized by Mikolajczak et al. [Ref. AE-101 who included the effects of mechanical damping and the drag force into their model.

The study of the coupled bending/torsion flutter in cascades is still in its early stages. Sendiksen and Friedmann [Ref. AE-111] were first to combine Theodorsen's model [Ref. AE-41] together with Lane's assumption [Ref. AE-181] and hence to model the cascade via a lumped parameter model where the blades were only aerodynamically coupled. They systematically investigated the effect of bending/torsion coupling on tuned cascade stability over a wide range of design parameters. Kieib [Ref. AE-16] and Kaza and Kieib [Ref. AE-141] used the same model to study the mistuned cascade stability and to predict the amplitude of blade vibration forced by wakes. They later extended this basic model [Ref. AE-201] to incorporate structural coupling among the blades via summation of in-vacuum modes of vibration. More recently, [Ref. AE-191] they considered the case of straight, slender, twisted, non-uniform elastic blades with a symmetric cross-section for which the equations of motion were derived using Hamilton's principle. A conceptually similar approach is due to Srinivasan and Fabunmi [Ref. AE-23] who, instead of using one typical section, defined the blade properties at several spanwise stations: a technique which allows complex blade geometries to be modelled with reasonable accuracy. Their analysis did not include structural interblade coupling and led to eigenproblems of prohibitive sizes for realistic blade numbers.

### 8.2.2 Aerodynamic Studies

The theory of vibrating incompressible, inviscid flow has been gradually built up by several authors. In spite of the earlier research by Giauert [Ref. AD-51] and Von Karman [Ref. AD-81], Theodorsen's work [Ref. AE-41]

is the first which derives analytical expressions for the lift and moment coefficients for an isolated aerofoil oscillating in incompressible flow. His analysis was later complemented by Postei and Leppert [Ref. AD-71] who calculated the corresponding pressure distribution on the aerofoil surface. Mendelson and Caroli [Ref. AD-81] derived the lift and moment equations for an infinite unstaggered cascade by assuming that air blades vibrated in phase. Lane and Wang [Ref. AD-91] presented a calculation method applicable to cascades of any stagger and phase angle. Their method was subsequently rationalized by Whitehead [Ref. AD-101] who presented the unsteady lift and moment coefficients in a standardized form.

The theoretical determination of the air forces acting on an oscillating two-dimensional aerofoil moving through a compressible fluid at subsonic speeds was first achieved by Possio in 1938 [Ref. AD-111]. Garrick [Ref. AD-121] extended his work and published extensive numerical tables for Mach numbers less than 0.7 beyond which he found the theory inapplicable. Woiston and Runyan [Refs. AD-1 and AD-21] studied the problem of subsonic tunnel interference effects for an isolated aerofoil. Their work was generalized by Lane and Friedman [Ref. AD-131] who presented a method of calculation for the generalized cascade and gave numerical results for the unstaggered case. Whitehead [Ref. AD-141] developed this technique to make it applicable to the transmission and reflection problems, and to the generation of sound by vibration and incoming flow disturbances. Smith [Ref. AD-151] considered the same problem but his analysis was based upon the work of Kaji and Okazaki [Ref. AD-161] who represented each blade by an unsteady distribution of pressure doublets.

The problem of a two-dimensional, oscillating, thin aerofoil moving with supersonic speed was first considered and solved by Possio in 1937 [Ref. AD-171]. The supersonic wind tunnel wall interference effects for an isolated aerofoil - equivalent to an unstaggered cascade with antiphase vibration of adjacent blades - were investigated by Miles [Ref. AD-31 and Drake [Ref. AD-41]. Their work was extended to staggered cascades with supersonic axial velocity (supersonic leading edge locus) by Lane [Ref. AD-181 using Lapiane transform techniques. The analysis of the practically more important but mathematically more difficult case of subsonic axial velocity was first treated by Goreiov [Ref. AD-191 who used a collocation method. Kurosaka [Ref. AD-201 obtained a closed form solution in the case of an infinite cascade oscillating at low frequencies using Laplace transform methods. Treatises for semi-finite cascades were published almost simultaneously by Verdon [Ref. AD-211, Brix and Platzer [Ref. AD-221, Nagashima and Whitehead [Ref. AD-231, Goldstein [Ref. AD-241 and Verdon and McCune [Ref. AD-251, all of whom considered a reference blade about which a finite number of neighbouring blades were taken into account until convergence towards a periodic solution was achieved. The first completely analytical solution is due to Goldstein. Sraun and Adamczyk [Ref. AD-261 and Adamczyk and Goldstein [Ref. AD-271 who applied the Wiener-Hopf technique to the solution of the integral equation for the velocity potential.

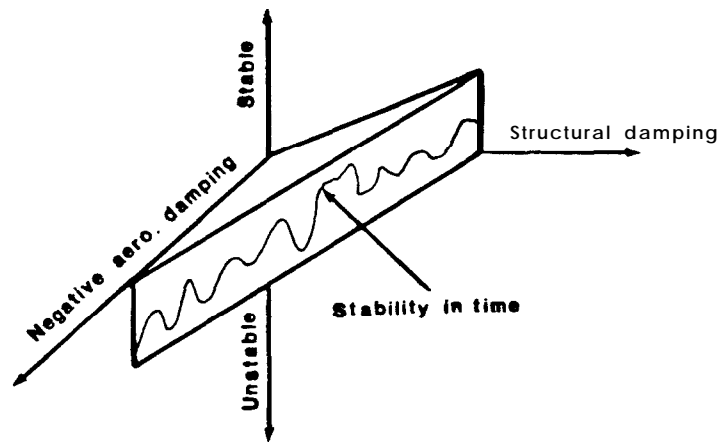
### 8.3 OBJECTIVES AND SCOPES OF THE PRESENT ANALYSIS

At the outset, the underlying objective of this research is to improve the basic understanding of the aeroelastic characteristics of bladed disc systems. To help to meet this rather general objective, it is proposed to

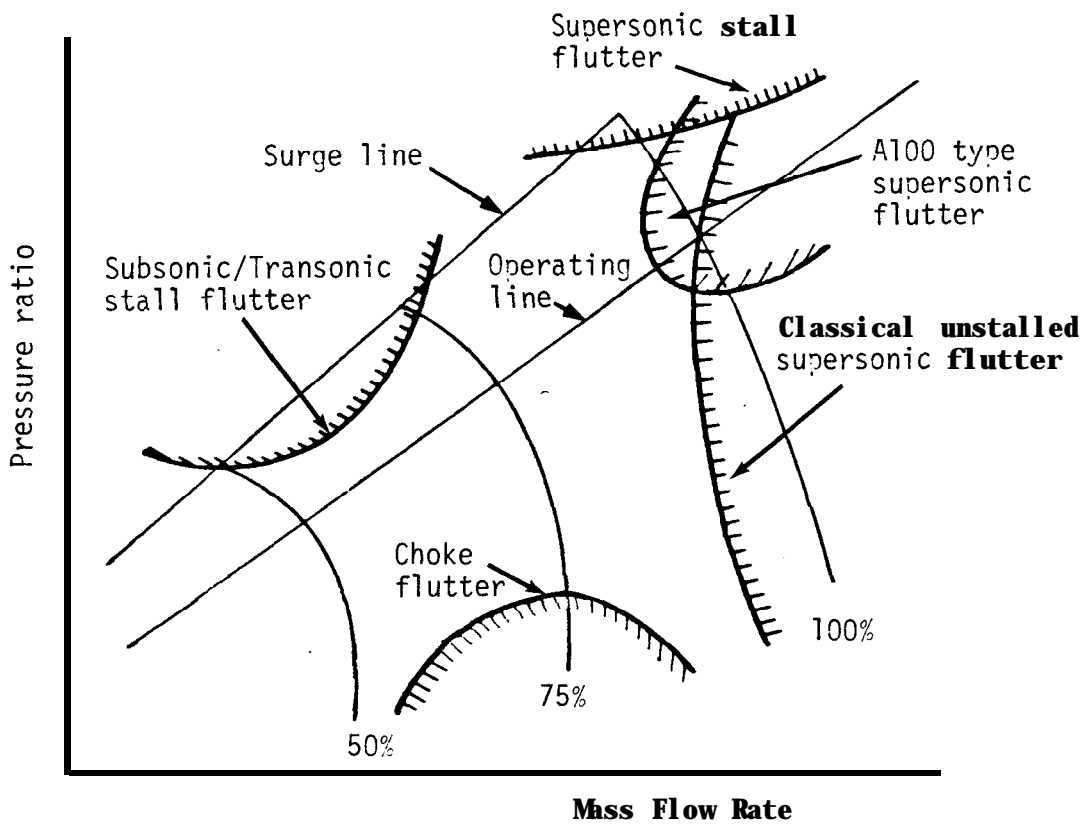


develop a numerical model which provides an acceptable interface of bladed disc structural dynamics with the existing unsteady aerodynamic theories. Although the formulation of the latter is not within the scope of this study, the choice and development of the former are and they will inevitably constitute its framework. As the aim of this study is to provide an overall representation of the aeroelastic phenomena rather than to seek the solution of a particular problem, it is appropriate to devise a strategy that yields a multi-purpose analysis and design tool based on effective numerical methods. A lumped parameter model, as documented in Chapter 9, will be used initially since it has been shown in Chapter 6 that such a model is adequately representative of structurally mistuned bladed disc systems and that it can provide a rapid and relatively cheap means of observing patterns of qualitative behaviour systematically.

The methods presented in this work, together with many others, can provide a theoretical basis for improved analysis and design capabilities for rotating machinery manufacturers. The long term effect should be a decrease in the amount of costly full scale engine testing and a reduction in the number of blade failures and resulting redesigns in the development process. Furthermore, the use of deliberate mistuning as a passive control tool for flutter could become a popular design feature for the next generation of turbo-machines.



**Fig. 8.1** Variation of system's stability in time



**Fig. 3.2** Types of fan/compressor flutter [Ref. AE-3]

## CHAPTER 9

### DERIVATION OF THE AEROELASTIC MODEL

#### 9.1 STRUCTURAL MODEL

As shown in Fig. 9. 1, the bladed disc assembly is discretized via a hybrid model of the original lumped parameter representation proposed by Dye and Henry [Ref. SD-131 and the isolated aerofoil of Theodorsen [Ref. AE-41. A modified version of the latter, as used in this study, is illustrated in Fig. 9.2. The blade is represented as a two degree-of-freedom oscillator in which the inertial coupling of the bending and torsional motions due to pretwist, rotation of the rotor, etc. is modelled through the offset distance  $d$  between the centre of twist and the centre of gravity. The elastic axis passes through this centre of twist at which a force normal to the blade surface causes only a translational displacement and no rotation. For most practical applications, the mass moment of inertia in the chordwise direction is much greater than that in the direction normal to the chord and hence the motion in the former can be neglected without any loss of expected accuracy. The inertial properties ( $m, I, d$ ) of the blades are usually represented at  $3/4$  spanwise position while the remaining model parameters ( $M, k, c, K, g, S_h, S_\alpha$ ) are determined by a trial-and-error process provided sufficient vibration data are available (see Section 6.2. 1). As can be seen from Figs. 9. 1 and 9.2, there are two degrees of freedom per blade (one translational and the other rotational) and one per disc sector, and

hence the model above leads to an eigenproblem of order  $3N$ , where  $N$  is the total number of blades.

If  $F_j$  and  $T_j$  are the external force and moment acting on the  $j^{\text{th}}$  blade, the equations of motion for the  $j^{\text{th}}$  blade and the  $j^{\text{th}}$  disc sector can be written as:

$$\begin{aligned}
 m_j \ddot{h}_j + m_j d \ddot{\alpha}_j - S_h h_{j-1} + (2S_h + k_j) h_j - S_h h_{j+1} - k_j y_j &= -F_j \\
 I_j \ddot{\alpha}_j + m_j d \ddot{h}_j - S_\alpha \alpha_{j-1} + (2S_\alpha + c_j) \alpha_j - S_\alpha \alpha_{j+1} &= T_j \quad (9-1) \\
 M \ddot{y}_j - K y_{j-1} + (2K + g + k_j) y_j - K y_{j+1} - k_j h_j &= 0
 \end{aligned}$$

where all other symbols have been defined in Figs. 9.1 and 9.2. The lumped parameter model is ideally suited for a systematic study of the mistuning effects since blade-to-blade differences can easily be introduced by changing any of the four section parameters, namely  $m_j$ ,  $I_j$ ,  $k_j$  and  $c_j$ . Although a more general approach is possible, the mistuning in this work will be restricted to the variation of the blade torsional frequencies about a reference value and hence all model parameters but  $c_j$  will be kept constant for a given bladed disc. Assuming simple harmonic motion and extending equation (9-1) to  $N$  blades in non-dimensional form gives :

$$\mu ([K] - \omega^2/\omega_0^2 [M]) \{q\} = \{Q\} \quad (9-2)$$

where  $[M]$  and  $[K]$  are the non-dimensional mass and stiffness matrices whose explicit form is given in **Appendix III**,  $\mu$  is a non-dimensional parameter defined in **Appendix III**,  $\omega_0$  is some arbitrary reference frequency;

and

$$\{q\}^T = \{h_1/b, \alpha_1, y_1/b, \dots, h_N/b, \alpha_N, y_N/b\}$$

$$\{Q\}^T = \{-F_1^*, T_1^*, 0, \dots, -F_N^*, T_N^*, 0\}$$

It should be noted that both the response and the force vectors are also in non-dimensional form. This being denoted by \*. Structural damping of the hysteretic type can easily be introduced by letting:

$$\begin{aligned}
 k_j & \rightarrow k_j(1+i\eta_h) \\
 c_j & \rightarrow c_j(1+i\eta_\alpha)
 \end{aligned}
 \tag{9-3}$$

where  $\eta_h$  and  $\eta_\alpha$  are the damping coefficients for bending and torsion respectively.

## 9.2 AERODYNAMIC MODEL

The choice of the particular expressions to replace F and T in equation (9-1) depends on the Mach number range in which flutter is expected to occur. The unsteady aerodynamic loads were calculated using Whitehead's theory [Ref. AD-101 for incompressible flow, Smith's theory [Ref. AD-151 for subsonic flow and Nagashima and Whitehead's theory [Ref. AD-231 for supersonic flow with subsonic or supersonic axial velocity. Although the formulation of these is outside the scope of this work. It is appropriate to review the basis of their derivation in reasonable detail in view of the common assumptions and solution techniques used.

### 9.2.1 Fundamentals of Two-Dimensional Cascade Flow Theories

The cascade flow model used in all three analyses is shown in Fig. 9.3.

The following common assumptions are made:

- (i) The system is two-dimensional. This means that the bending vibration of a blade may be represented by the translational motion of the equivalent two-dimensional aerofoil in a direction normal to the chord and that the torsional vibration becomes simply a rotation about a fixed axis.
- (ii) The blades are represented as flat plates of negligible thickness.
- (iii) The effects of fluid viscosity are neglected so that there are no boundary layers on the blades and the flow follows the blade surface without stalling.
- (iv) The blades operate at zero mean incidence so that the mean deflection is also zero.
- (v) The blades undergo simple harmonic motion whose amplitude is small. They all vibrate with the same amplitude and with a constant phase angle between adjacent blades. For a stage with  $N$  blades, this phase angle is restricted to  $N$  values which are integral fractions of  $2\pi$ . Both flutter and forced vibration of identical blades is of this form but any motion of the blade row can be synthesised by superposing modes of this kind so that this assumption does not lead to any loss of generality.
- (vi) The flow is isentropic and irrotational.
- (vii) The wakes shed from upstream periodic obstructions are limited to sinusoidal distortions represented by vorticity perturbations so that they are convected downstream at the mainstream

velocity  $V$ .

- (viii) The unsteady blade loading at the trailing edge is finite for incompressible and subsonic flows. This is a statement of the Kutta-Joukowski condition.
- (ix) All **perturbations** from the uniform main flow are small so that the continuity and momentum equations may be **linearized** and the principle of superposition may be applied to the solutions obtained.

The main objective of the aerodynamic analyses is to predict the aerodynamic forces and moments acting on a cascade of fiat plates due to:

- (a) translational vibration of the plates normal to their chord line, this corresponding to the **flapwise** vibration of a three-dimensional blade;
- (b) torsional vibration about a given axis;
- (c) wakes convected into the cascade from periodic upstream obstructions.

The general method of calculation is based on equating the total induced velocity normal to the blade surface to the input **upwash** velocities corresponding to (a), (b) and (c); that is to say:

$$V_{\text{induced}} = V_{\text{upwash}} \quad (94)$$

The induced velocity can be determined by regarding the blades and their wakes as vortex sheets [Refs. AD-10 and AD-151 or pressure dipoles [Ref. AD-231 in which case the convected **wave** equation has to be used. In any event, equation (9-4) leads to an integral equation of Fredholm type of the first kind which can be expressed as:

$$\int_{-b}^b K(\tau - e) f(\tau) d\tau = Vu(e) \quad (9-5)$$

where  $f$  is the unknown pressure or vorticity distribution,  
 $K$  kernel function,  
 $V_u$  inputupwash velocity,  
 $b$  semi chord length,  
 $e$  a co-ordinate along the blade chord,  
 $\tau$  a dummy integration variable.

The kernel in equation (9-5) is a very complicated (complex) function of five parameters. namely: the reduced frequency  $A$ . the Mach number  $M$ . the cascade stagger angle  $\xi$ . the gap to chord ratio  $g/c$  and the Interblade phase angle  $\beta_r$ . Some analytical formulations can be obtained under certain simplifying assumptions [Refs. AD-20 and AD-231. and a closed form solution is discussed in Ref. AD-27. The problem is further complicated by the presence of singularities in the kernel function and these must be extracted prior to the numerical solution. This is discussed in detail in Ref. MA-4.

Once the pressure (or vorticity) distribution is determined. the unsteady aerodynamic lift force and moment per unit span length are given by:

$$F = \int_{-b}^b f(\tau) d\tau$$

$$T = \int_{-b}^b f(\tau) \tau d\tau \quad (9-6)$$

where  $f$  denotes the pressure distribution function across the blade chord.



### 9.2.2 Force and Moment Coefficients

As mentioned earlier, the force and moment defined by equation (9-6) are due to three input upwash velocities and hence they can explicitly be written as:

$$\begin{aligned} F &= -2\pi\gamma VbL (\dot{h} C_{Fh} + \alpha V C_{F\alpha} - w C_{Fw}) \\ T &= 4\pi\gamma Vb^2L (\dot{h} C_{Mh} + \alpha V C_{M\alpha} - w C_{Mw}) \end{aligned} \quad (9-7)$$

where  $V$  is the relative flow velocity,

- $\gamma$  fluid density,
- $w$  velocity of disturbance due to wakes,
- $L$  blade span,

and  $C_{Fh}$ ,  $C_{F\alpha}$  and  $C_{Fw}$  are the force (or moment) coefficients due to blade translational velocity, blade rotation and wake disturbances respectively. it should be noted that these coefficients are normally computed at the leading edge and hence they are an explicit function of a sixth parameter, the elastic axis position. The conversion formulae can be found in Ref. AD-10.

When the frequency of vibration approaches zero, the coefficients tend to a finite limit which, in the general case, is not zero. it can be shown that:

$$\begin{aligned} \lim_{\omega \rightarrow 0} C_{Fh} &= \lim_{\omega \rightarrow 0} C_{F\alpha} = \lim_{\omega \rightarrow 0} C_{Fw} = c_p \\ \lim_{\omega \rightarrow 0} C_{Mh} &= \lim_{\omega \rightarrow 0} C_{M\alpha} = \lim_{\omega \rightarrow 0} C_{Mw} = C_M \end{aligned}$$

This is the main reason for basing  $C_{Fh}$  and  $C_{Mh}$  on the velocity of the translational vibration rather than the displacement since the force and the moment are expected to vanish once the motion has stopped.

For a tuned cascade. In which there is no structural coupling among the blades and the inertial coupling is weak, the bending flutter stability of unstalled blades is dictated by the real part of  $C_{Fh}$  since this determines the component of the blade force which is in phase with the velocity of the motion. If  $\text{Re}(C_{Fh})$  is positive and there is no mechanical damping present, the blades will flutter. This can easily be seen by considering the corresponding equation of motion:

$$m \ddot{h} + m \dot{d} \ddot{\alpha} + k \omega_o^2 (1 + i \eta_h) h = 2\pi \rho V b L (\dot{h} C_{Fh} + \alpha V C_{F\alpha})$$

Assuming harmonic motion and equating the imaginary parts gives:

$$\eta_h - A [\omega \text{Re}(C_{Fh}) + \alpha/h V \text{Im}(C_{F\alpha})] = 0 \quad (9-8)$$

where  $A$  is a positive constant. Equation (9-8) represents the equilibrium condition for which the aerodynamic damping effect is cancelled by its structural counterpart. Assuming that there is no mechanical damping and  $a/h$  is small (i.e. weak coupling between bending and torsional motions), the condition for stability becomes:

$$\text{Re}(C_{Fh}) < 0$$

The torsional stability is similarly controlled by  $\text{Im}(C_{M\alpha})$ . Although the  $C_{Fw}$  and  $C_{Mw}$  coefficients do not contribute to the stability analysis, they can be used to predict the amplitude of the forced vibration due to wakes provided the disturbance velocity  $w$  can be estimated.

### 9.3 AEROELASTIC MODEL

#### 9.3.1 Derivation of the Aeroelastic Equations of Motion

The overall equations of motion for the bladed system under aerodynamic loading will be derived by substituting the aerodynamic forces and moments of equation (9-7) into equation (9-2). The motion is assumed to be simple harmonic with a constant phase angle between adjacent blades. the values of which are restricted to:

$$\beta_r = 2\pi r/N \text{ where } r = 0, N-1$$

and N is the total number of blades. For a tuned system, the modal shapes corresponding to different interblade phase angles (or nodal diameters) are always pure and hence the motion of the  $j^{\text{th}}$  sector for vibration in a single mode can be written as:

$$\begin{Bmatrix} h_j/b \\ a_j \\ y_j/b \end{Bmatrix} \exp(i\omega t) = \begin{Bmatrix} h_{ar}/b \\ \alpha_{ar} \\ y_{ar}/b \end{Bmatrix} \exp[i(\omega t + \beta_r j)] \quad (9-9)$$

where

- $h_j$  is the bending amplitude of the  $j^{\text{th}}$  blade,
- $a_j$  torsional amplitude of the  $j^{\text{th}}$  blade,
- $y_j$  amplitude of the  $j^{\text{th}}$  disc sector,
- $h_{ar}$  bending deflection of the  $j^{\text{th}}$  blade in the  $r^{\text{th}}$  tuned system mode,
- $\alpha_{ar}$  torsional deflection of the  $j^{\text{th}}$  blade in the  $r^{\text{th}}$  tuned system mode,
- $y_{ar}$  deflection of the  $j^{\text{th}}$  disc sector in the  $r^{\text{th}}$  tuned system mode,
- $\omega$  frequency of vibration,

t time,  
and  $i = \sqrt{-1}$ .

In the case of a mistuned system, the blades have different response amplitudes and the phase angle between adjacent blades may vary. In view of the spatial periodicity, the overall motion can be expressed as a superposition of all possible motions of the corresponding tuned system and hence the motion of the  $j$ th sector takes the form:

$$\begin{pmatrix} h_j/b \\ \alpha_j \\ y_j/b \end{pmatrix} \exp(i\omega t) = \sum_{r=0}^{N-1} \begin{pmatrix} h_{ar}/b \\ \alpha_{ar} \\ y_{ar}/b \end{pmatrix} \exp[i(\omega t + \beta_r j)] \quad (9-10)$$

For an  $N$  bladed disc, equation (9-10) can be generalized as:

$$\begin{matrix} \{q\} & = & [E] \{q_{ar}\} & (9-11) \\ \text{system response} & & \text{modal deflection} & \\ \text{vector} & & \text{vector} & \end{matrix}$$

where

$$[E] = [\exp(2\pi i s r / N)] = \begin{bmatrix} E(0,0) & 0 & E(0,1) & E(0,2) & \dots & 0 \\ E(1,0) & 0 & E(1,1) & 0 & E(1,2) & \dots \\ 0 & E(2,0) & 0 & E(2,1) & 0 & \dots \\ \dots & \dots & \dots & \dots & \dots & \dots \end{bmatrix}$$

$$s = j - 1$$

$$\{q_{ar}\}^T = \{ h_{a0}/b, \alpha_{a0}, y_{a0}/b, \dots, h_{aN-1}/b, \alpha_{aN-1}, y_{aN-1}/b \}$$

and  $\{q\}$  is defined in equation (9-2). Also, it can be shown that:

$$\{q_{ar}\} = [E]^{-1} \{q\} = 1/N [\bar{E}] \{q\} \quad (9-12)$$

Using equation (9-10), equation (9-7) can be re-written to express the aerodynamic forces and moments in terms of the non-dimensional coefficients and modal deflections. Such a formulation leads to:

$$\begin{aligned} P_j &= -\gamma b^3 \omega^2 L \sum_{r=0}^{N-1} [l_{hhr} h_{ar}/b + l_{har} \alpha_{ar} + l_{hwr}] \exp[i(\omega t + \beta_r j)] \\ T_j &= \gamma b^4 \omega^2 L \sum_{r=0}^{N-1} [l_{ahr} h_{ar}/b + l_{aar} \alpha_{ar} + l_{awr}] \exp[i(\omega t + \beta_r j)] \end{aligned} \quad (9-13)$$

where

$$\begin{aligned} l_{hhr} &= 4i/\lambda C_{Ph} & l_{ahr} &= 8i/\lambda C_{Mh} \\ l_{har} &= 8/\lambda^2 C_{F\alpha} & l_{aar} &= 16/\lambda^2 C_{M\alpha} \\ l_{hwr} &= -8/\lambda^2 w/V C_{FW} & l_{awr} &= -16/\lambda^2 w/V C_{MW} \end{aligned}$$

and  $\lambda = 2b\omega/V$  is often termed as the reduced frequency.

The non-dimensional form of equation (9-13) can be generalised for an N-bladed disc to give:

$$\{Q\} = \omega^2/\omega_0^2 [E][A]\{q_{ar}\} + \omega^2/\omega_0^2 [E]\{F_w\} \quad (9-14)$$

where  $\{Q\}$  is defined in equation (9-2),  
 $\{q_{ar}\}$  and  $[E]$  are defined in equation (9-11),  
 $[A]$  is the aerodynamic matrix whose explicit form is given in Appendix III,  
 $\{F_w\}$  is the force vector due to wakes whose explicit form is also given in Appendix III,  
and  $\omega_0$  is some arbitrary reference frequency.

Equation (9-14) constitutes the aerodynamic part of the analysis while equation (9-2) represents the structural side. Thus the aeroelastic equation of motion is:

$$([\mathbf{K}] - \omega^2/\omega_0^2[\mathbf{M}] + 1/(\mu N)[\mathbf{E}][\mathbf{A}][\bar{\mathbf{E}}])(\mathbf{q}) = 1/\mu \omega^2/\omega_0^2[\mathbf{E}]\{\mathbf{F}_w\} \quad (9-15)$$

where use of equation (9-12) has been made. Let:

$$[\mathbf{C}] = [\mathbf{M}] + 1/(\mu N)[\mathbf{E}][\mathbf{A}][\bar{\mathbf{E}}] \quad (9-16)$$

$$[\mathbf{P}] = [\mathbf{C}]^{-1}[\mathbf{K}]$$

in which case equation (9-15) becomes:

$$([\mathbf{P}] - \omega^2/\omega_0^2 [\mathbf{I}]) (\mathbf{q}) = 1/\mu \omega^2/\omega_0^2 [\mathbf{C}]^{-1}[\mathbf{E}]\{\mathbf{F}_w\} \quad (9-17)$$

it should be noted that the above complex eigenproblem is not linear since the elements of  $[\mathbf{A}]$  (and hence of  $[\mathbf{P}]$ ) are very complicated functions of frequency. Thus, an iterative solution technique must be used and this will be discussed in Section 10.1. The aeroelastic stability of the cascade is determined by the eigenvalues of the characteristic matrix  $[\mathbf{P}]$ . Let:

$$\omega_r = \Omega_r + i\eta_r \quad (9-18)$$

where  $\Omega_r$  and  $\eta_r$  represent the natural frequency and the aerodynamic damping factor of the  $r^{\text{th}}$  mode. Flutter occurs if:

$$\eta_r < 0 \quad (9-19)$$

### 9.3.2 Forced Aeroelastic Response

In the foregoing analysis, it is possible to consider a forcing function which, in the general case, contains all harmonics  $r$  of the rotational speed  $n$  up to  $r = N-1$ , where  $N$  is the total number of blades and  $r$  is

termed as the engine order of the excitation. For the sake of clarity, only one harmonic  $r = R$ , will be considered at a time, though this restriction brings no loss of generality since the principle of superposition holds. Physically, this corresponds to the case in which there are  $R$  symmetrically placed obstructions located upstream from the rotor and the circumferential wake distribution is perfectly sinusoidal. Thus:

$$\omega = nR \quad (9-20)$$

Remembering that the coefficients  $l_{hwR}$  and  $l_{\alpha wR}$  in equation (9-13) represent the part of the aerodynamic loading due to wakes, the non-dimensional forcing function corresponding to the  $R^{\text{th}}$  engine order excitation can be written as:

$$\begin{aligned} \{F_R\} &= \left\{ \begin{array}{c} l_{hwR} \\ l_{\alpha wR} \\ 0 \end{array} \right\}_{j=1, N} e^{iR[nt + 2\pi(j-1)/N]} = \left\{ \begin{array}{c} l_{hwR} \\ l_{\alpha wR} \\ 0 \end{array} \right\}_{s=0, N-1} e^{2\pi isR/N} e^{i\omega t} \\ &= 1/N [E(s, R)] \{F_{wR}\} \end{aligned} \quad (9-21)$$

where the notation  $[E(s, R)] \{F_{wR}\}$  indicates that excitation for only one harmonic, namely  $r=R$ , is considered at a time. Using equation (9-16), equation (9-15) can be rewritten as:

$$\{q\} = p/\mu ([K] - P [C])^{-1} [E] \{F_w\} \quad (9-22)$$

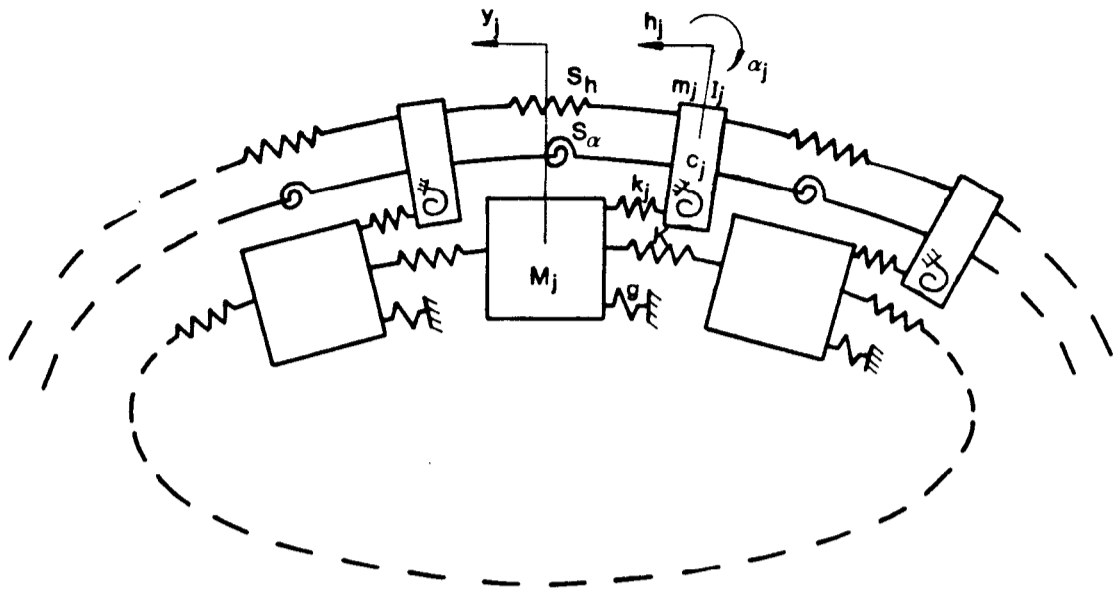
where  $p = \omega^2/\omega_0^2$  is the non-dimensional forcing frequency parameter,  
 $\{q\}$  cascade aerodynamic response vector,  
 $\{F_w\}$  vector of wake amplitude coefficients.

The notation  $[E] \{F_w\}$  corresponds to the general case where all possible harmonics ( $r = 0, N-1$ ) are considered at any one instant. Since interest is confined to the  $R^{\text{th}}$  engine order excitation only, equation (9-22) must be modified to read:

$$\{q\} = p/(\mu N) ([K] - p [C])^{-1} [E(s, R)] \{F_{wR}\} \quad (9-23)$$

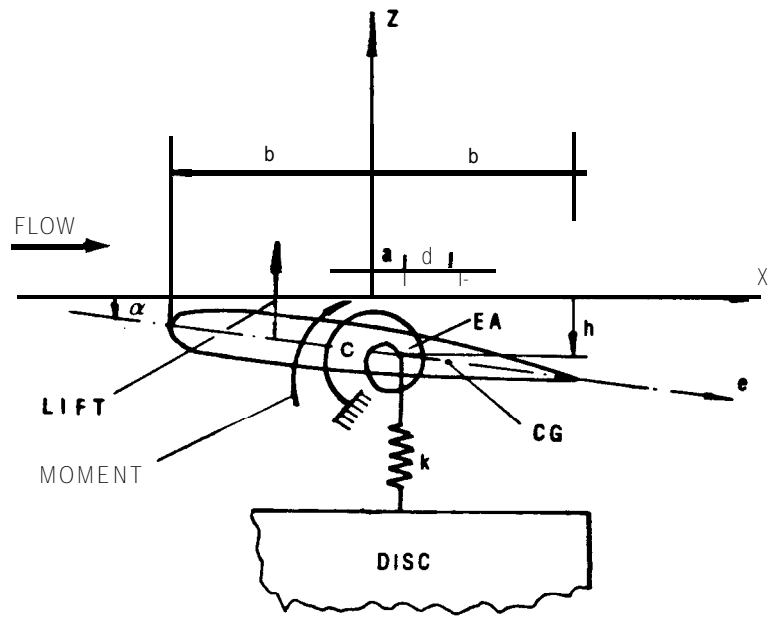
Equation (9-23) differs from its structural counterpart equation (6-10) by the fact that the forcing frequency is implicitly present in the  $[C]$  matrix. It should also be noted that the quantity  $\omega^2$  appears both on the numerator of the forcing frequency parameter  $p$  and on the denominator of the  $l_{hwR}$  and  $l_{\alpha wR}$  coefficients so that it only affects  $([K] - p[C])^{-1}$  term.



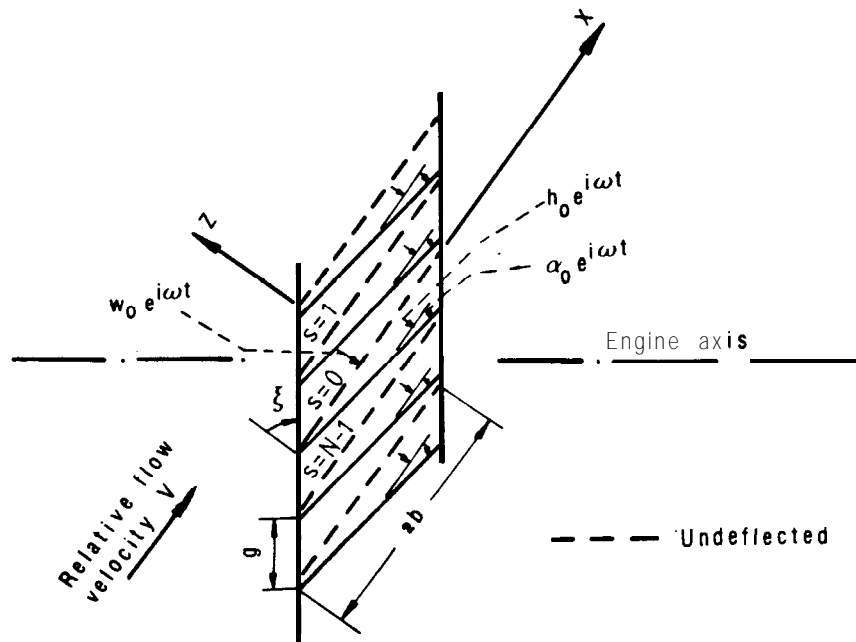


**Fig. 9.1 Lumped parameter model**

- $h_j$  Translational co-ordinate for  $j^{\text{th}}$  blade,  
 $\alpha_j$  Rotational co-ordinate for  $j^{\text{th}}$  blade,  
 $y_j$  Co-ordinate for  $j^{\text{th}}$  disc sector;
- $m_j$  Mass of  $j^{\text{th}}$  blade,  
 $I_j$  Second moment of inertia for  $j^{\text{th}}$  blade,  
 $c_j$  Rotational stiffness for  $j^{\text{th}}$  blade,  
 $k_j$  Translational stiffness for  $j^{\text{th}}$  blade;
- $M_j$  Mass of  $j^{\text{th}}$  disc sector,  
 $K$  Interdisc stiffness,  
 $\beta$  Grounding stiffness;
- $S_h$  Shroud stiffness in translation,  
 $S_\alpha$  Shroud stiffness in rotation.



**Fig. 9.2 Aerofoil details**



**Fig. 9.3 Geometry of tuned cascade**

## CHAPTER 10

### NUMERICAL STUDY

#### 10.1 DETAILS OF THE COMPUTER PROGRAM

A digital computer program, namely FLUT1, was written to perform the aeroelastic analysis described in Chapter 9. Through its modular structure, the following options can be considered.

(I) Computation of force and moment coefficients for different flow conditions.

As mentioned earlier, the unsteady aerodynamic loads were calculated by using Whitehead's theory [Ref. AD-101 for incompressible flow, Smith's theory [Ref. AD-151 for subsonic flow, and Nagashima and Whitehead's theory [Ref. AD-231 for supersonic flow with subsonic or supersonic axial velocity. In all three cases, the solution methods presented in the original source were followed closely and good agreement was obtained with the published results. Some numerical problems, however, were encountered in the case of subsonic flow and it was concluded that the present formulation could lead to erroneous results for Mach numbers above 0.9.

(II) Determination of flutter stability.

The eigenproblem given by equation (9-17) was solved using standard routines from the Numerical Algorithms Group (NAG) library. The

recommended path for eigen-analysis is first to balance the complex matrix by reducing its norm. then to put it into upper Hessenberg form using stabilized elementary similarity transformations and finally to extract the eigenvalues via the LR algorithm with shifts of origin. Both the original and the balanced matrix have the same eigenvalues and the eigenvectors of the former can be recovered by back-substitution. Further details can be found in Ref. MA-S.

Unfortunately, the analysis is further complicated by the fact that the stability matrix  $[P]$  is also a function of frequency, a feature which renders the eigenproblem below non-linear and mathematically very complex indeed:

$$([P(\omega)] - \omega^2 [I]) \{q\} = \{0\} \quad (10-1)$$

where  $\omega = \Omega + i\eta$ ,  $\Omega$  being the frequency and  $\eta$  the damping part. After some deliberation. It was recalled that the natural frequencies of the aerodynamically loaded system would be close to the in-vacuum ones. in which case the latter could be used as initial guesses to an iterative solution for the real part of the complex eigenvalue. That is to say:

$$\begin{aligned} ([P(\Omega_0)] - (\Omega_1 + i\eta_1)^2 [I]) \{q\} &= \{0\} \\ ([P(\Omega_1)] - (\Omega_2 + i\eta_2)^2 [I]) \{q\} &= \{0\} \\ ([P(\Omega_{j-1})] - (\Omega_j + i\eta_j)^2 [I]) \{q\} &= \{0\} \end{aligned} \quad (10-2)$$

until  $(\Omega_j - \Omega_{j-1})/\Omega_j <$  a prescribed value,  $j$  being the iteration number.

**(III) Forced *aeroelastic* response.**

The amplitude of the forced response induced by wakes, as given by equation (9-23), was computed using a standard complex matrix inversion routine from the NAG library. The frequency-dependence of the [C] matrix was taken into account by setting it up at the natural frequency of interest or, in some cases, at the central frequencies of subdivided intervals.

Although the correctness of the program could not be checked for the general case (for which there are no published results available), the following test runs were made:

- (i) the in-vacuum natural frequencies and associated mode shapes of various bladed discs were checked against those given in Refs. SD-26 and SD-28;
- (ii) in the case of a 12-bladed cascade, the loci of the uncoupled torsional eigenvalues were checked against Refs. AE-8 and AE-12;
- (iii) in the case of a 25-bladed rotor, the locus of the coupled torsional eigenvalues was determined in parallel with Ref. AE-16. The stability plots resulting from both calculations are given in Fig. 10. 1, which incidentally provides a direct comparison of Adamczyk-Goldstein and Nagashima-Whitehead theories for supersonic flow with subsonic axial velocity.

Good agreement was obtained in all three cases. However, it should be noted that in (ii) and (iii) above, the blades are only coupled aerodynamically: that is to say there are no mechanical connections between them and hence they behave as isolated cantilevers from a structural viewpoint.

## 10.2 AERODYNAMIC FORCE AND MOMENT COEFFICIENTS

### 10.2.1 Direct Use of the Coefficients for Flutter Predictions

In the case of a tuned **bladed** disc where the **interblade** structural coupling is weak (for example, relatively **stiff** disc, flexible blades and no shroud attachment) and bending and torsional motions are uncoupled, the flutter boundaries can be deduced from the calculation of the aerodynamic force and moment coefficients without resorting to the full **aeroelastic** model. As discussed in Chapter 9, the **torsional stability** is then governed by  $\text{Im}(C_{M\alpha})$  and the deviation from the in-vacuum frequencies by  $\text{Re}(C_{M\alpha})$ .

Consider the following hypothetical cascade whose characteristic parameters are:

Number of blades = 12  
Stagger angle = **48°**  
Gap/chord = 1.0  
Elastic axis = 43% chord  
Reduced frequency = **.42**

and for which it is proposed to calculate the force and moment **coefficients in eight different** cases of **increasing** Mach number, i.e. **M = 0.4, 0.6, 0.7, 1.1, 1.2, 1.3 and 1.5**. As there are 12 blades in the cascade, the only allowable values of the **interblade** phase angle are **integer** multiples of  $\pi/6$ , each one **giving** rise to an **aerodynamic mode**, the stability of which depends on the sign of  $\text{Re}(C_{Fh})$  and  $\text{Im}(C_{M\alpha})$ . For the eight cases above, it has been found that in all cases  $\text{Re}(C_{Fh})$  is negative so that the bending vibration is stable and this

observation is in total agreement with Refs. AD-10, AD-15 and AD-23. The  $C_{M\alpha}$  coefficient, however, shows significant variations between modes and  $\text{Re}(C_{M\alpha})$  is plotted against  $\text{Im}(C_{M\alpha})$  in Figs. 10.2a to 10.2h. Fig. 10.2a shows the stability behaviour of the cascade when subjected to incompressible flow ( $M=0$ ). The aerodynamic modes 1, 2, 3, and 4 have positive imaginary part and hence they are unstable according to the criterion presented in Section 9.2.2. In the subsonic regime, the locus of the coefficients does not show any significant changes at  $M = 0.4$  (Fig. 10.2b) but the isolated behaviour of mode 1 becomes dominant at  $M = 0.6$  and  $0.7$  (Figs. 10.2c and 10.2d). In the supersonic regime, the loci change rather rapidly in an apparently random manner (Figs. 10.2e to 10.2h) from one Mach number plane to the next, at least half of the modes being unstable in all four cases.

The deviation from the in-vacuum natural frequencies is governed by the real part of  $C_{M\alpha}$ , and its generally positive value leads to lower damped frequencies. For this particular cascade, it is interesting to note that  $\text{Re}(C_{M\alpha})$  becomes negative at supersonic Mach numbers only.

### 10.2.2 Further Considerations

(i) Lack of symmetry. An obvious but rather important feature of the loci shown in Fig. 10.2 is the asymmetry of the aerodynamic modes which are dependent on the wave direction, this being given by the sign of the interblade phase angle. In other words, the cascade distinguishes between forward and backward travelling waves and hence, for a 12-bladed system, mode 1 ( $\beta_1 = \pi/6$ ) is different from mode 11 ( $\beta_{11} = -\pi/6$ ), 2 from 10, 3 from 9, etc ... Furthermore, in most

cases. the loci are of elliptical shape, the unstable modes usually opposing the stable ones. it will be shown later how this feature can be exploited to stabilise a biaded disc system by means of mistuning.

(II) Blade Interactions in the cascade. The force and moment acting on any given blade are dependent in some way on the blade's own position, velocity and rotation, and the position, velocity and rotation of all the other blades in the cascade, as well as the aerodynamic parameters. The blade interactions can best be viewed in a global sense by taking the discrete Fourier transform of a set of aerodynamic coefficients comprising all possible values of the interblade phase angle. Fig. 10.3 shows plots of the Fourier components in the case of the  $C_{M\alpha}$  coefficients for increasing values of the gap to chord ratio parameter. it is seen that the non-zero components are grouped on either side of the 0<sup>th</sup> order component which is the largest. This suggests that only a limited number of neighbouring blades can influence the reference blade, the interactions being roughly proportional to their respective distance. As the  $g/c$  parameter increases, all  $C_{M\alpha}$  coefficients tend to the same limiting value, irrespective of the value of the phase angle, and the cascade flow coincides with that past a single aerofoil: the reference blade. in this case, the DFT of a set of identical values returns all Fourier terms but the constant one as zero or, as expected, there is no contribution from other blades which are too distant. Similar calculations were performed for extending the validity of the result above to other aerodynamic coefficients ( $C_{Fh}$ ,  $C_{F\alpha}$ ,  $C_{Fw}$ ,  $C_{Mh}$  and  $C_{Mw}$ ) as well as to subsonic and supersonic flows. The same pattern was observed in all cases.



(III) Sensitivity tests\* Although three of the cascade parameters, namely  $g/c.\xi$  and  $\beta_r$ , are determined by its geometry. the remaining two, Mach number and reduced frequency, depend on the flow conditions and hence their evaluation may somehow be less accurate. To investigate the sensitivity of the aerodynamic coefficients to small changes in these two parameters, It was decided to compute their values at a series of neighbouring points as tabulated below:

$\lambda^-, M^-$	$\lambda^-, M$	$\lambda^-, M^+$
$\lambda, M^-$	$\lambda, M$	$\lambda, M^+$
$\lambda^+, M^-$	$\lambda^+, M$	$\lambda^+, M^+$

where  $-$  denotes a value under the nominal and  $+$  above. The test was performed at two points marked as A and B in Figs. 10.24 and 10.2g. The results for the  $C_{M\alpha}$  coefficient are tabulated below and plotted In Fig. 10.4.

T e s t  p o i n t  A: $M^\pm = 0.7 \pm .02, \lambda^\pm = .42 \pm .04$		
.50087 - .08295i	.62771 + .08450i	.59387 + .25643i
.73132 + .18769i	.58956 + .42477i	.43165 + .45305i
.50064 + .59905i	.31361 + .53301i	.24843 + .45937i
T e s t  p o i n t  B: $M^\pm = 1.3 \pm .03, \lambda^\pm = .42 \pm .04$		
-.12031 + .09655i	-.03374 + .08916i	-.00032 + .05334i
-.07218 - .06696i	-.10765 + .07365i	-.04277 + .07384i
-.05540 - .01068i	-.09843 - .07287i	-.09621 + .05509i

Table 10.1 Variation of the  $C_{M\alpha}$  coefficient for small changes in  $\lambda$  and  $M$

As can be seen from Figs. 10.4a and 10.4b, the  $C_{M\alpha}$  coefficient is quite sensitive to changes in both parameters, a property which must be considered duly if quantitative flutter predictions are required.

(iv) Pressure distribution along the blade chord. As mentioned earlier, once the pressure distribution function along the blade chord is known, the unsteady aerodynamic loads can be computed in a straightforward manner by integrating this function between the leading and trailing edges. Fig. 10.5 illustrates the pressure difference across the blade due to torsional vibration in the case of subsonic and supersonic flows. In both examples the integral equation was solved using 30 collocation points and hence the pressure distribution function was discretized at 30 points along the blade chord. As can be seen from Fig. 10.5a, the subsonic pressure distribution has a smooth shape as opposed to the supersonic one - shown in Fig. 10.5b - which exhibits a discontinuity at the point where the shock wave emanating from the leading edge of the blade below hits the reference blade. In agreement with these two examples above, further calculations showed that the pressure distribution function could, in most cases, be approximated by a series of quadratics each defined for a specific interval along the blade chord. This idea will be developed later in Chapter 11, to yield an aerodynamic model of finite element type.

### 10.3 CASE STUDY: TWELVE-BLADED DISC

Using the lumped parameter model described in Chapter 9, a detailed stability analysis and forced response study was made of a hypothetical twelve-bladed disc, henceforth referred to as disc A, with emphasis on

mistuning. Modern fans and compressors operate with flow velocities which are supersonic relative to the blades while the axial velocity entering the blade row remains subsonic. Accordingly, the aerodynamic computations will be restricted to this particular flow type which is of current practical interest. The aeroelastic system data are given below in Table 10.2.

Number of Blades	= 12
Stagger angle	= 62°
Distance between adjacent blades	= 86 mm
Distance between the CT and the CG	= 1 mm
Distance between the LE and the CT	= 75 mm
Blade length	= 500 mm
Chord length	= 100 mm
Blademass	= 0.785 Kg
Blade mass moment of inertia wrt CG	= 1.43 x 10 <sup>-3</sup> Kg. m <sup>2</sup>
First cantilever frequency in bending	= 50 Hz
First cantilever frequency in torsion	= 500 Hz
Reference frequency	= 500 Hz
Structural damping factor for bending	= 0
Structural damping factor for torsion	= 0 and 0.003
Disc sector mass	= 1.000 Kg
Interdisc stiffness	= 1.0 x 10 <sup>8</sup> N/m
Grounding stiffness	= 6.0 x 10 <sup>4</sup> N/m
Shroud stiffness in translation	= 1.0 x 10 <sup>6</sup> N/m
Shroud stiffness in rotation	= 1.0 x 10 <sup>3</sup> N/m
Relative flow velocity	= 375 m/s
Mach number	= 1.25
Fluid density	= 1.3 Kg/m <sup>3</sup>

Table 10.2 Aeroelastic system data

LE: Leading edge. TE: Trailing edge

CG: Centre of gravity. CT: Centre of twist

### 10.3.1 Tuned System

Preliminary Calculations.

Fig. 10.6 shows the natural frequency spectrum of disc A under vacuum conditions. Although the system under vacuum cannot differentiate between forward and backward travelling waves, the aerodynamically loaded one will and this is the reason for plotting the natural frequencies against the harmonic number instead of the more usual variable, the nodal diameter number. As the model allows three degrees of freedom per sector, the resulting modes are grouped into three families. The first one corresponding to blade bending, the second to blade torsion and the third exhibiting disc dominated modes. As there are no aerodynamic loads acting on the disc sector, the behaviour of this third family is of no interest in aeroelastic studies. Also, as pointed out in Ref. AD-23, and confirmed by independent calculations, the real part of the force coefficient  $C_{Fh}$  never becomes positive so that the uncoupled bending flutter is always stable (see also Ref. AD-30). Further calculations revealed that in order to make the bending modes of the coupled motion unstable, a series of rather unrealistic conditions (e. g. centre of gravity at the leading edge and centre of twist at the trailing edge or vice versa) would have to be imposed on the system and hence the first family was also excluded from the analysis. However, it is stressed that this result is specific to disc A and no wider generalization would be made at this stage. Although the model above covers a 3N eigen-spectrum for all cases studied, only those results related to the second family will be reported and discussed and hence when frequency or damping is mentioned, torsional motion is implied. The mode shapes of this family are displayed in Fig. 10.7.

Convergence of the aeroelastic modes.

As mentioned earlier, the convergence of the calculation of damped natural frequencies and associated aerodynamic damping factors requires an iterative technique in which the in-vacuum frequencies are taken as initial guesses. In view of the computational effort involved in calculating the aerodynamic coefficients and solving the eigenproblem, any such method would be unacceptably expensive unless a very rapid convergence rate was assured. A series of calculations, as formulated by equation (10-2), was conducted to check the numerical viability of the iterative scheme. The results are given below in Table 10.3 and plotted in Fig. 10.0.

r	$\Omega_0$	$\Omega_1$	$\Omega_2$	$\Omega_3$
0	500.27	498.62	490.61	<b>498.62</b>
1	506.17	498.83	498.64	490.64
2	521.97	509.65	509.04	508.97
3	542.82	<b>527.46</b>	526.43	526.31
4	562.90	546.76	545.55	545.40
5	577.17	562.08	561.01	560.71
6	582.31	570.02	569.00	568.80
7	577.17	567.92	567.40	567.11
<b>8</b>	562.90	557.19	556.92	556.24
9	542.82	546.29	546.29	546.29
10	521.97	527.86	527.75	527.68
11	506.17	511.17	511.06	511.01

Table 10.3 Convergence of the damped natural frequency (Hz)  
r: harmonic number;  $\Omega_j$ : frequency at j<sup>th</sup> iteration.

As can be seen from Table 10.2 and Fig. 10.8, the natural frequencies reach a stable value after the first iteration and further cycles do not

bring about any significant improvement which could justify the additional computational effort required. The same trend is also observed for the aerodynamic damping factor obtained from the imaginary part of the eigenvalue. Further calculations, not presented here, confirmed that the iteration could be stopped after the first cycle without significant loss of accuracy and this procedure was adopted for all subsequent calculations. Another interesting feature of Fig. 10.8 is the asymmetry of the damped natural frequencies on the  $\Omega_1$ ,  $\Omega_2$  and  $\Omega_3$  curves, contrasting the ones on the  $\Omega_0$  curve which correspond to the unloaded case.

#### Stability analysis.

In common with many other studies, it is found that the flutter stability is best visualized by plotting the real part of the eigenvalue (here, natural frequency) against the imaginary part (here, aerodynamic damping factor) on the Argand plane. Fig. 10.9 shows such a plot for the aeroelastic modes of disc A, the solid line determining the locus of the eigenvalues. As can be seen from Fig. 10.9, there is a wide variation in the stability of the aeroelastic modes, the ones associated with interblade phase angles 0,  $\pi/6$  and  $n/3$  (or harmonic numbers 0, 1 and 2) being unstable. These are opposed by modes 6, 7 and 8 which possess strong aerodynamic damping. The stability of the first three modes can be improved by:

- (i) stabilizing them at the expense of the remaining ones, especially numbers 6, 7 and 8; and/or
- (ii) altering the corresponding mode shapes since the amount of aerodynamic damping in each mode is motion dependent.

Techniques (i) and (ii) above are concurrent, though not necessarily

compatible. in the sense that they are both Introduced using some means of structural modification. This Idea will be developed in the next section under the heading of mistuning.

The correlation between the imaginary part of the  $C_{M\alpha}$  coefficient and the aerodynamic damping value was investigated by plotting the latter against the former in Fig. 10.10a. It is clearly seen that damping is almost directly proportional to  $\text{Im}(C_{M\alpha})$  and this is an expected result since the centre of twist being very close to the centre of gravity, coupling between bending and torsion is weak.

The deviation from the in-vacuum natural frequencies - defined by  $(\Omega_0^2 - \Omega^2) / 100$  as in Ref. AE-8 - is simiariy controlled by  $\text{Re}(C_{M\alpha})$  and this is shown in Fig. 10.10b. The relative percentage deviation - defined by  $100 \times (\Omega_0 - \Omega) / \Omega$  - is small and rarely exceeds 1%. the largest occuring for  $\beta_r = \pi$  with 2%. This is an expected result since the ratio of material to air densities is large for most aeroelastic applications, and so the damped frequency is usually close to the in-vacuum one.

#### Effect of structural damping.

The broken line in Fig. 10.9 corresponds to the case where some structural damping of the hysteretic type was introduced by setting  $\eta_\alpha$  to 0.003. It is immediately seen that its only effect, as predicted by equation (9-8), is simply to shift the locus bodily towards stability without changing the natural frequencies. This was true for all the cases computed and these other results will therefore not be presented.

### 10.3.2 Effects of Mistuning

in recent years, the idea of utilizing blade mistuning as a passive means of flutter control has been suggested by several authors (see for instance Refs. AE-13, AE-15 and AE-23). The purpose of this section is to extend this popular approach to a model where the blades are both aerodynamically and structurally coupled, a feature which was absent from previous studies. As explained earlier, the mistuning is introduced through the torsional stiffness parameter  $c$ , thus restricting the blade-to-blade differences to the variation in individual blade cantilever frequencies in torsion.

Fig. 10. 11 shows six stability plots, each corresponding to a different type of mistuning with comparable levels of deviation from the reference blade frequency at 500 Hz. The corresponding data are given in Table 10.4. As can be seen from Fig. 10. 11, each mistuning pattern leads to a different stability locus with at least one mode being unstable. Before studying in some detail each of the six mistuning cases, it should be stressed that modal interferences due to mistuning occur and hence there is always more than one harmonic present in any one mode. Although the dominant interblade phase angle can usually be identified without much difficulty (that is how the individual points of Fig. 10. 11 are labelled), the assumption stating that all blades move with the same amplitude and a constant phase angle is violated. Also, Fig. 10. 12 shows the discrete Fourier transform components of the eigenvectors associated with the unstable modes 0, 1 and 2.



- (i) The first type of mistuning to be considered is random mistuning which is simulated by defining the mean (500 Hz) and the standard deviation (25 Hz) of the population and then using a random number generator to calculate the individual blade frequencies which constitute the sample. The stability plot shown in Fig. 10. 11a corresponds to a sample mean of 493 Hz and a sample standard deviation of 21 Hz. Compared to their tuned counterparts, all mistuned modes are shifted in a random manner which, to a certain extent, can be explained with the aid of Fig. 10. 12a. It is immediately seen that each mode shape contains all possible harmonics ( $r = 0, 11$ ) and hence the change in stability of any one mode is dictated by all the others depending on how the harmonics are coupled. Due to all these modal interferences, it is very difficult, if at all possible, to find a pattern from which changes in stability could be predicted.
- (ii) The second type is cosine mistuning governed by the detuning function  $0.05 \cos 2\theta$ . As can be seen from Fig. 10. 11b, the marked improvement of modes 0, 1 and 2 is balanced by the deterioration of modes 7, 8 and 11. These six are the *active* modes as opposed to the remaining ones which are the *passive* modes. From a structural viewpoint, this result may be seem unexpected since in the case of a 12-bladed disc, any detuning function of the form  $\cos 2\theta$  is known to split all double modes into pairs of single ones such as (1,11), (2,10), (3,9), (4,8), and (5,7). Fig. 10. 12b reveals, however, that either all even (including 0) or all odd harmonics are coupled in any one mode, suggesting that modes 0 and 2 are stabilized at the expense of mode 8; mode 1 at the expense of 7 and 11, etc.
- (iii) The third type is single blade mistuning where the first blade's cantilever frequency is set to 525 Hz, all the other ones remaining unchanged at 500 Hz. Fig. 10. 11c shows that, there is no significant improvement in the stability of the first three modes, a

phenomenon which can easily be explained with the aid of Fig. 10.12c. All three modes contain major harmonics of order 0, 1, 2, 10 and 11, and hence the interactions take place mainly among these already unstable modes. It is also seen that modes 10 and 11 are both destabilized to compensate for 1 and 2, and mode 0 is shifted further towards instability.

(iv) The fourth type is alternate mistuning of 10% in which even and odd numbered blades have different cantilever frequencies, these being at 525 Hz and 475 Hz respectively. Because of the symmetry inherent in this type of mistuning, the harmonic associated with the phase angle  $\beta_r$  becomes coupled with that associated with  $(\beta_r + \pi)$ . In the case of a 12-bladed disc, 0 is coupled with 6, 1 with 7, 2 with 8, etc. This is illustrated in Fig. 10.12d. As can be seen from Fig. 10.11d, alternate mistuning results in a strong stabilizing effect on the system since unstable modes 0, 1 and 2 are opposed by the heavily damped ones, i.e. 6, 7 and 8. Another interesting feature of Fig. 10.11d is the split of the stability locus into two distinct loops. This is due to the forced grouping of the individual blade frequencies into high and low families under the effect of mistuning.

(v) The fifth type of mistuning to be considered is a special arrangement, henceforth referred to as SA1 mistuning, in which two high frequency blades at 525 Hz are followed by two low frequency blades at 475 Hz. In this case the symmetry group consists of four blades, analogous in some respects to a four-bladed packet, and as can be seen from Fig. 10.12e, the harmonics which couple with  $\beta_r$  are  $(\beta_r + \pi/2)$ ,  $(\beta_r + \pi)$  and  $(\beta_r + 3\pi/2)$ . As in the previous case, and due to the same reason, this type of mistuning has a strong stabilizing effect on the system. The stability plot is seen to split into four distinct loops of three modes each, this being due to the individual blades grouping into two low and two high frequency families.

(vi) The sixth and the last type of mistuning is another special arrangement. henceforth referred to as SA2 mistuning, in which two high frequency blades at 525 Hz are followed by one low frequency blade at 475 Hz. This causes harmonic  $\beta_r$  to be coupled with  $(\beta_r + 2\pi/3)$  and  $(\beta_r + 4\pi/3)$  and the stability locus splits into three families of four modes each (see Figs. 10.11f and 10.120).

Random mistuning				Cosine mistuning		
r	$\Omega_0$	n	$\eta$	$\Omega_0$	n	$\eta$
0	484.2	484.9	-1.0	490.2	487.5	-0.8
1	488.1	481.3	-5.9	491.0	488.0	-4.4
2	506.1	498.4	5.7	519.0	512.1	2.4
3	532.6	524.9	32.1	541.0	528.9	16.0
4	557.4	548.1	58.6	557.7	545.4	44.1
5	570.6	577.7	69.1	571.1	559.9	64.9
6	588.8	577.0	90.0	591.4	579.9	89.8
7	573.8	562.8	87.8	590.8	579.5	85.7
8	562.3	554.1	80.7	566.0	557.0	87.2
9	540.3	535.5	40.6	545.3	544.9	59.9
10	521.5	518.4	28.8	528.3	528.6	40.2
11	500.2	500.5	19.2	513.4	512.4	20.9
Single blade mistuning				Alternate mistuning		
r	$\Omega_0$	n	$\eta$	$\Omega_0$	n	$\eta$
0	501.2	499.2	-8.3	494.3	492.2	3.2
1	506.2	500.6	-7.8	499.4	492.2	-7.8
2	522.0	511.1	-3.0	511.7	500.8	4.1
3	542.8	529.9	34.0	519.9	511.4	22.4
4	562.9	549.3	51.8	573.4	562.7	43.1
5	577.2	563.9	68.9	584.1	571.3	58.6
6	588.2	576.6	88.1	588.5	577.0	83.5
7	580.0	569.1	95.7	584.1	574.9	90.7
8	566.3	668.9	100.9	573.4	566.2	89.7
9	546.4	547.2	50.2	568.0	560.9	41.9
10	525.5	528.8	21.2	511.7	513.0	40.6
11	509.3	512.9	23.2	499.4	502.7	30.4

Table 10.4 Mistuning data (Continued)  
r: harmonic number;  $\Omega_0$ : vacuum frequency;  
 $\Omega$ : damped frequency;  $\eta$ : damping factor.

(vi) The sixth and the last type of mistuning is another special arrangement. henceforth referred to as SA2 mistuning, in which two high frequency blades at 525 Hz are followed by one low frequency blade at 475 Hz. This causes harmonic  $\beta_r$  to be coupled with  $(\beta_r + 2\pi/3)$  and  $(\beta_r + 4\pi/3)$  and the stability locus splits into three families of four modes each (see Figs. 10.11f and 10.120).

Random mistuning				Cosine mistuning		
r	$\Omega_0$	n	$\eta$	$\Omega_0$	n	$\eta$
0	484.2	484.9	-1.0	490.2	487.5	-0.8
1	488.1	481.3	-5.9	491.0	488.0	-4.4
2	506.1	498.4	5.7	519.0	512.1	2.4
3	532.6	524.9	32.1	541.0	528.9	16.0
4	557.4	548.1	58.6	557.7	545.4	44.1
5	570.6	577.7	69.1	571.1	559.9	64.9
6	588.8	577.0	90.0	591.4	579.9	89.8
7	573.8	562.8	87.8	590.8	579.5	85.7
8	562.3	554.1	80.7	566.0	557.0	87.2
9	540.3	535.5	40.6	545.3	544.9	59.9
10	521.5	518.4	28.8	528.3	528.6	40.2
11	500.2	500.5	19.2	513.4	512.4	20.9
Single blade mistuning				Alternate mistuning		
r	$\Omega_0$	n	$\eta$	$\Omega_0$	n	$\eta$
0	501.2	499.2	-8.3	494.3	492.2	3.2
1	506.2	500.6	-7.8	499.4	492.2	-7.8
2	522.0	511.1	-3.0	511.7	500.8	4.1
3	542.8	529.9	34.0	519.9	511.4	22.4
4	562.9	549.3	51.8	573.4	562.7	43.1
5	577.2	563.9	68.9	584.1	571.3	58.6
6	588.2	576.6	88.1	588.5	577.0	83.5
7	580.0	569.1	95.7	584.1	574.9	90.7
8	566.3	668.9	100.9	573.4	566.2	89.7
9	546.4	547.2	50.2	568.0	560.9	41.9
10	525.5	528.8	21.2	511.7	513.0	40.6
11	509.3	512.9	23.2	499.4	502.7	30.4

Table 10.4 Mistuning data (Continued)

r: harmonic number;  $\Omega_0$  vacuum frequency;  
n: damped frequency;  $\eta$ : damping factor.

SA1 mistuning				SA2 mistuning		
r	$\Omega_0$	$\Omega$	$\eta$	$\Omega_0$	$\Omega$	$\eta$
0	489.5	486.9	2.0	499.9	497.3	7.7
1	492.1	407.1	-6.0	503.6	497.5	-4.5
2	524.8	490.8	11.9	508.6	502.7	7.2
3	533.0	524.5	31.5	554.7	545.0	20.7
4	561.4	550.3	34.5	564.4	554.2	44.0
5	590.3	578.1	79.1	591.3	579.3	59.7
6	592.4	581.9	82.1	595.2	584.2	84.2
7	590.3	580.2	86.3	591.3	582.2	92.4
8	561.4	554.3	68.0	585.2	575.3	86.5
9	533.7	549.5	44.4	554.7	554.3	45.3
10	524.8	524.2	45.1	546.0	543.6	22.9
11	492.1	518.5	28.4	503.6	504.1	27.7

Table 10.4 Mistuning data (Concluded)

r: harmonic number;  $\Omega_0$  vacuum frequency;  
 $\Omega$ : damped frequency;  $\eta$ : damping factor.

It is difficult to assess the most beneficial type of mistuning because:

ta) although the mistuning levels are compatible. there is no real one-to-one correspondence: and

(b) as the aerodynamic effects depend on both the frequency and amplitude of vibration. the amount of global damping - defined as the algebraic sum  $\sigma$  of all damping values - varies in each case. The following values. each corresponding to a different type of mistuning. were calculated from Table 10.4:

$$\sigma_i = 505.6, \quad \sigma_{ii} = 505.9, \quad \sigma_{iii} = 514.8$$

$$\sigma_{iv} = 500.5, \quad \sigma_v = 508.1, \quad \sigma_{vi} = 494.6$$

and in the case of the tuned system  $\sigma$  is 519.2. This suggests that in spite of stabilizing a number of modes. mistuning may well decrease the global amount of damping, thus degrading the overall stability. further calculations with different system data showed that the global damping could also be increased by mistuning. this being a very complicated

function of the motion because of the aerodynamic coefficients involved.

### 10.3.3 The Special Case of Alternate Mistuning

Although all the last three mistuning types studied gave quite similar results, the case of alternate mistuning is somewhat special and requires further consideration.

- (i) The Fourier analysis of some research fan data provided by a well-known engine manufacturer showed that this type of mistuning already existed in more than 80% of the assemblies studied, probably due to dynamic balancing considerations.
- (ii) As the harmonic associated with  $\beta_r$  is coupled *on/y* with that associated with  $(\beta_r + \pi)$ :
  - the success of the method can be predicted straight away;
  - under certain simplifying conditions (stiff disc, flexible blades) the analysis can be reduced to the study of a two-bladed cascade with phase angles  $\beta_r$  and  $(\beta_r + \pi)$ ;
  - the susceptibility of each mode to forced response is restricted to two harmonics.

Figure 10.13 shows the variation of modal aerodynamic damping with increasing degree of alternate mistuning. Once again, it is clearly seen that  $\beta_r$  modes are stabilized at the expense of  $(\beta_r + \pi)$  modes. Also, certain pairs, namely (4, 10) and (5, 11), do not play an active part in the stability transfer, their modal damping values being subject to fluctuations of the aerodynamic load rather than changing with structural mistuning. Further calculations showed that this is always the case with alternate mistuning, the number and identity of these passive modes being determined by the number of blades in the system; though a

rational pattern could not be identified. As can be seen from Fig. 70.13c, mode 2 exhibits a drop towards instability at 20% mistuning and the situation is not improved at 22%. The cause to this phenomenon is of aerodynamic origin and can be traced back to the moment coefficient associated with the interblade phase angle  $\beta_8 = 4\pi/3$ . Table 10.5 gives values for the  $C_{M\alpha}$  coefficient calculated at the undamped natural frequencies of mode 8.

% Mist.	$\Omega$ (Hz)	$\lambda$	$Re(C_{M\alpha})$	$Im(C_{M\alpha})$
16	584.84	.9799	.077977	-.316625
18	588.99	.9887	.076338	-.316664
20	593.22	.9939	.007528	-.202775
22	597.54	1.0012	.006331	-.202775

Table 10.5 Variation of the  $C_{M\alpha}$  coefficient with frequency  
 $\Omega$ : damped frequency;  $\lambda$ : reduced frequency.

The imaginary part of  $C_{M\alpha}$ , shown to be directly proportional to damping, exhibits a sudden jump at 20% mistuning which in turn effects the stability of mode 8 dramatically. The loss in damping is partly recovered by mode 2, which inevitably is shifted towards the instability boundary. Assuming that it is not due to a numerical problem - a number of tests including a search for acoustic resonance suggested it was not - this type of behaviour is a good example of how interactions take place between the structural and aerodynamic parts within the aeroelastic model. It further suggests that mistuning can have unpredictable effects on the system's stability by altering the aerodynamic load beyond expected levels.

As mentioned earlier, the global amount of aerodynamic damping is a

rational pattern could not be identified. As can be seen from Fig. 70.13c, mode 2 exhibits a drop towards instability at 20% mistuning and the situation is not improved at 22%. The cause to this phenomenon is of aerodynamic origin and can be traced back to the moment coefficient associated with the interblade phase angle  $\beta_8 = 4\pi/3$ . Table 10.5 gives values for the  $C_{M\alpha}$  coefficient calculated at the undamped natural frequencies of mode 8.

% Mist.	$\Omega$ (Hz)	$\lambda$	$Re\{C_{M\alpha}\}$	$Im\{C_{M\alpha}\}$
16	584.84	.9799	.077977	-.316625
18	588.99	.9887	.076338	-.316664
20	593.22	.9939	.007528	-.202775
22	597.54	1.0012	.006331	-.202775

Table 10.5 Variation of the  $C_{M\alpha}$  coefficient with frequency  
 $\Omega$ : damped frequency;  $\lambda$ : reduced frequency.

The imaginary part of  $C_{M\alpha}$ , shown to be directly proportional to damping, exhibits a sudden jump at 20% mistuning which in turn effects the stability of mode 8 dramatically. The loss in damping is partly recovered by mode 2, which inevitably is shifted towards the instability boundary. Assuming that it is not due to a numerical problem - a number of tests including a search for acoustic resonance suggested it was not - this type of behaviour is a good example of how interactions take place between the structural and aerodynamic parts within the aeroelastic model. It further suggests that mistuning can have unpredictable effects on the system's stability by altering the aerodynamic load beyond expected levels.

As mentioned earlier, the global amount of aerodynamic damping is a



system property which is effectively constant for given structural and flow conditions. Fig. 10. 14 shows the variation of this quantity with increasing alternate mistuning. Particular attention must be paid to the drop at 20% mistuning and to the partial recovery at 22% mistuning as a result of which some of the modes of Figs. 10. 13b and 10. 13c, namely 5, 10 and 11, have been individually stabilized.

Finally, It was proposed to investigate the effects of alternate mistuning on systems with odd number of blades. To this end the number of blades in disc A was decreased by one and the new 11-bladed assembly was called disc B. In this case, because of the broken cyclic symmetry, all permissible harmonics ( $r=0, 10$ ) are present in any one mode, thus giving rise to more complex modal interactions than previously. Nevertheless, as can be seen from Fig. 10. 15, the global picture is quite similar to the previous case, harmonic  $\beta_r$  being primarily coupled either to:

$$[\beta_r + (N - 1)\pi/N] \quad \text{or to} \quad [\beta_r + (N + 1)\pi/N]$$

or sometimes to both. From the formulation above, it is obvious that the odd numbered case will tend to coincide with the even numbered one with increasing number of blades.

#### 10.4 AEROELASTIC RESPONSE TO FORCED VIBRATION

it was shown in Chapter 9 that the analytical model developed in this study could also be used to predict the response levels of the assembly to various forms of harmonic forcing induced by wakes: The forced

response will be presented for disc A at a lower relative flow velocity ( $V = 340$  m/s) so that the system is aeroelastically stable in all modes. Furthermore, the velocity  $W$  of the disturbance induced by wakes is assumed to be equal to that of the main flow so that the ratio  $W/V$  reduces to unity. Calculations were first made for the tuned system, and Fig. 10.16 shows the response curves (which are identical for all 12 blades) for the three cases of 2, 3 and 6 engine order (EO) excitations. The reason for exciting these particular modes is that the first one has the lowest amount of aerodynamic damping, the third has the highest and the second is representative of the average value. As can be seen from Fig. 10.16, the level of the forced response maximum is inversely proportional to aerodynamic modal damping, a well-known characteristic of structurally-damped systems.

A further set of results is shown in Fig. 10.17 for 2% alternate mistuning of the same assembly subjected to a 3<sup>rd</sup> engine order (3EO) excitation. Only two harmonics, of order 3 and 9, are present in mode 3 as a result of which odd and even numbered blades vibrate with different amplitudes. The 3EO response curve of the tuned system is consequently split into two, the first one corresponding to low frequency blades and the second to high frequency ones. Each of these curves exhibits two resonances, one primary and one secondary, and hence the single resonance peak corresponding to the tuned system is replaced by four distinct peaks one of which is very heavily damped. Also in Fig. 10.17 are shown the response curves (broken line) of the same mistuned system on which no aerodynamic forces act. It is immediately seen that these exhibit only the primary resonances and the same is also true of the tuned system. The presence of the secondary resonances is

due to mistuning under which effect the system distinguishes between forward and backward travelling waves. it is of further interest to notice that these secondary resonances occur slightly earlier than the primary ones. the relative difference being about 0. 1%.

In this particular example, the forced response level caused by mistuning is comparable to that for the tuned system. Additional calculations. which are not presented here. showed that alternate mistuning could also have a beneficial effect by lowering the forced response level. though it was a rare occurrence.

#### 10.5 CONCLUDING REMARKS

An analytical model. based on the lumped parameter technique and two-dimensional cascade theory. has been set up and used successfully to investigate the flutter stability and the aeroelastic response of bladed-disc systems subjected to various flow regimes. It has been found that:

- (i) In the case of subsonic and supersonic flows. the convergence rate of computing the aerodynamic coefficients is unexpectedly slow and the solution of the Integral equation usually requires more than 20 collocation points, 30 having been used in most cases. For large numbers of blades the calculations become too expensive to conduct parametric studies and hence the present analysis was restricted to a 12-bladed system.
- (ii) Single degree-of-freedom torsional Instabilities encountered in subsonic and supersonic flows and known as acoustic resonance have been excluded from the present analysis. This phenomenon is of aerodynamic origin and is due to the singular behaviour of

the generating power series for certain very narrow ranges of the interblade phase angle which, in the general case, do not coincide with the discretized values corresponding to the finite number of blades. Further details can be found in Refs. AD-30 and AD-31.

- (iii) For a given aeroelastic system, the calculations are quite sensitive to small changes in both the reduced frequency and the Mach number but less so to the fluid density. The reduced frequency and the Mach number, both functions of the velocity, show considerable variations from blade root to tip, a feature which cannot be represented accurately by the typical section approach unless the blade's hub to tip ratio is close to unity. A realistic solution should consider modelling the entire blade from root to tip but the problem size would then become prohibitive for including any form of mistuning.
- (iv) Although the effect of mistuning generally results in the stabilization of certain particular modes, the opposite may also result due to sudden changes in the modal damping amount which in turn are caused by unpredictable variations of the aerodynamic coefficients.
- (v) In Ref. AE-24 it is reported that mistuning can have an adverse effect on the system's stability. Using the principle of virtual work, the blades are classified into two categories, namely dampers which dissipate aerodynamic energy via friction and *exciters* which act as sources of external force through which the excess energy is transmitted. The stability of the system is a function of the damper to exciter ratio which depends on the amount of mistuning introduced. The disagreement with the present analysis is believed to be due to the underlying assumption that the interblade phase angle remains constant, even in the mistuned case.
- (vi) Finally, there is a one-to-one correspondence between a packeted bladed disc and a symmetrically mistuned one. In both cases, the cyclic symmetry is symmetrically destroyed and the mode shapes

contain several Fourier components which can be predicted from knowledge of the total number of blades and the mistuning (or packeting) configuration.

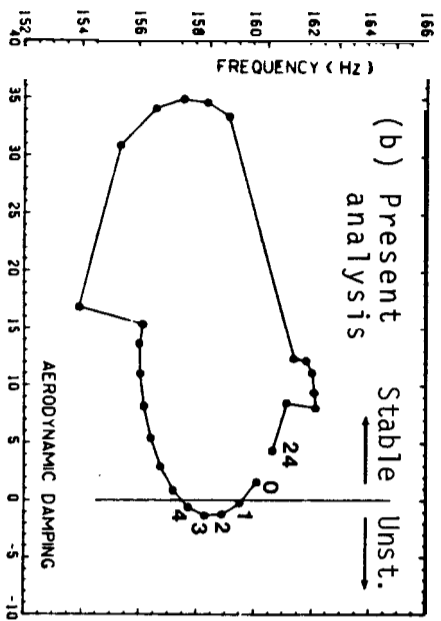
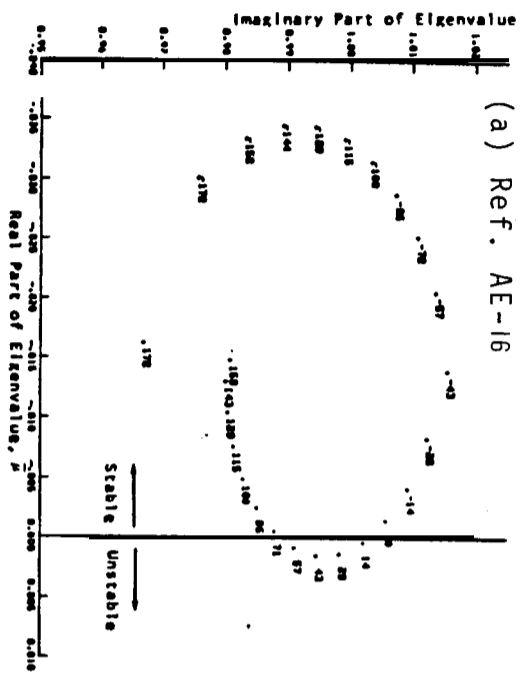


Fig. 10.1 Test case : 25-b ded cascade

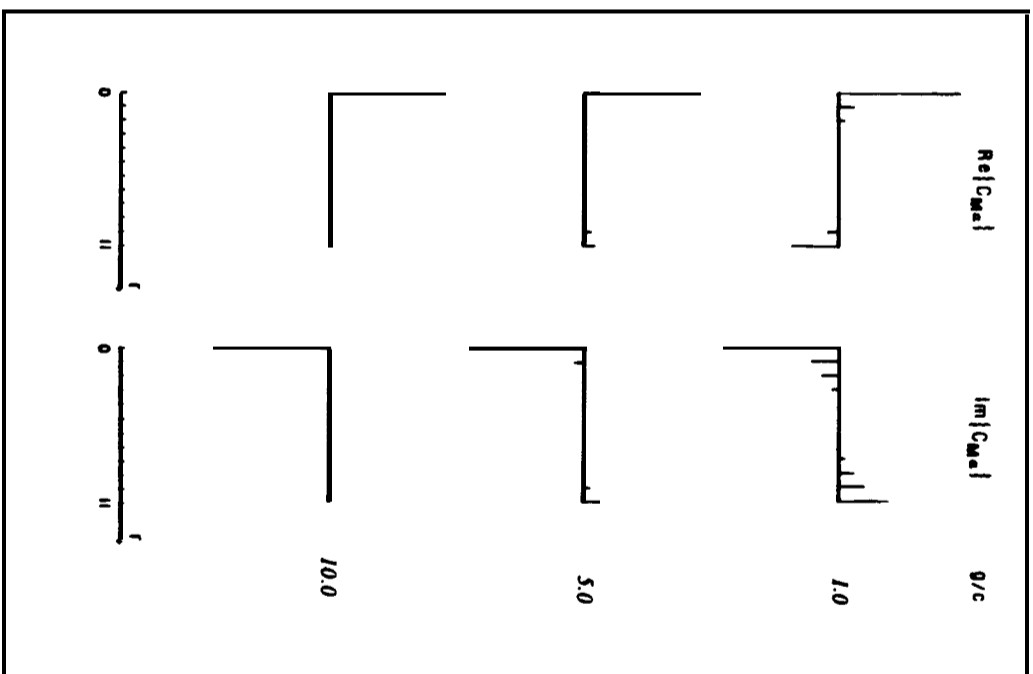


Fig. 10.3 Variation of the Fourier components with  $g/c$   
 $M=0$ ,  $\lambda=.42$ ,  $EA=.43$ ,  $\xi=48$

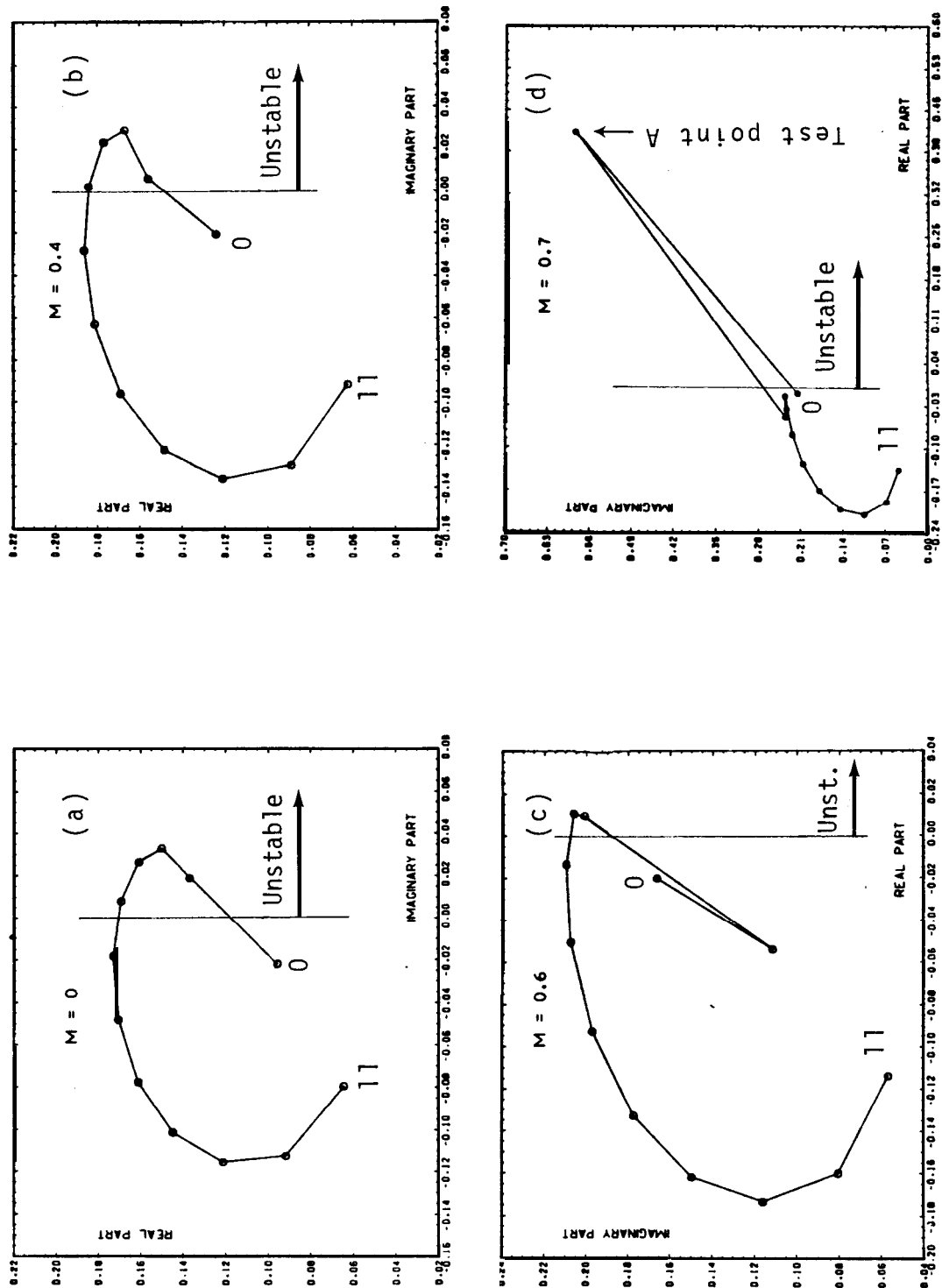


Fig. 10.2 Stability plots for various flow regimes (Continued)

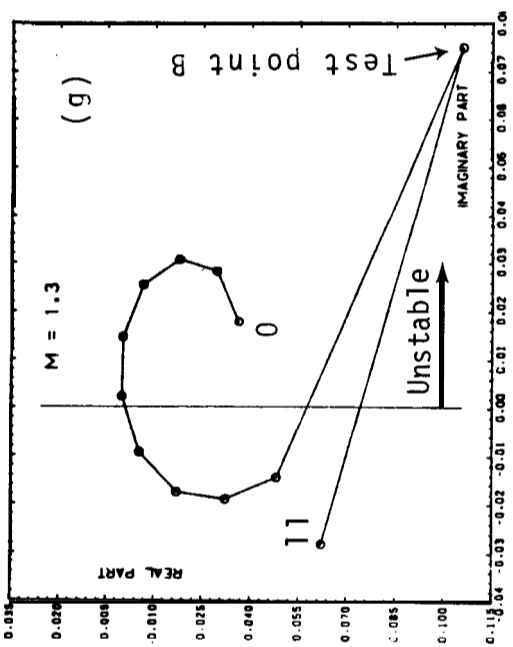
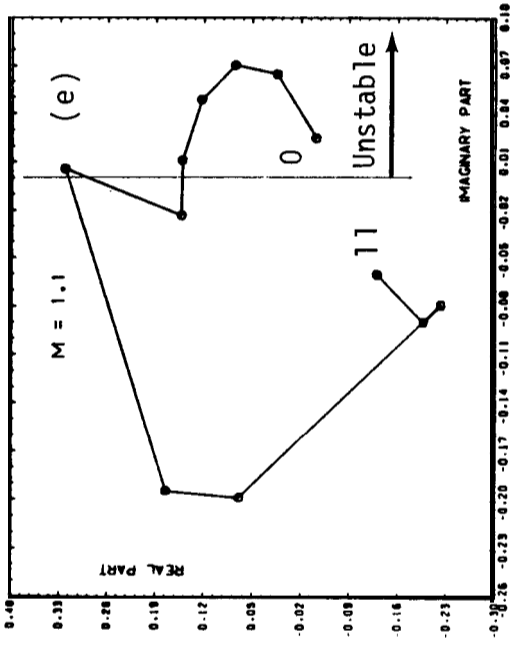
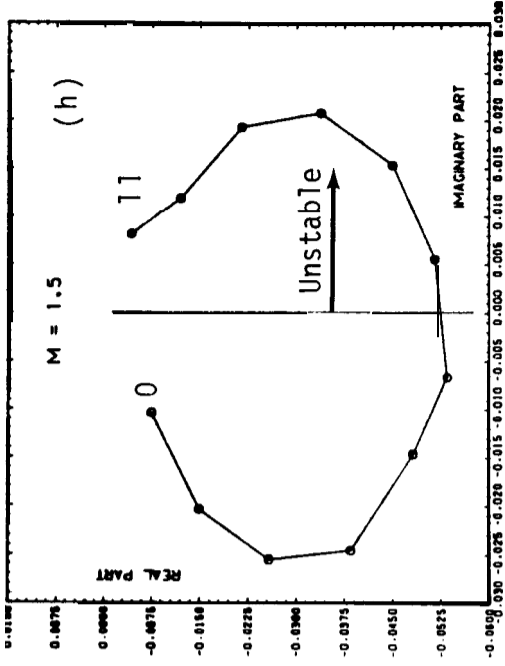
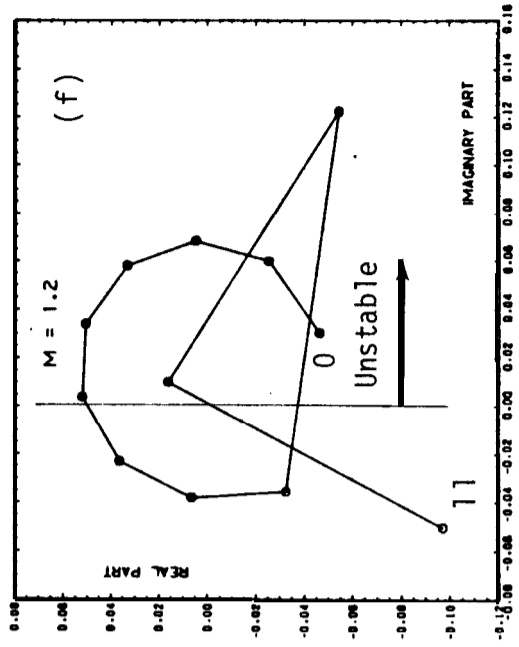


Fig. 10.2 Stability plots for various flow regimes (Concluded)



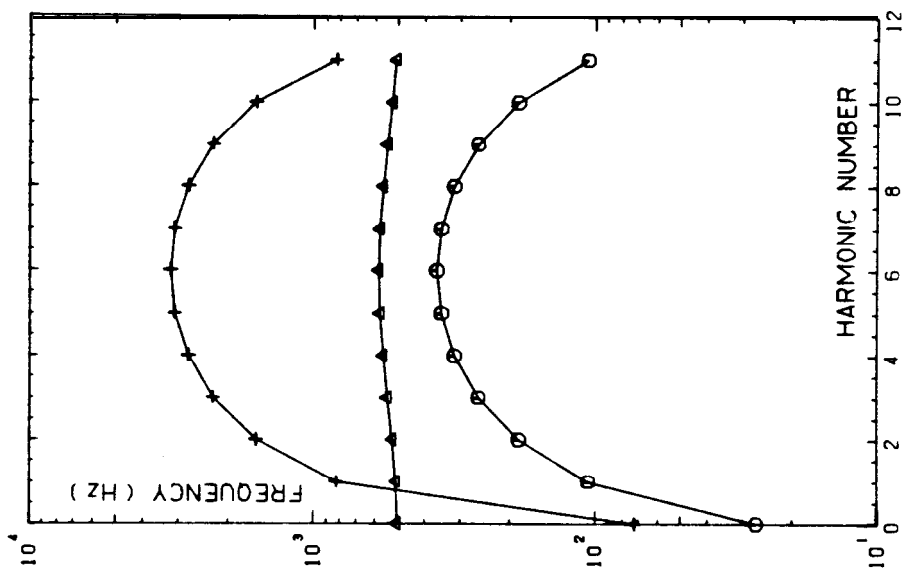


Fig. 10.6 Natural frequencies of the unloaded system.

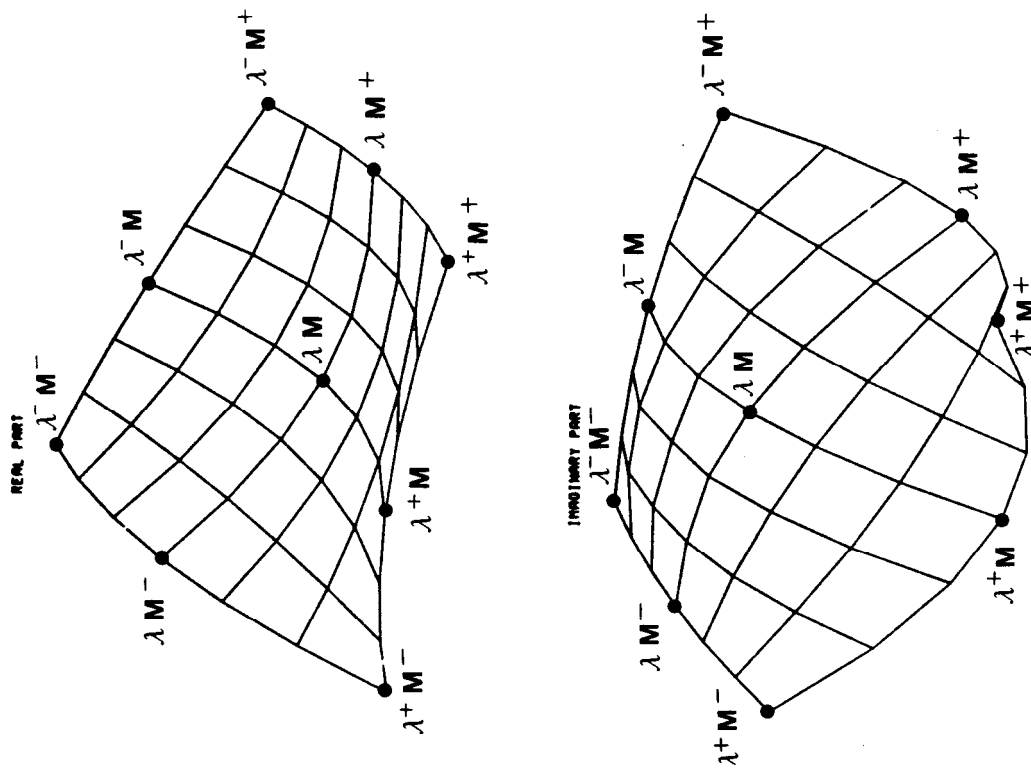
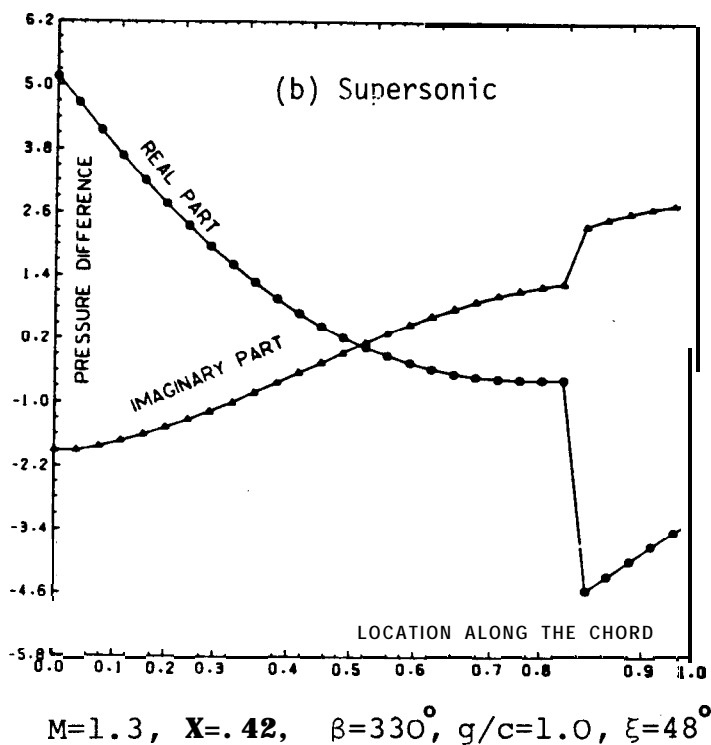
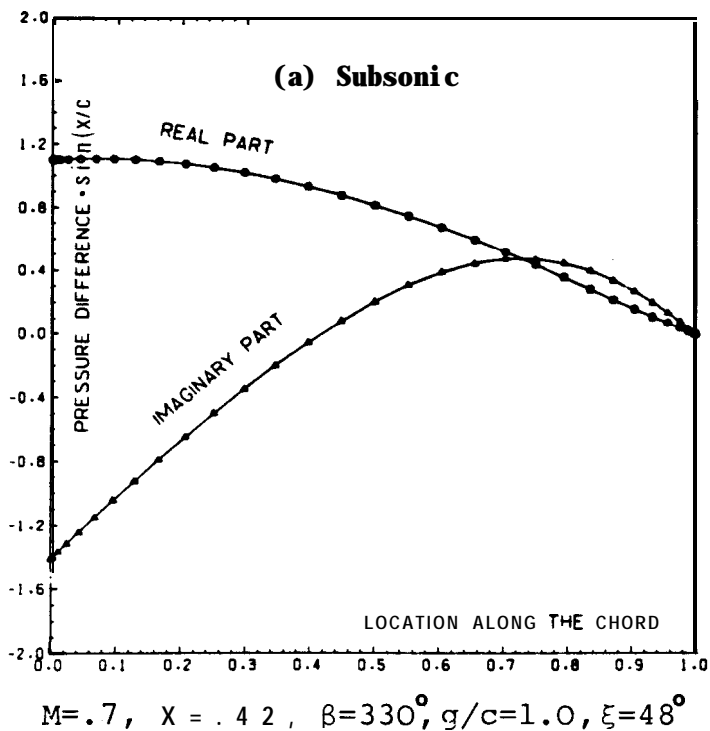


Fig. 10.4 Variation of the  $C_{M\alpha}$  coefficient for small changes in  $\lambda$  and  $M$



**Fig. 10.5** Pressure distribution due to torsional motion

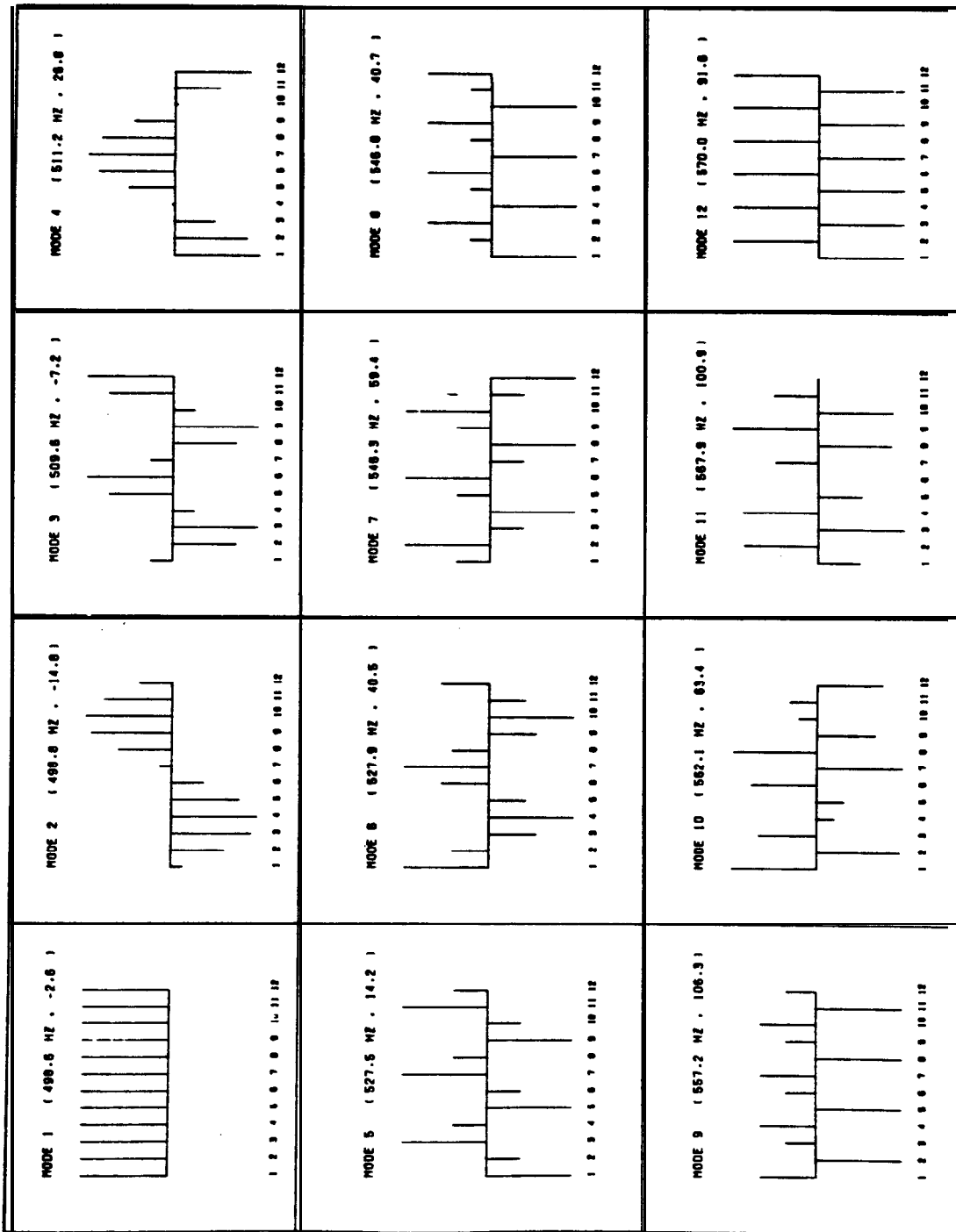
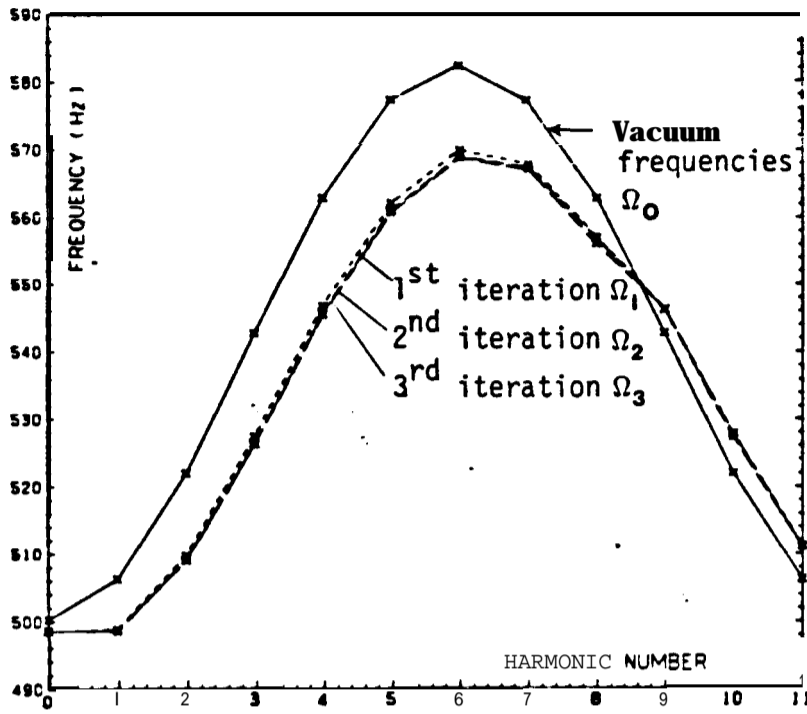
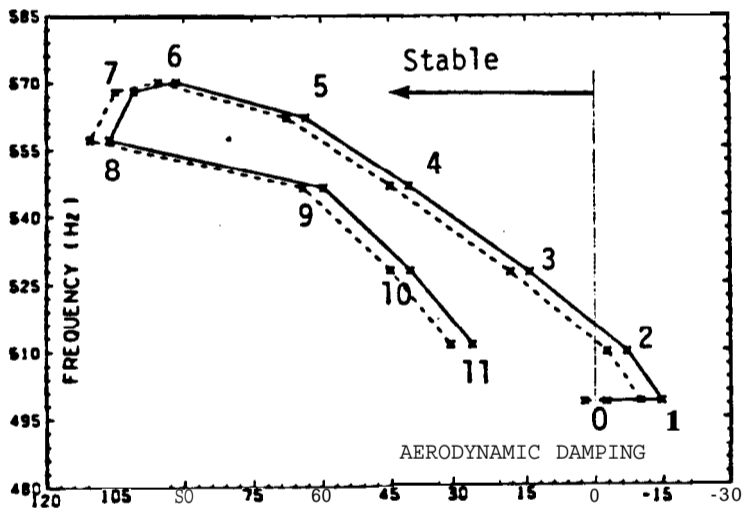


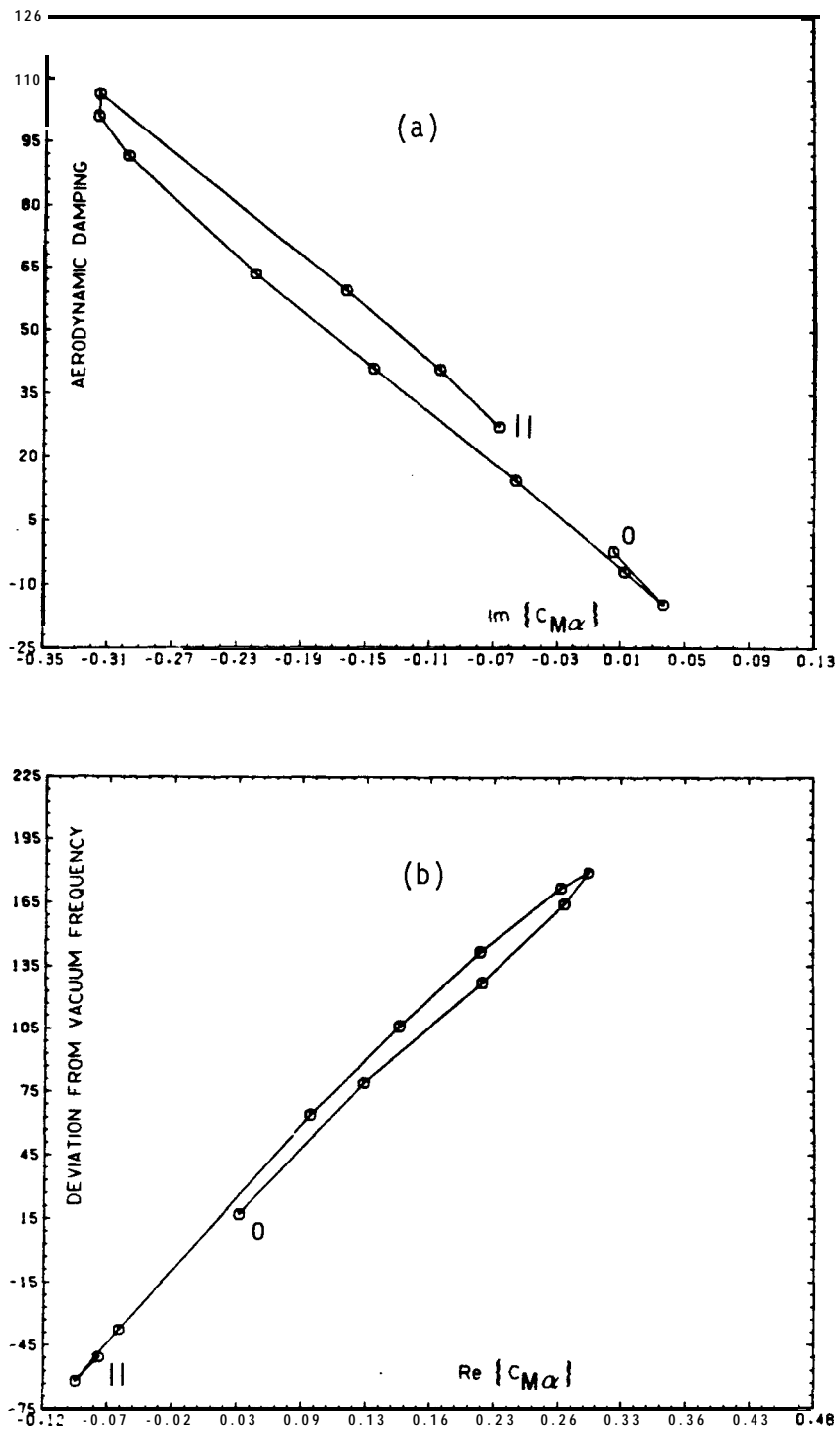
Fig. 10.7 Modal properties of the 12-bladed system under aerodynamic load



**Fig. 10.8** Convergence of the damped natural frequency



**Fig. 10.9** Effect of structural damping



**Fig. 10.10** Correlation between the computed eigenvalue and the  $C_{M\alpha}$  coefficient

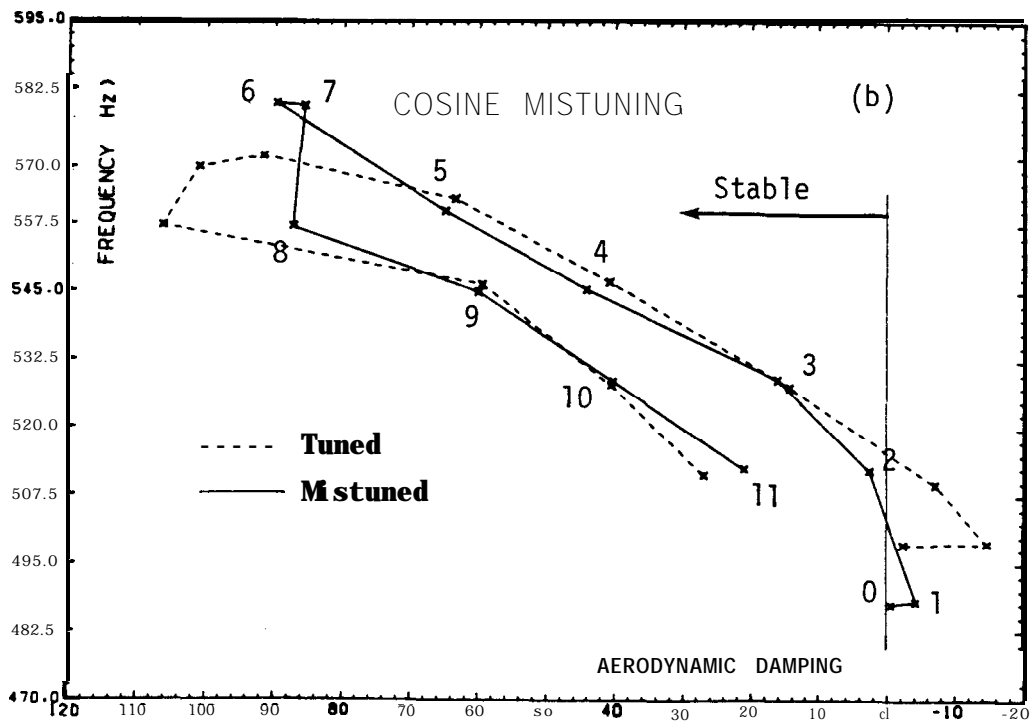
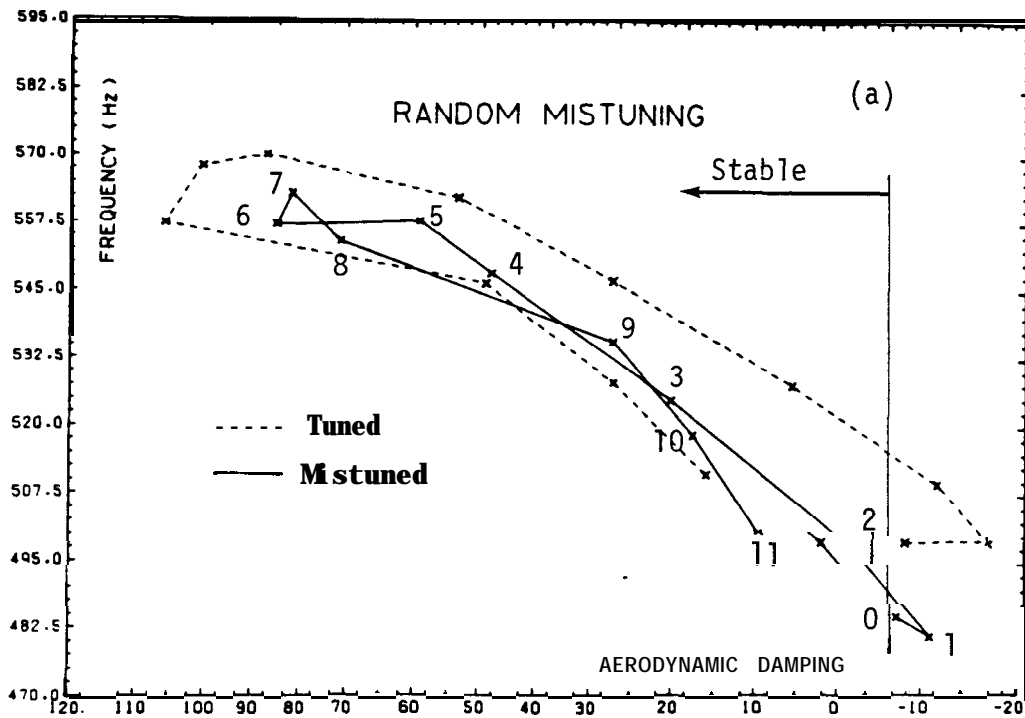
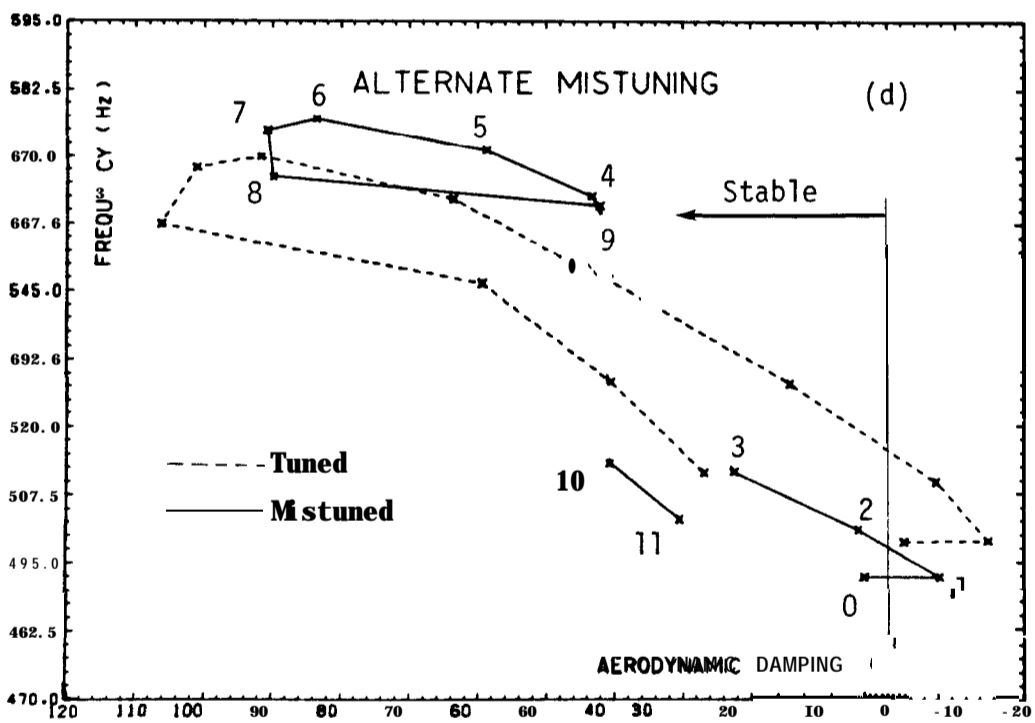
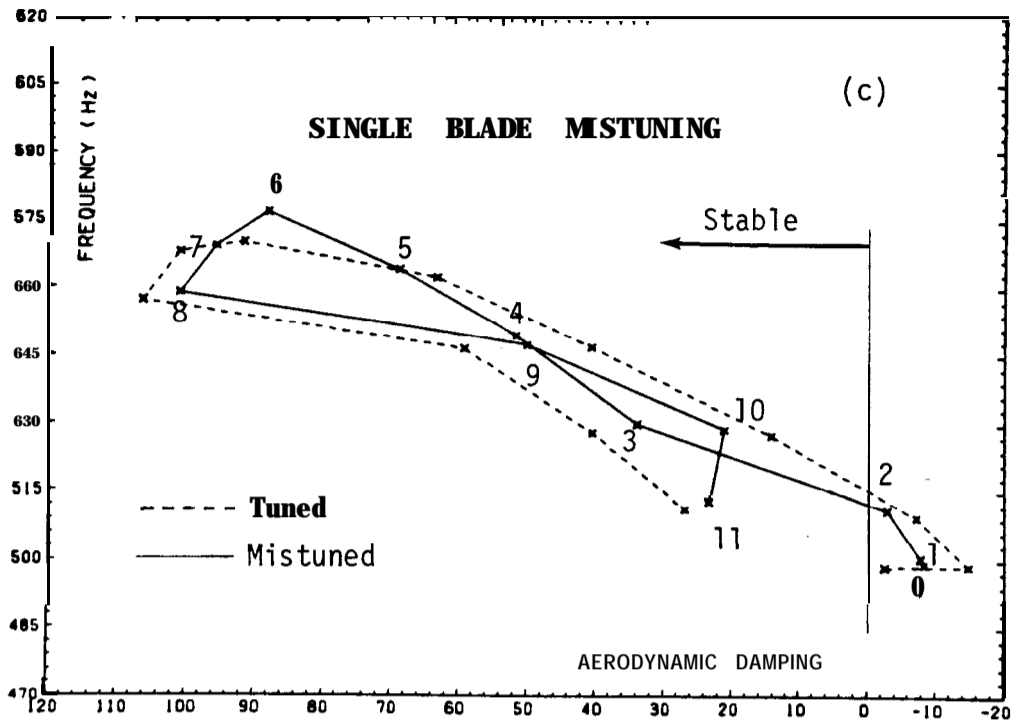


Fig. 10.11 Stability diagrams for various types of mistuning (Continued)



**Fig. 10.11** Stability diagrams for various types of mistuning  
**(Continued)**

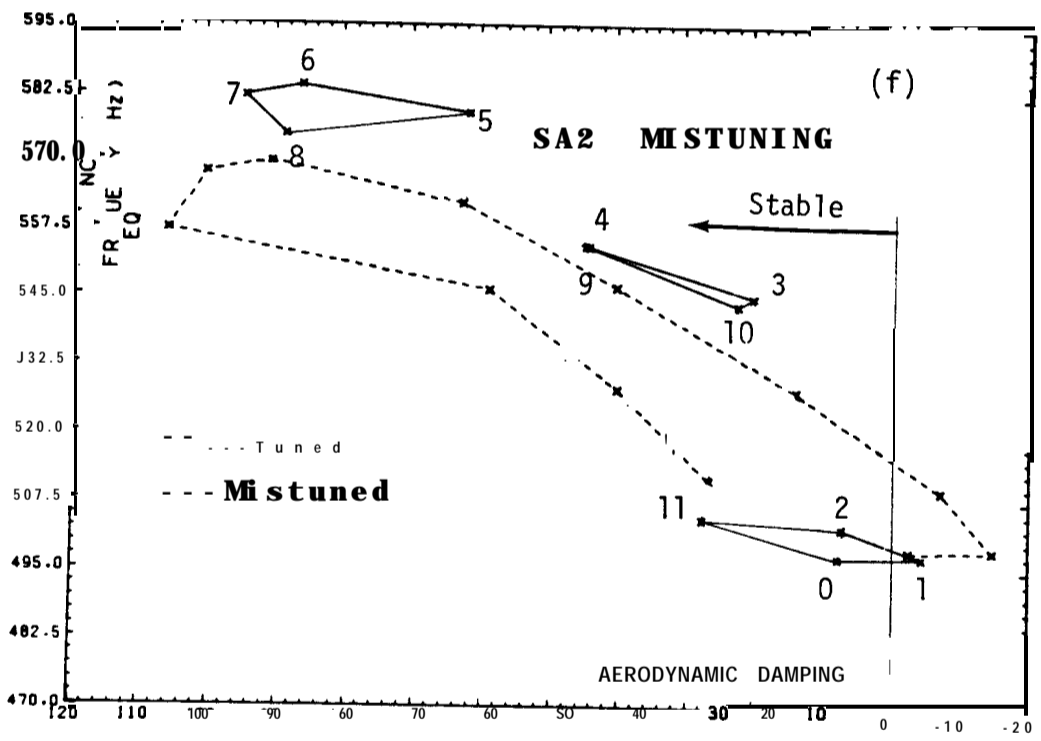
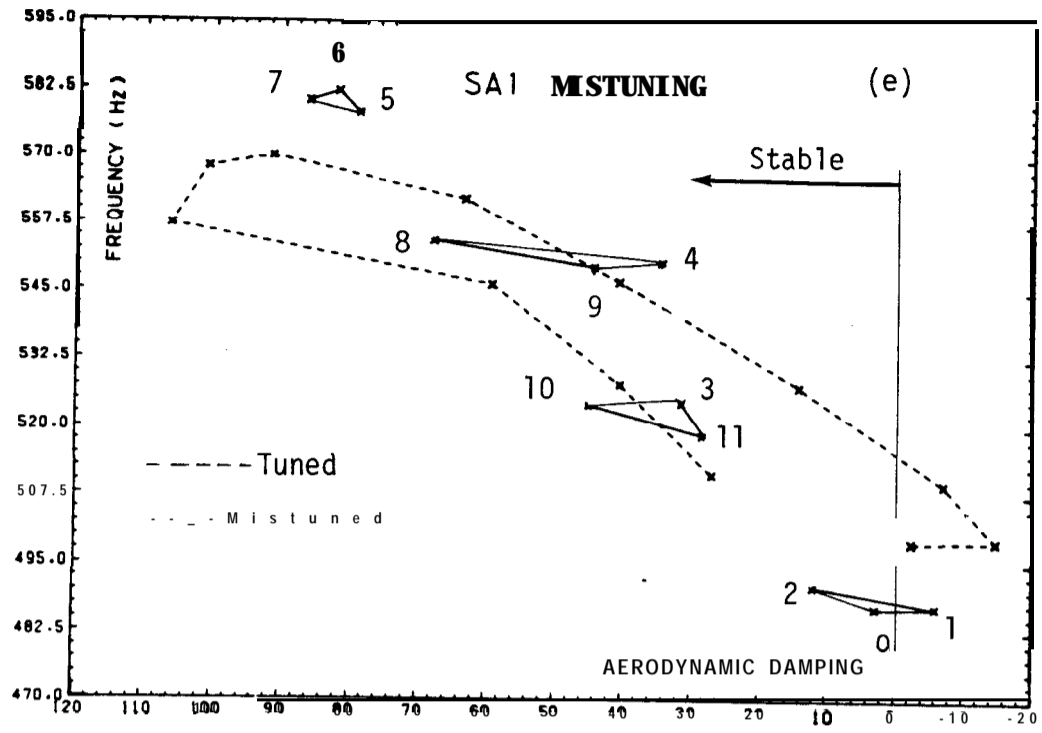
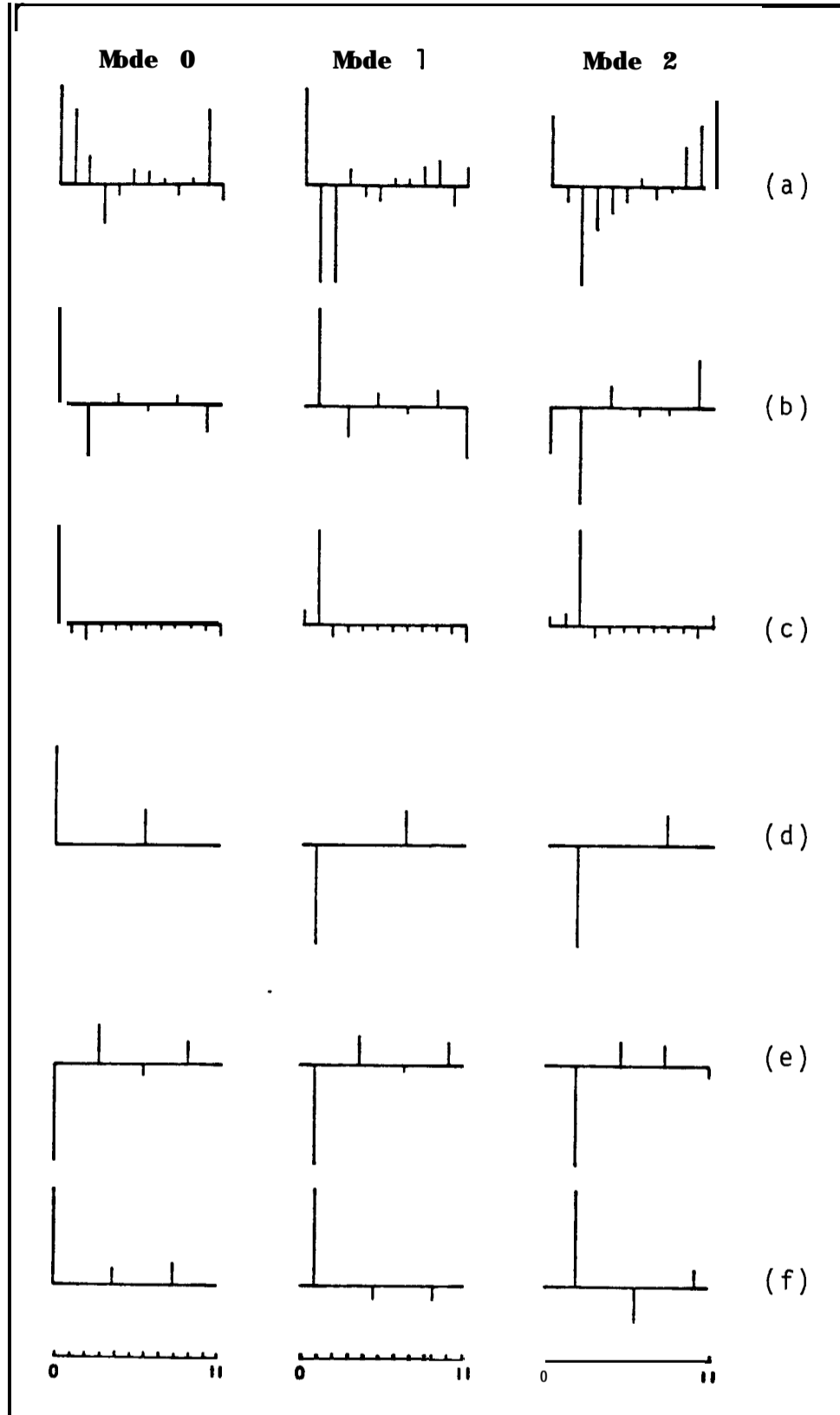


Fig. 10.11 Stability diagrams for various types of mistuning (Concluded)





**Fig. 10.12** DFT components of the eigenvectors associated with modes C, 1 and 2

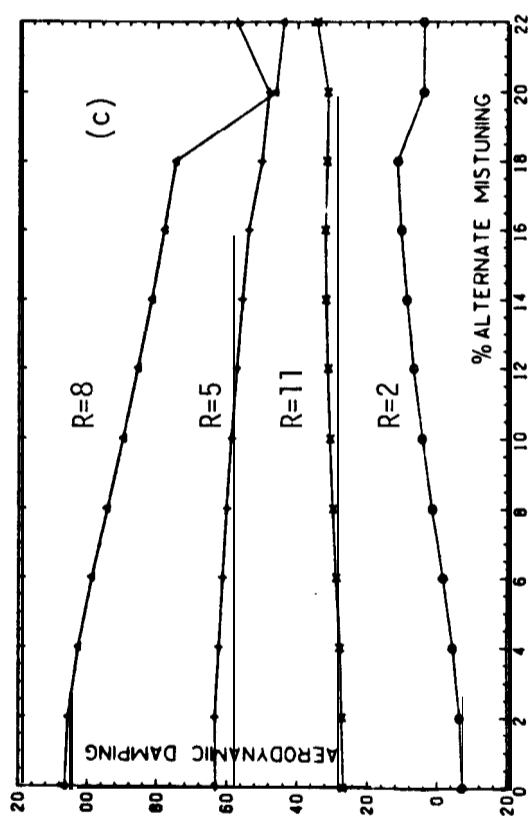
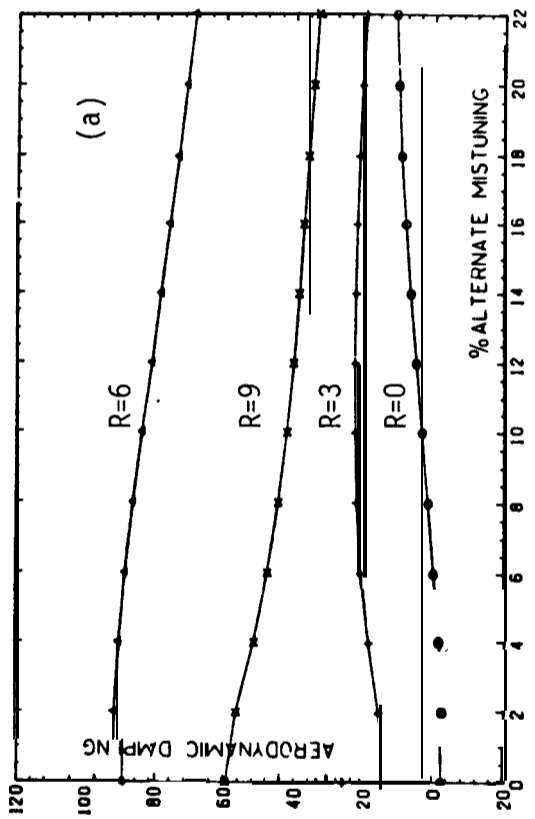
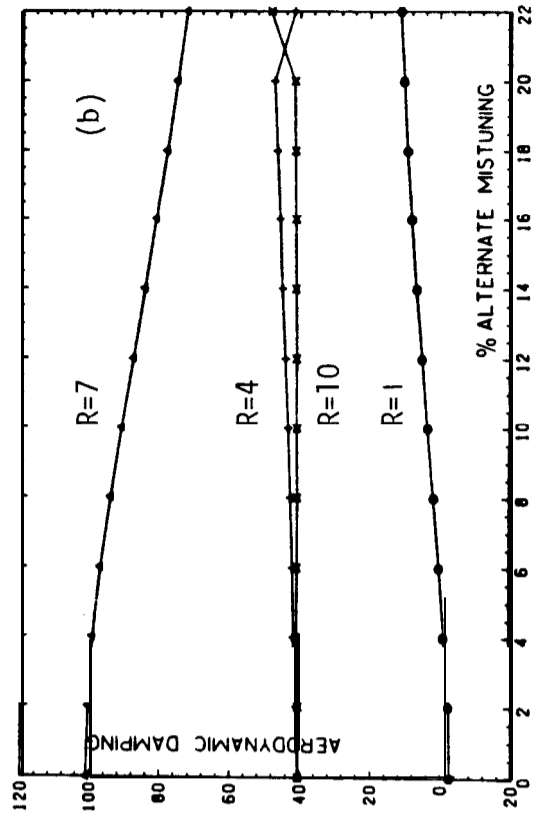
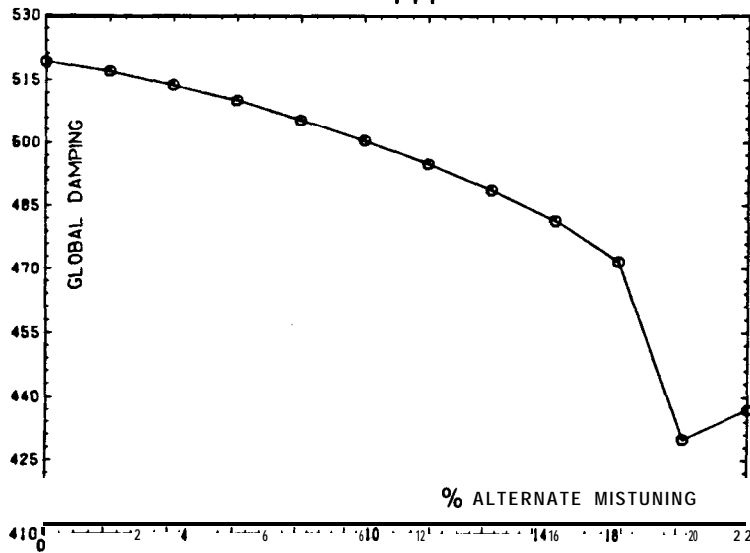
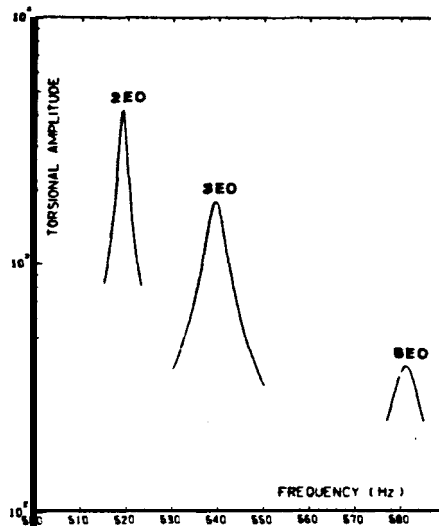
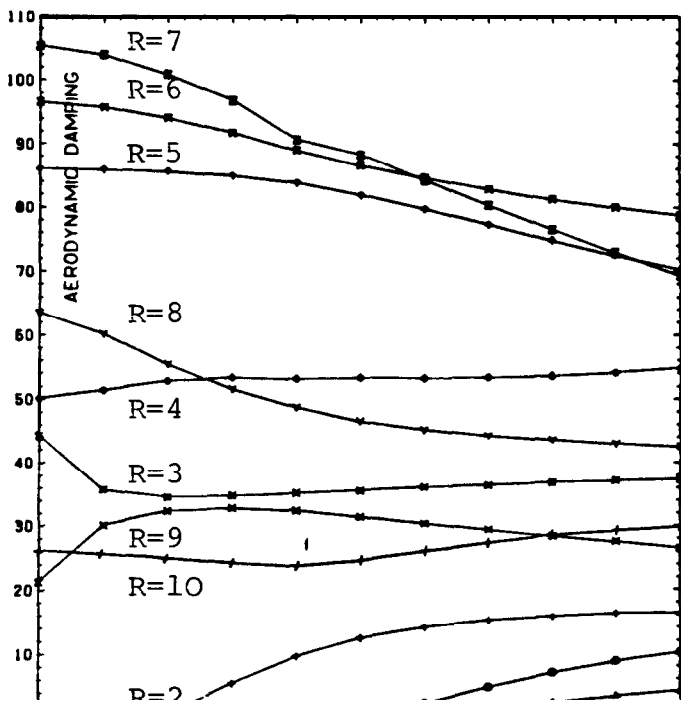


Fig. 10.13 Variation of modal damping with increasing mistuning (Disc A)



**Fig. 10.14** Variation of global damping with increasing mistuning



**Fig. 10.16** Effect of modal damping on forced response levels

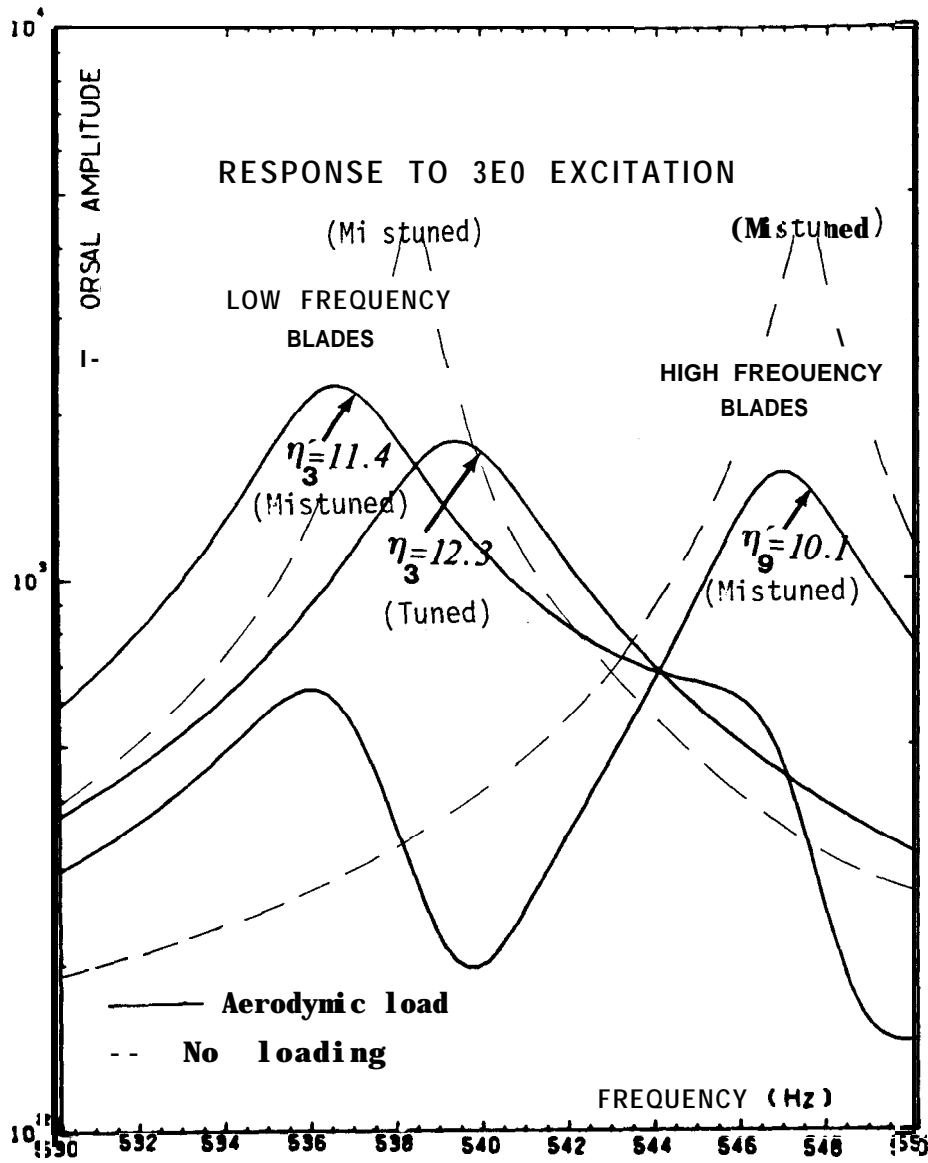


Fig. 10.17 Forced response of the tuned and alternately mistuned systems

## CHAPTER 11

### FLUTTER ANALYSIS OF A CANTILEVERED PLATE

#### 11.1 INTRODUCTION

Although the flutter analysis presented In Chapter 9 can provide the designer with sufficient qualitative data. It can be criticized because of its oversimplified structural representation and inadequacy for quantitative work. The need for a more advanced model is obvious and the objective of this chapter is to establish the basic steps towards a more complete aeroelastic analysis. The biaded disc studies initiated from a cantilevered beam model, disc flexibility and radius were later incorporated in the analysis and the effects of mistuning and packeting were Investigated last. It is logical to follow the same historical trend In aeroelastic analysis In which case the starting point would be the study of a cantilevered plate under aerodynamic loading.

#### 11.2 STRUCTURAL MODEL

As shown In Fig. 11.1, the structure is modelled using rectangular isotropic plate elements with three degrees of freedom at each node. Although the greatest advantage of finite element modelling over other techniques lies In its general applicability to non-uniform components. this work is restricted to outlining the method of approach and to indicating the order of accuracy which can be expected. To this end.

the element mass, stiffness and aeroelastic matrices were derived for untwisted flat plates of uniform thickness and the procedure is summarized in Appendix IV. The derivation of more elaborate elements is discussed in Ref. FE-3

### 11.3 AERODYNAMIC MODEL

#### 11.3.1 Pressure Distribution

In Chapter 9. we have seen that the aerodynamic force and moment coefficients may be calculated by integrating the pressure difference across the blade. this being a function of the flow conditions and cascade parameters. In this chapter, we shall assume that the pressure distribution along the plate chord -with respect to an elastic axis passing through the centre of gravity and per unit span length- is a known function of the form:

$$P(y) = -\omega y [p_h(y)\dot{h} + c\omega p_\alpha(y)\alpha] \quad (11-1)$$

where  $\omega$  denotes the frequency of vibration,  
 $y$  the fluid density,  
 $c$  a constant which will later coincide with the blade chord,  
 $\dot{h}$  the translational velocity,  
 $\alpha$  the rotational co-ordinate,  
 $y$  a co-ordinate along the blade chord.

$p_h$  and  $p_\alpha$  are the given non-dimensional pressure distribution functions due to the translational and rotational motions respectively. Results from Chapter 10 (see Fig. 10.5) suggest that they can be approximated by a second order polynomial in most cases.

$$\begin{aligned}
 p_h &= r_1 y^2 + r_2 y + r_3 \\
 p_\alpha &= s_1 y^2 + s_2 y + s_3
 \end{aligned}
 \tag{11-2}$$

The definition of  $P(y)$  above in equation (11-1) is totally arbitrary and a choice has been made to facilitate the mathematical analysis. There are, however, some analytical expressions available for incompressible flow, a classical example being Theodorsen's expression for the non-circulatory part [Ref. AE-6].

### 11.3.2 Finite Element Discretization

As shown in Fig. 11.2. the pressure distribution function given in equation (11-1) is applied in turn to each finite element row in the X direction. For the first element in each row the values of  $p_h$  and  $p_\alpha$  are specified at 3 points, namely at  $y=0, y=b/2$  and  $y=b$  and the coefficients of the pressure parabolae are determined using the Lagrange interpolation formula.

Consider the finite element illustrated in Fig. 11. 1. Using the principle of virtual work it can be shown [Ref. FE-31 that the element load vector for any distributed load  $P$  the Z direction is given by:

$$\{Q\}_e = \begin{Bmatrix} F_r \\ M_{\alpha r} \\ M_{\theta r} \end{Bmatrix} = -[B]^T \int_{x=0}^l \int_{y=0}^c \{w\} P \, dx dy \tag{11-4}$$

$r=k, l, m, n$

where elements of  $[B]$  and  $\{w\}$  depend on the shape functions chosen for the element. Inserting equation (11-1) into equation (11-4) and

integrating over the element area yields:

$$\begin{aligned}
 F_r &= \omega \gamma ab [C_{hhr} \cdot \dot{h}_r + c\omega C_{h\alpha r} \cdot \alpha_r]/720 \\
 M_{\alpha r} &= \omega \gamma ab^2 [C_{\alpha hr} \cdot \dot{h}_r + c\omega C_{\alpha\alpha r} \cdot \alpha_r]/720 \\
 M_{\theta r} &= \omega \gamma a^2 b [C_{\theta hr} \cdot \dot{h}_r + c\omega C_{\theta\alpha r} \cdot \alpha_r]/720 \quad r=k, l, m, n
 \end{aligned}
 \tag{11-5}$$

where  $C_{hhr}$ ,  $C_{h\alpha r}$ ,  $C_{\alpha hr}$ ,  $C_{\alpha\alpha r}$ ,  $C_{\theta hr}$ ,  $C_{\theta\alpha r}$  etc. are the non-dimensional aeroelastic force and moment coefficients. It should be noted that these are termed "aeroelastic" and not 'aerodynamic' as in Chapter 9 since their formulation requires knowledge of the element shape function and hence they are structurally dependent. As can be seen from equation (11-5), there are  $6 \times 4 = 24$  coefficients which define the aeroelastic behaviour of the element. Unlike in Chapter 9, it is not possible here to predict the flutter stability from the sign of real or imaginary parts since in the general case these coefficients will have different values at each node which, in turn, will be common to more than one element. Nevertheless, it is expected that flutter in a pure bending mode will depend largely on the real part of  $C_{hhr}$ . Similarly, torsional flutter will be controlled by the imaginary part of  $C_{\alpha\alpha r}$  which, for any asymmetric elastic axis position, depends also on  $C_{hhr}$ ,  $C_{h\alpha r}$  and  $C_{\alpha hr}$ . The  $C_{\theta hr}$  and  $C_{\theta\alpha r}$  coefficients are of secondary importance since it is assumed that there is no flutter motion in spanwise torsion. Rearranging equation (11-5) gives:

$$\{Q\}_e = \omega^2 [A]_e \{\delta\}
 \tag{11-6}$$

where  $[A]_e$  is the element aeroelastic coefficient matrix and the elements of  $\{\delta\}$  are the nodal displacements. Equation (11-6) is derived fully in Appendix IV.



#### 11.4 AEROELASTIC MODEL

If [A] is the global aeroelastic inertia matrix, the overall equation of motion becomes:

$$\begin{array}{l} [\mathbf{K} - \omega^2 \mathbf{M}] \{\mathbf{q}\} = \omega^2 [\mathbf{A}] \{\mathbf{q}\} \\ \text{Structural part} \quad \text{Aerodynamic part} \end{array} \quad (11-7)$$

Of

$$([\mathbf{K}] - \omega^2 [\mathbf{M} + \mathbf{A}]) \{\mathbf{q}\} = \{\mathbf{0}\} \quad (11-8)$$

it should be noted that the eigenproblem given by equation (11-8) is linear and hence it does not require an iterative solution as was the case for equation (9-17). Since the elements of [A] are complex, the eigenvalues and eigenvectors of equation (11-7) are also expected to be complex in the general case. Let:

$$\omega_r = \Omega_r + i\eta_r \quad (11-9)$$

where  $\Omega_r$  is the natural frequency for mode  $r$  and  $\eta_r$  is the aerodynamic damping associated with that mode of vibration. Proceeding as previously, the  $r^{\text{th}}$  mode will be considered as stable if:

$$\eta_r > 0 \quad (11-10)$$

and unstable otherwise. Although there is no structural damping term in equation (11-8), this feature can easily be incorporated into the stiffness matrix. Assuming hysteretic damping:

$$[\mathbf{K}] \rightarrow [\mathbf{K} + i\mathbf{H}]$$

in which case equation ( 11-10) becomes:

$$(\eta_{\text{ aerodynamic}} + \eta_{\text{ structural}}) > 0$$

As the structural damping is a positive defined quantity. It plays no significant part in the stability analysis in the sense that it will always have a stabilizing effect and hence it can be omitted without any loss of generality and added linearly if required.

## 11.5 NUMERICAL STUDY

### 11.5.1 Preliminary Calculations

A computer program, namely FLUT2. was written to perform the complex eigen-analysis discussed above. To this end equation (11-7) must be re-ordered as:

$$([P] - \omega^2[I]) \{q\} = \{0\} \quad (11.11)$$

where  $[P] = ([M] + [A])^{-1}[K]$  is the aeroelastic stability matrix.

Once the element mass, stiffness and aeroelastic coefficient matrices are computed, the corresponding global matrices can be assembled using the direct stiffness method of Ref. FE-4 and the complex eigensolution path of FLUT1 (see Section 10.1) is also used here.

To check the correctness of the computer program and to determine the minimum mesh size in order to obtain the first 10 modes accurately, a series of calculations were made using the data given in Ref. FE-5. These are reproduced in Table 11.1 and the resulting natural frequencies are presented in Table 11.2 In the following non-dimensional form:

$$\lambda = \omega \sqrt{\rho t l^4 / D} \quad \text{Where} \quad D = Et^3 / 12(1 - \nu^2)$$

The type of the vibration mode is also given for each case where F denotes flexural bending, T torsion and PM a plate mode i.e. a mode which would not be predicted by simple beam theory. The corresponding mode shapes are plotted in Fig. 11.3

Length	= 233 mm
<b>Chord</b>	= 100 mm
Thickness	= 2.3 mm
Density	= 2764 Kg/m <sup>3</sup>
Elastic modulus	= 68.9 GN/m <sup>2</sup>
Poisson's ratio	= .3

Table 11.1 Plate data

Mode	3x1	4x2	5x3	6x4	7x5	Ref. FE-5	
						24x11	Exp
<b>1F</b>	3.42	3.43	3.43	3.43	3.43	3.43	3.45
<b>1T</b>	17.00	16.95	16.93	16.92	16.92	16.74	16.79
<b>2F</b>	21.66	21.68	21.56	21.51	21.48	21.36	21.50
2T	54.87	54.96	54.33	54.29	54.26	53.66	53.76
3F	56.19	61.49	61.04	60.73	60.55	59.94	60.37
<b>PM0</b>						81.01	
3T	103.26	101.63	101.58	101.52	101.49	100.3	100.8
4F	132.27	118.79	119.06	116.36	117.89	115.4	117.2
<b>PM1</b>	146.73	125.43	127.11	127.18	127.19	124.2	131.8
<b>PM2</b>	182.87	149.64	153.30	154.70	155.67	153.6	161.2
<b>4T</b>	194.31	160.60	163.71	163.65	163.55	161.3	

Table 11.2 **Convergence of the non-dimensional natural frequency with mesh size**  
(Number of elements along the x axis is given first. )

As can be seen from Table 11.2. the convergence is rapid for all modes and there is very good agreement with the published results except for the PM0 mode which is not predicted at all. This is probably due to the differences in element formulation in the two sets of calculations and as pointed out in Ref. FE-S. this mode is not . . . typical of classical plate response. . . and . . . rather unusual. .!"

Using the same structural data, a second test was carried out to check the convergence of the complex eigenvalue with particular attention to the imaginary part. To this end both  $\rho_h$  and  $\rho_\alpha$  were set to  $(1+i)$  and the elastic axis was taken at the three-quarter chord point. Results are summarized in Table 11.3.

Mode	4x2	5x3	6x4	7x5	8x6
<b>1F</b>	3.35	3.35	3.35	3.35	3.35
	5.00	4.96	4.93	4.92	4.92
<b>1T</b>	15.27	15.30	15.31	15.31	15.31
	-20.75	-23.21	-24.05	-24.43	-24.48
<b>2F</b>	21.07	20.99	20.95	20.93	20.90
	34.43	32.85	32.06	31.61	31.12
<b>2T</b>	48.52	48.80	48.91	48.96	49.00
	-75.76	-76.64	-76.39	-76.09	-75.97
<b>3F</b>	58.90	58.89	58.25	58.67	58.42
	97.99	88.68	64.63	82.50	82.19
<b>3T</b>	87.23	90.04	90.90	91.28	91.36
	-209.68	-157.49	-143.37	-137.08	-135.10
<b>4F</b>	89.61	91.04	91.64	91.96	92.03
	620.13	-639.65	-641.93	-642.51	-642.77
<b>PM1</b>	103.83	109.82	112.56	114.10	115.26
	-854.13	-820.36	-807.04	-803.38	-801.14
<b>PM2</b>	107.40	115.56	115.96	115.81	115.38
	36.55	100.90	82.82	83.04	83.06
<b>4T</b>	125.37	138.88	143.69	145.47	196.62
	-849.31	-342.50	-231.47	-196.09	-181.39

Table 11.3 **Convergence of  $\omega = \Omega + i\eta$  with mesh size**  
 For each mode, the real part is shown on the upper line.

As can be seen from Table 11.3, the frequency part converges very rapidly for all modes while the damping part shows a somewhat slower convergence rate, especially for torsional and plate modes. This is apparently due to the complexity of these modes (see Fig. 11.3) whose shapes cannot be computed accurately for a small mesh size. Further calculations revealed that the elastic axis position is also of significant importance for the convergence of torsional modes. Nevertheless, a mesh size of 7x5 was found to be adequately representative of both the structural part and the aerodynamic loading and all subsequent

calculations were performed for that particular mesh size.

11.52 Case Study

Using the model described above. the flutter stability of a cantilevered plate was investigated. The structural data are listed in Table 11. 1 and the aeroelastic coefficients, due to the pressure distribution functions illustrated in Fig. 11.4, are plotted in Fig. 11.5. Results from the complex eigensoiution are given below in Table 11.4 and also the real part of each normaiized mode shape vector is plotted in Fig. 11.6.

Mode	$\Omega(\text{Hz})$	$(\Omega - \Omega_0)/\Omega_0$	$\eta$
<b>1F</b>	34.68	-.15	1.33
<b>1T</b>	168.90	-1.32	-7.33
<b>2F</b>	216.95	-.15	8.40
2T	541.55	-1.35	-23.80
3F	611.50	-.18	23.52
3T	1012.06	-1.44	-46.96
4F	1176.63	-1.35	-72.48
<b>PM1</b>	1244.38	-3.29	-65.76
<b>PM2</b>	1505.75	-4.40	-227.58
4T	1628.49	-1.58	-85.10

Table 11.4 Natural frequency and aerodynamic damping values for the first 10 modes.

As can be seen from Table 11.4. the aerodynamic loading not only produces a damping effect but also results in a natural frequency shift from the in-vacuum values. According to the stability criterion given by equation (11-10) . only the first three modes are stable, all remaining

ones being prone to flutter. As the  $C_{hr}$  ( $r=k,l,m,n$ ) coefficients have negative real parts for all five finite element rows, the instability of the 4F mode is somewhat unexpected. A closer inspection reveals, however, that both bending and torsional motions are present in that mode (see Fig. 17.8) and hence its flutter instability is caused structurally, a phenomenon which could not be predicted using the lumped parameter model of Chapter 9.

The instability of the torsional and plate modes follows from the fact that most of the  $C_{\alpha r}$  ( $r=k,l,m,n$ ) coefficients have positive imaginary part and the same applies to the plate modes in which a great deal of torsional motion is present.

The natural frequency shift is observed not to correlate with the amount of aerodynamic damping present in any one mode but it seems to be dependent on the type of motion present in that mode: about 0.2% for bending, 1.5% for torsion and 4% for plate modes. Also, the damped natural frequency is always lower than the undamped one, a well-known characteristic of single-degree-of-freedom systems.

The differences in mode shapes for the loaded and unloaded cases are illustrated in Fig. 11.7. It should be noted that these plots had to be magnified about 50 times for better visualization of the aerodynamic effect. Also, Figs. 11.3, 11.6 and 11.7 are replotted in Fig. 11.8 from a different viewpoint on the OY axis. Let A denote the surface resulting from the difference of the loaded and unloaded mode shape plots. As can be seen from Fig. 11.7,  $\Delta 1F$ ,  $\Delta 2F$  and  $\Delta 3F$  are all twisted, a feature more clearly illustrated in Fig. 11.8. This suggests

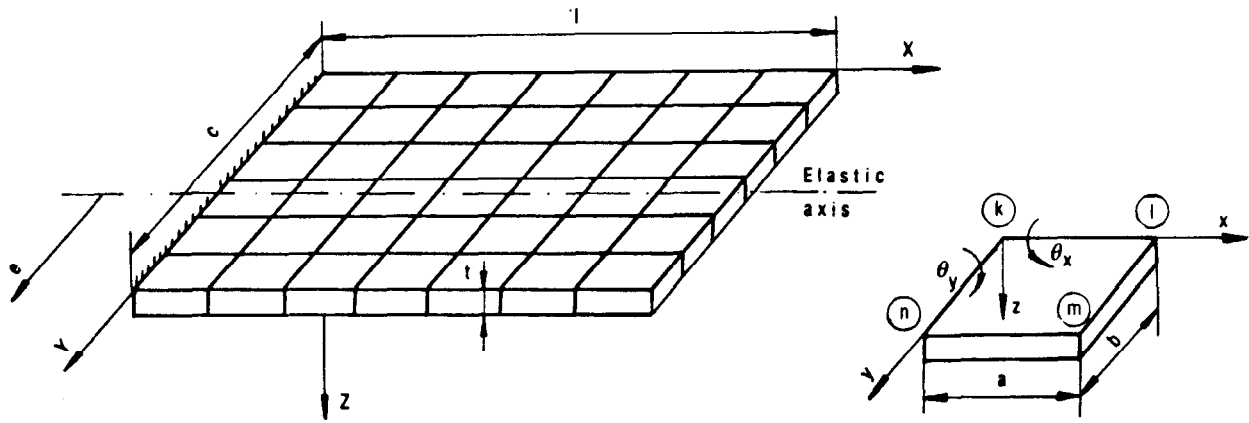
that the aerodynamic load can always introduce a torsional motion. irrespective of the in-vacuum mode shapes. or amplify the existing one as for the remaining modes. A comparison of Figs. 11.3 and 11.6 reveals that under load, 4F behaves more like a plate mode than a flexural one and conversely. PM1 exhibits pronounced bending characteristics. As a result  $\Delta 4F$  and  $\Delta PM1$  look remarkably similar in shape and the implications of this phenomenon on stability have been discussed earlier.

#### 11.6 CONCLUDING REMARKS

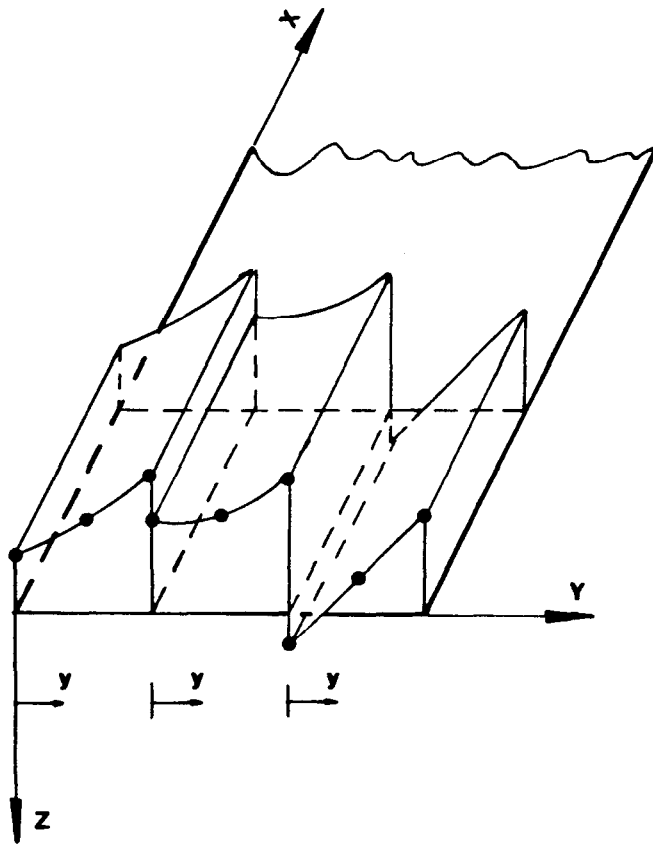
A finite element based model to investigate the flutter stability of a cantilevered plate has been introduced. The main advantage of this model over the lumped parameter one lies in its realistic aero/structural dynamics interface, an indispensable feature for any quantitative analysis.

As the major aim of the chapter was to devise and apply a general method of attack rather than to undertake a systematic analysis of cantilevered plates under different loading conditions. only one case study - on the rigour of which it is not possible to reach any specific conclusions - has been presented. It may, however, be stated that the aerodynamic loading always produces a damping effect as well as a natural frequency shift, both of which depend on the type of motion(s) present in any given mode. Hence, a more correct formulation of the flutter problem has been achieved since the modal stability is a simultaneous function of both the structural behaviour and the flow conditions.



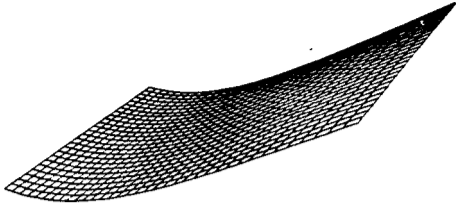


**Fig. 11.1** Finite element model of a cantilevered plate



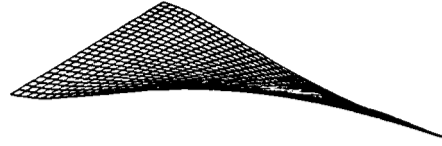
**Fig. 11.2** Pressure distribution along the chord  
Note that only the real (or imaginary) part is shown.

1F (F=34.7 HZ ETR = 01

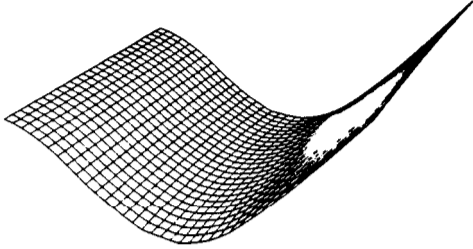


- 159 -

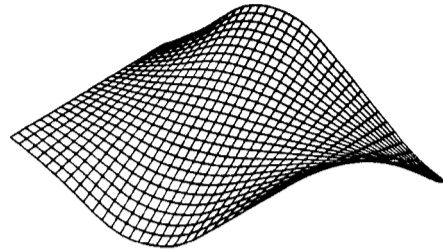
1T (F=171.2 HZ ETR = 01



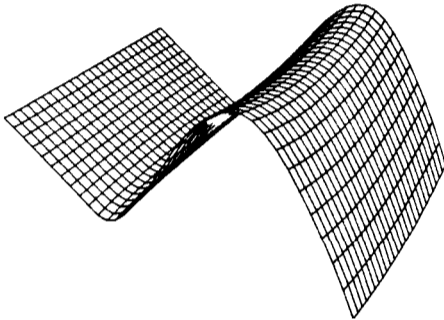
2F (F=217.3 HZ ETR = 01



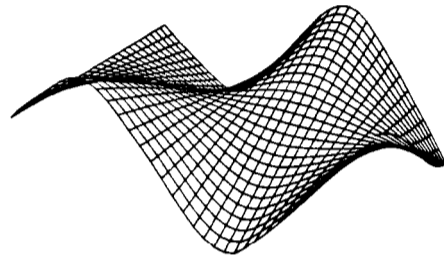
2T (F=549.0 HZ ETR = 01



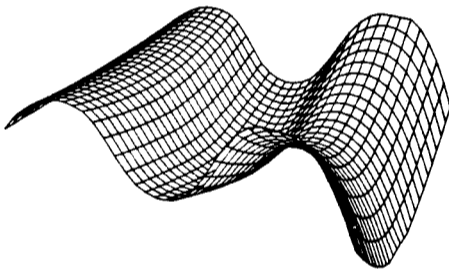
3F (F=612.6 HZ ETA = 0)



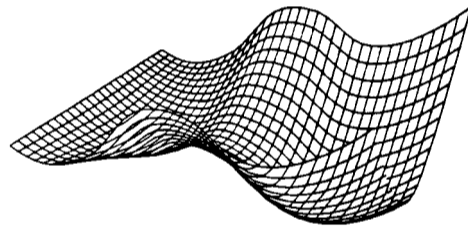
3T (F=1026.8 HZ ETA = 0)



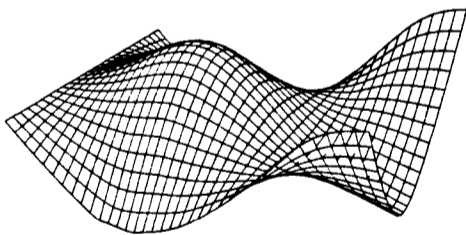
4F (F=1192.7 HZ ETR = 01



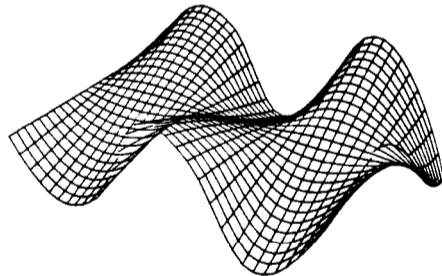
PM1 (F=1286.7 HZ ETA = 0)



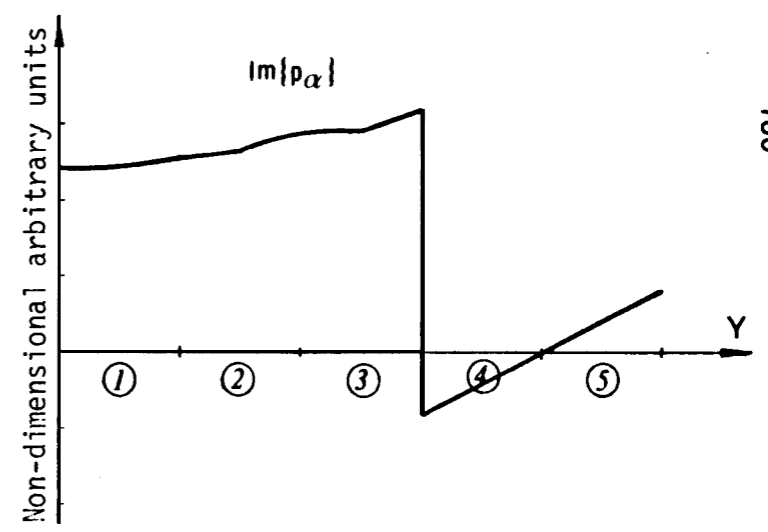
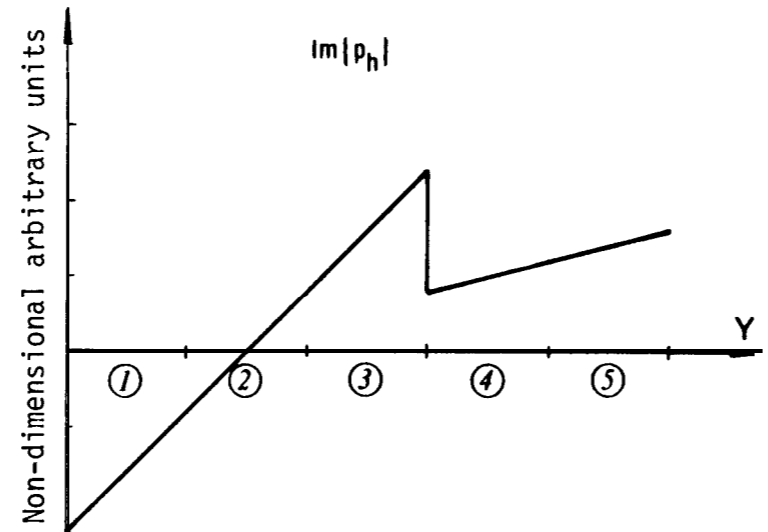
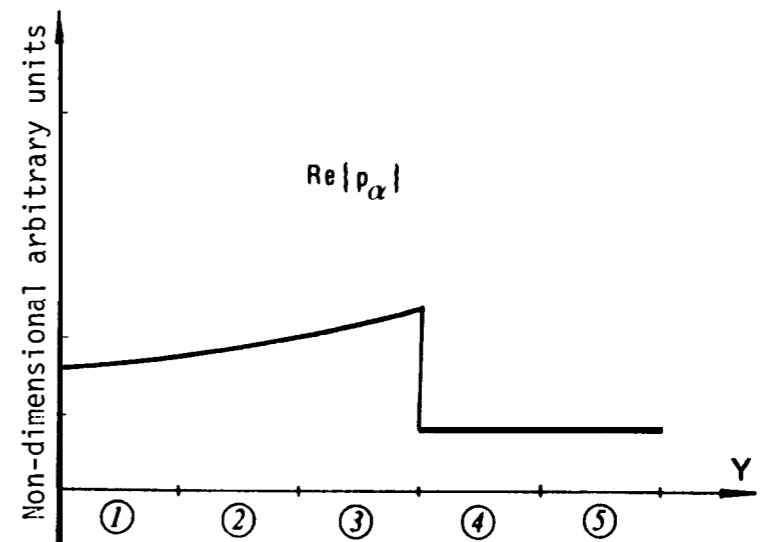
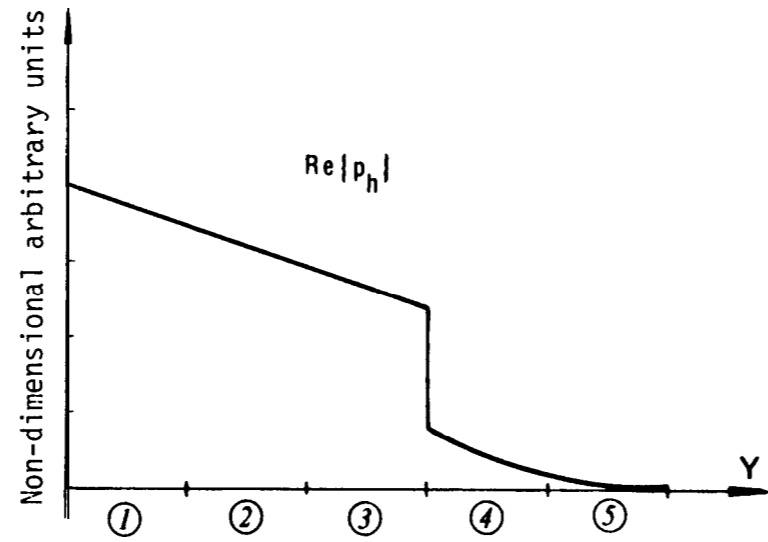
PM2 (F=1574.9 HZ ETR = 0)



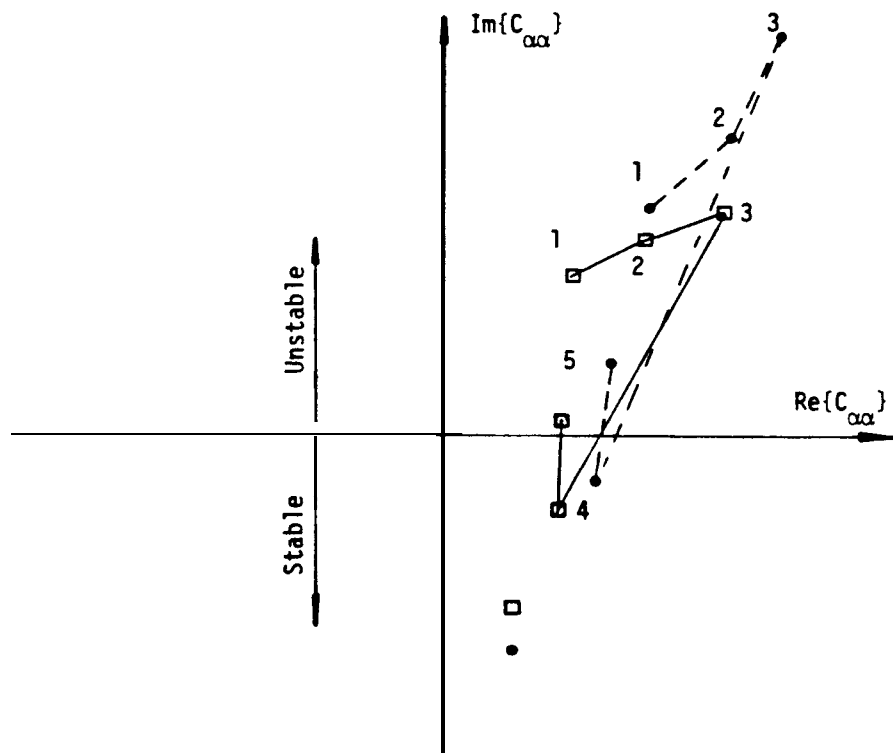
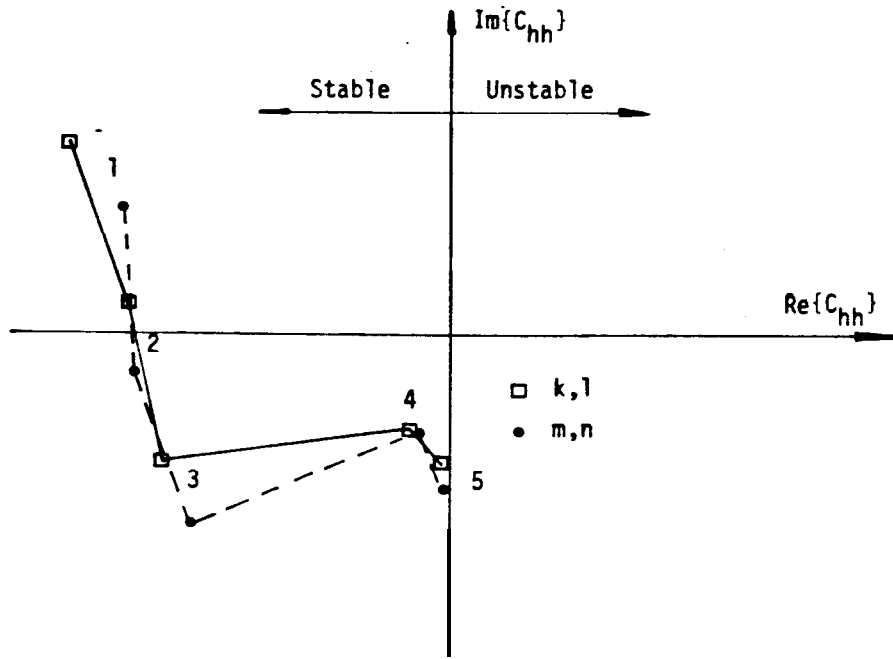
4T (F=1654.6 HZ ETA = 01



**Fig. 11.3** The first 10 modes of the cantilevered plate for vacuum conditions

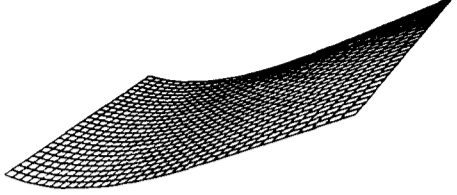


**Fig. 11.4** Pressure distribution functions  $p_h$  and  $p_\alpha$  for each of the 5 finite element rows in the Y direction. The elastic axis is at  $3/4$  chord position.

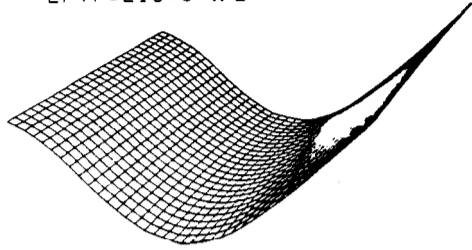


**Fig. 11.5** Aeroelastic coefficients resulting from the pressure distribution given in Fig. 11.4 ( $e=\frac{1}{4}$ ,  $\gamma=1.3 \text{ Kg/m}^3$ )

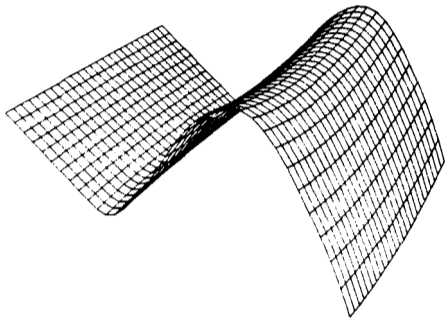
1F (F=34.7 HZ ETA=1.3)



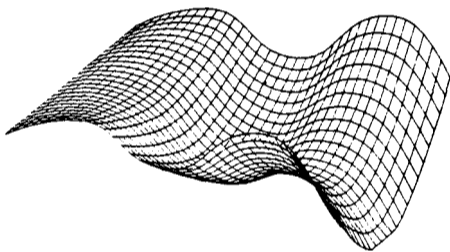
2F (F=216.9 HZ ETA=8.4)



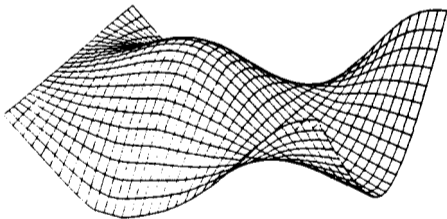
3F (F=611.5 HZ ETA=23.5)



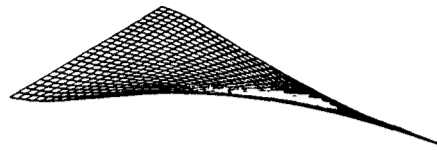
4F (F=1176.6 HZ ETA=-72.5)



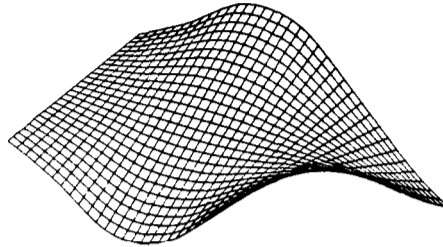
PM2 (F=1505.8 HZ ETA=-227.6)



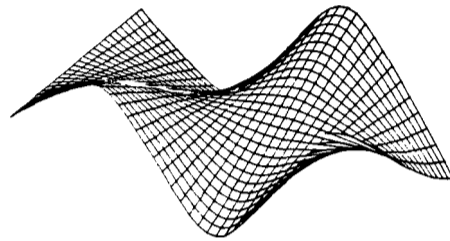
1T (F=168.9 HZ ETA=-7.3)



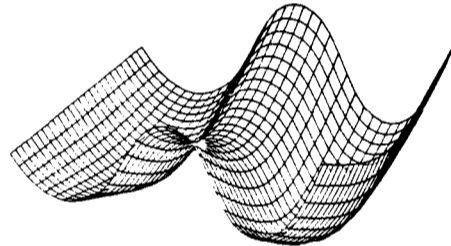
2T (F=541.5 HZ ETA=-23.8)



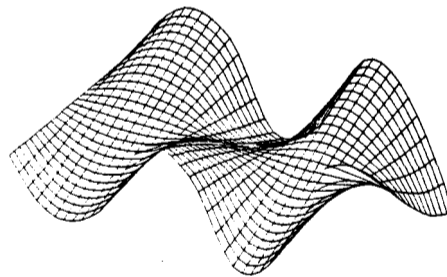
3T (F=1012.1 HZ ETA=-47.0)



PM1 (F=1244.4 HZ ETA=-65.8)



4T (F=1628.5 HZ ETA=-85.1)



**Fig. 11.6** The first 10 modes of the cantilevered plate under aerodynamic load

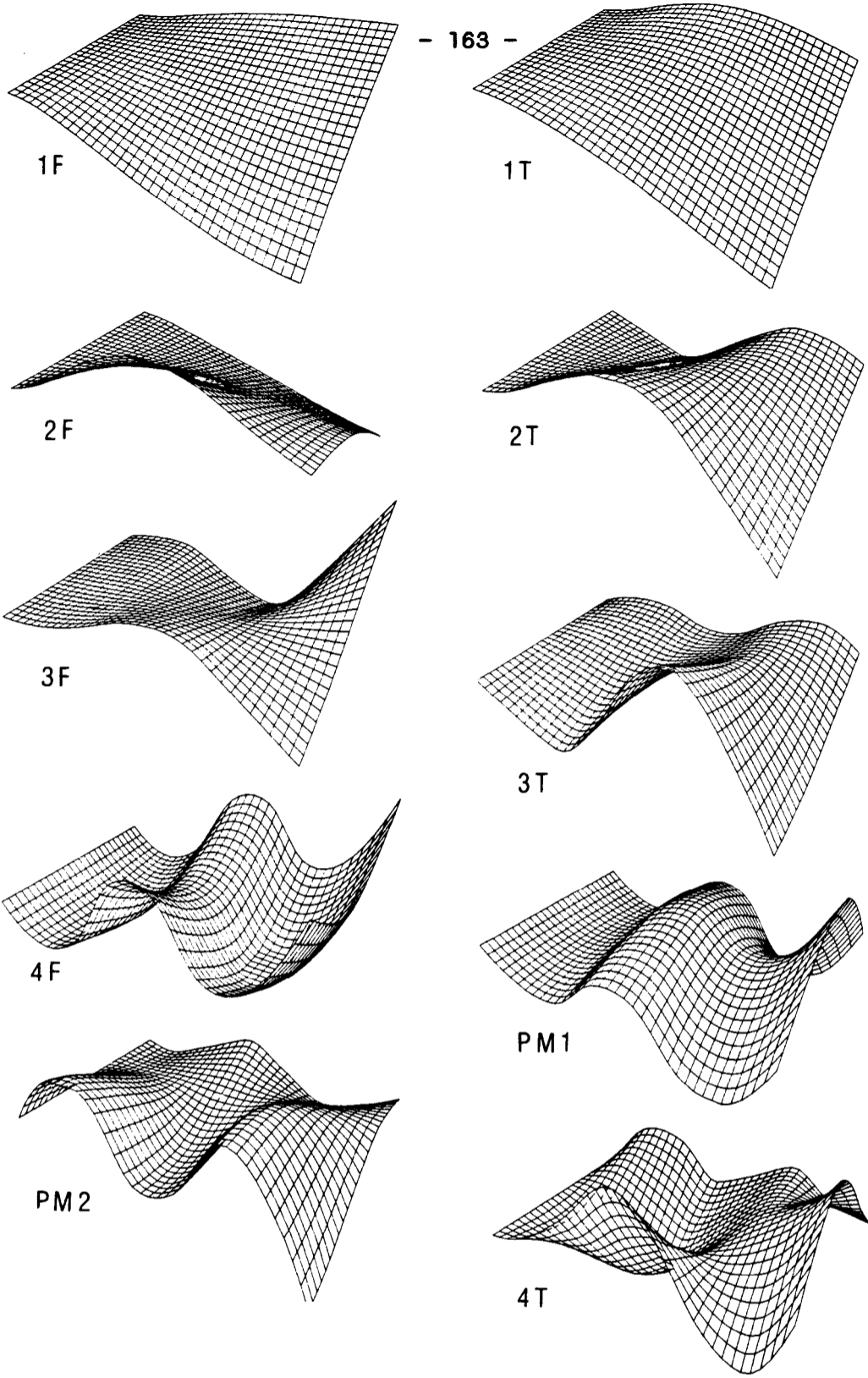


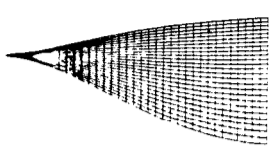
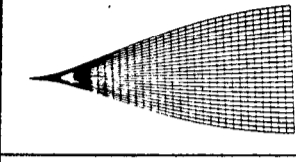
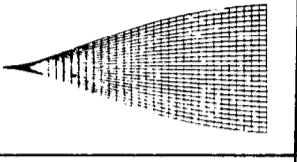
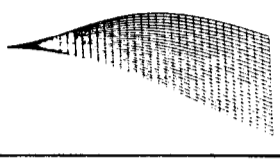


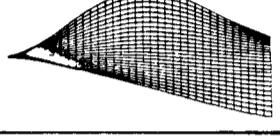
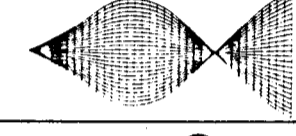
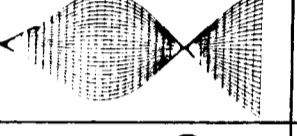
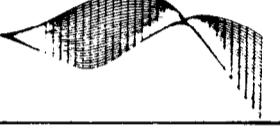
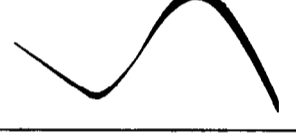
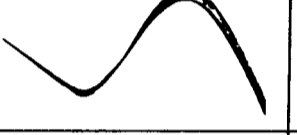
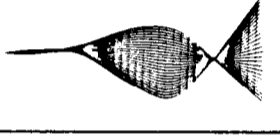
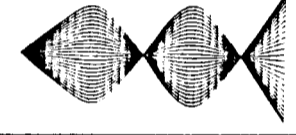
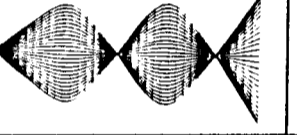
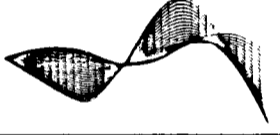

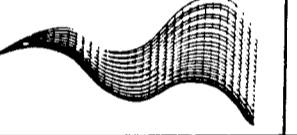
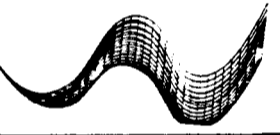
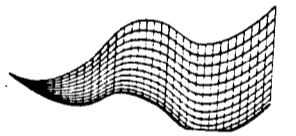
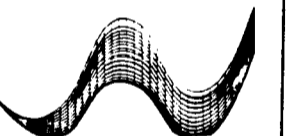
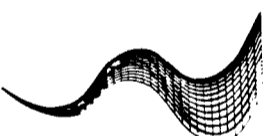
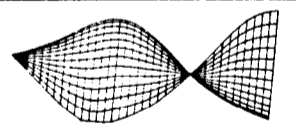
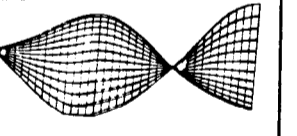
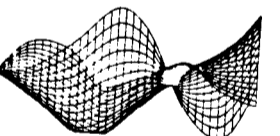
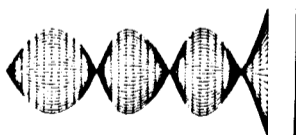
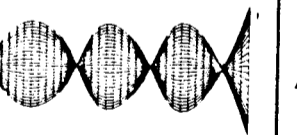
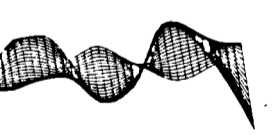


Fig. 11.7 A surfaces **resulting from the difference of the**  
loaded and **unloaded mode shapes**

Mode	(1) No aero. load	(2) Under aero. load	$\Delta = (2) - (1)$
1F			
1T			
2F			
2T			
3F			
3T			
4F			
PM1			
PM2			
4T			

**Fig. 11.8** Mode shapes of the cantilevered plate with and without aerodynamic loading

CHAPTER 12

CONCLUSIONS

12.1 SUMMARY OF CONCLUSIONS OF PRECEDING FOUR CHAPTERS

The work described in the second part of this thesis represents an attempt to improve the basic understanding of the aeroelastic characteristics of bladed disc systems. To this end, two analytical models, based on completely different approaches, have been developed and used with success to conduct qualitative and/or quantitative studies of a number of bladed systems. The first model, which is an integration of the existing two-dimensional cascade flow theories with a lumped parameter representation of a bladed disc assembly, was found to be ideally suited for parametric studies yielding qualitative results.

- (1) Due to the dependence of the aerodynamic coefficients on the wave direction imposed by the interblade phase angle, the aeroelastic structure distinguishes between forward and backward travelling waves: a feature totally ignored by its structural counterpart. This results in  $N$  distinct aeroelastic modes as opposed to  $\lfloor N/2 + 1 \rfloor$  or  $\lfloor (N-1)/2 + 1 \rfloor$  single and double structural modes where  $N$  is the total number of blades. Furthermore, each aeroelastic mode is characterized by a complex number, the real part of which gives the natural frequency and the imaginary part the aerodynamic damping. For all tuned cases studied, it has been found that these two values are very strongly correlated with the real and imaginary parts of the moment coefficient in torsion (or force coefficient in bending). This



suggests that the tuned system analysis does not require the full model when the coupling between bending and torsional motions is weak. Furthermore, the damped frequencies are observed to be within  $\pm 3\%$  of the in-vacuum values while the modal aerodynamic damping amount showed a rather wide scatter on both ends of the stability spectrum.

- (ii) Structural mistuning has the effect of coupling travelling waves associated with different interblade phase angles and thus of causing modal interference. The quantitative and qualitative characteristics of this coupling process are determined by the amount and form of mistuning present: symmetric arrangements result in an orderly grouping of the harmonics which can be predicted from the total number of blades.
- (iii) Since the aerodynamic loads and hence the coefficients are frequency-dependent, mistuning can have unpredictable effects on the stability of a particular mode and, furthermore, the overall amount of damping may decrease with increasing mistuning. However, in general, mistuning has a beneficial effect on the system's stability in the sense that critical modes are very often stabilized at the expense of the well-damped ones.
- (iv) Alternate mistuning, which couples only out-of-phase harmonics, is particularly useful if the least and most stable modes are separated by approximately 180 degrees interblade phase angle. It has been found that this is usually the case, the phenomenon being of aerodynamic origin. However, alternate mistuning is not the most beneficial type and other symmetrical arrangements may require lower levels of detuning to stabilize the same system.
- (v) From an aeroelastic viewpoint, mistuning can lower the level of the response to forced vibration and this finding is in contrast with the common belief. It should however, be noted that this is a relatively rare occurrence, as mistuning usually imposes more severe conditions.

The second model, derived from the finite element discretization of a cantilevered flat plate and its surrounding fluid flow, was used to study quantitatively the behaviour of an isolated blade subjected to a known pressure function. It has been found that:

- (i) the mode shapes of the aerodynamically loaded system can be significantly different from the in-vacuum ones:
- (ii) the aerodynamic loading always produces a damping effect as well as a frequency shift, both of which depend on the type of motion(s) present in any given mode rather than the sign of the aeroelastic coefficients. The damped natural frequency is always lower than the in-vacuum one, the relative difference sometimes exceeding 4%.

### 12.2 Limitations and Extension of the Present Work

The studies presented herein constitute an introduction to the aeroelastic analysis of bladed disc assemblies, a multi-disciplinary subject whose complete understanding will defy many workers for years to come. The simplifying assumptions that have had to be made are too numerous to mention individually: Non-linear effects, interactions between various stages, three dimensional flow, blade camber and twist, etc.

The most serious limitation of the first model is perhaps the typical section approach which was developed some fifty years ago for fixed wing geometry. As the relative flow velocity is usually supersonic at the tip and subsonic towards the hub, spanwise variation of blade mode shapes must be incorporated into the model to account for the variation in both the reduced frequency and Mach number with the radius. On the other

hand. the assumption which considers the Interblade phase angle as constant even in the mistuned case must be re-examined and the flow models modified if necessary. Furthermore, the case of the stalled flow must also be addressed.

The structural part of the second model can easily be extended to include blade camber and twist, root flexibility and finite disc effects. A more accurate formulation of the aerodynamic load would require a two-dimensional integration (both spanwise and chordwise) and this is more difficult because of the transonic regime which will be encountered between the subsonic and supersonic regions. An alternative approach is to extract the aerodynamic data from measurements and incorporate these into the model.

Finally, there is an obvious need for experimental verification of the theoretical findings. Although some practical work to check the validity of the aerodynamic coefficients is reported in the original publications, aeroelastic data are almost non-existent. An experimental programme to investigate the effects of symmetric mistuning on flutter stability is strongly recommended.

**APPENDICES AND REFERENCES**

APPENDIX I

LIST OF COMPUTER PROGRAMS DEVELOPED IN THIS STUDY

<u>Name</u>	<u>Description</u>
BLISC	Computes the natural frequencies of a continuously-shrouded disc via coupling of shroud, blade and disc receptances. A cyclic symmetry approach is used.
FINPAC	Computes the natural frequencies and mode shapes of an isolated blade packet (cantilevered or free-free) using a finite element based model.
MULPAC	Computes the natural frequencies and mode shapes of a packeted biaded disc by coupling disc and packet receptances at the blade roots. This is a <i>full</i> analysis in the sense that each blade is considered in turn without taking advantage of the cyclic symmetry. The packet receptance matrix is either formed by coupling Individual blade and shroud segments or derived from a free-free eigensoiution obtained via FINPAC.
SINPAC	As above for MULPAC except that advantage of the cyclic symmetry has been taken to minimize the size of the matrix equations of motion.
LUMPAC	Computes the natural frequencies and mode shapes of a packeted biaded disc using a lumped parameter model.
FLUT1	Computes the flutter boundaries and the aeroelastic response of biaded disc systems subjected to incompressible, subsonic or supersonic unstaiied flows. The structural model is a mass-spring one and the aerodynamic models are based on two-dimensional cascade flow theory.
FLUT2	Computes damped natural frequencies and aerodynamic damping values of an isolated cantilevered blade subjected to a prescribed pressure distribution using a finite element approach. The associated mode shapes are also determined and can be plotted if required.

APPENDIX II

TABULATED RESULTS FROM CHAPTERS 4.5 AND 6

Natural Frequencies (Hz) of the 30-bladed disc

n: Nodal diameter number: s: nodal circle number

n/s	0	1	2	3	4	5
0		139.02	498.18	1215.63	2067.88	3396.52
1		248.55	808.89	1573.37	2673.34	3946.40
2	<b>98.36</b>	370.31	1124.02	1969.05	3317.06	
3	156.27	546.00	1381.80	2455.01	3859.82	
4	201.23	750.67	1615.86	3056.37	4346.98	
5	250.14	936.39	1883.70	3524.58	4475.43	
6	310.50	1077.00	2201.03	3907.11	<b>4669.02</b>	
7	383.49	1177.92	2585.61	4241.86	4772.52	
8	444.91	1255.86	3110.83	4627.00	4834.52	
9	556.49	1325.19	3336.41	5054.12	4875.07	
10	638.24	1369.94	3541.82	5564.36	4904.92	
11	714.68	1443.08	3703.39	6224.74	4921.56	
12	779.28	1546.47	3832.69		4942.43	
13	825.18	1654.90	3938.11		4968.90	
14	857.72	1777.46	4022.18		4985.39	
15	866.82	1860.03	4080.65		4994.65	

Table II-1 Continuous uniform shroud

n/s	0	1	2	3	4	5
0		138.20	497.37	1215.50	2070.61	3393.01
1		248.56	809.16	1575.96	2680.85	3943.27
2	95.91	369.68	1124.92	1969.31	3322.24	
3	145.69	544.54	1388.99	<b>2465.47</b>	3879.28	
4	171.14	747.72	1620.13	3012.62		
5	185.06	930.33	1892.02	3506.36		
6	193.53	1064.96	2220.41	3901.38		
7	199.14	1155.37	2577.63	4248.96		
8	203.10	1216.01	2912.51	<b>4620.31</b>		
9	206.06	1258.19	<b>3184.46</b>	5053.59		
10	202.65	1256.45	3384.33	5536.79		
11	202.00	1273.55	3526.32	6020.80		
12	202.96	1285.27	3628.45			
13	203.62	1292.92	3704.14			
14	204.03	1297.24	3762.06			
15	205.12	1298.64	3807.64			

Table II-2 Non-interlocking shroud

n/s	0	1	2	3	4	5
<b>0</b>		142.70	497.91	1222.05	2054.01	3406.12
<b>1</b>		253.30	821.63	1600.85	2673.91	3960.31
<b>2</b>	109.2	373.73	1143.78	1973.95	3277.12	
<b>3</b>	163.45	519.21	1469.30	2463.05		
<b>4</b>	187.4	819.06	1666.10	3019.45		
<b>5</b>	194.01	948.95	1884.07	3407.41		
	340.49	1087.59	1977.90	3585.03		
6	340.60	1176.23	2262.15			
7	340.75	1257.55	2633.33			
8		1314.30	2935.76			
9	345.37	1330.45	3128.80			
10	345.34	1334.91	3305.11			
	670.36	1451.15	3472.50			
11	664.99	1422.97	3774.84			
12	669.18	1423.64	3811.43			
13	694.80	1358.08	3928.02			
14		1379.03	4006.70			
15		1379.78	3912.46			

Table II-3 10 Packets of 3 blades (Direct method)

Packet receptances are derived via receptance coupling.

n/s	0	1	2	3	4	5
0		142.67	498.11	1227.03	2065.94	3452.84
1		255.63	820.89	1615.18	2691.84	4002.21
2	105.2	390.90	1143.54	1977.83	3299.06	
3	161.6	559.31		2471.07		
4	186.5	775.01	1663.05	3000.06		
5	193.5	950.5	1882.83	3442.84		
		983.2	1928.16	3627.66		
6		1111.88	2239.45			
7		1236.76	2600.53			
8		1283.03	2918.71			
9	342.05	1333.14	3104.90			
10	345.94	1346.6	3348.80			
	667.12	1458.55	3535.50			
11	656.01	1444.53	3824.08			
12	661.06					
13	661.64	1488.62	3972.14			
14	667.59		4071.02			
15	661.79	1522.51				

Table II-4 10 Packets of 3 blades (Direct method)  
 Packet receptances are derived via modal summation.

n/s	0			1			2		
0			54.5	142.8	260.5	387.5	497.5	535.0	758.8
1		110.8	142.1	252.3	349.4	597.5	817.5	840.0	961.3
2	98.9	202.0	269.1	371.6	433.8	706.9	1133.8	1168.1	1256.3
3	150.2	274.7	425.6	548.8	583.1	797.5	1377.5	1425.0	1510.0
4	175.8	307.7	544.7	757.4	786.8	937.5	1596.3	1648.3	1724.8
5	189.5	323.1	604.1	942.2	979.2	1108.6	1862.3	1909.4	1973.0
6	197.7	331.6	632.5	1071.9	1120.0	1247.5	2193.8	2236.3	2297.0
7	202.8	336.6	647.7	1153.8	1210.0	1338.8	2550.0	2590.9	2665.0
8	206.4	340.1	656.9	1206.3	1267.5	1397.5	2863.0	2889.1	3014.1
9	209.1	342.5	663.1	1240.6	1305.0	1435.0	3077.5	3085.0	3281.3
10	210.9	344.4	667.5	1263.8	1330.0	1461.3	3174.0	3230.0	3462.5
11	212.3	345.6	670.6	1280.0	1347.5	1478.8	3224.4	3320.3	3576.6
12	213.3	346.6	672.5	1291.3	1360.0	1492.0	3250.0	3375.0	3648.1
13	214.0	347.2	673.8	1298.8	1368.8	1500.0	3265.0	3410.6	3691.6
14	214.4	347.4	674.4	1303.8	1372.5	1503.8	3274.4	3429.4	3715.3
15	214.6	374.5	675.2	1305.0	1375.0	1506.3	3276.9	3437.5	3723.8

Table II-5 10 Packets of 3 blades (Cyclic symmetry method)



n/s	0	1	2	3	4	5
0		143.2	504.5	1251.8	2053.1	3253.1
1		256.6	826.0	1585.5	2663.0	3873.1
2	103.4	372.0	1148.5	1968.9	3196.4	
3	157.7	572.9	1386.8	2461.8		
4	185.0	m . 7	1642.6	2969.5		
5	199.1	969.5	1911.0			
6	206.4	1109.5	2243.4			
7	209.6	1192.5	2599.3			
8	470.5	1309.0	2945.5			
9	470.5	1341.5	3165.2			
10	470.5	1371.6	3239.8			
11	469.8	1394.7	3476.3			
12		1438.4	3684.5			
13	486.0	1432.2	3660.9			
14	482.2	1439.3				
15	482.3	1442.5	3719.7			

Table II-6 15 Packets of 2 blades (Direct method)

n/s	0	1	2	3	4	5
<b>0</b>		147.6	<b>496.5</b>	1247.6	2032.8	3347.7
1		230.1	789.2	1573.3	2657.5	
2	121.5	333.2	1155.1	1962.8		
3	162.2	516.7	1405.3	2426.8		
	258.1	562.7	1465.1	2476.3		
4	264.6	761.0	1678.7	2999.7		
<b>5</b>	279.6	981.1	1916.7			
6	279.6	1107.0	2223.6			
	355.2	1180.1	2239.2			
7		1246.3	2580.0			
8		1299.1	2900.0			
9	388.5	1306.6	3105.8			
		1350.3	3168.3			
10	591.0		3253.6	3420.9		
11	591.1	1369.6	3385.6	3529.1		
12	590.9	1369.5	3514.5	3553.3		
	800.6	1616.6	3553.3	3801.1		
13	801.1	1623.3	3685.8	3921.5		
14	835.3	1573.9	3706.0	4064.2		
15	811.0	1610.9	3625.7	3924.7		

Table II-7 6 Packets of 5 blades (Direct method)

n/s	0	1	2
0		146.6	488.8
1		253.1	810.0
2	100.9	366.3	1129.4
3	152.8	540.9	1373.4
	214.2	558.8	1414.0
4	242.7	770.5	1602.5
5	256.6	970.6	1872.3
6	264.7	1109.8	2196.5
	392.1	1138.9	2214.9
7	396.9	1230.3	2567.1
8	400.0	1287.0	2882.2
9	402.2	1323.4	3106.9
	610.0	1393.9	3131.7
10	613.3	1419.9	3263.1
11	615.0	1436.5	3361.3
12	616.0	1448.9	3422.6
	798.5	1618.8	3655.0
13	800.5	1626.3	3697.5
14	802.3	1630.5	3722.5
15	802.5	1632.0	3730.0

**Table II-8** 6 Packets of 5 blades (Cyclic symmetry method)

n/s	0	1	2	3	4	5
0		152.5	499.7	1255.7	2030.4	3336.0
1		269.5	817.3	1585.0	2644.7	
2	124.8	386.4	1155.3	1953.5	3262.6	
3	231.6	558.3	1419.6	2438.1		
4	242.7	766.0	1711.8	2989.3	4278.2	
5	268.5	967.2	1893.2	3406.5		
	335.8	1009.4	1919.2	3537.7		
6		1135.4	2212.8			
7	315.8	1239.7	2569.0			
8		1320.5	2905.1			
9	676.3	1366.7	3154.3			
10	691.0	1385.3	3246.4			
	808.3	1631.0	3684.7			
11		1618.3	3829.6			
12		1665.0	3867.0			
13	828.2					
14						
15						

**Table II-9** 5 Packets of 6 blades (Direct method)

n/s	0	1	2	3	4	5
0					1978.3	3454.1
1			814.5		2628.1	
2	139.8	391.2	1230.1			4421.1
3	177.5	493.2		2422.2		
	226.8	554.3		2440.5		
4	319.8	782.7		3020.0		
5	343.6	972.9	1907.2	3534.1		
6	374.8	1184.1	2166.8			
	425.6	1212.3				
7		1321.3	2551.2			
8	449.0	1405.5	2926.2			
9		1410.9	3195.2			
	600.4	1505.8	3208.3			
10		1515.2	3311.3			
11						
12	647.5		3600.8			
	823.2	1750.2	4002.7			
13		1705.1				
14	877.9	1769.6	3847.6			
15			3899.2			

Table II-10 3 Packets of 10 blades (Direct method)

n/s	0	1	2
0	1.19	278.19	1879.11
1	275.80	613.36	2359.49
2	315.61	818.64	3518.14
3	369.45	886.91	4874.10
4	430.90	922.90	6251.11
5	495.07	949.73	7591.26
6	558.73	973.40	8864.87
7	619.68	995.78	10051.46
8	676.33	1016.87	11134.69
9	727.49	1036.47	12110.57
10	772.22	1054.12	12938.26
11	809.77	1069.33	13636.98
12	839.56	1081.66	14188.92
13	861.14	1090.75	14587.73
14	874.22	1096.31	14828.85
15	078.59	1098.18	14909.52

Table II-11 Continuous uniform shroud (Lumped parameter model)

n/s	0	1	2
0	1.17	251.14	1879.08
1	51.08	252.00	1879.34
2	100.33	255.02	1880.10
3	145.17	261.79	1881.33
4	181.08	275.98	1882.99
5	203.69	301.29	1885.02
6	215.14	334.92	1887.34
7	220.85	370.92	1889.87
8	223.97	405.65	1892.49
9	225.82	437.38	1895.09
10	227.00	465.17	1897.55
11	227.77	488.46	1899.76
12	228.28	506.90	1901.61
13	228.60	520.22	1903.00
14	228.78	528.28	1903.87
15	228.84	530.97	1904.16

**Table** II-12 Non-interlocking shroud (Lumped parameter model)

n/s	0	1	2
<b>0</b>	1.19	278.18	1879.11
<b>1</b>	80.86	279.80	1879.91
<b>2</b>	152.414	285.97	1881.97
<b>3</b>	203.20	300.65	1884.49
<b>4</b>	227.00	321.54	1886.50
<b>5</b>	232.93	331.65	1887.27
	495.07	949.73	7591.26
6	495.07	957.35	7591.26
7	495.07	977.09	7591.26
8	495.07	1002.17	7591.26
9	495.07	1026.28	7591.26
10	495.07	1041.54	7591.26
	772.22	1054.12	12938.26
11	772.22	1064.10	12938.26
12	772.22	1073.92	12938.26
13	772.22	1080.19	12938.26
14	772.22	1083.61	12938.26
15	772.22	1084.68	12938.26

**Table** II-U 10 Packets of 3 blades (Lumped parameter model)

0 Nodal Diameters						
<b>M</b>		143.0	499.9	1207.	2030.	3337.
C1		142.7	497.9	1222.	2054.	3406.
E1		-.2	-.4	1.2	1.2	.9
c2		<b>142.8</b>	<b>497.5</b>	1210.	2041.	3349.
E2		-.1	-.5	.1	-.5	-.4
1 Nodal Diameter						
<b>M</b>		248.4	815.9	1575.	2623.	
C1		253.3	824.6	1601.	2674.	
E1		2.0	1.1	1.7	1.9	
<b>C2</b>		252.3	817.5	1582.	2651.	
E2		1.6	.2	.4	1.1	
2 Nodal Diameters						
<b>M</b>	103.6	392.4	1121.	1936.	3341.	
C1	109.2	373.3	1144.	1974.	3277.	
E1	5.4	-4.9	2.1	2.0	-1.9	
c2	98.9	371.6	1134.	1957.	3310	
E2	-4.0	-5.3	1.2	1.1	-.9	
3 Nodal Diameters						
<b>M</b>	154.8	544.2	1364.	2403.		
C1	163.5	519.2	<b>1469.</b>	<b>2463.</b>		
E1	5.6	-4.6	7.7	2.5		
<b>C2</b>	150.2	548.8	1378.	2388.		
E2	-3.0	.8	1.0	-.7		
4 Nodal Diameters						
<b>M</b>	179.7	804.0	1597.	2909.		
C1	187.4	819.1	1666.	3019.		
E1	4.3	1.9	4.3	3.8		
c2	175.8	757.4	1596.	2889.		
E2	-2.2	-5.8	-.1	-0.7		
5 Nodal Diameters						
<b>M</b>	187.7	1010.	1834.	3321.		
C1	194.0	948.0	1884.	34'07.		
E1	3.4	-6.1	2.7	2.6		
c2	189.5	942.2	1862.	3365.		
E2	1.0	-6.7	1.5	1.3		

Table II-14 Packeted-bladed disc (10 Packets of 3 blades)

**M:** Measured  
**C1:** Computed via MULPAC  
**c2:** Computed via SINPAC  
**E1 = (C1 - M) x 100/M**  
**E2 = (C2 - M) x 100/M**

Continued

5 Nodal Diameters			
<b>M</b>	345.0	NI	1872.
<b>C1</b>	340.5		1978.
<b>E1</b>	-1.3		5.7
<b>C2</b>	323.1		1909
<b>E2</b>	-6.3		2.0
6 Nodal Diameters			
<b>M</b>	<b>NI</b>	1118.	2171.
<b>C1</b>		1176.	2262.
<b>E1</b>		5.2	4.1
<b>c2</b>		1120.	2236.
<b>E2</b>		.2	2.9
7 Nodal Diameters			
<b>M</b>	<b>NI</b>	1202.	2507.
<b>C1</b>		1258.	2633.
<b>E1</b>		4.7	5.0
<b>C2</b>		1210.	2590.
<b>E2</b>		.7	3.3
8 Nodal Diameters			
<b>M</b>	<b>NI</b>	1261.	2776.
<b>C1</b>		1314.	2936.
<b>E1</b>		4.2	5.8
<b>C2</b>		1267.	2889.
<b>E2</b>		.5	4.1
9 Nodal Diameters			
<b>M</b>	<b>NI</b>	1291.	2941.
<b>C1</b>		1330.	3129.
<b>E1</b>		3.0	6.4
<b>C2</b>		1305.	3085.
<b>E2</b>		1.1	4.9
10 Nodal Diameters			
<b>M</b>	<b>NI</b>	1305.	3193.
<b>C1</b>		1335.	3305.
<b>E1</b>		2.3	3.5
<b>C2</b>		1330.	3230.
<b>E2</b>		1.9	1.2

**Table** II-14 Packeted-bladed disc (10 Packets of 3 blades)

**M:** Measured  
**C1:** Computed via MULPAC  
**c2:** Computed via SINPAC  
**E1 = (C1 - M) x 100/M**  
**E2 = (C2 - M) x 100/M**

Continued

10 Nodal Diameters			
<b>M</b>	665.8	1456.	3580.
<b>c1</b>	670.4	1451.	3473.
<b>E1</b>	.7	-.3	-3.0
<b>c2</b>	667.5	<b>1461.</b>	<b>3463.</b>
<b>E2</b>	.2	.3	-3.2
11 Nodal Diameters			
<b>M</b>	675.4	1479.	3602.
<b>C1</b>	665.0	1423.	3775.
<b>E1</b>	-1.5	-3.8	4.8
<b>C2</b>	670.6	1479.	3576.
<b>E2</b>	-.7	0.0	-.7
12 Nodal Diameters			
<b>M</b>	678.5	1488.	3647.
<b>c1</b>	669.2	1424.	3811.
<b>E1</b>	-1.4	-4.3	5.0
<b>C2</b>	672.5	1492.	3648.
<b>E2</b>	-.9	.3	0.0
15 Nodal Diameters			
<b>M</b>	<b>NI</b>	1507.	<b>NI</b>
<b>C1</b>		1380.	
<b>E1</b>		-8.4	
<b>C2</b>		1506	
<b>E2</b>		-.1	

**Table II-14** Packeted-bladed disc (10 Packets of 3 blades)

**M:** Measured  
**C1:** Computed via MULPAC  
**C2:** Computed via SINPAC  
 $E1 = (C1 - M) \times 100/M$   
 $E2 = (C2 - M) \times 100/M$   
  
**NI:** Not identified

Concluded

0 Circles, 3 Diameters mode					1 Circle, 10 diameters mode				
Predicted at 163.4 Hz			Measured at 154.8 Hz		Predicted at 1334. Hz			Measured at 1305. Hz	
No	Displ.	DFT	Displ.	DFT	No	Displ.	DFT	Displ.	DFT
0		.00		-100.000	0		.68		-47.202
1	-23	.00	-59.361	1.964	1	-100.00	.01	-91.333	1.726
2	-55.54	.00	-89.352	2.132	2	98.90	.00	26.001	.895
3	-87.15	100.00	-96.209	48.792	3	3.46	.01	-36.177	2.904
4	-91.76	.00	-93.980	1.463	4	-100.00	.01	-96.050	.608
5	-65.67	.00	-75.638	2.224	5	98.89	.00	26.747	.757
6	-13.54	.00	-59.158	.530	6			-30.625	1.648
7	96.13	56.93	6.32	.00	7	-99.99	3.46	.01	.00
8			-34.668	1.250	8	98.87	.00	30.309	5.586
9	95.52	.00	-34.305	.827	9	3.45	.00	-29.369	2.335
10	56.57	.00	-39.987	1.426	10	-99.99	100.00	-87.713	100.000
11	6.27	.00	-68.856	.924	11	98.89	.00	21.306	1.304
12	-45.49	.00	-84.845	.817	12	3.46	.00	-30.214	1.275
13	-91	89	1.75	-92.022	13	-99.99	.01	-90.839	1.746
14	-100.00	.00	100.000	1.534	14	98.90	.00	1e.508	2.017
15	-67.40	.00	-77.187	-.307	15	3.46	.00	-30.713	.195
16	.22		-71.024		16	-99.99		-89.797	
17	55.54		-41.354		17	96.88		27.180	
18	87.14		-33.312		18	3.46		-31.739	
19	91.76		-34.391		19	-99.99		-83.434	
20	65.68	13.55	-53.402		20	98.87		29.501	
21			-71.409		21	3.46		-34.608	
22	-56.93		-77.091		22	-99.99		-95.557	
23	-96.13		-94.083		23	98.89		34.668	
24	-95.52		-88.690		24	3.46		-28.645	
25	-56.56		-85.058		25	-99.99		-100.000	
26	-6.27		-54.715		26	98.89		25.387	
27	45.48		-39.346		27	3.46		-25.228	
28	91.89		-34.476		28	-100.00		-88.206	
29	100.00		-36.035		29	98.80		23.297	
30	67.40		-47.944		30	3.44		-32.957	

**Table II-15 Predicted and measured mode shapes**



APPENDIX III

EXPLICIT FORMULATION OF THE  
NON-DIMENSIONAL AEROELASTIC EQUATIONS

Combining equations (9-1) and (9-13), the motion of the  $j^{\text{th}}$  sector can be written as:

$$\left( \begin{bmatrix} (2S_h + k)b & 0 & -kb \\ 0 & 2S_{\alpha} + c_j & 0 \\ -kb & 0 & (2K + k + g)b \end{bmatrix} - \omega^2 \begin{bmatrix} mb & md & 0 \\ md & I & 0 \\ 0 & 0 & Mb \end{bmatrix} \right) \begin{Bmatrix} h_j/b \\ \alpha_j \\ y_j/b \end{Bmatrix} \quad (\text{III-1})$$

$$= \gamma b^3 \omega^2 L \sum_{r=0}^{N-1} \left( \begin{bmatrix} l_{hhr} & l_{har} & 0 \\ b l_{\alpha hr} & b l_{\alpha ar} & 0 \\ 0 & 0 & 0 \end{bmatrix} \begin{Bmatrix} h_{ar}/b \\ \alpha_{ar} \\ y_{ar}/b \end{Bmatrix} + \begin{Bmatrix} l_{hwr} \\ b l_{\alpha wr} \\ 0 \end{Bmatrix} \right) \exp(i\beta_r j)$$

It is easily seen that the quickest way of non-dimensionalising equation (III-1) is to divide the  $h_j/b$  row by  $\gamma b^3 \omega_0^2 L$  and the  $\alpha_j$  one by  $\gamma b^4 \omega_0^2 L$ , where  $\omega_0$  is some arbitrary reference frequency. Extending this resulting equation to  $N$  blades and using equations (9-11) and (9-12) gives:

$$([K] - \omega^2 [M]) \{q\} = 1/\mu \omega^2 / \omega_0^2 (1/N [E][A][\bar{E}]\{q\} + [E]\{F_w\}) \quad (\text{III-2})$$

where  $\mu = m/\pi \gamma L b^2$

$$[K] = \begin{bmatrix} [G_1] & [H] & \cdot & [H] \\ [H] & [G_2] & \cdot & [H] \\ \cdot & \cdot & \cdot & \cdot \\ [H] & [H] & \cdot & [G_N] \end{bmatrix} \quad 3N \times 3N$$

$$[G_j] = \begin{bmatrix} \gamma_h^2 + 2\delta_h & 0 & -\gamma_h^2 \\ 0 & \chi^2 \gamma^2 \alpha_j + 2\delta_\alpha & 0 \\ -\gamma_h^2 & 0 & \gamma_h^2 + \delta_g + 2\delta_K \end{bmatrix}; [H] = \begin{bmatrix} -\delta_h & 0 & 0 \\ 0 & -\delta_\alpha & 0 \\ 0 & 0 & -\delta_K \end{bmatrix}$$

with

$$\gamma_h^2 = k(1 + i\eta_h)/m\omega_0^2, \quad \gamma^2 \alpha_j = c_j(1 + i\eta_\alpha)/I\omega_0^2, \quad \chi^2 = I/m_b^2$$

$$\delta_h = S_h/m\omega_0^2, \quad \delta_\alpha = S_\alpha/m_b^2\omega_0^2, \quad \delta_K = K/m\omega_0^2$$

$$[M] = \begin{bmatrix} [F] & & & \\ & [F] & & \\ & & \cdot & \\ & & & [F] \end{bmatrix}; \quad [F] = \begin{bmatrix} 1 & x & 0 \\ x & \chi^2 & 0 \\ 0 & 0 & t \end{bmatrix}$$

with  $t = m/M$  and  $x = d/b$

$$[A] = \begin{bmatrix} [a_0] & & & \\ & [a_1] & & \\ & & \cdot & \\ & & & [a_{N-1}] \end{bmatrix} \quad \text{and} \quad [a_r] = \begin{bmatrix} l_{hhr} & l_{h\alpha r} & 0 \\ l_{\alpha hr} & l_{\alpha\alpha r} & 0 \\ 0 & 0 & 0 \end{bmatrix}$$

$$F_w)^T = \{l_{hw0}, l_{\alpha w0}, 0, \dots, l_{hwN-1}, l_{\alpha wN-1}, l_{\alpha wN-1}, 0\}$$

and the cascade response vector (q) and the [E] matrix are defined in equations (9-2) and (9-11) respectively.

APPENDIX IV

DERIVATION OF THE MASS, STIFFNESS AND AEROELASTIC MATRICES  
FOR AN UNTWISTED ISOTROPIC RECTANGULAR PLATE ELEMENT OF  
UNIFORM THICKNESS

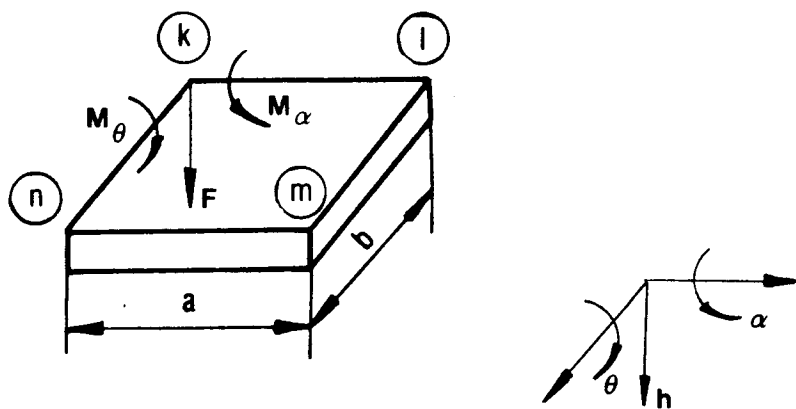


Fig. IV-1 Rectangular plate element of uniform thickness

Fig. IV-1 illustrates one of the rectangular elements forming the complete plate in which  $k, l, m$  and  $n$  are the nodal point indexes. At each node there are three load components, one lateral force  $F$  and two moments  $M_\alpha$  and  $M_\theta$ , to which correspond the three displacements  $h$ ,  $\alpha$  and  $\theta$ .

It is assumed that the deflected form of the element can be approximated by a shape function of the form:

$$H = \left\{ 1, \frac{x}{a}, \frac{y}{b}, \frac{x^2}{a^2}, \frac{xy}{ab}, \frac{y^2}{b^2}, \frac{x^3}{a^3}, \frac{x^2y}{a^2b}, \frac{xy^2}{ab^2}, \frac{y^3}{b^3}, \frac{x^3y}{a^3b}, \frac{xy^3}{ab^3} \right\}$$

$$\{A_1, A_2, A_3, A_4, A_5, A_6, A_7, A_8, A_9, A_{10}, A_{11}, A_{12}\} \quad (IV-1)$$

$$= \{w\}^T \cdot \{A\}$$

The elements of  $\{A\}$  can be found using the boundary conditions which must be satisfied at each node in turn, that is to say:

$$(h)_r = h_r$$

$$(\partial h / \partial y)_r = \alpha_r$$

$$(\partial h / \partial x)_r = \theta_r \quad \text{where } r = k, l, m, n$$

Inserting these conditions gives:

$$\{\delta\} = [B] \{A\}$$

where  $\{\delta\}^T = \{h_k, \alpha_k, \theta_k, \dots, h_n, \alpha_n, \theta_n\}$  (IV-2)

and hence:

$$\{A\} = [B]^{-1} \{\delta\} \quad (W-3)$$

The bending strain energy of an isotropic plate of uniform flexural rigidity  $D$  is:

$$U = D/2 \int_{y=0}^b \int_{x=0}^a [ (\partial^2 h_r / \partial x^2)(\partial^2 h_r / \partial y^2) + 2\nu (\partial^2 h_r / \partial x^2)(\partial^2 h_r / \partial y^2) + 2(1 - \nu)(\partial^2 h_r / \partial x \partial y)^2 ] dx dy$$

$r = k, l, m, n$

$$= 1/2 \int_{y=0}^b \int_{x=0}^a \{C\}^T [D] \{C\} dx dy \quad (W-4)$$

where  $\{C\}^T = \{\partial^2 h_r / \partial x^2, \partial^2 h_r / \partial y^2, \partial^2 h_r / \partial x \partial y\}$   
 $r = k, l, m, n$

and

$$[D] = \begin{bmatrix} d & 0 & 0 & 0 \\ 0 & 0 & d & 0 \\ 0 & 0 & 0 & d \\ 0 & d & 0 & 0 \end{bmatrix} \quad \text{with } d = \begin{bmatrix} \nu D & D & 0 \\ 0 & \nu D & 2(1 - \nu)D \\ 0 & 0 & 0 \end{bmatrix}$$

The curvatures can easily be obtained by differentiating equation (IV-1).

$$\{C\} = [E]\{A\} = [E][B]^{-1}\{\delta\} \quad (\text{IV-5})$$

Substituting equation (IV-5) into equation (IV-4) and noting that only  $[E]$  is a function of  $x$  and  $y$  gives:

$$U = 1/2 \{\delta\}^T \left[ [B]^{-T} \left\{ \int_{y=0}^b \int_{x=0}^a [E]^T [D] [E] dx dy \right\} [B]^{-1} \right] \{\delta\}$$

$$= 1/2 \{\delta\}^T [K]_e \{\delta\} \quad (\text{IV-6})$$

Applying Castigliano's theorem,  $\partial U / \partial \delta_r = F_r$ , yields:

$$\{F\} = [K]_e \{\delta\} \quad (\text{W-7})$$

where  $\{F\}^T = \{F_x, M_{\alpha x}, M_{\theta x}\}$   
 $r = k, l, m, n$

and  $[K]_e$  is the element stiffness matrix for which an explicit expression is given in Fig. IV-2a.

The external work done by the equivalent nodal inertia forces  $\{F_{In}\}$  in

moving through virtual nodal displacements  $\{\delta_v\}$  is equal to the external work done by the actual distributed inertia loading  $f$  in moving through a virtual deflection  $h_v$ . Hence:

$$\{\delta_v\}^T \cdot \{F_{in}\} = \int_{y=0}^b \int_{x=0}^a h_v f \, dx dy \quad (IV-8)$$

The inertia force per unit area when the plate is vibrating sinusoidally with circular frequency is:

$$f = \omega^2 \rho h = \omega^2 \rho \{w\}^T \{A\} = \omega^2 \{w\}^T [B]^{-1} \{\delta\} \quad (IV-9)$$

Also from equation (IV-1)

$$h_v = \{A_v\}^T \{w\} = (\{\delta_v\}^T [B]^{-T}) \{w\} \quad (rv-10)$$

Substituting equations (IV-9) and (IV-10) into equation (IV-8) gives:

$$\{\delta_v\}^T \cdot \{F_{in}\} = \omega^2 \rho \{\delta_v\}^T [B]^{-T} \left\{ \int_{y=0}^b \int_{x=0}^a \{w\} \{w\}^T \, dx dy \right\} [B]^{-1} \{\delta\} \quad (rv-11)$$

Each element of the virtual displacement vector  $\{\delta_v\}$  can be given the value of unity in turn while the remaining ones are all set to zero, in this case equation (IV-11) becomes:

$$\{F_{in}\} = \omega^2 \left[ [B]^{-T} \left\{ \int_{y=0}^b \int_{x=0}^a \{w\}^T \rho \{w\} \, dx dy \right\} [B]^{-1} \right] \{\delta\} \quad (IV-12)$$

Identifying with Newton's second law

$$\{F_{in}\} = \omega^2 [M]_e \{\delta\} \quad (IV-13)$$

where  $M_e$  is the element inertia matrix for which an explicit expression is given in Fig. (IV-2b)

Using the principle of virtual work again, it can be shown in a similar manner that nodal forces due to a distributed axial loading P per unit element area can be determined as:

$$\{Q\}_e = \begin{Bmatrix} F_r \\ M_{\alpha r} \\ M_{\theta r} \end{Bmatrix}_{r = k,l,m,n} = -[B]^{-T} \int_{y=0}^b \int_{x=0}^a \{w\} P(x,y) dx dy \quad (Iv-14)$$

In Chapter 11 It was assumed that the pressure distribution per unit span length is given by:

$$P(x,y) = P(y) = -\omega y [P_h(y)h + c\omega P_a(y)\alpha] \quad (Iv-15)$$

where both  $p_h$  and  $p_a$  are second order polynomials of the form:

$$P_s = c_2 y^2 + c_1 y + c_0$$

where  $s = h$  or  $a$  depending on the motion. It can be shown that:

$$-[B]^{-T} \int_{y=0}^b \int_{x=0}^a \{w\} (c_2 y^2 + c_1 y + c_0) dx dy = - \frac{ab}{720} \begin{Bmatrix} c_{hsk} \\ b.c_{\alpha sk} \\ a.c_{\theta sk} \\ c_{hsl} \\ b.c_{\alpha sl} \\ a.c_{\theta sl} \\ c_{hsm} \\ b.c_{\alpha sm} \\ a.c_{\theta sm} \\ c_{hsn} \\ b.c_{\alpha sn} \\ a.c_{\theta sn} \end{Bmatrix} \quad (Iv-15)$$

$s = h \text{ or } a$

where

$$\begin{aligned}
 C_{hsk} &= C_{hsl} = 24C_2 b^2 + 54C_1 b + 180C_0 \\
 C_{hsm} &= C_{hsn} = 96C_2 b^2 + 126C_1 b + 180C_0 \\
 C_{ask} &= C_{asl} = 6C_2 b^2 + 12C_1 b + 30C_0 \\
 C_{asm} &= C_{asn} = -12C_2 b^2 - 18C_1 b - 30C_0 \\
 C_{esk} &= -C_{esl} = 5C_2 b^2 + 10C_1 b + 30C_0 \\
 C_{esm} &= -C_{esn} = -15C_2 b^2 - 20C_1 b - 30C_0
 \end{aligned}
 \tag{IV-17}$$

$s = h \text{ or } \alpha$

Inserting equation (IV-15) into (IV-14) and using (IV-17) gives:

$$\{Q\}_e = \begin{Bmatrix} F_r \\ M_{\alpha r} \\ M_{\theta r} \end{Bmatrix}_{r=k,l,m,n} = \omega y ab / 720 \begin{Bmatrix} C_{hhr} \dot{h}_r + c\omega \cdot C_{\alpha\alpha r} \alpha_r \\ b \cdot C_{\alpha hr} \dot{h}_r + b\omega \cdot C_{\alpha\alpha r} \alpha_r \\ a \cdot C_{\theta hr} \dot{h}_r + a\omega \cdot C_{\theta\alpha r} \alpha_r \end{Bmatrix}_{r=k,l,m,n}
 \tag{IV-18}$$

Assuming simple harmonic motion. equation (IV-18) can be written as:

$$\{Q\}_e = \omega^2 y ab / 720 \cdot [A]_e \{\delta\}
 \tag{IV-19}$$

where  $[A]_e$  is the element aeroelastic load matrix given by:

$$[A]_e = \begin{vmatrix} [A]_k & & & & \\ & [A]_l & & & \\ & & [A]_m & & \\ & & & [A]_n & \\ & & & & [A]_n \end{vmatrix}
 \tag{IV-20}$$

with

$$[A]_r = \begin{bmatrix} i & C_{hhr} & c & C_{\alpha\alpha r} & 0 \\ ib & C_{\alpha hr} & cb & C_{\alpha\alpha r} & 0 \\ ia & C_{\theta hr} & ca & C_{\theta\alpha r} & 0 \end{bmatrix}$$

$r = k, l, m, n$

and  $\{\delta\}$  is defined in equation (IV-2).



The aeroelastic coefficients given in equation (IV-20) are referred to an axis position passing through the centre of gravity. It is therefore necessary to generalise for any axis position distant  $e$  from the centre of gravity. These two cases will be distinguished by the suffices 0 and 1 respectively. The lateral force is not affected by the change of axis but the radial moment is. Hence:

$$\begin{aligned} F_1 &= F_0 \\ M_1 &= M_0 - eF_0 \end{aligned} \tag{IV-21}$$

The transformation formulae can be found by inserting equation (IV-21) into equation (IV-18).

$$\begin{aligned} (C_{h\dot{h}r})_1 &= (C_{h\dot{h}r})_0 \\ (C_{h\dot{\alpha}r})_1 &= (C_{h\dot{\alpha}r})_0 - ie_1(C_{h\dot{h}r})_0 \\ (C_{\dot{\alpha}hr})_1 &= (C_{\dot{\alpha}hr})_0 - e_2(C_{h\dot{h}r})_0 \\ (C_{\dot{\alpha}\dot{\alpha}r})_1 &= (C_{\dot{\alpha}\dot{\alpha}r})_0 - e_2(C_{\dot{\alpha}\dot{\alpha}r})_0 - ie_1(C_{\dot{\alpha}hr})_0 + ie_1e_2(C_{h\dot{h}r})_0 \end{aligned} \tag{IV-22}$$

$r = k, l, m, n$

where  $e_1 = e/c$  and  $e_2 = e/b$ .

$$[K]_e = D/150b [L] ([K_1] + [K_2]) [L]$$

where

	<table border="0" style="width: 100%; border-collapse: collapse;"> <tr><td>60p+60q</td><td></td><td></td><td></td><td></td><td></td><td></td><td></td><td></td><td></td><td></td><td></td><td></td><td></td><td></td></tr> <tr><td>30p</td><td>20q</td><td></td><td></td><td></td><td></td><td></td><td></td><td></td><td></td><td></td><td></td><td></td><td></td><td></td></tr> <tr><td>30q</td><td>0</td><td>20q</td><td></td><td></td><td></td><td></td><td></td><td></td><td></td><td></td><td></td><td></td><td></td><td></td></tr> <tr><td>30p-60q</td><td>15p</td><td>-30q</td><td>60p+60q</td><td></td><td></td><td></td><td></td><td></td><td></td><td></td><td></td><td></td><td></td><td></td></tr> <tr><td>15p</td><td>10p</td><td>0</td><td>30p</td><td>20p</td><td></td><td></td><td></td><td></td><td></td><td></td><td></td><td></td><td></td><td></td></tr> <tr><td>30q</td><td>0</td><td>10q</td><td>-30q</td><td>0</td><td>20q</td><td></td><td></td><td></td><td></td><td></td><td></td><td></td><td></td><td></td></tr> <tr><td>-30p-30q</td><td>-15p</td><td>-15q</td><td>-60p+30q</td><td>-30p</td><td>-15q</td><td>60p+60q</td><td></td><td></td><td></td><td></td><td></td><td></td><td></td><td></td></tr> <tr><td>15p</td><td>5p</td><td>0</td><td>30p</td><td>10p</td><td>0</td><td>-30p</td><td>20p</td><td></td><td></td><td></td><td></td><td></td><td></td><td></td></tr> <tr><td>15q</td><td>0</td><td>-5q</td><td>-15q</td><td>0</td><td>10q</td><td>-30q</td><td>0</td><td>20q</td><td></td><td></td><td></td><td></td><td></td><td></td></tr> <tr><td>-60p+30q</td><td>-30p</td><td>15q</td><td>-30p-30q</td><td>-15p</td><td>15q</td><td>30p-60q</td><td>-15p</td><td>30q</td><td>60p+60q</td><td></td><td></td><td></td><td></td><td></td></tr> <tr><td>30p</td><td>10p</td><td>0</td><td>15p</td><td>5p</td><td>0</td><td>-15p</td><td>10p</td><td>0</td><td>-30p</td><td>20p</td><td></td><td></td><td></td><td></td></tr> <tr><td>15q</td><td>0</td><td>10q</td><td>-15q</td><td>0</td><td>5q</td><td>-30q</td><td>0</td><td>10q</td><td>30q</td><td>0</td><td>20q</td><td></td><td></td><td></td></tr> </table>	60p+60q															30p	20q														30q	0	20q													30p-60q	15p	-30q	60p+60q												15p	10p	0	30p	20p											30q	0	10q	-30q	0	20q										-30p-30q	-15p	-15q	-60p+30q	-30p	-15q	60p+60q									15p	5p	0	30p	10p	0	-30p	20p								15q	0	-5q	-15q	0	10q	-30q	0	20q							-60p+30q	-30p	15q	-30p-30q	-15p	15q	30p-60q	-15p	30q	60p+60q						30p	10p	0	15p	5p	0	-15p	10p	0	-30p	20p					15q	0	10q	-15q	0	5q	-30q	0	10q	30q	0	20q				<p align="center">SYMMETRIC</p> <p><math>p = a^2/b^2</math> <math>q = b^2/a^2</math></p>	
60p+60q																																																																																																																																																																																							
30p	20q																																																																																																																																																																																						
30q	0	20q																																																																																																																																																																																					
30p-60q	15p	-30q	60p+60q																																																																																																																																																																																				
15p	10p	0	30p	20p																																																																																																																																																																																			
30q	0	10q	-30q	0	20q																																																																																																																																																																																		
-30p-30q	-15p	-15q	-60p+30q	-30p	-15q	60p+60q																																																																																																																																																																																	
15p	5p	0	30p	10p	0	-30p	20p																																																																																																																																																																																
15q	0	-5q	-15q	0	10q	-30q	0	20q																																																																																																																																																																															
-60p+30q	-30p	15q	-30p-30q	-15p	15q	30p-60q	-15p	30q	60p+60q																																																																																																																																																																														
30p	10p	0	15p	5p	0	-15p	10p	0	-30p	20p																																																																																																																																																																													
15q	0	10q	-15q	0	5q	-30q	0	10q	30q	0	20q																																																																																																																																																																												
	<table border="0" style="width: 100%; border-collapse: collapse;"> <tr><td>42-12v</td><td></td><td></td><td></td><td></td><td></td><td></td><td></td><td></td><td></td><td></td><td></td><td></td><td></td><td></td></tr> <tr><td>3+12v</td><td>4-4v</td><td></td><td></td><td></td><td></td><td></td><td></td><td></td><td></td><td></td><td></td><td></td><td></td><td></td></tr> <tr><td>3+12v</td><td>v</td><td>4-4v</td><td></td><td></td><td></td><td></td><td></td><td></td><td></td><td></td><td></td><td></td><td></td><td></td></tr> <tr><td>-42-12v</td><td>-3-12v</td><td>-3+3v</td><td>42-12v</td><td></td><td></td><td></td><td></td><td></td><td></td><td></td><td></td><td></td><td></td><td></td></tr> <tr><td>-3-12v</td><td>-4+4v</td><td>0</td><td>3+12v</td><td>4-4v</td><td></td><td></td><td></td><td></td><td></td><td></td><td></td><td></td><td></td><td></td></tr> <tr><td>3-3v</td><td>0</td><td>-1+v</td><td>-3-12v</td><td>-v</td><td>4-4v</td><td></td><td></td><td></td><td></td><td></td><td></td><td></td><td></td><td></td></tr> <tr><td>42-12v</td><td>3-3v</td><td>3-3v</td><td>-42+12v</td><td>-3+3v</td><td>3+12v</td><td>42-12v</td><td></td><td></td><td></td><td></td><td></td><td></td><td></td><td></td></tr> <tr><td>-3+3v</td><td>1-v</td><td>0</td><td>3-3v</td><td>-1+v</td><td>0</td><td>-3-12v</td><td>4-4v</td><td></td><td></td><td></td><td></td><td></td><td></td><td></td></tr> <tr><td>-3+3v</td><td>0</td><td>1-v</td><td>3+12v</td><td>0</td><td>4-4v</td><td>-3-12v</td><td>v</td><td>4-4v</td><td></td><td></td><td></td><td></td><td></td><td></td></tr> <tr><td>-42+12v</td><td>-3+3v</td><td>-3-12v</td><td>42-12v</td><td>3-3v</td><td>-3+3v</td><td>-42+12v</td><td>3+12v</td><td>3-3v</td><td>42-12v</td><td></td><td></td><td></td><td></td><td></td></tr> <tr><td>3-3v</td><td>-1+v</td><td>0</td><td>-3+3v</td><td>1-v</td><td>0</td><td>3+12v</td><td>-4+4v</td><td>0</td><td>-3-12v</td><td>4-4v</td><td></td><td></td><td></td><td></td></tr> <tr><td>-3-12v</td><td>0</td><td>-4+4v</td><td>3-3v</td><td>0</td><td>1-v</td><td>-3+v</td><td>0</td><td>-3+3v</td><td>3+12v</td><td>-v</td><td>4-4v</td><td></td><td></td><td></td></tr> </table>	42-12v															3+12v	4-4v														3+12v	v	4-4v													-42-12v	-3-12v	-3+3v	42-12v												-3-12v	-4+4v	0	3+12v	4-4v											3-3v	0	-1+v	-3-12v	-v	4-4v										42-12v	3-3v	3-3v	-42+12v	-3+3v	3+12v	42-12v									-3+3v	1-v	0	3-3v	-1+v	0	-3-12v	4-4v								-3+3v	0	1-v	3+12v	0	4-4v	-3-12v	v	4-4v							-42+12v	-3+3v	-3-12v	42-12v	3-3v	-3+3v	-42+12v	3+12v	3-3v	42-12v						3-3v	-1+v	0	-3+3v	1-v	0	3+12v	-4+4v	0	-3-12v	4-4v					-3-12v	0	-4+4v	3-3v	0	1-v	-3+v	0	-3+3v	3+12v	-v	4-4v				<p align="center">SYMMETRIC</p> <p><math>v</math> Poisson's ratio <math>D</math> Flexural rigidity</p>	
42-12v																																																																																																																																																																																							
3+12v	4-4v																																																																																																																																																																																						
3+12v	v	4-4v																																																																																																																																																																																					
-42-12v	-3-12v	-3+3v	42-12v																																																																																																																																																																																				
-3-12v	-4+4v	0	3+12v	4-4v																																																																																																																																																																																			
3-3v	0	-1+v	-3-12v	-v	4-4v																																																																																																																																																																																		
42-12v	3-3v	3-3v	-42+12v	-3+3v	3+12v	42-12v																																																																																																																																																																																	
-3+3v	1-v	0	3-3v	-1+v	0	-3-12v	4-4v																																																																																																																																																																																
-3+3v	0	1-v	3+12v	0	4-4v	-3-12v	v	4-4v																																																																																																																																																																															
-42+12v	-3+3v	-3-12v	42-12v	3-3v	-3+3v	-42+12v	3+12v	3-3v	42-12v																																																																																																																																																																														
3-3v	-1+v	0	-3+3v	1-v	0	3+12v	-4+4v	0	-3-12v	4-4v																																																																																																																																																																													
-3-12v	0	-4+4v	3-3v	0	1-v	-3+v	0	-3+3v	3+12v	-v	4-4v																																																																																																																																																																												
	<table border="0" style="width: 100%; border-collapse: collapse;"> <tr><td>1</td><td>0</td><td>0</td><td>0</td><td></td></tr> <tr><td>0</td><td>0</td><td>1</td><td>0</td><td></td></tr> <tr><td>0</td><td>0</td><td>0</td><td>1</td><td></td></tr> <tr><td>0</td><td>1</td><td>0</td><td>0</td><td></td></tr> </table>	1	0	0	0		0	0	1	0		0	0	0	1		0	1	0	0		<p>and</p> <table border="0" style="width: 100%; border-collapse: collapse;"> <tr><td>1</td><td>0</td><td>0</td></tr> <tr><td>0</td><td>b</td><td>0</td></tr> <tr><td>0</td><td>0</td><td>a</td></tr> </table>	1	0	0	0	b	0	0	0	a																																																																																																																																																								
1	0	0	0																																																																																																																																																																																				
0	0	1	0																																																																																																																																																																																				
0	0	0	1																																																																																																																																																																																				
0	1	0	0																																																																																																																																																																																				
1	0	0																																																																																																																																																																																					
0	b	0																																																																																																																																																																																					
0	0	a																																																																																																																																																																																					

Fig. IV-2a Element stiffness matrix

$$[M]_e = \rho tab/6300 [L][M][L]$$

where

	<table border="0" style="width: 100%; border-collapse: collapse;"> <tr><td>-3454</td><td></td><td></td><td></td><td></td><td></td><td></td><td></td><td></td><td></td><td></td><td></td><td></td><td></td><td></td></tr> <tr><td>-461</td><td></td><td></td><td></td><td></td><td></td><td></td><td></td><td></td><td></td><td></td><td></td><td></td><td></td><td></td></tr> <tr><td>-461</td><td>4 3</td><td>-80</td><td></td><td></td><td></td><td></td><td></td><td></td><td></td><td></td><td></td><td></td><td></td><td></td></tr> <tr><td>-1226</td><td>-199</td><td>-274</td><td>-3464</td><td></td><td></td><td></td><td></td><td></td><td></td><td></td><td></td><td></td><td></td><td></td></tr> <tr><td>-199</td><td>-40</td><td>-42</td><td>-461</td><td>-80</td><td></td><td></td><td></td><td></td><td></td><td></td><td></td><td></td><td></td><td></td></tr> <tr><td>274</td><td>42</td><td>60</td><td>461</td><td>63</td><td>-60</td><td></td><td></td><td></td><td></td><td></td><td></td><td></td><td></td><td></td></tr> <tr><td>-394</td><td>-116</td><td>-116</td><td>-1226</td><td>-274</td><td>199</td><td>-3464</td><td></td><td></td><td></td><td></td><td></td><td></td><td></td><td></td></tr> <tr><td>116</td><td>30</td><td>28</td><td>274</td><td>60</td><td>-42</td><td>461</td><td>-60</td><td></td><td></td><td></td><td></td><td></td><td></td><td></td></tr> <tr><td>116</td><td>28</td><td>30</td><td>199</td><td>42</td><td>-40</td><td>461</td><td>4 3</td><td>-80</td><td></td><td></td><td></td><td></td><td></td><td></td></tr> <tr><td>-1226</td><td>-274</td><td>-199</td><td>-394</td><td>-116</td><td>116</td><td>-1226</td><td>199</td><td>274</td><td>-3454</td><td></td><td></td><td></td><td></td><td></td></tr> <tr><td>274</td><td>60</td><td>42</td><td>116</td><td>30</td><td>-26</td><td>199</td><td>-40</td><td>-42</td><td>461</td><td>-80</td><td></td><td></td><td></td><td></td></tr> <tr><td>-199</td><td>-40</td><td>-166</td><td>-166</td><td>-28</td><td>30</td><td>-274</td><td>42</td><td>60</td><td>-461</td><td>63</td><td>-90</td><td></td><td></td><td></td></tr> </table>	-3454															-461															-461	4 3	-80													-1226	-199	-274	-3464												-199	-40	-42	-461	-80											274	42	60	461	63	-60										-394	-116	-116	-1226	-274	199	-3464									116	30	28	274	60	-42	461	-60								116	28	30	199	42	-40	461	4 3	-80							-1226	-274	-199	-394	-116	116	-1226	199	274	-3454						274	60	42	116	30	-26	199	-40	-42	461	-80					-199	-40	-166	-166	-28	30	-274	42	60	-461	63	-90				<p align="center">SYMMETRIC</p>	
-3454																																																																																																																																																																																							
-461																																																																																																																																																																																							
-461	4 3	-80																																																																																																																																																																																					
-1226	-199	-274	-3464																																																																																																																																																																																				
-199	-40	-42	-461	-80																																																																																																																																																																																			
274	42	60	461	63	-60																																																																																																																																																																																		
-394	-116	-116	-1226	-274	199	-3464																																																																																																																																																																																	
116	30	28	274	60	-42	461	-60																																																																																																																																																																																
116	28	30	199	42	-40	461	4 3	-80																																																																																																																																																																															
-1226	-274	-199	-394	-116	116	-1226	199	274	-3454																																																																																																																																																																														
274	60	42	116	30	-26	199	-40	-42	461	-80																																																																																																																																																																													
-199	-40	-166	-166	-28	30	-274	42	60	-461	63	-90																																																																																																																																																																												
	<p>a Element width b length t thickness <math>\rho</math> density <math>v</math> Poisson's ratio D flexural rigidity</p>																																																																																																																																																																																						

and [L] is defined in Fig N-21

Fig. IV-2b Element mass matrix

REFERENCES

Aerodynamics [AD]

- AD-1 Woolston, D. S. and Runyan. H. L. , "Some Considerations on the Air Forces on a Wing Oscillating Between Two Walls for Subsonic Compressible Flow", J. Aero. Sci. , Voi 22, p 41. January 1955
- AD-2 Runyan. H. L. , Woolston. D. S. and Rainey. A. G. , 'Theoretical and Experimental Investigation of the Effect of Tunnel Walls on the Forces of an Oscillating Aerofoil in Two-Dimensional Subsonic Compressible Flow', NACA TR 1262, 1956
- AD-3 Miles. J. W. , "The Compressible Flow Past an Oscillating Aerofoil in a Wind Tunnel". J. Aero. Sci. , Voi 24, pp 671-678, July 1956
- AD-4 Drake, D. G. , 'The Oscillating Two-Dimensional Aerofoil Between Porous Walls'. Aero. Quart. ,Vol 8. p 226. 1958
- AD-5 Giauert. H. , 'The Force and Moment of an Oscillating Airfoil'. Br. ARC R&M 1216. 1928
- AD-6 Von Karman, T. and Burgers. J. M. , 'Aerodynamic Theory', J. Springer, Berlin. 1934
- AD-7 Postei. E. E. and Leppert. E. L. , 'Theoretical Pressure Distributions for a Thin Airfoil Oscillating in incompressible Flow'. J. of the Aeronaut. Sci. , pp 486-492. August 1948.
- AD-6 Mendelson, A. and Caroi. R. W. , 'Lift and Moment Equations for Oscillating Aerofoils in an Infinite Unstaggered Cascade". NACA TN 3263, October 1954
- AD-9 Lane. F. and Wang, C.T.. 'A Theoretical Investigation of the Flutter Characteristics of Compressor and Turbine Blade Systems'. WADC TR 54-449, 1954
- AD-10 Whitehead. D. S. , 'Force and Moment Coefficients for Vibrating Aerofoils in Cascade". British Aeronautical Research Council R 8 M 3254. February 1960
- AD-11 Posslo. c. , 'Aerodynamic Forces on an Oscillating Profile in a Compressible Fluid at Subsonic Speeds'. British Aeronautical Research Council. ARC 3799 0.128, November 1938
- AD-12 Garrick. I. E. , 'Bending-Torsion Flutter Calculations Modified by Subsonic Compressibility Corrections', NACA TN 1034, 1946

- AD-13 Lane, F and Friedman, M., 'Theoretical investigations of Subsonic Oscillatory Blade Row Aerodynamics'. NACA TN 4136, February 1958
- AD-14 Whitehead, D. S., "Vibration and Sound Generation in a Cascade of Flat Plates in Subsonic Flow". ARC, R&M 3684. 1972
- AD-15 Smith, S. N., 'Discrete Frequency Generation in Axial Flow Turbomachines', ARC R&M 3709, March 1972
- AD-16 Kaji, S. and Okazaki, T., 'Propagation of Sound Waves through a Blade Row'. J. Sound Vib., Voi 11, No 3. 1970
- AD-17 Possio, c.. 'L'azione Aerodinamica sul Profilo Oscillante alle Velocita Ultrasonore'. Acta Pont. Accad. Sci. Roma. Toma 1. pp 93-105, 1937 (Trans. in Br. ARC 7668. May 1944)
- AD-18 Lane, F., 'Supersonic Flow Past an Oscillating Cascade with Supersonic Leading Edge Locus'. J. Aero. Sci., Voi 24. pp 65-66, 1957
- AD-19 Goreiov, D. N., 'Lattice of Plates in an Unsteady Supersonic Flow'. Ahidi Gaza. Vol 1. No 4. 1966; Trans. Fluid Dynamics Vol 1, No 4. p 34. 1966
- AD-20 Kurosaka, M., 'On the Unsteady Supersonic Cascade with Subsonic Leading Edge - An Exact First Order Theory -' Parts 1 and 2. J. of Eng. for Power. pp 13-31, January 1974
- AD-21 Verdon, J. M., \*The Unsteady Aerodynamics of a Finite Supersonic Cascade with Subsonic Axial Flow". J. Appi. Mech., pp 667-671, September 1973
- AD-22 Brix, C. W., Jr. and Platzler, M. F., .Theoretical investigation of Supersonic Flow Past Oscillating Cascades with Subsonic Leading Edge Locus'. AIAA Paper No 72-14. 1974
- AD-23 Nagashima, T. and Whitehead, D.S.. 'Aerodynamic Forces and Moments for Vibrating Supersonic Cascade Blades'. CUED/A - Turbo/TR 59, 1974: See also "Linearized Supersonic Flow in Cascades". ARC R&M 3811, February 1977
- AD-24 Goldstein, M. W., "Cascade with Subsonic Edge Locus". AIAA J. Vol 73, p 1117. 1975
- AD-25 Verdon, J. M. and McCune, J. E.. 'Unsteady Supersonic Cascade in Subsonic Axial Flow'. AIAA J., Vol 13. pp 193-201, February 1975
- AD-26 Goldstein, M. E., Braun, W. and Adamczyk, J. J., 'Unsteady Flow in a Supersonic Cascade with Strong in-Passage Shocks'. J. of Fluid Mech., Voi 83, Pt. III, pp 569-605. December 1977

- AD-27 Adamczyk. J. J and Goldstein, M. E. , 'Unsteady Flow in a Supersonic Cascade with Subsonic Leading Edge Locus'. AIAA J.. Vol 16. pp 1248-1254. December 1978
- AD-28 Kerlick. D.G. and Nixon, D.. 'A High Frequency Transonic Small Disturbance Code for Unsteady Flows in a Cascade'. AIAA paper No 82-0955, June 1982
- AD-29 Favrat. D. and Suter. P. , 'interaction of the Rotor Blade Shock Waves in Supersonic Compressors with Upstream Stator Vanes", ASME paper No 77-GT-93,1977
- AD-30 Whitehead. D. S. , 'Vibration and Sound Generation in a Cascade of Flat Plates in subsonic Flow'. ARC R&M 3685, February 1970
- AD-31 Verdon, J. M. , 'Further Developments in the Aerodynamic Analysis of Unsteady Supersonic Cascades". Parts 1 and 2. J. of Eng. for Power, Vol 99. pp 509-525. October 1977
- AD-32 Whitehead. D. S.. 'Bending Flutter of Unstalled Cascade Blades at Finite Deflection', ARC, R & M 3386. October 1962

**Aeroelasticity [AE]**

- AE-1 Den Hartog. J. P. . 'Mechanical Vibrations'. McGraw-Hill, New York, 1956
- AE-2 Schnittger. J. R. and Sisto. F. . 'Blade Flutter in Axial Turbomachines', App. Mech. Surveys. Spartan Books, Washington D. C. , 1966
- AE-3 Fleeter, S. . "Aeroelasticity Research for Turbomachine Applications". AIAA Paper No 77-437. 1977
- AE-4 Theodorsen. T. . 'General Theory of Aerodynamic Instability and the Mechanism of Flutter'. NACA TR 496, 1934
- AE-5 Theodorsen, T. and Garrick, I. E. . "Mechanism of Flutter: A Theoretical and Experimental Investigation of the Flutter Problem'. NACN TR 685, 1940
- AE-6 Bisplinghoff, R. L. , Ashley, H. and Hoffman, R. L. . 'Aeroelasticity', Addison-Wesley, 1957
- AE-7 Scanlan, R. H. and Rosenbaum. R. . "Aircraft Vibration and Flutter'. Dover Publications, 1968
- AE-6 Whitehead. D. S. . 'Torsional Flutter of Unstalled Cascade Blades at Zero Deflection', ARC. R & M No 33429, March 1964
- AE-9 Carta. F. O. . 'Coupled Blade-Disc-Shroud Flutter instabilities in Turbojet Engine Rotors'. J. of Eng. for Power. pp 419-425, July 1967
- AE-10 Mikolajczak. A. A. , Arnoldi. R. A. , Snyder, L. E. and Stargardter. H. , 'Advances In Fan and Compressor Blade Flutter Analysis and Predictions'. J. Aircraft, Vol 12, No 4, pp 325-332. April 1975
- AE-11 Bendiksen, O. and Friedmann. P. . 'Coupled Bending-Torsion Flutter In Cascades', AIAA J. , Vol 18. No 2. pp 194-201. 1979
- AE-12 Srinivasan. A. V. . 'Influence of Mistuning on Blade Torsional Flutter'. NASA CR 165137, August 1980
- AE-13 Hanamura, Y. and Tanaka, H. . 'A Modification of Flutter Characteristics by Changing Elastic Nature of Neighbouring Blades In Cascades'. Presented at Tokyo Joint Gas Turbine Congress. Gas Turbine Society of Japan. Tokyo. 1972
- AE-14 Kaza. K. R. V. and Kielb. R. E. . • Effects fo Mistuning on Bending-Torsion Flutter and Response of a Cascade in Incompressible Flow'. AIAA J. , Vol 20, No 8, pp 1120-1127. August 1982

- AE-15 Klelb, R. E. and Kaza, K. R. V. , 'Aeroelastic Characteristics of a Cascade of Mistuned Blades in Subsonic and Supersonic Flows', ASME paper No 81-DET-1222. September 1981
- AE-16 Klelb. R. E. , 'Aeroelastic Characteristics of a Mistuned Bladed-Disc Assembly'. Ph. D. Thesis. The Ohio State University , Columbus. Ohio, 198 1
- AE-17 Goland. M. , 'The Flutter of a Uniform Cantilever Wing". J. of App. Mech. , Vol 12. No 4. December 1945
- AE-18 Lane, F. , 'Supersonic Flow Past an Oscillating Cascade with Supersonic Leading Edge Locus'. J. Aeronaut. Sci.. Vol 24. pp 54-66. January 1956
- AE-19 Kaza . K.R.V. and Klelb, R. E. , 'Coupled Bending-Torsion Flutter of a Mistuned Cascade with Non-uniform Blades'. NASA TM-82813, 1982
- AE-20 Klelb, R. E. and Kaza, K. R. V.. 'Effects of Structural Coupling on Mistuned Cascade Flutter and Response., NASA TM-83049. 1983
- AE-21 Whitehead. D. S. , 'Effect of Mistuning on the Vibration of Turbo-Machine Blades Induced by Wakes'. J. Mech. Eng. sci. . Vol 8, No 1, pp 15-21. 1966
- AE-22 Whitehead, D. S. , "Research Note: Effect of Mistuning on Forced Vibration of Blades with Mechanical Coupling', J. Mech. Eng. Sci. . Vol 18, No 6. pp 306-307. 1976
- AE-23 Srinivasan. A.V. and Fabunmi, J.A. , 'Cascade Flutter Analysis of Cantilevered Blades', ASME paper No. 83-GT-129. 1983
- AE-24 Movshovlch, I. M. , 'Self-Induced Vibrations of Axial Compressor Blades". NASA, TT F-547, pp 71-82. 1969
- AE-25 Blevins. R. D. , 'Flow-Induced Vibration', Van Nostrand, 1977
- AE-26 MacDonald, A. J. , "Wind Loading on Buildings". Applied Science Publishers, 1975
- AE-27 Houghton. E. L. and Carruthers. N. B. , 'Wind Forces on Buildings and Structures". Edward Arnold, 1976
- AE-28 Platzer. M. F.. "Transonic Blade Flutter - A Survey'. The Shock and Vib. Dig. , July 1975
- AE-29 Platzer. M. F. , 'Transonic Blade Flutter - A Survey of New Developments'. The Shock and Vib. Dig. , September 1978
- AE-30 Platzer. M. F. , "Transonic Blade Flutter - A Survey of New Developments'. The Shock and Vib. Dig. , July 1982

- AE-31 Woolston. D. S. and Runyan. H. L. . 'On the use of Coupled Modal Functions In Flutter Analysis'. NACA TN 2375, 1951
- AE-32 Whitehead. D. S. . 'The Vibration of Cascade Blades Treated by Actuator Disc Methods". Proc. I. Mech. Eng. . Vol 173, p 555. 1959
- AE-33 Halliwell, D. G. . 'Fan Supersonic Flutter: Prediction and Test Analysis'. ARC, R & M 3789, 1977
- AE-34 Legendre. R. . 'Aerodynamic Damping of Two-Mode Blade Vibrations". Proceedings of the Symposium on Flow Research on Blading. Brown Boveri & Co. Baden. 1969
- AE-35 Halliwell. D. G., Newton. S.G. and Lit. K. S. . "A Study of Unsteady Pressures Near the Tip of a Transonic Fan in Unstalled Supersonic Flutter'. Presented at the ASME 9th Biennial Conference on Mechanical Vibration and Noise of the Design and Production, Dearborn. Michigan. September. 1983



**Finite Elements [FE]**

- FE-1 Thomas. J. and Belek, H. T. , 'Free Vibration of Blade Packets', J. Mech. Eng. Sci. . Vol 19, No 1, 1977
- FE-2 Salama. A.M., Petyt. M. and Motat Soares. C. A., 'Dynamic Response of Packets of Blades by the Finite Element Method'. ASME, J. Mech. Des.. Vol 100. No 4. p 660. 1978
- FE-3 Zienkiewicz, O. C. , "The Finite Element Method in Engineering Science". McGraw Hill. 1971
- FE-4 Nath, B. , 'Fundamentals of Finite Elements for Engineers". Athleon Press. 1973
- FE-5 MacBain, J. C. , 'Vibrating Behaviour of Twisted Cantilevered Plates'. J. Aircraft. Vol 12, No 4. April 1975
- FE-8 Desai, C. S. and Abel. J. F. , "Introduction to the Finite Element Method". Van Nostrand. 1972
- FE-7 Dawe. D. J.. 'A Finite Element Approach to Plate Vibration Problems'. J. Mech. Eng. Sci., Vol 7, No 1, 1965
- FE-8 Henry. R. and Hagopian. J. . "Sous Structuration ou Propagation d'Ondes? Pourquoi pas l'une et l'autre? Application aux Disque-Aube de Turbomachines'. Laboratoire Mechanique des Structures, ERA-CNRS. INSA. Lyon. 1982
- FE-Q Melosh. Robert J. , "Basis for Derivation of Matrices for the Direct Stiffness Method". AIAA J. . Voi 1, No 7. July 1963
- FE-10 Salama. A. M. , Petyt. M. and Mota Soares. C. A. , 'Dynamic Analysis of Bladed Disks by Wave Propagation and Matrix Difference Techniques'. presented at the ASME Winter Annual Meeting, New York. December 1976
- FE-I 1 Mota Soares. C. A. , Petyt. M. and Salama. A. M. , 'Finite Element Analysis of Bladed-Disks'. presented at the ASME Winter Annual Meeting. New York. December 1976
- FE-12 Orris. R. M. and Petyt. M. , 'A Finite Element Study of Harmonic Wave Propagation in Periodic Structures'. J. Sound and Vib. . Vol 33. No 2. 1974
- FE-13 Dokainish, M. A. and Rawtani. S. , 'Vibration Analysis of Rotating Cantilever Plates'. Int. J. Num. Mech.Eng. , Vol 3. pp 233-248. 1971
- FE-14 Zienkiewicz, O. C. and Cheung, Y. K. , 'The Finite Element Method for Analysis of Elastic Isotropic and Orthotropic Slab'. Proc. Inst. Civ. Eng. , Vol 28, 1964

- FE-15 Wright, P. M. , "Simplified Formulation of Stiffness Matrices'. Proc. Amer. Soc. Civ. Eng., April 1963
- FE-16 Hitchings, D. , Ewins. D. J. and Singh. M., 'Dynamic Analysis of Turbine Blades'. ASME Advances in Comp. Tech., Vol 2, 1982
- FE-17 Singh, M. and Schiffa. D. , 'Vibrational Characteristics of Packeted Bladed Disks'. ASME 87-DET-137
- FE-18 Rockey, K. C. and al.. 'The Finite Element Method'. Granada Publishing Co. , 1980
- FE-19 Weisshaar. T. A. , 'Panel Flutter Optimization - A Refined Finite Element Approach'. Int. J. Num. Meth. In Eng.. Vol 10. pp 77-91. 1 976

Mathematics **[MA]**

- MA- 1     Davis. P. J. . "Circulant Matrices", John Wiley. 1979
- MA-2     Noble. B., 'Methods Based on the Wiener-Hopf Technique'. Pergamon Press. New York. 1958
- MA-3     Sneddon. I. , 'Use of Integral Transformations'. McGraw Hill. New York, 1972
- MA-4     Fox. L. and Goodwin, E. T. , 'The Numerical Solution of Non-Singular Linear Integral Equations'. Proc. Royal Soc. A. , Vol 245, pp 501-535. February, 1953
- MA-5     Wilkinson, J. H. and Reinsch. C. , "Handbook for Automatic Computation". Volume II. Springer-Verlag , 1971
- MA-6     Crout. P. D. , 'A Short Method for Evaluating Determinants and Solving Systems of Linear Equations with Real or Complex Coefficients", Trans AIEE. Vol 60, pp 1235-1240, 1941

**Structural Dynamics [SD]**

- SD-1 Smith, D. M. , 'Vibrations in Turbomachinery'. Proc IMech Eng, Voi 180. 1966
- SD-2 Stodoia. A. , 'Steam and Gas Turbines', Vois. 1 and 2. McGraw Hill, New York, 1927
- SD-3 Sezewa, K.. 'Vibrations of Turbine Blades with Shrouding'. Phil. Mag. XVI. Ser 7. pp 164-174. 1933
- SD-4 Smlth, D. M. . 'Vibration of Turbines Blades In Packets". Proc. 7<sup>th</sup> int. Cong. App. Mech. , p 178. London. 1949
- SD-S Prohl, M.A. , 'Method for Calculating Vibration Frequencies and Stresses of a Banded Croup of Turbine Buckets'. Trans. ASME, Vol 80, pp 169-180, 7958
- SD-6 Weaver, F. L. and Prohl. M. A. , 'High Frequency Vibrations of Steam Turbine Buckets", Trans ASME. Vol 80. pp 181-194. 1958
- SD-7 Ellngton, J. P. and McCallion, H. , 'The Vibration of Laced Turbine Blades'. J. Roy. Aero. Soc. , Vol 61. p 563. 1957
- SD-8 Bishop, R. E. D. and Johnson. D. C. , 'The Mechanics of Vibration'. CUP. 1960
- SD-9 Rieger, F. and McCallion, H. , 'The Natural Frequencies of Portal Frames'. Parts 1 and 2, int. J. Mech. Sci., Vol 7. pp 253-261 and 263-276. 1965
- SD-10 Afolabi. H. O. , 'The Vibration of Turbine Blade Packets". M. Sc. Thesis. Imperial College. 1978
- SD-1 1 Dimitriadis, E. K. , 'The Vibration of Packeted-Bladed Discs', M. Sc. Thesis. Imperial College, 1979
- SD-12 Stathanopoulos, A. , 'Using a Mathematical Model to investigate the Vibration Properties of Packeted-Bladed Disc Assemblies'. M. Sc. Thesis. Imperial College. 1978
- SD-13 Dye, R. C. F. and Henry. T.A.. 'Vibration Amplitudes of Compressor Blades Resulting from Scatter in Natural Frequencies'. ASME J. Eng for Power. Vol 91. No 3. 1969
- SD-14 Ewins. D. J. , 'Further Studies of Bladed Disc Vibration - Effects of Packeting", presented at IMech Eng Conf 'Vibrations in Rotating Machinery'. Cambridge. September 1980
- SD-15 Singh. M. and Schiffer. D. , "Vibrational Characteristics of Packeted Bladed Discs'. ASME 82-DET-137

- SD-16 Ewins. D. J. , "The Vibration of Bladed Discs". Ph. D. Thesis. Cambridge University. 1966
- SD-17 Cottney. D. J. , 'The Receptance Analysis of Disc. Blade and Shroud Vibration'. Ph. D. Thesis. Imperial College. 1975
- SD-18 Ewins. D. J. , 'Vibration Characteristics of Bladed Disc Assemblies'. J. Mech. Eng. Sci.. Vol. 15. No. 3. 1973
- SD-19 Cottney. D. J. and Ewins. D. J.. 'On Predicting the Natural Frequencies of Shrouded Bladed Discs'. ASME75-DET-113
- SD-20 Cottney, D. J. and Ewins. D. J.. 'Towards the Efficient Vibration Analysis of Shrouded Bladed Disc Assemblies'. Trans ASME. J. of Eng. for Ind. , Vol. 96, No. 3. 1974
- SD-21 Bishop, R. E. D. and McCleod, A. J., 'The Forced Vibration of Circular Flat Plates'. Mech. Eng. Sci. Monograph No 1. March 1965
- SD-22 Armstrong. E. K. , 'Blade and Disc Vibration'. Ph. D. Thesis. Cambridge University. 1955
- SD-23 Wittrick. W. H. and Williams. F. W. , 'A General Algorithm for Computing Natural Frequencies of Repetitive Structures'. Quart. Journ. Mech. and Appt. Math, Vol. 24, pp 264-284. 1971
- SD-24 Williams, F. W. , 'Natural Frequencies of Repetitive Structures\*', Quart. Journ. Mech. and Appl. Math, Vol 24, pp 285-310. 1971
- SD-25 Lim. S. , 'The Effect of Root Flexibility on Turbine Blade Vibration Properties'. M. Sc. Thesis. imperial College, 1980
- SD-26 Afolabi. D. H. , 'Vibration of Mistuned Bladed Disc Assemblies'. Ph. D. Thesis. Imperial College, 1982
- SD-27 Imregun. M. , 'User's Guide to Computer Program BLISC'. Imperial College Dynamics Section, Report No 81005. January 1981
- SD-28 Wong, H. W. , "Using a Mathematical Model to Investigate the Vibration Properties of Bladed-Disc Assemblies". M. Sc. Thesis. Imperial College, 1978
- SD-29 Levy. S. and Wilkinson. J. P. P. , 'The Component Element Method In Dynamics". McGraw Hill, 1976
- SD-30 Henshall. R. D. and Warburton. G. B. , 'Transmission of Vibration in Beam Systems'. Int. J. Num. Meth. in Eng. Vol 1. pp 47-66. 1969
- SD-31 Campbell. W. and Heckman, W. C. , 'Tangential Vibration of Steam Turbine Buckets'. Trans ASME Vol 47, pp 643-671. 1925

- SD-32 Hurty, w. c. , 'Dynamic Analysis of Structural Systems Using Component Modes'. AIAA J. Voi 3, No 4. pp 678-685. 1965
- SD-33 Al Jumaiiy, A. M. and Fauikaer. L. L. , 'Vibration Characteristics of Hollow Symmetrical Blades Based on Thin Shell Theory'. J. Ivlech. Des.. Vol. 100. No 1. pp 183-187. 1978
- SD-34 Bishop. R. E. D.. 'The Treatment of Damping Forces in Vibration Theory'. J. Roy. Aero. Soc., Voi 59. pp 738-74. November 1955
- SD-35 Ewins. D. J. and Cottney. D. J.. \*Towards the Efficient Vibration Analysis of Shrouded Assemblies', ASME 73-DET-144
- SD-38 Crawiey. E. F. , 'in-plane inertial Coupling in Tuned and Severely Mistuned Biaded Disks'. ASME 82-GT-288
- SD-37 Wiidheim. S. J., 'Dynamics of Circumferentialiy Periodic Structures'. Ph. D. Thesis. Linkoping University. Linkoping (Sweden), 1971